FEDERAL UNIVERSITY OF SÃO CARLOS

EXACT AND TECHNOLOGY SCIENCES CENTER

POSTGRADUATE PROGRAM IN CHEMICAL ENGINEERING

RONALDO CORREIA DE BRITO

INTERMITTENT DRYING AND DRAFT TUBE DESIGN FOR SPOUTED BEDS

SÃO CARLOS

2021

FEDERAL UNIVERSITY OF SÃO CARLOS

EXACT AND TECHNOLOGY SCIENCES CENTER

POSTGRADUATE PROGRAM IN CHEMICAL ENGINEERING

RONALDO CORREIA DE BRITO

INTERMITTENT DRYING AND DRAFT TUBE DESIGN FOR SPOUTED BEDS

Doctoral thesis presented to the Postgraduate Program in Chemical Engineering at the Federal University of São Carlos as part of the necessary requirements to obtain the title of D.Sc. in Chemical Engineering.

Supervisor: Prof. Dr. José Teixeira Freire

Co-supervisor: Prof. Dr. Rodrigo Béttega

BEPE supervisor: Prof. Dr. Martin Olazar

SÃO CARLOS

2021

UNIVERSIDADE FEDERAL DE SÃO CARLOS

Centro de Ciências Exatas e de Tecnologia
Programa de Pós-Graduação em Engenharia Química

Folha de Aprovação

Defesa de Tese de Doutorado do candidato Ronaldo Correia de Brito, realizada em 08/12/2021.

Comissão Julgadora:

Prof. Dr. Jose Teixeira Freire (UFSCar)

Prof. Dr. Rodrigo Béttega (UFSCar)

Prof. Dr. Marcos Antônio de Souza Barrozo (UFU)

Prof. Dr. Nehemias Curvelo Pereira (UEM)

Prof. Dr. Wanderley Pereira Oliveira (USP)

O presente trabalho foi realizado com apoio da Coordenação de Aperfeiçoamento de Pessoal de Nível Superior - Brasil (CAPES) - Código de Financiamento 001.
O Relatório de Defesa assinado pelos membros da Comissão Julgadora encontra-se arquivado junto ao Programa de Pós-Graduação em Engenharia Química.

Dedico este trabalho à minha esposa, Natállia Lamec, e aos meus pais, com muito amor.

AGRADECIMENTOS

Primeiramente agradeço à Deus por estar ao meu lado em cada instante, me dando forças para superar os obstáculos e guiando meu caminho.

Aos meus pais, cujo amor, carinho e educação foram primordiais para a realização deste trabalho. À minha amada esposa, Natállia Lamec, por todo amor, carinho, companheirismo e paciência. Agradeço por ter ficado ao meu lado em cada momento dessa difícil jornada, abrindo mão por vezes dos próprios sonhos e desejos em prol desta conquista.

Ao meu orientador, Prof. Dr. José Teixeira Freire, pela amizade, pelo carinho, pela dedicação e pelos ensinamentos. Ensinamentos esses que colaboram continuamente para meu crescimento profissional e pessoal.

Aos meus coorientadores, Prof. Dr. Rodrigo Béttega e Prof. Dr. Martin Olazar, por toda atenção, carinho, confiança, dedicação, incentivo, paciência e todo tipo de apoio que me foi dado. Agradeço aos demais professores do Centro de Secagem, que sempre contribuem e dedicam-se diariamente à formação de pessoas, em especial ao Prof. Dr. Fábio Freire, Prof.ª Dra. Maria do Carmo e Prof. Dr. Thiago Faggion.

Aos técnicos do Centro de Secagem Edilson, Oscar e Samuel, pela disposição e ajuda constante. Agradeço também ao Prof. Dr. Victor Forti e Marina Zacharias por todas contribuições.

Aos amigos do Centro de Secagem e do doutorado, pela amizade, contribuições e inúmeros momentos de alegria. Agradeço também aos meus amigos de Bilbao, Mikel Tellabide e Idoia Estiati, por todo carinho, amizade e companheirismo.

À CAPES e ao CNPq pelo apoio financeiro.

Por fim, agradeço à FAPESP (Processos 2017/01856-7 e 2018/22655-2) pelo apoio financeiro e confiança no desenvolvimento desta tese.

TABLE OF CONTENTS

LIST OF FIGURES

CHAPTER 2

CHAPTER 3

CHAPTER 4

CHAPTER 5

CHAPTER 6

CHAPTER 7

CHAPTER 8

LIST OF TABLES

CHAPTER 8

ABSTRACT

The conventional spouted bed has presented several limitations that restrict the use on an industrial scale. Thus, studies of different methodologies and configurations have been performed to overcome such limitations. Limited processing capacity (scaling-up) and energy issues are some of the main problems considered from an industrial point of view. Alternatives as a heat recovery system lost in the exhaust air, intermittent drying, and draft tube can be promising and have not been explored in the spouted bed. Therefore, the main objective of this Ph.D. thesis is to design a spouted bed with a heat recovery system lost in the exhaust air, coupling the methodology of the intermittency and the use of the draft tube. Two types of intermittency (reduction and total interruption of the air flow) and five different intermittency profiles have been evaluated, including the use of time-variant intermittency ratios. Alumina, soybean, and barley have been used as particulate materials. Regarding the internal devices, three different configurations have been employed: without, nonporous, and open-sided. Based on particle image velocimetry (PTV), a new draft tube is designed for the equipment proposed, i.e., a spouted bed with a heat recovery system built according to the results obtained and the design criteria of our research group. Thus, the current Ph.D. thesis contributed to obtain energy-efficient equipment with suitable and feasible characteristics for industrial applications.

Keywords: Spouted bed; Intermittent drying; Energy efficiency; Energy consumption; Draft tube.

RESUMO

Apesar de suas vantagens, o leito de jorro tem apresentado diversas limitações que impedem sua aplicação em escala industrial e vem motivando o estudo de diferentes configurações e metodologias. Como principais problemas do ponto de vista industrial, destaca-se as restrições na capacidade de processamento e as questões energéticas do equipamento, que lhe atribuem uma baixa eficiência e alto consumo energético. Para contornar os problemas descritos, a utilização do tubo draft, de um sistema de recuperação do calor perdido no ar de exaustão e a metodologia da intermitência constituem alternativas que não têm sido exploradas no leito de jorro e combinadas podem representar uma solução promissora para a aplicação do equipamento no setor industrial. Deste modo, o objetivo da presente tese foi avaliar a metodologia intermitente e a inserção de tubos draft em leito de jorro para o processamento de sólidos particulados, visando a aplicação em leito de jorro com sistema de recuperação de calor do ar de exaustão. Dois tipos de intermitência (redução e interrupção total da vazão de ar) e cinco diferentes razões de intermitência foram avaliados, incluindo a razão de intermitência variável. Alumina, soja e cevada foram os materiais particulados utilizados para a análise da intermitência e design dos tubos draft. Em relação aos tubos, três diferentes configurações foram utilizadas: tubos sólidos, com as laterais abertas e sem tubos. Baseando-se em uma técnica de rastreamento de partículas (*Particle tracking velocimetry – PTV*), um novo critério de design foi proposto para o desenvolvimento de tubos draft. Deste modo, os resultados obtidos na presente tese contribuíram para obtenção de um equipamento energeticamente eficiente com características viáveis e adequadas para aplicações industriais.

PALAVRAS-CHAVE: Leito de jorro; Intermitência; Eficiência energética; Consumo energético; Tudo *draft*.

CHAPTER 1 - INTRODUCTION

Among the different equipment and methods currently available to perform the drying process, the spouted bed has been stood out for providing high rates of heat and mass transfer due to the high degree of mixture between phases and solid recirculation in the bed. Thus, the spouted bed has been employed in a wide variety of chemical and physical processes, such as drying of solids, pastes, and solutions (BARROS; FERREIRA; FREIRE, 2019; ESTIATI et al., 2019; SOUSA et al., 2019; VIEIRA et al., 2018), coating (ALI; AL-JUWAYA; AL-DAHHAN, 2017; LIU et al., 2020; PIETSCH et al., 2019), pyrolysis (AZIZI et al., 2020; LOPEZ et al., 2019; SANTAMARIA et al., 2020), feeding (MASSARO SOUSA et al., 2020; MASSARO SOUSA; FERREIRA, 2020), etc.

Despite these advantages, several difficulties restrict the spouted bed application on an industrial scale and the processing of large amounts of material. The energy issues inherent to convective dryers and the existence of a maximum spoutable bed height are some of such difficulties. Besides, the conventional spouted bed has a crucial parameter that limits scaling up, which is the ratio between the inlet diameter and particle diameter. The inlet diameter should be smaller than 20–30 times the average particle diameter to reach spouting status (EPSTEIN, 2011; MATHUR; EPSTEIN, 1974; OLAZAR; SAN JOSÉ; BILBAO, 2011).

Besides the energy inefficiency, which is observed in most convective dryers, spouted bed requires a large amount of mechanical energy to break the packed bed and to maintain the spouting stable regime (BRITO et al., 2017). Furthermore, the residence time of air flow in the spout is negligible when compared to the annulus region, thus providing an inefficient air utilization because most of the air supplied to the system flows through the spout region. Accordingly, most

of the air supplied in the spouted bed is wasted in the air exhaust system and its energy and drying potential are not effectively employed in the process (BECKER; SALLANS, 1961; CORRÊA; FREIRE; CORRÊA, 2009).

Several designs, configurations, and processing methodologies have been proposed to overcome such limitations and disadvantages, providing suitable and advantageous equipment, especially for industrial applications. The recovery of heat lost in the exhaust air and the intermittent drying are some promising alternatives for application in the spouted bed, mainly considering the energy issues. Besides the energy potential, the exhaust air in the spouted bed also has a high potential for removal of moisture since the air drying is often not completely saturated, mainly due to the short residence time mentioned above. Therefore, the recovery of heat loss in the exhaust air is one of the most attractive methods for reducing energy consumption and providing better utilization of the air during the drying process (KEMP, 2014; KROKIDA; BISHARAT, 2004; STRUMILLO; KUDRA, 1987).

The intermittent drying consists of alternating between active and passive drying periods (CHUA; MUJUMDAR; CHOU, 2003; KUMAR; KARIM; JOARDDER, 2014). This methodology can be incorporated into the process by periodically changing the drying operating conditions, such as inlet air temperature and air flow. In addition to the benefits related to the energy cost, intermittency can also be advantageous in terms of product quality (FILIPPIN et al., 2018; ZHU; YANG; WANG, 2016). When applied in the spouted bed, the advantages and characteristics of the fixed bed could also be harnessed with the application of intermittent drying changing the air flow (KUMAR; KARIM; JOARDDER, 2014; LIMA et al., 2015).

Regarding the limitations related to the scaling up and processing of large amounts of material, the use of a draft tube is a common and promising alternative (ALTZIBAR et al., 2009;

OLAZAR et al., 2012). These internal devices also may influence and be significant in the intermittent drying due to the impact on the air percolation in the bed. In this sense, some studies have evaluated the effect of the draft tube on the air flow through the bed. Makibar et al. (2012) have observed the deviation of the air flow through the outside of the tube for tube diameters smaller than the spout diameter, except when the air flow was rapidly increased. Stable spouting has been obtained for any flow rate increasing ramp for tube diameters larger than the spout. Besides the intermittent drying, the diameter of the tube can affect the heat loss in the exhaust air because this factor plays a crucial role in the residence time. As previously mentioned, the residence time of air flow in the spout is shorter than annulus, providing a low utilization of the energy and drying potential of the air.

As well as the intermittency and the heat recovery system, the draft tube may also be important for energy and quality issues. Concerning the energy issues, the draft tube provides a smaller minimum spouting velocity and operating pressure drop than the conventional configuration (ALTZIBAR et al., 2013, 2014; OLAZAR et al., 2012). Both parameters affect significantly the energy performance of the equipment. Regarding the quality issues, both type and geometry factors of the draft tube play a critical role in the particle cycle times and solid circulation rates. According to Makibar et al. (2012), a suitable control of solid circulation is mandatory for the operation with heat-sensitive materials.

1.1 OBJECTIVES

Given the above background, the main aims of this thesis are to evaluate the intermittent methodology and the draft tube insertion in spouted beds for the processing of particulate solids,

aiming the application in a spouted bed with a heat recovery system. For this purpose, the following specific objectives are required:

1) Design and development of a spouted bed with a heat recovery system.
2) Analysis of the intermittent methodology in spouted beds considering both energy and quality aspects.
3) Mathematical modelling of the intermittent drying in spouted beds.
4) Hydrodynamic analysis of spouted bed with different types of draft tubes.
5) Analysis of the drying of particulate solids in draft tube spouted beds.
6) Proposing of a new design criterion for the development of draft tubes to be used in spouted beds.

1.2 THESIS STRUCTURE

Given the above objectives described, a structure based on the journal papers written is adopted for this thesis to provide a clear understanding concerning the development of this work. Consequently, chapters can be read independently and some overlap may be found between them. Thus, in addition to the introduction chapter (Chapter 1) described above, this thesis is structured in 9 chapters. Chapter 2 presents a summary of the main results obtained in this thesis. Chapters 3 and 4 are focused on intermittency analysis, which deals with the energy and quality aspects of the intermittent drying, respectively. Chapter 5 describes the mathematical modelling proposed for intermittent drying in a conical spouted bed. Chapters 6, 7, and 8 provide the studies related to the design and development of the draft tubes for the spouted bed. Chapter 6 describes the hydrodynamic study of a conical spouted bed with conventional draft tubes, which is based on the

application of pressure fluctuation analysis for the estimation of the minimum spouting velocity. Chapter 7 presents the energy analysis of the drying of particulate materials in a draft tube spouted bed. Chapter 8 presents the design and development of a new draft tube using particle tracking velocimetry (PTV). Finally, Chapter 9 describes the final considerations obtained in this thesis and some recommendations and outlook for future work are discussed.

REFERENCES

ALI, N.; AL-JUWAYA, T.; AL-DAHHAN, M. An advanced evaluation of spouted beds scale-up for coating TRISO nuclear fuel particles using Radioactive Particle Tracking (RPT). **Experimental Thermal and Fluid Science**, v. 80, p. 90–104, jan. 2017.

ALTZIBAR, H. et al. Hydrodynamics of conical spouted beds using different types of internal devices. **Chemical Engineering and Technology**, v. 32, n. 3, p. 463–469, 2009.

ALTZIBAR, H. et al. Minimum Spouting Velocity of Conical Spouted Beds Equipped with Draft Tubes of Different Configuration. **Industrial & Engineering Chemistry Research**, v. 52, p. 2995–3006, 27 fev. 2013.

ALTZIBAR, H. et al. Operating and peak pressure drops in conical spouted beds equipped with draft tubes of different configuration. **Industrial and Engineering Chemistry Research**, v. 53, n. 1, p. 415–427, 2014.

AZIZI, K. et al. On the pyrolysis of different microalgae species in a conical spouted bed reactor: Bio-fuel yields and characterization. **Bioresource Technology**, v. 311, n. April, 2020.

BARROS, J. P. A. A.; FERREIRA, M. C.; FREIRE, J. T. Spouted bed drying on inert particles: Evaluation of particle size distribution of recovered, accumulated and elutriated powders. **Drying**

Technology, v. 0, n. 0, p. 1–12, 2019.

BECKER, H. A.; SALLANS, H. R. Drying wheat in a spouted bed. **Chemical Engineering Science**, v. 18, n. 3, p. 97–112, 1961.

CHUA, K. J.; MUJUMDAR, A. S.; CHOU, S. K. Intermittent drying of bioproducts - An overview. **Bioresource Technology**, v. 90, n. 3, p. 285–295, 2003.

CORRÊA, N. A.; FREIRE, F. B.; CORRÊA, R. G. Controle do Processo de Secagem em Leito de Jorro. In: FREIRE, J. T.; SILVEIRA, A. M. (Eds.). . **Fenômenos de Transporte em Sistemas Particulados: Fundamentos e Aplicações**. São Carlos: Suprema, 2009. p. 237–272.

DE BRITO, R. C. et al. Effect of mechanical energy on the energy efficiency of spouted beds applied on drying of sorghum [Sorghum bicolor (L) moench]. **Chemical Engineering and Processing: Process Intensification**, v. 117, p. 95–105, jul. 2017.

EPSTEIN, N. Empirical and analytical hydrodynamics. In: EPSTEIN, N.; GRACE, J. R. (Eds.). . **Spouted and Spout-Fluid Beds: Fundamentals and Applications**. First ed. New York: Cambridge University Press, 2011. p. 340.

ESTIATI, I. et al. Influence of the fountain confiner in a conical spouted bed dryer. **Powder Technology**, v. 356, p. 193–199, 2019.

FILIPPIN, A. P. et al. Thermal intermittent drying of apples and its effects on energy consumption. **Drying Technology**, p. 1–16, 2018.

KEMP, I. C. Fundamentals of Energy Analysis of Dryers. **Modern Drying Technology**, v. 4–4, p. 1–45, 2014.

KROKIDA, M. K.; BISHARAT, G. I. Heat Recovery from Dryer Exhaust Air. **Drying Technology**, v. 22, n. 7, p. 1661–1674, 2004.

KUMAR, C.; KARIM, M. A.; JOARDDER, M. U. H. H. Intermittent drying of food products: A

critical review. **Journal of Food Engineering**, v. 121, n. 1, p. 48–57, 2014.

LIU, M. et al. Scale-up strategy study of coating furnace for TRISO particle fabrication based on numerical simulations. **Nuclear Engineering and Design**, v. 357, p. 110413, 2020.

LOPEZ, G. et al. Kinetic modeling and experimental validation of biomass fast pyrolysis in a conical spouted bed reactor. **Chemical Engineering Journal**, v. 373, p. 677–686, 2019.

MAKIBAR, J. et al. Pilot scale conical spouted bed pyrolysis reactor: Draft tube selection and hydrodynamic performance. **Powder Technology**, v. 219, p. 49–58, 2012.

MASSARO SOUSA, L. et al. Feeding spent coffee grounds into reactors: TFM simulation of a non-mechanical spouted bed type feeder. **Waste Management**, v. 109, p. 161–170, 2020.

MASSARO SOUSA, L.; FERREIRA, M. C. On the performance of a spouted bed type device for feeding spent coffee grounds to a circulating fluidized bed reactor. **Chemical Engineering Research and Design**, v. 160, p. 31–38, 2020.

MATHUR, K. B.; EPSTEIN, N. **Spouted Beds**. New York: Academic Press, 1974.

OLAZAR, M. et al. Drying of Biomass in a Conical Spouted Bed with Different Types of Internal Devices. **Drying Technology**, v. 30, n. 2, p. 207–216, 2012.

OLAZAR, M.; SAN JOSÉ, M. J.; BILBAO, J. Conical spouted beds. In: EPSTEIN, N.; GRACE, J. R. (Eds.). . **Spouted and Spout-Fluid Beds: Fundamentals and Applications**. First ed. New York: Cambridge University Press, 2011. p. 340.

PIETSCH, S. et al. Measurement of granule layer thickness in a spouted bed coating process via optical coherence tomography. **Powder Technology**, v. 356, p. 139–147, 2019.

SANTAMARIA, L. et al. Effect of La2O3 promotion on a Ni/Al2O3 catalyst for H2 production in the in-line biomass pyrolysis-reforming. **Fuel**, v. 262, n. September 2019, p. 116593, 2020.

SOUSA, R. C. et al. Drying of pasty and granular materials in mechanically and conventional

spouted beds. **Particuology**, v. 42, p. 176–183, 2019.

VIEIRA, G. N. A. et al. Real-time monitoring of milk powder moisture content during drying in a spouted bed dryer using a hybrid neural soft sensor. **Drying Technology**, v. 3937, n. 9, p. 1184–1190, 2018.

ZHU, Z.; YANG, Z.; WANG, F. Experimental research on intermittent heat pump drying with constant and time-variant intermittency ratio. **Drying Technology**, v. 34, n. 13, p. 1630–1640, 2 out. 2016.

CHAPTER 2 - SUMMARY OF THESIS RESULTS

The first steps of this research were focused on the development of the equipment and the definition of critical design parameters that play a key role in the dynamic stability of the equipment. Such parameters are related to both geometric factors of the contactor and particulate solid properties. Thus, the following parameters were considered for the equipment design: column diameter (D_c), contactor base diameter (D_i), gas inlet diameter (D_o), contactor angle (γ), static bed height (H_o), and particle diameter (d_p). Thus, based on the main design criteria presented, a prototype of the experimental unit was developed considering standards already established in the Drying Center DEQ/UFSCar. The experimental unit built is schematized in Figure 2.1.

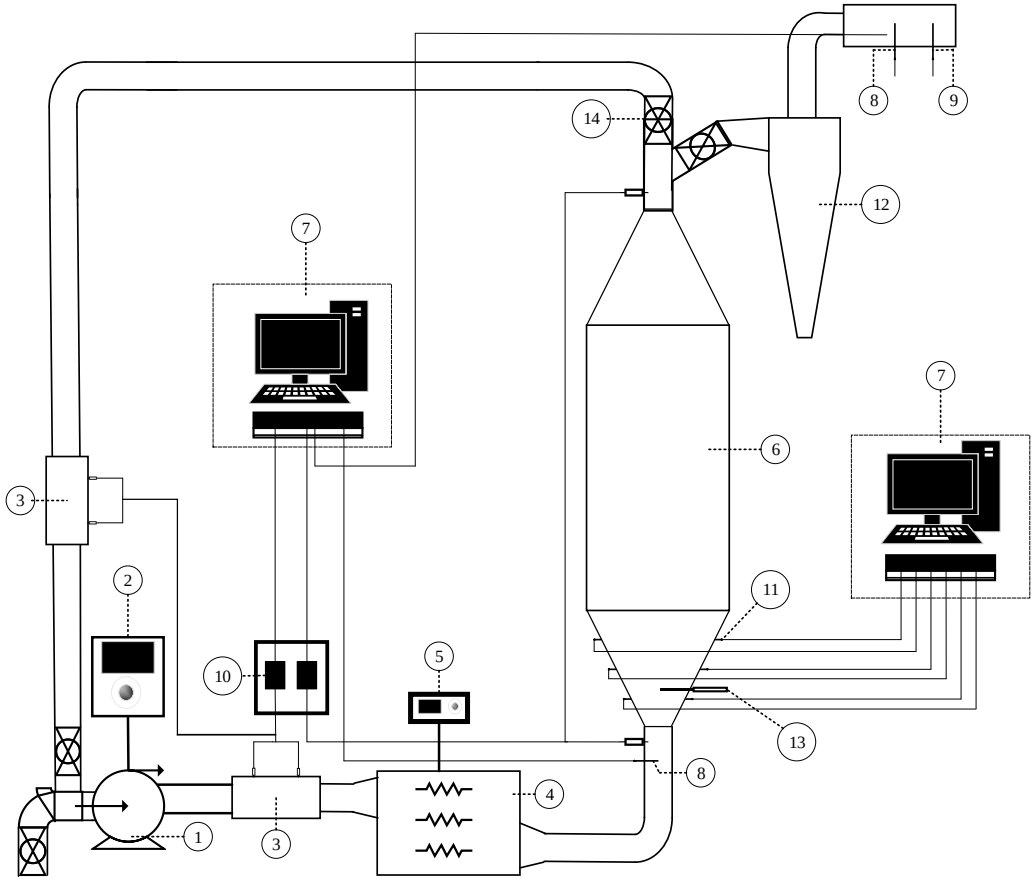

Figure 2.1. Components of the experimental unit used for the drying experiments: (1) blower; (2) frequency inverter; (3) Venturi flow meter; (4) heater; (5) temperature controller; (6) drying chamber; (7) data acquisition system; (8) T type thermocouple; (9) T type wet bulb thermocouple; (10) pressure transducers; (11) K type thermocouple; (12) cyclone; (13) sampler; (14) spherical valves.

Based on the experimental unit developed, a comprehensive analysis of the intermittency has been performed considering both the energy and quality aspects. It is worth mentioning that the next stages of this study were performed in the spouted bed without a heat recovery system. Thus, the results obtained will push forward the knowledge frontier and provide the theoretical basis for further applications in the equipment developed with heat recovery systems.

In the study of intermittent methodology, two types of intermittencies are considered, which consist of periodic reduction (intermittency **A**) and periodic interruption (intermittency **B**) of the air flow. The former attributed to the equipment a "hybrid" regime so that the advantages of the fixed bed configuration could be coupled with the advantages of the spouted bed configuration. This coupling was possible due to the alternating periods under low and high air flows, taking the minimum spouting velocity as a reference. The second type of intermittency allowed the alternating between active and passive drying periods, providing a resting period for the process, which has previously been described as "refreshing effect"(ISHIKURA; NAGASHIMA; IDE, 2003). Such a period provides the decrease of moisture gradients that produce tensile stress at the surface and compressive stress in the interior of the material and, therefore, providing a product with better quality and less effective drying time. Five different intermittency profiles have been evaluated, including the use of time-variant intermittency ratios, and three different particulate materials (alumina, soybean, and barley) have been used for both intermittent methodologies described above.

Energy analysis of intermittent drying was performed with alumina particles and three different parameters were employed to evaluate the energy performance: energy efficiency, specific energy consumption, and exhaust heat loss. Some of the main results are presented in Figures 2.2 and 2.3.

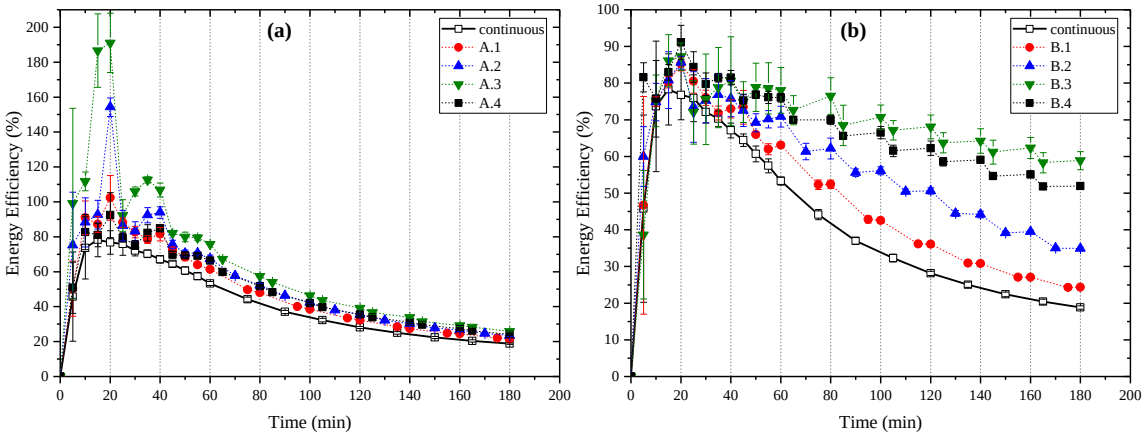

Figure 2.2. Energy efficiency, as a function of time, for the continuous process and the processes performed with (a) periodic decreases (intermittency A) and (b) periodic interruption of the air flow.

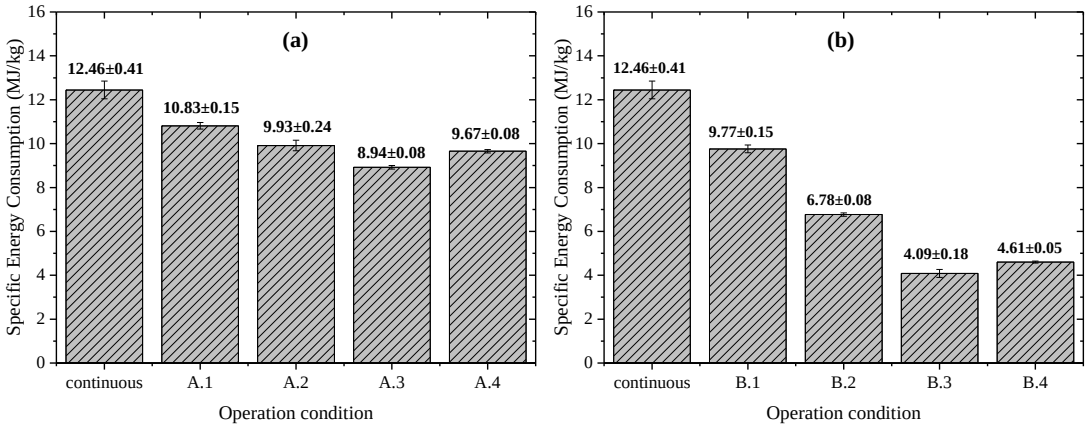

Figure 2.3. Specific energy consumption for the continuous process and the processes performed with (a) periodic decreases (intermittency A) and (b) periodic interruption of the air flow.

As observed, the use of intermittency in spouted beds provided increases in energy efficiency and decreases in specific energy consumption, improving the energy use compared to the conventional process. Reductions of energy consumption in a range from 13,2 to 67,2% were obtained. Overall, the energy results obtained suggest the intermittency methodology as a promising alternative for application in spouted beds. These results have already been published in *Drying Technology* (BRITO; BÉTTEGA; FREIRE, 2019) and are presented later in full in Chapter 3.

The effects of intermittency on product quality were evaluated by physical and physiological quality analysis of intermittent soybean seeds drying in the spouted bed. Mechanical damages and physiological properties were analyzed by tests of germination, first germination count, seedling length, tetrazolium, sodium hypochlorite, and X-ray. These analyses were performed in partnership with the Department of Agro-Industrial Technology and Rural Socioeconomics (DTAiSER/UFSCar), Araras campus e Luiz de Queiroz College of Agriculture (ESALQ/USP). Some of the main results are presented in Figures 2.4 and 2.5.

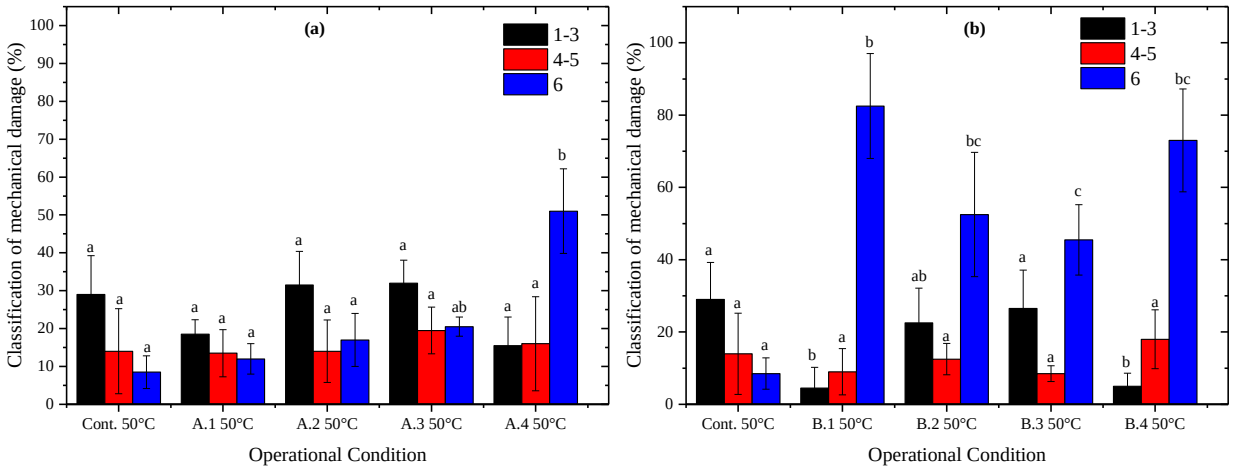

Figure 2.4. Mechanical damage classification of soybean seeds obtained in tetrazolium tests, as a function of intermittent conditions, for (a) the processes with reduction of the air flow (intermittency A) and (b) the processes with interruption of the air flow (intermittency B) at 50°C.

*Means followed by a different letter at a given column are significantly different at p<.05 by Tukey test.

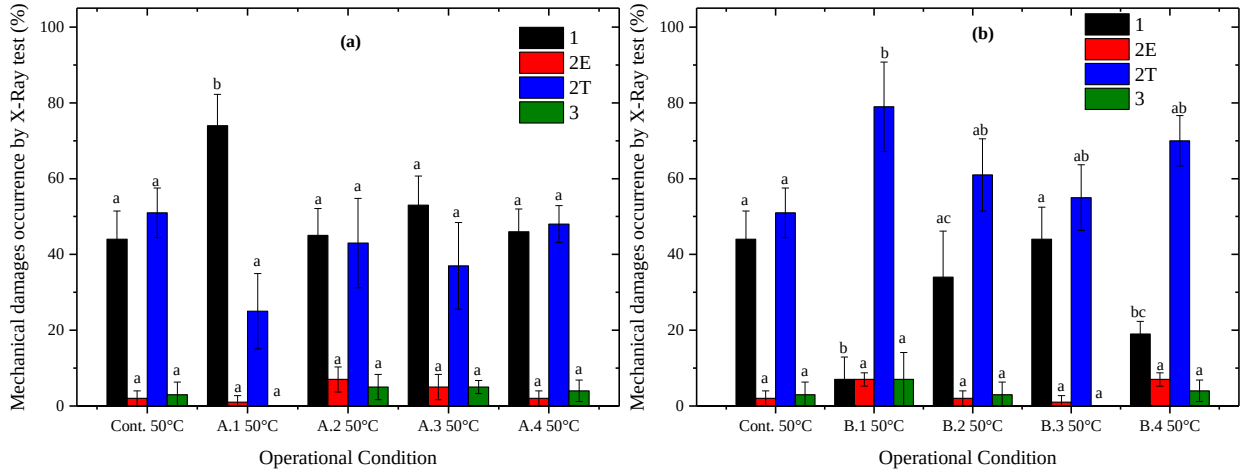

Figure 2.5. Mechanical damage classification of soybean seeds obtained in X-Ray tests, as a function of intermittent conditions, for (a) the processes with reduction of the air flow (intermittency A) and (b) the processes with interruption of the air flow (intermittency B) at 50°C.

*Means followed by a different letter at a given column are significantly different at p<.05 by Tukey test. *1 = intact seeds; 2E = non-severe damage to the embryo; 2T = non-severe damage to the tegument; 3 = severe damage.

According to the quality results obtained, most of the mechanical damages observed in the continuous processes due to the high degree of agitation were not as harmful to physiological properties as heating damages. Likewise, mechanical damages caused by intermittency with periodic interruption of the air flow were more harmful to physiological properties than damages caused by intermittency with periodic reductions. Finally, the findings of this quality study indicated a distinct trend of intermittency application in the spouted bed compared to other dryers when seed quality attributes are demanded, mainly due to the gas-solid flow pattern. These quality results have already been published in *Drying Technology* (BRITO et al., 2021) and are also presented in full later in Chapter 4.

Based on the results obtained in energy and quality analysis, a fully predictive mathematical model for intermittent drying in a conical spouted bed was proposed. Accordingly, soybeans particles have been used due to their healthy nutrients and wide application in the animal feed and the human food industry. Thus, a single-phase model is proposed for a single particle, and then, the assumptions usually adopted in spouted bed systems to represent the whole bed are evaluated in both continuous and intermittent processes. Figure 2.6 presents some of the predictions obtained with the model proposed.

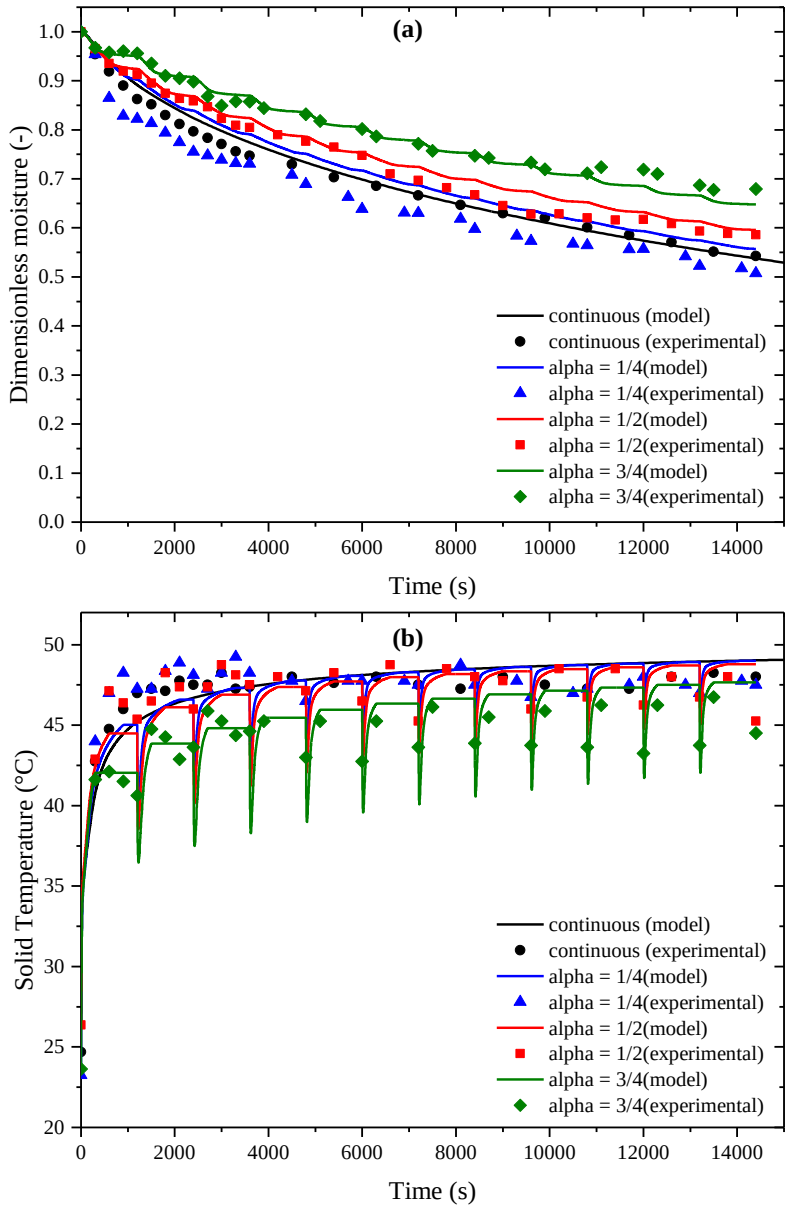

Figure 2.6. (a) Dimensionless moisture and (b) average solid temperature (predicted and measured experimentally), as a function of drying time, for intermittent drying conditions at 50 °C.

Good agreement between predicted and experimental results were obtained for continuous drying under moderate air temperature, as well as for intermittent drying with medium and long resting periods. Poor predictions were obtained for high air temperatures and short resting periods, mainly due to heat loss and particle-particle interactions. Therefore, the assumptions adopted are less accurate for such conditions in the spouted bed, and, thereby, different terms should be implemented in the model. Nevertheless, the model employed provides predictions physically consistent of the internal gradients of moisture and temperature, which are essential results in the intermittent drying for product quality and energy optimization. A full description of the proposed model and the results obtained are presented in Chapter 5.

After obtaining the intermittent results described above, the next steps of this thesis were focused on the draft tube design. As previously mentioned, these internal devices are promising alternatives to overcome the limitations related to the scaling up and processing of large amounts of material, which are fundamental aspects in the development of industrially feasible and advantageous equipment. All stages of draft tube design were performed at the Department of Chemical Engineering of the University of the Basque Country (UPV/EHU), Bilbao/ESP, during the international research internship (BEPE/FAPESP).

Firstly, the hydrodynamic analysis of spouted beds with different types of draft tubes was performed. Thus, the conventional draft tubes were evaluated and three different configurations related to the draft tubes were used: nonporous tubes, open-sided tubes, and without draft tubes. Besides the hydrodynamic characterization usually performed in spouted beds, which is based on the characteristic curves (pressure drop vs. air velocity), the analysis of pressure fluctuation signals (PFS) and spectral analysis (Power Spectral Density, PSD) were also used for a comprehensive hydrodynamic analysis. In addition to the particulate materials used in the study of intermittent

drying (alumina, soybean, and barley), other materials commonly used by the UPV/EHU research group were also included in the hydrodynamic analysis, such as sand and glass beads. Figure 2.7 presents some of the main results obtained.

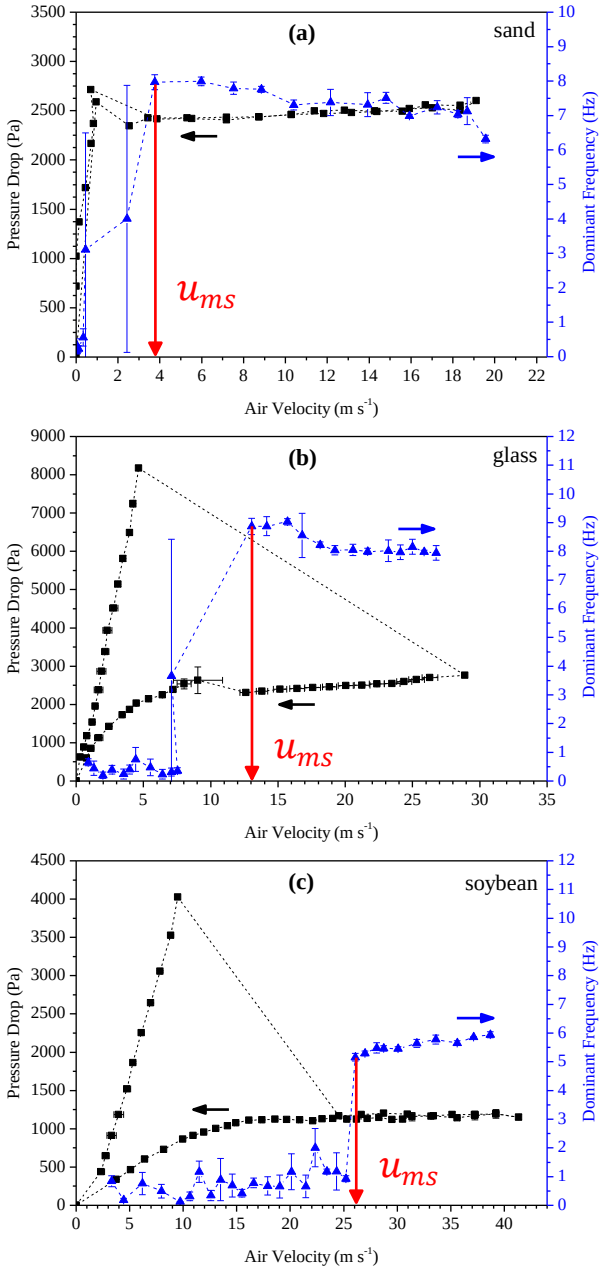

Figure 2.7. Evolution of pressure drop and dominant frequency with air velocity for the systems without draft tube and beds of (a) sand, (b) glass beads, and (c) soybeans.

As observed in Figure 2.7, the methodology proposed based on both hydrodynamic and spectral analyses allows estimating the minimum spouting velocity. Such methodology was also suitable for draft tube configurations, especially those characterized by pulsating spouting regimes. The results presented in Figure 2.7, jointly with the other results obtained for all configurations evaluated and discussed, are presented in full in Chapter 6. These results have already been published in *Journal of the Taiwan Institute of Chemical Engineers* (BRITO et al., 2020).

Based on the hydrodynamic results obtained, the drying and energy performance of draft tubes in spouted beds were evaluated for the processing of particulate materials. Thus, drying of alumina, soybean, and barley were performed with three different configurations: without tube and with nonporous and open-sided tubes. Energy Efficiency, Drying Efficiency, and Specific Energy Consumption were the parameters considered for energy analysis. Some of the main results obtained are presented in Figure 2.8.

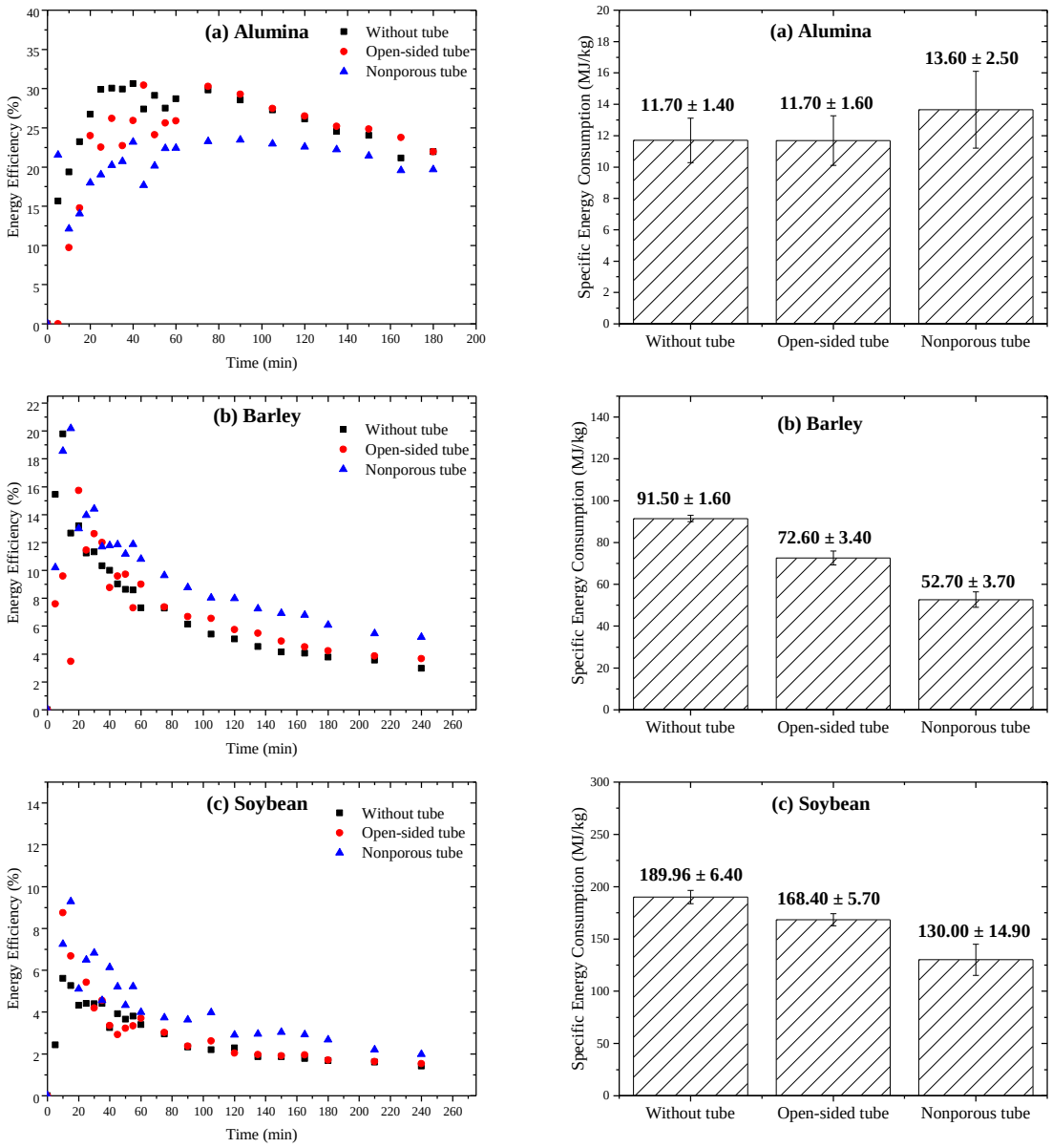

Figure 2.8. Evolution of energy efficiency with time and specific energy consumption for the processes without draft tube and with nonporous and open-sided ones: (a) alumina beads, (b) barley, and (c) soybean.

As observed in Figure 2.8, the open-sided draft tube provided the best energy utilization in the processing of alumina particles, due to the better stability, control, and advantages related to

scaling-up of this internal device when compared to the configuration without draft tube. Nonporous tubes provided the best energy performance in the processing of barley and soybean. Such results implied that the improvement in energy performance provided by draft tubes in spouted bed is highly dependent on the air percolation and particulate material to be dried. Nevertheless, the findings obtained in this study contribute to support the draft tubes as promising devices for improving energy issues in spouted beds, mainly in the processing of low moisture materials. The full description and discussion of all the results obtained are presented in Chapter 7. Such results have already been published in *Powder Technology* (BRITO et al., 2021).

The hydrodynamic and drying results obtained were key findings for the development of a new criterion for the design of draft tubes (nonporous and open-sided). The methodology proposed was based on the average spout diameter measured by a borescopic technique in conical spouted beds without draft tube. The technique employed enabled the capture of particle velocity (*particle tracking velocimetry – PTV*) inside the spouted bed by an image processing algorithm developed in Matlab® 2017b, which is schematized in Figure 2.9.

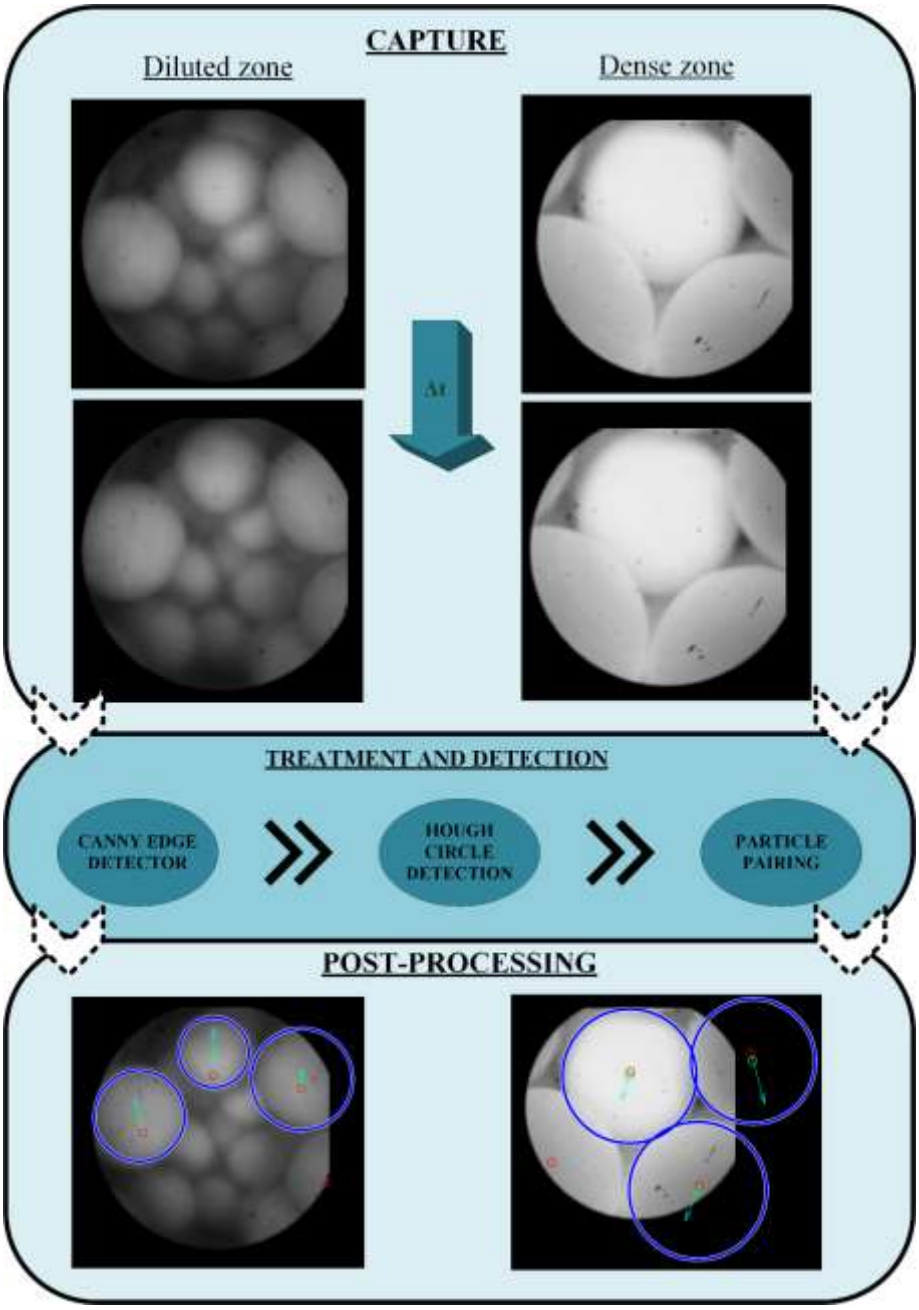

Figure 2.9. Schematic representation of the methodology used for the particle velocity estimation.

Thus, the assumption of the vertical solid displacement as the main velocity component in all regions in the spouted bed was adopted and the spout limits were determined based on the points where particle movement changes from upward to downward. Finally, the new draft tubes

based on the equivalent spout diameter of the configuration without draft tube was designed and built, as shown in Figure 2.10.

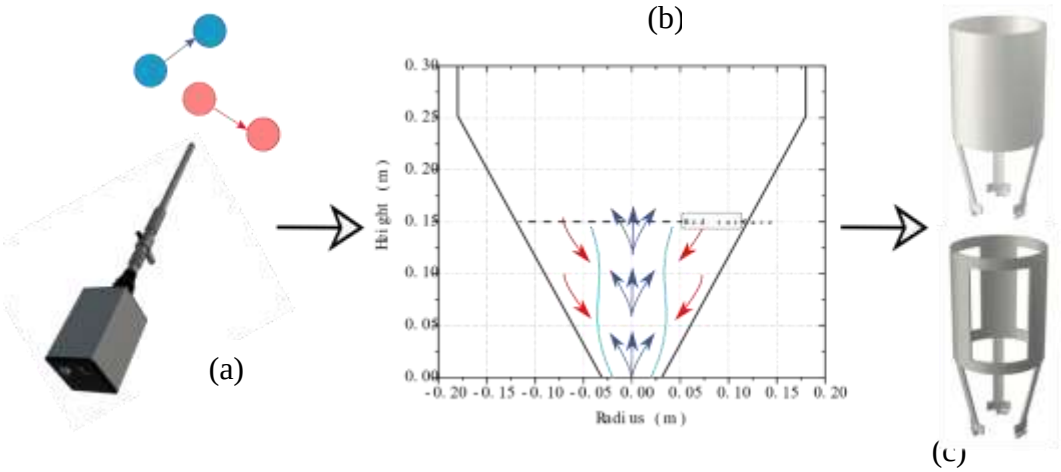

Figure 2.10. Schematic figure of the proposed methodology for design of draft tubes: (a) borescope, (b) delimitation of the spout-annulus interface, and (c) new draft tubes.

The conventional draft tubes are usually designed based on gas inlet diameter, whereas the new draft tubes were developed based on the average spout diameter. Therefore, the new draft tubes, especially the open-sided one, provided a more efficient gas-solid contact than any conventional one, as it increases the spout volume, as well as the contact time in this zone. Furthermore, the new open-sided tube presented an interesting hydrodynamic similarity with the configuration without tube, which was evidenced by both the spout geometry and hydrodynamic parameters (differences in the range from 2% to 6%). These findings are fundamental when the scaling up aspects are considered for any industrial applications. The full description and discussion of these results are presented in Chapter 8. Such results have already been published in *Advanced Powder Technology* (de BRITO et al., 2021b).

REFERENCES

BRITO, R. C. et al. Physical and physiological quality of intermittent soybean seeds drying in the spouted bed. **Drying Technology**, v. 39, n. 6, p. 820–833, 31 mar. 2021.

BRITO, R. C.; BÉTTEGA, R.; FREIRE, J. T. Energy analysis of intermittent drying in the spouted bed. **Drying Technology**, v. 37, n. 12, p. 1498–1510, 10 set. 2019.

DE BRITO, R. C. et al. Estimation of the minimum spouting velocity based on pressure fluctuation analysis. **Journal of the Taiwan Institute of Chemical Engineers**, v. 113, p. 56–65, ago. 2020.

DE BRITO, R. C. et al. Drying of particulate materials in draft tube conical spouted beds: Energy analysis. **Powder Technology**, v. 388, p. 110–121, ago. 2021a.

DE BRITO, R. C. et al. Draft tube design based on a borescopic technique in conical spouted beds. **Advanced Powder Technology**, n. xxxx, out. 2021b.

ISHIKURA, T.; NAGASHIMA, H.; IDE, M. Hydrodynamics of a spouted bed with a porous draft tube containing a small amount of finer particles. **Powder Technology**, v. 131, n. 1, p. 56–65, 2003.

CHAPTER 3

ENERGY ANALYSIS OF INTERMITTENT DRYING

This chapter describes the analysis of the intermittent methodology in spouted beds considering energy aspects, which refers to specific objective (2) of this thesis. Thus, the paper described in this chapter aimed to evaluate different intermittency ratios applied to a spouted bed used to dry alumina, from the energy perspective. Two types of intermittencies (reduction and total interruption of the air flow) and five different intermittency profiles were evaluated, including the use of time-variant intermittency ratios. The use of intermittency provided higher energy efficiency and better use of the energy supplied, compared to the continuous process. Reductions of energy consumption in the range from 13.2% to 67.2% were obtained, relative to the continuous process. The findings showed that the use of intermittency is a promising way to optimize energy consumption in spouted beds.

This chapter is based on:

R. C. Brito, R. Béttega & J. T. Freire (2019) Energy analysis of intermittent drying in the spouted bed, Drying Technology, 37:12, 1498-1510, DOI: 10.1080/07373937.2018.1512503.

3.1 INTRODUCTION

Drying is one of the oldest and most important ways to preserve and store different kinds of materials. Used in numerous industrial sectors and processing operations, the drying process reduces the moisture content of the material to suitable levels, retarding and avoiding biological activity and deterioration. In addition to biological materials, drying also plays an important role in the processing of other kind of materials, such as alumina (Al_2O_3), which is a material widely employed in industry [1]. Industrial applications of alumina include its use as a catalyst, catalyst support, adsorbent, and template for the fabrication of nanomaterials [1–4]. When used as a catalyst support, drying of alumina is essential to ensure satisfactory mechanical strength of the final product [5]. However, drying is highly energy intensive and may account for about 27 - 70% of the total energy use in industries, depending on the product manufactured [6]. The latent heat required for removal of water, together with inefficient air-to-material heat transfer and significant loss of energy, are among the factors that contribute to this energy demand. This is especially the case for convective dryers, which account for about 85% of all industrial dryers [7].

Such energy issues inherent in the drying process clearly indicate the need to develop novel technologies and to identify ways of using energy that are more efficient. New drying technologies can provide significant improvements in terms of energy use, but these alternatives often involve high investment and operating costs. Considering these issues, the use of intermittency during drying appears to offer a promising methodology that could help to resolve energy issues. The intermittency method consists of alternating periods of drying and reduction/interruption of the process [8,9]. Intermittency can be incorporated into a process by periodically changing the drying operating conditions, such as inlet air temperature and air flow. In addition to the benefits related to the cost of

energy, intermittency can also be advantageous in terms of product quality. Filippin et al. [10] used thermal intermittency in the drying of apples and evaluated the effects on product quality and energy consumption. The application of thermal intermittency provided energy savings of up to 17%, while maintaining certain quality parameters, such as color and chlorogenic acid retention. Zhu et al. [11] performed intermittent heat pump drying of green soybean seeds, using constant and time-variant intermittency ratios. In addition to energy advantages, the intermittent drying provided a better drying rate, with the use of time-variant intermittency ratios being most suitable for the drying of green soybean.

Despite its advantages, few studies have employed intermittency in spouted bed technology. The spouted bed offers important advantages and properties, especially in the processing of particulate materials [12,13], since it can provide high degrees of agitation and mixing between the phases [14,15]. Oliveira and Rocha [16] described the intermittent drying of beans in a spouted bed and found that intermittency was a promising technique for the drying of beans and grains in general, due to the gain in energy efficiency. Bon and Kudra [17] analyzed several optimization problems relevant to intermittent drying, using process simulations of the batch drying of corn in a rotating jet spouted bed (RJSB), an example of intermittent drying related to the dryer design. The authors reported several advantages of intermittent drying over continuous drying and developed a tool to resolve each optimization problem analyzed. In addition to energy-related aspects, the advantages and characteristics of the fixed bed could also be harnessed with application of intermittent drying in a spouted bed. Hence, due to the potential of intermittent drying in the spouted bed, together with the lack of evaluation of the influence of the intermittency ratio or of the energy efficiency profile over time in this configuration, further studies are required in order to obtain a better understanding of this methodology.

Therefore, the objective of this work was to analyze the application of intermittency and the use of different intermittency ratios in the spouted bed, from the energy point of view. For this purpose, an experimental study of the intermittent drying of alumina in a spouted bed was performed. Five different intermittency profiles were evaluated, defined based on four constant intermittency ratios and one time-variant intermittency ratio. Two different types of intermittency were applied, using periods of reduction or total interruption of the air flow.

3.2 MATERIALS AND METHODS

3.2.1 Materials and Equipment

All the different operating conditions employed 2 kg of activated F-200 alumina particles (mean diameter of 3.42 mm). For both intermittent and continuous processes, the alumina particles were saturated with water for 24 h before each drying process. The equipment used is shown in Figure 3.1.

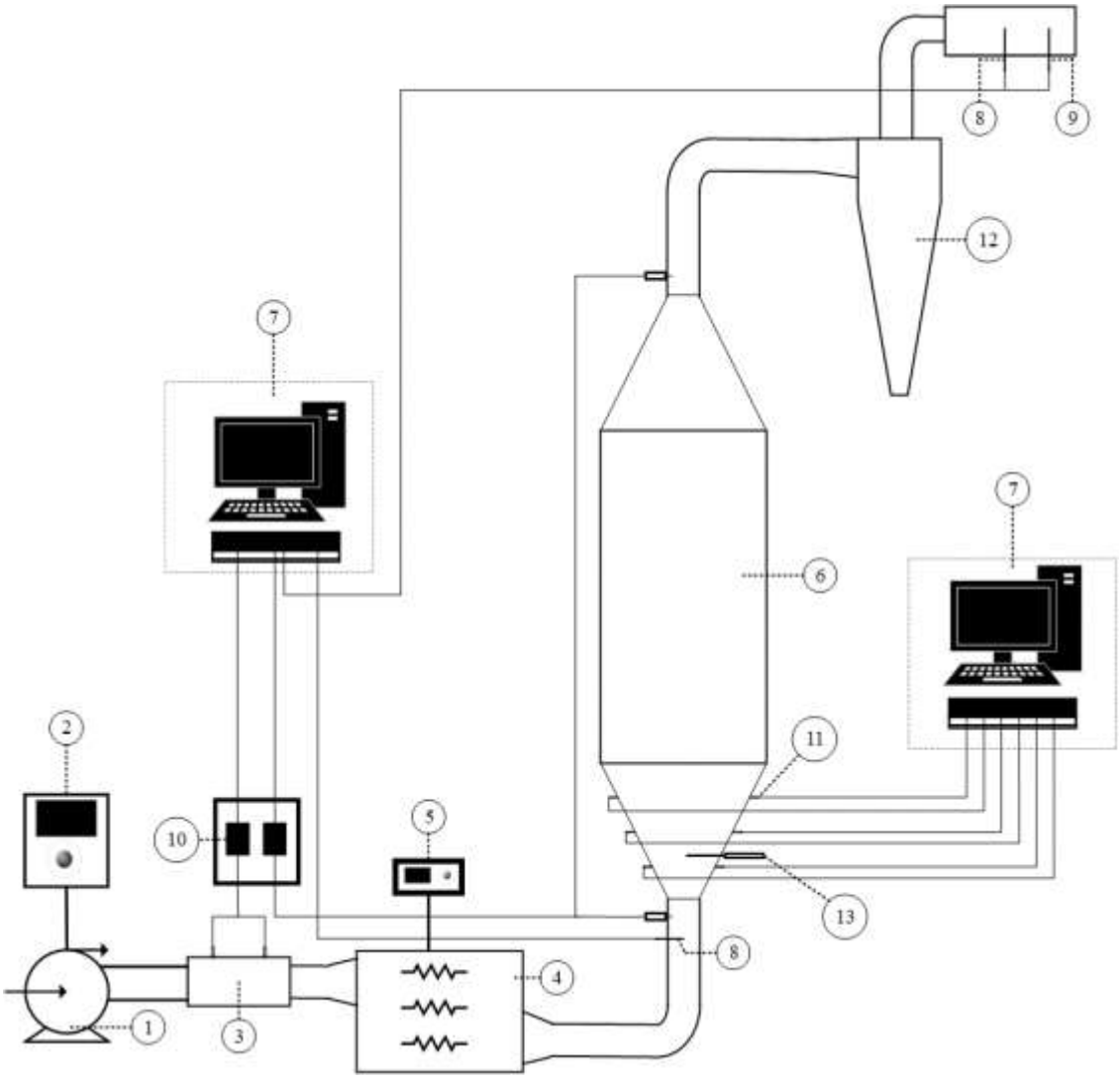

Figure 3.1. Components of the experimental unit used for the drying experiments: (1) blower; (2) frequency inverter; (3) Venturi flow meter; (4) heater; (5) temperature controller; (6) drying chamber; (7) data acquisition system; (8) T type thermocouple; (9) T type wet bulb thermocouple; (10) pressure transducers; (11) K type thermocouple; (12) cyclone; (13) sampler.

The air was supplied by a 7.5 HP blower (1) controlled by a frequency inverter (2). A Venturi meter (3) was employed to measure the air flow. The air was heated by an electric heater (4) with three resistances that were controlled by a temperature controller (5). The drying chamber (6) consisted of

a cylindrical stainless steel vessel (60 cm height, 30 cm diameter) with identical 60° conical sections (23 cm height) at the top and bottom. The data acquisition system (7) was composed of two acquisition boards. One board was used to acquire the inlet and outlet drying air temperatures, as well as the pressures at the Venturi meter and in the drying chamber. The air temperatures were measured with T type thermocouples (8) positioned in the inlet and outlet of the drying chamber. A T type thermocouple covered with a wet bulb (9) was also located in the outlet. Pressure transducers (10) were employed to measure the pressure. Another board was used to acquire temperature data for the walls of the conical region. Six K type thermocouples (11) were used, which were evenly distributed in the conical region in order to obtain the average temperature in this area. For both acquisition boards, the data were acquired at intervals of 3 s. A dust collection cyclone (12) was positioned in the outlet. A sampler (13) was placed in the conical region, at 7 cm from the inlet nozzle.

3.2.2 Experimental procedure

Two intermittency protocols (A and B) were employed to evaluate the advantages of intermittent drying in the spouted bed. Intermittency A consisted of periodic reductions of the air flow to values lower than the minimum spouting air flow (u_{mj} = 24.93 ± 0.08 m s^{-1}), which was obtained previously from fluid dynamics characterization, according to the methodology described by Mathur and Epstein [14]. Intermittency B consisted of periodic interruptions of the air flow. The intermittency intervals were based on cycles and on a parameter known as the intermittency ratio (α). Each cycle was set at 20 min. As described by Kumar et al. [8], the intermittency ratio was defined as the ratio of the time of reduction or interruption of the air flow (τ_{off}) to the total drying time ($\tau_{off} + \tau_{on}$), as follows:

$$\alpha = \frac{\tau_{off}}{\tau_{off} + \tau_{on}} \quad (1)$$

The intermittency ratios employed in the two methods (A and B) are shown in Table 3.1. In addition to the processes with fixed intermittency ratios, conditions with time-variant intermittency ratios were also employed (A.4 and B.4). The time-variant intermittency ratios were used because, theoretically, the time required for redistribution of the internal moisture of the material, with movement of the moisture towards the surface, varies throughout the process as the moisture content decreases [11].

Table 3.1. Intermittency ratios used to evaluate the application of intermittency with periodic reduction (intermittency A) and periodic interruption (intermittency B) of the air flow during the drying of alumina in the spouted bed.

Intermittency ratio		***α=1/4***		***α=1/2***		***α=3/4***		***α=time-variant***		***α=0***
Run		***A.1**	***B.1**	**A.2**	**B.2**	**A.3**	**B.3**	**A.4**	**B.4**	**Continuous**
1st cycle	τ_{on} ***(min)***	15		10		5		15		20
	τ_{off} ***(min)***	5		10		15		5		0
2nd cycle	τ_{on} ***(min)***	15		10		5		10		20
	τ_{off} ***(min)***	5		10		15		10		0
3rd – 9th cycles	τ_{on} ***(min)***	15		10		5		5		20
	τ_{off} ***(min)***	5		10		15		15		0

* A and B indicate intermittency with periodic reduction and interruption of the air flow, respectively.

In both the intermittent and continuous processes, the air temperature was maintained constant at 60 °C. The air flow was also maintained constant in the continuous process (1.25 u_{mj}). In the intermittent process with periodic flow reduction (intermittency A), the air flow was changed between 0.85 u_{mj} and 1.25 u_{mj}.

Samples were regularly collected from the conical region, for determination of the moisture content and solids temperature. The sampling intervals were defined following preliminary tests. In both intermittent and continuous processes, these intervals were 5 min up to 60 min of drying. Thereafter, the sampling intervals were 15 min for the continuous process and at each instant of air flow change for the intermittent processes (Table 3.1). The moisture content was obtained by measuring the weight loss after heating at 105 °C for 24 h. For the solid temperature measurements, the samples were immediately placed into small thermally insulated containers. K type thermocouples installed inside each container measured the solids temperature. All the experiments were carried out in triplicate. The drying curves were constructed using a dimensionless moisture parameter (X^*), given by the following equation:

$$X^*(t) = \frac{\bar{X}_t}{\bar{X}_i} \tag{2}$$

3.2.3 Energy analysis

The advantages of intermittent drying, from an energy point of view, were evaluated by energy analysis considering a theoretical dryer similar to that described by Kudra [7], based on several studies available in the literature [15,16,18,19]. The system considered was composed of alumina particles and air, with the drying chamber being adopted as the control volume.

The energy required to evaporate water from the samples was calculated based on the latent heat of free water vaporization ($\Delta H_{v,s}$), as follows:

$$Q_w = \Delta H_{v,s} m_{ds} (\bar{X}_t - \bar{X}_i) \quad (3)$$

The latent heat of free water vaporization was obtained using Equation 4 [20]:

$$\Delta H_{v,s} = 2502.535259 - 2.38576424\ T_s(°C) \quad (4)$$

where $T_s(°C)$ represents the temperature of the solids (in Celsius).

The thermal energies supplied to the system and lost in the exhaust were determined using the following equations:

$$Q_{in} = \dot{m} \int_{T_a}^{T_{in}} c_p dT \quad (5)$$

$$Q_{out} = \dot{m} \int_{T_a}^{T_{out}} c_p dT \quad (6)$$

The specific heat of air was estimated based on the specific heat of vapor ($c_{p,v}$), the specific heat of dry air ($c_{p,g}$), and the absolute air humidity (Y), as follows:

$$c_p = c_{p,g} + c_{p,v} Y \quad (7)$$

$$c_{p,g} = 1.05 - 0.365\left(\frac{T(K)}{1000}\right) + 0.85\left(\frac{T(K)}{1000}\right)^2 - 0.39\left(\frac{T(K)}{1000}\right)^3 \quad (8)$$

$$c_{p,v} = 1.79 + 0.107\left(\frac{T(K)}{1000}\right) + 0.586\left(\frac{T(K)}{1000}\right)^2 - 0.20\left(\frac{T(K)}{1000}\right)^3 \quad (9)$$

where $T(K)$ represents the temperature of the drying air (in Kelvin). The specific heat relations were obtained from Borgnakke and Sonntag [21]. The absolute air humidity in the inlet and outlet were obtained using a dry bulb and wet bulb psychrometer.

The mechanical energy (W_m) required to maintain the characteristic flow regime was obtained according to the methodology described in detail by Brito et al. [18]. The following equation was used:

$$W_m = \dot{m}\left(\frac{\Delta v^2}{2} + \frac{\Delta P}{\rho}\right) \quad (10)$$

where Δv is the difference between the air velocities in the inlet and outlet positions, ΔP is the pressure drop in the bed, obtained by the pressure transducers, and ρ is the specific mass of air.

The specific mass of air was obtained using the following equation [13]:

$$\rho = 2.2538 - 0.003588\,T(K) \quad (11)$$

Based on these terms, the energy efficiency (*EE*), the specific energy consumption (*SEC*), and the exhaust heat loss (*EHL*) were employed to evaluate the energy performance of the intermittent and continuous drying processes. The energy efficiency was calculated as the ratio of the energy required

to evaporate the water and the total energy supplied to the system (thermal and mechanical energy). The specific energy consumption was considered to be the ratio between the total energy supplied to the system and the amount of water removed from the alumina particles. The exhaust heat loss was obtained from the relation between the energy lost in the exhaust and the total energy supplied to the system.

Energy efficiency (*EE*)

$$EE\ (t) = \frac{Q_w(t)}{\int_0^{\tau_{on}}\left(Q_{in,on} + W_{m,on}\right)dt + \int_{\tau_{on}}^{t}(Q_{in,off} + W_{m,off})dt} \quad (12)$$

Specific energy consumption (*SEC*)

$$SEC = \frac{\int_0^{\tau_{on,end}}\left(Q_{in,on} + W_{m,on}\right)dt + \int_{\tau_{on,end}}^{t_{end}}(Q_{in,off} + W_{m,off})dt}{m_{ds}\left(\bar{X}_{t,end} - X_i\right)} \quad (13)$$

Exhaust heat loss (*EHL*)

$$EHL = \frac{Q_{out}}{Q_{in} + W_m} \quad (14)$$

It should be noted that the energy efficiency and exhaust heat loss were determined throughout the drying, while the specific energy consumption was only determined at the end of process.

The heat lost to the walls was calculated based on the solutions of the boundary layer equations reported by Na and Chiou [22] for natural laminar convection over the frustum of a cone, considering that values of the Rayleigh number (Ra) in the range from 3.9 x 10^6 to 3.0 x 10^7 were obtained. The authors proposed the Nusselt (*Nu*) and Grashof (*Gr*) numbers based on a coordinate system developed for the vertical frustum of the cone, according to the following equations:

$$Nu_{x^*} = Gr_{x^*}^{1/4}[-g'(\xi, 0)] \quad (15)$$

$$Gr_{x^*} = \frac{g\beta \cos\gamma\,(T_{wall} - T_a)x^{*3}}{\nu^2} \quad (16)$$

Further details concerning Equations 14 and 15 can be found in Na and Chiou [22], together with the values of $[-g'(\xi, 0)]$, which are tabulated.

The Nusselt number was used to obtain the coefficient of heat transfer (h_{x^*}). Equation 16 was used to estimate the rate of heat transfer from the walls of the conical region to the environment:

$$Q_{wall} = h_{x^*}A_c(T_{wall} - T_a) \quad (17)$$

where A_c and T_{wall} are the area and wall temperature of the conical region, respectively. The wall temperature was an average value obtained using the data for the six K type thermocouples and the area of the conical region.

3.3 RESULTS AND DISCUSSION

3.3.1 Drying curves

Figure 3.2 presents the results for the dimensionless moisture, as a function of time, for the different operating conditions employed.

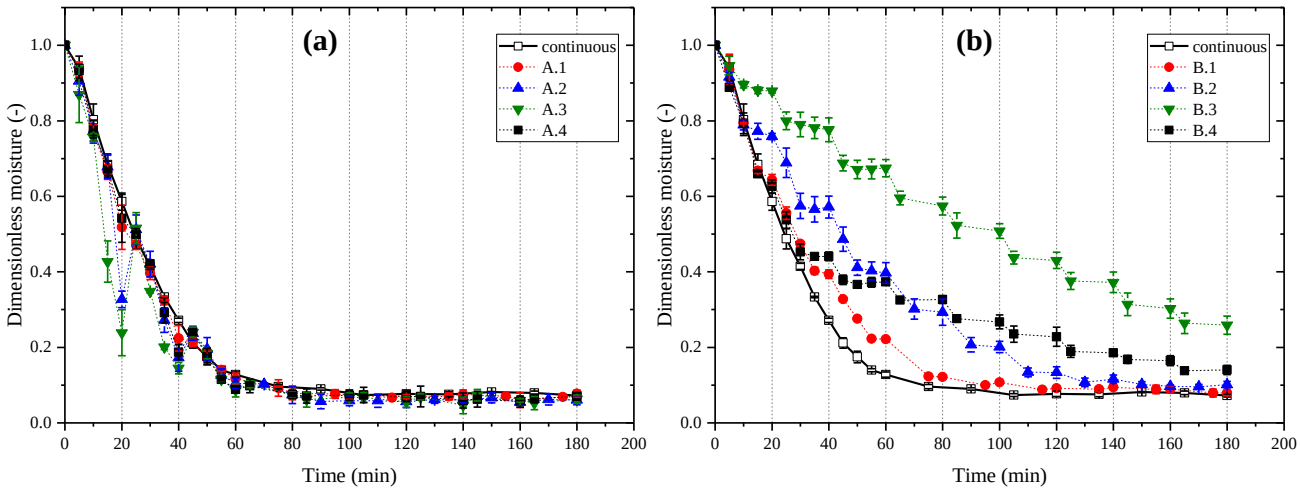

Figure 3.2. Dimensionless moisture, as a function of drying time, for (a) the processes with reduction of the air flow (intermittency A) and (b) the processes with interruption of the air flow (intermittency B).

Typical drying curves of alumina particles were observed for the continuous process, with a sharp initial decrease of the dimensionless moisture, followed by an exponential decrease and approach to a condition of dynamic equilibrium. Calçada et al. [23] and Perazzini et al. [24] reported similar results for the drying of alumina in a fluidized bed and a vibro-fluidized bed, respectively.

As shown in Figure 3.2(a), processes A.2 and A.3 presented sharper decreases in the first two intermittency cycles (40 min), compared to the continuous process. These decreases could be attributed to the reduction of the air flow, in the intermittent periods, to values lower than the minimum spouting flow, which probably resulted in the confinement of most of the drying air in an internal spout. The phenomenon of the internal spout is inherent to the mechanism of transition from a static to a spouted bed, as described in greater detail by Malek and Lu [25] and Mathur and Epstein [14]. Consequently, the drying air remained in direct contact with the alumina particles located in the lower regions of the system, where the sampling of the material was performed. Furthermore, the reduction of the air flow

led to a longer residence time, relative to the continuous process, enabling greater removal of moisture. However, a longer residence time could also result in a more heterogeneous drying process. A similar phenomenon also occurs in the fixed bed, as described by Souza et al. [26]. A decrease of the intermittency ratio, as well as use of a time-variant intermittency ratio (processes A.1 and A.4), resulted in smaller differences, relative to the continuous process.

The use of intermittency B resulted in periods during which the dimensionless moisture remained practically constant (Figure 3.2(b)), with the decrease occurring in a stepwise way. These periods coincided with the times when the air flow was interrupted, becoming more evident with increase of the intermittency ratio, due to the longer interruption periods. The dimensionless moisture was always lower in the continuous process, compared to the processes with intermittency B, with the greatest difference for run B.3. These results could be explained by the shorter effective drying times in the intermittent processes. The effective drying times are shown in Table 3.2, together with the final dimensionless moisture values.

Table 3.2. Effective drying time and final dimensionless moisture for different operating conditions in the alumina drying process with interruption of the air flow (intermittency B).

Operating condition	**Effective drying time (min)**	**Final dimensionless moisture**
Continuous	180	0.07 ± 0.02
B.1	135	0.08 ± 0.01
B.2	90	0.10 ± 0.01
B.3	45	0.25 ± 0.02
B.4	60	0.14 ± 0.01

Despite the shorter effective drying times, the final dimensionless moistures reached in the processes with intermittency B were close to that for the continuous process, with the exception of run B.3. The interruption of the air flow allowed redistribution of the internal moisture of the material, with constant transfer towards the surface, due to the moisture gradient. This transfer was favorable to the rapid removal of moisture when the air supply was restarted, since there was a greater vapor pressure difference between the interface and the air flow. This phenomenon has previously been described as a "refreshing effect" [27]. The higher vapor pressure near the surface was demonstrated by Defraeye [28], who performed a parametric study of intermittent drying of fruits. The effect of intermittency B in the drying process was also described by Zhao et al. [29] for the intermittent heat pump drying of green soybean seeds. Zhao et al. [29] reported peak drying rates in processes with interruption of air flow that were 6 - 8 times higher, compared to the same moments in a continuous drying process.

The process B.4, performed with a time-variant intermittency ratio, resulted in lower dimensionless moisture than the processes with constant intermittency ratio, considering the cycles with the same intermittency ratio values (Table 3.3). The results demonstrated the importance of use of a time-variant intermittency ratio, since the time required for the redistribution of the internal moisture of the material and movement of the moisture towards the surface varies throughout the process. A time-variant intermittency ratio was also employed by Zhu et al. [11] for the intermittent heat pump drying of green soybean, with similar results being obtained.

Table 3.3. Average dimensionless moisture values for different operating conditions, considering cycles with the same intermittency ratios.

Operating conditions		Average dimensionless moisture (-)		
		1st cycle	2nd cycle	3rd cycle
$\alpha = \frac{1}{4}$	**B.1**	0.64 ± 0.01	0.39 ± 0.01	0.22 ± 0.01
	B.4	0.62 ± 0.02	-	-
$\alpha = \frac{1}{2}$	**B.2**	0.76 ± 0.01	0.57 ± 0.01	0.40 ± 0.01
	B.4	-	0.44 ± 0.01	-
$\alpha = \frac{3}{4}$	**B.3**	0.88 ± 0.01	0.78 ± 0.01	0.67 ± 0.01
	B.4	-	-	0.37 ± 0.01

3.3.2 Energy analysis

3.3.2.1 Energy efficiency

Kudra and Ratti [30] highlighted the importance of the instantaneous energy efficiency. This parameter is particularly useful for analysis and comparison of the influence of different operational conditions on the energy performance of dryers. Figure 3.3 shows the instantaneous energy efficiencies, as a function of time, for the continuous process and the processes performed with periodic decreases in the air flow (intermittency A).

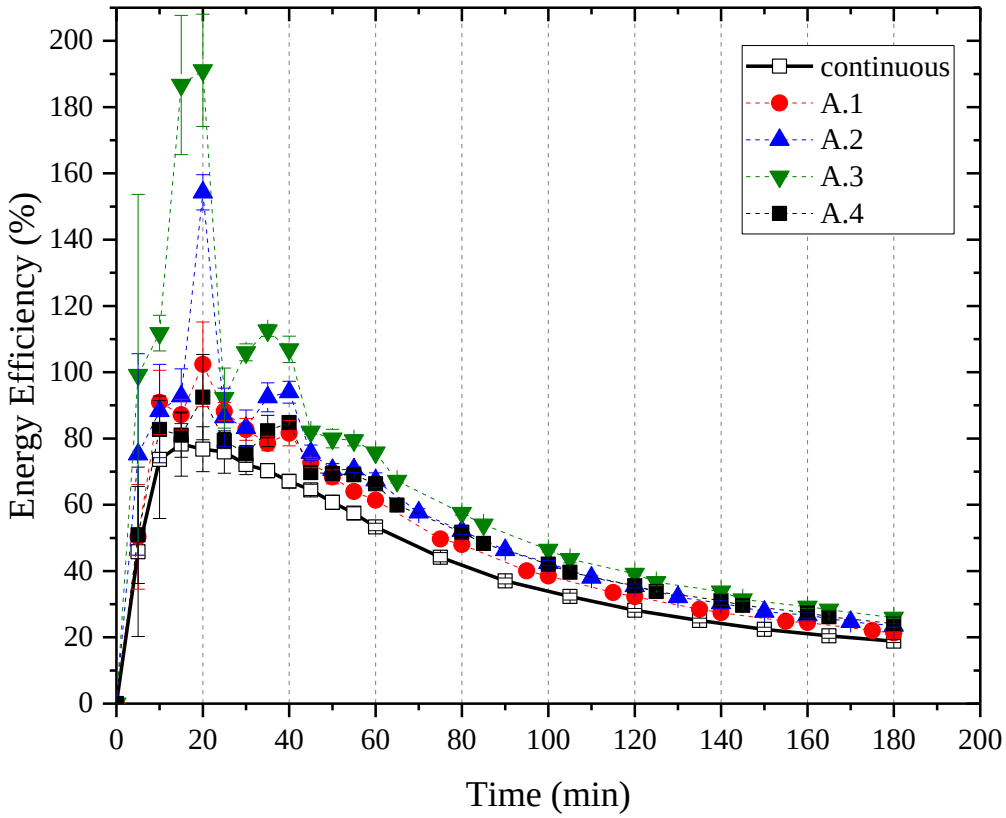

Figure 3.3. Energy efficiency, as a function of time, for the continuous process and the processes performed with periodic decreases of the air flow (intermittency A).

In the case of continuous drying, higher efficiencies were obtained at the start of the process, with a sharp increase followed by an apparent stabilization period that lasted up to approximately 40 min, after which there was a continuous and exponential decrease over time. The apparent stabilization period could be explained by a possible predominance of the external mass transfer resistance. The observed behavior was consistent with the results reported by Kudra [6], who found that most of the energy supplied during this period was effectively employed to remove moisture. Furthermore, a greater amount of energy was required initially, due to the higher moisture content of the material.

The period of apparent stabilization was not observed clearly in the intermittent processes.

Instead, greater instabilities and deviations were observed in this period, for all the intermittent conditions applied. These results provided support for the hypothesis of predominance of the external mass transfer resistance, as suggested previously. With the predominance of the external mass transfer, the process becomes more susceptible to external conditions such as the air flow and the fluid dynamics. The observed features could therefore be explained by the fact that the external conditions changed over time in the intermittent processes.

From the second cycle onwards, the energy efficiencies were slightly higher for the intermittent processes, compared to the continuous process, which could be attributed to the smaller amounts of total energy (thermal and mechanical energy) supplied to the system in the intermittent processes. This finding highlighted the importance of using lower air flows, especially at the end of the drying operation, when the internal mechanisms of mass transfer control the process. In addition, the amount of energy required varies throughout the drying process, as demonstrated by Nazghelichi et al. [31] in thermodynamic analysis of fluidized bed drying of carrot cubes.

Increase of the intermittency ratio in the processes with reduction of air flow (intermittency A) resulted in improved energy efficiency, which could be explained by the longer duration of the process under lower air flow. However, distinct energy efficiency peaks were observed in processes A.2 and A.3. These peaks occurred in the first two cycles, coinciding with the decreases of dimensionless moisture, as discussed previously for the same processes (Figure 3.2(a)). Therefore, a possible explanation for these peaks was that in these processes, higher amounts of moisture were removed during this period. However, as discussed previously, the periods of reduced air flow in these processes (A.2 and A.3) were likely to have led to a more heterogeneous drying. In addition, these peaks were not physically coherent, since they suggested that the amounts of energy used were greater than the energy supplied to the processes.

These results, together with the dimensionless moisture data, indicated that long periods of reduced air flows might not be appropriate in intermittent drying processes. However, this finding was not supported by the results obtained by Oliveira and Rocha [16], who performed the intermittent drying of beans in a spouted bed with reduction of air flow. This divergence could be explained, in part, by the different periods of intermittency, intermittent drying using a single intermittency ratio, and determination of the energy efficiency only at the end of the process.

As the drying processes progressed, the differences between the energy efficiencies obtained using the different intermittency ratios became less clear. This suggested that the amounts of energy wasted at the end of the processes were similar and were independent of the intermittency ratio. It could therefore be inferred that a promising strategy might be interruption of the air flow at the end of the drying, when the process is controlled by the internal mass transfer mechanism.

Figure 3.4 shows the instantaneous energy efficiencies, as a function of time, for the continuous process and the processes performed with periodic interruption of the air flow (intermittency B). No significant differences in the energy efficiencies were observed in the two first cycles of the processes. From the second cycle, the efficiencies for intermittent drying were higher than for the continuous process, as observed for intermittency A, which could be attributed to the shorter effective drying time, as can also be seen from Table 3.2. When the air flow was interrupted, the thermal energy supplied to the system was also interrupted, as well as the mechanical energy, since the bed remained static, without flow of the fluid phase. Nonetheless, the migration of moisture from within the particle to the surface continued, due to the moisture gradient, resulting in the formation of a liquid surface film. Hence, when the supply of air was restarted, the energy was more effectively employed as latent heat, similarly to the beginning of the drying process. This mechanism could also explain the stepwise decrease in energy efficiency, with periods of almost constant energy efficiency. Therefore, in addition

to reducing the effective drying time, interruption of the air flow during the drying process provided better energy utilization.

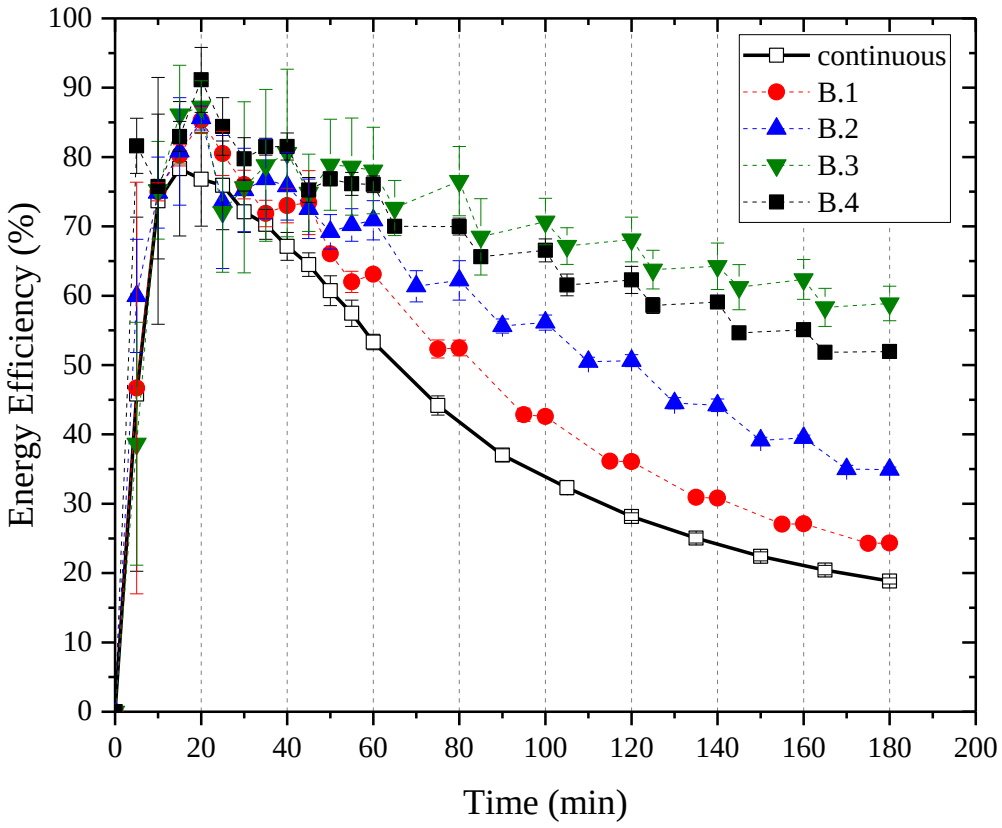

Figure 3.4. Energy efficiency, as a function of time, for the continuous process and the processes performed with periodic interruption of the air flow (intermittency B).

Considering the different intermittency ratios employed in the processes with interruption of air flow (intermittency B), an increase of this parameter resulted in greater energy efficiency (Figure 3.4), due to the shorter effective drying time, as described previously and indicated in Table 3.2. Table 3.4 provides the energy efficiencies obtained at the end of the different processes with periodic interruption of the air flow (intermittency B), together with the effective drying times. It can be seen that higher

energy efficiency was achieved using a higher intermittency ratio and, consequently, a shorter effective drying time. The energy efficiency obtained for the process with a time-variant intermittency ratio (run B.4) was lower than for run B.3, which had the same intermittency ratio at the end of the process. This finding could be attributed to the greater amount of moisture removed in process B.4, as shown in Figure 3.2(b). Hence, the energy required for process B.4 was lower than for process B.3, resulting in lower energy efficiency, since similar amounts of energy were supplied to the two processes. However, the use of a time-variant intermittency ratio was justifiable, considering that the time required for the moisture to move from within the particle to the surface increased as the moisture content decreased. As a result, the best strategy would be the use of short intermittency intervals at the beginning of the process, followed by longer intervals during the later stages.

Table 3.4. Final energy efficiencies reached in the continuous process and the processes with periodic interruption of the air flow (intermittency B).

Operating condition	Effective drying time (min)	Final energy efficiency (%)
Continuous	180	18.90 ± 0.40
B.1	135	24.30 ± 0.50
B.2	90	34.90 ± 0.40
B.3	45	58.90 ± 2.50
B.4	60	51.90 ± 0.80

The energy efficiency results were consistent with the findings of Zhu et al. [11], who also evaluated the use of different intermittency ratios. However, Zhu et al. [11] employed the specific moisture extraction rates to analyze the intermittent processes from an energy point of view. Likewise,

most studies reported in the literature have generally used parameters such as specific or total energy consumption for energy evaluation of intermittent drying processes [10,32,33].

3.3.2.2 Specific energy consumption

Figure 3.5 presents the results obtained for the specific energy consumptions of the continuous and intermittency A processes.

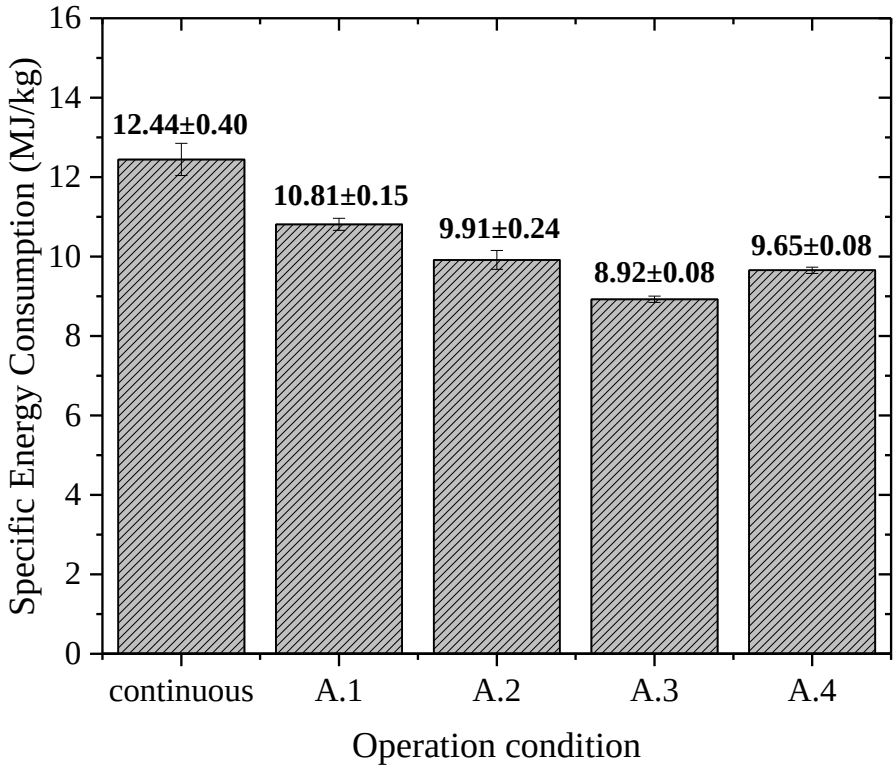

Figure 3.5. Specific energy consumption for the continuous process and the processes performed with periodic decreases of the air flow (intermittency A).

As shown in Figure 3.5, the highest specific energy consumption was obtained for the continuous process, while a higher intermittency ratio resulted in lower energy consumption. The lowest specific energy consumption was obtained in process A.3, which was the condition with the longest

intermittency period. Compared to the continuous process, a relative reduction of 28.3% was observed for process A.3. Reductions of 13.1% and 20.3% were obtained for processes A.1 and A.2, respectively. Considering the processes with constant intermittency ratios, the results indicated that there was a near-linear relation between the relative energy reduction and increase of the intermittency ratio, which could be explained by the smaller amounts of energy supplied to the system in the intermittent processes. In terms of the amount of moisture removed, there were no significant differences between the processes (Figure 3.2a). Thus, the use of intermittency A provided analogous amounts of moisture removed, relative to the continuous process, with a smaller energy demand. The advantage of intermittency A over the continuous process, in terms of the specific energy consumption, was also observed by Oliveira and Rocha [16], who performed the intermittent drying of beans in a spouted bed.

The specific energy consumption values obtained for processes A.2 and A.4 (performed with time-variant intermittency ratios) were similar. From this, it could be inferred that process A.4 would be more suitable from the energy point of view, since processes A.2 and A.3 presented behaviors different to that of the continuous process, as shown in the results for drying (Figure 3.2a) and energy efficiency (Figure 3.3a).

Figure 3.6 presents the specific energy consumptions of the processes with periodic interruption of the air flow (intermittency B).

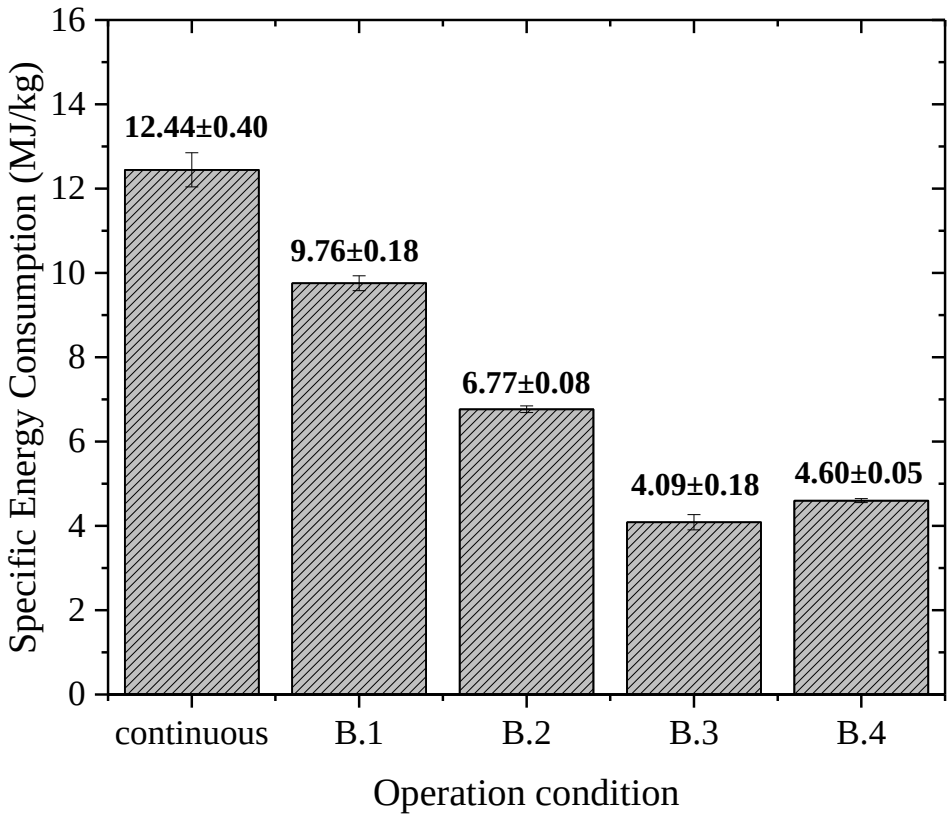

Figure 3.6. Specific energy consumption for the continuous process and the processes performed with periodic interruption of the air flow (intermittency B).

It can be seen from Figure 3.6 that process B.3 provided the lowest specific energy consumption, including in comparison to the other intermittent conditions (Figure 3.5). As observed for intermittency A, increase of the intermittency ratio resulted in lower specific energy consumption. In comparison with the continuous process, the relative decreases for processes B.1, B.2, and B.3 were 21.5, 45.6, and 67.1%, respectively. In addition, a linear relation was observed between the relative energy reduction and increase of the intermittency ratio. These results could be attributed to the shorter effective drying times in the processes with interruption of air flow (Tables 3.2 and 3.4). Despite the smaller amount of moisture removed, this was compensated by the shorter effective drying time, resulting in lower

specific energy consumption. In addition, the greatest relative reduction was observed for the condition with the longest period of intermittency. These findings were consistent with the work of Yang et al. [34], who reported relative reductions ranging from 24.4 to 48.1% for intermittent heat pump drying of Chinese cabbage.

A relative reduction of 63.0% was obtained for process B.4 (performed with a time-variant intermittency ratio), compared to the continuous process. Significant differences were observed between process B.4 and the other intermittency conditions, with the exception of process B.3. At the end of the process, the period of intermittency was longer for both processes (B.3 and B.4). This longer period was likely to have contributed to better energy use, since the time required for the moisture to move from within the particle to the surface increased with decrease of the moisture content, which could be attributed to a greater predominance of the internal mass transfer mechanism. Furthermore, additional energy would not be wasted in overheating the material. Despite differences in methodology, material, equipment, and energy parameters, qualitatively similar results were obtained by Zhu et al. [11], since the energy results for processes with longer periods of intermittency and time-variant intermittency ratios were similar at the end of the process. These results indicated that from the energy perspective, processes B.3 and B.4 were more satisfactory, compared to the continuous process and processes B.1 and B.2.

It is important to note that in practice, especially in the processing of seeds and grains, the drying process should, in principle, be stopped after reaching the desired moisture content. This could lead to significantly different specific energy consumption and energy efficiencies at the end of drying (Table 3.4) for processes with periodic interruption of the air flow (intermittency B). In this case, comparison between the continuous and intermittent processes should be revised, together with the quality parameters.

3.3.2.3 Heat losses in the exhaust and on the walls

The heat losses for the continuous and intermittency A processes are shown in Figure 3.7. For the continuous condition, there was a sharp decrease of the EHL in the first cycle (Figure 3.7a). In subsequent cycles, the EHL values gradually increased, until a dynamic equilibrium condition was reached after approximately 60 min. The values indicated that a smaller portion of the energy supplied to the process was lost in the exhaust at the beginning of the drying. As described previously, higher amounts of energy were required at the beginning of the process, due to the high initial moisture content of the material. The findings were consistent with the energy efficiency results presented previously (Figure 3.3). Furthermore, greater removal of moisture at the beginning caused a decrease in the air temperature, as well as an increase in the relative humidity. Consequently, the humidity of the exhaust air tended towards a condition of saturation (adiabatic saturation temperature). Jokiniemi and Ahokas [35] obtained similar results for the relative humidity of the exhaust air during the drying of oats and barley.

The profiles of the heat losses to the walls (Figure 3.7b) were qualitatively similar to the EHL profiles. The gradual increase of heat losses on the walls could also be explained by the smaller amounts of energy required as the moisture content decreased. In addition, with the decrease of moisture, a greater proportion of the supplied energy was used as sensible heat, providing the heating of the material. Consequently, there was greater heat transfer from the particles to the walls by molecular mechanisms (conduction).

The use of intermittency A resulted in lower EHL, relative to the continuous process (Figure 3.7a), for all the intermittency ratios employed. No significant differences were observed between the intermittency processes. Periodic decreases of EHL were observed in the intermittent processes,

coinciding with the times when the air flow was decreased. A possible explanation was that the decrease of the air flow provided better use of the drying potential of the air, due to increase of the residence time. Hence, a smaller proportion of the energy supplied was wasted in the exhaust air. This hypothesis was supported by the results obtained for the energy efficiency (Figure 3.3) as well as by the work of Jokiniemi and Ahokas [35], who investigated the drying of oats and observed an increase in the relative humidity of the air as the air flow decreased.

Comparison of the continuous and intermittent processes (Figure 3.7b) revealed no significant differences in the heat losses on the walls. These results could be explained by the increased wall temperatures of the lower regions caused by the reduction of the air flow and formation of the static bed. It should be noted that the wall temperature used was an average value considering the area of the conical region.

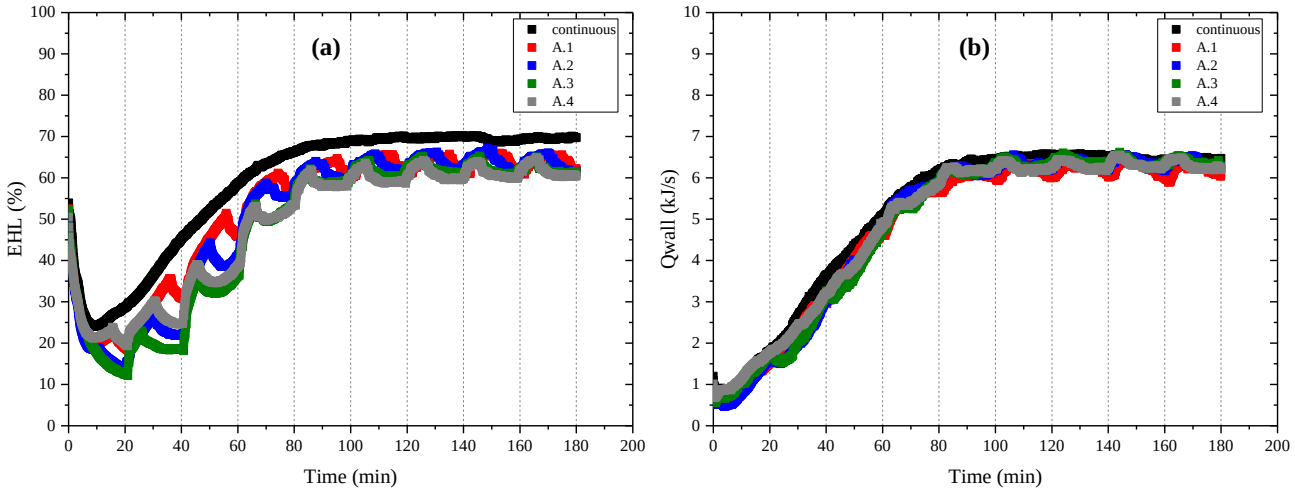

Figure 3.7. (a) Exhaust heat loss and (b) heat loss on the walls, as a function of time, for the continuous process and the processes performed with periodic decreases of the air flow (intermittency A).

The heat losses of the continuous and intermittency B processes are shown in Figure 3.8. The use of intermittency B resulted in lower EHL, compared to the continuous process (Figure 3.8a). Periodic sharp decreases of EHL were observed in the intermittent processes, coinciding with the times that the air supply was restarted. These periodic reductions of EHL could be attributed to the "refreshing effect", as described previously. This phenomenon probably contributed to better use of the energy supplied, due to the liquid film formed on the surface of the material, as occurred at the beginning of the process. Therefore, the amount of energy wasted in the exhaust air decreased when intermittency B was used, resulting in lower EHL values. Furthermore, discontinuities of EHL were observed (Figure 3.8a), which could be explained by the periodic interruptions of air flow.

The differences of EHL for the different intermittency ratios were more significant for intermittency B, compared to intermittency A. The lowest EHL values were obtained for run B.3, while decrease of the intermittency ratio caused the EHL values to increase. These findings could be explained by the longer duration of interruption of the air flow in the processes with higher intermittency ratios, since this provided better redistribution of moisture in the material. Similar behavior was observed for the heat losses on the walls (Figure 3.8b), which decreased with increase of the intermittency ratio.

Based on the results obtained for the heat losses of both intermittency conditions, it could be inferred that reductions or interruptions of the air flow led to smaller energy losses. Similarly, Darvishi et al. [36] dried mushrooms in a fluidized bed and observed that the heat losses increased with the air flow. Heat losses were represented by the authors as the sum of the energy lost from the dryer body by natural convection, the energy transferred to the environment in the exhaust air from the drying chamber, and sensible heating of the solids.

The observed heat losses suggested that it might be beneficial to employ recirculation of the

drying air, especially during the period of greater predominance of internal mass transfer mechanisms, since the highest losses occurred at the end of the process. In addition to the energy considerations, control of the air flow supplied to the process could assist in stabilizing the inlet air humidity conditions, with mixing of the exhaust with the feed air, as also highlighted by Golman and Julklang [37].

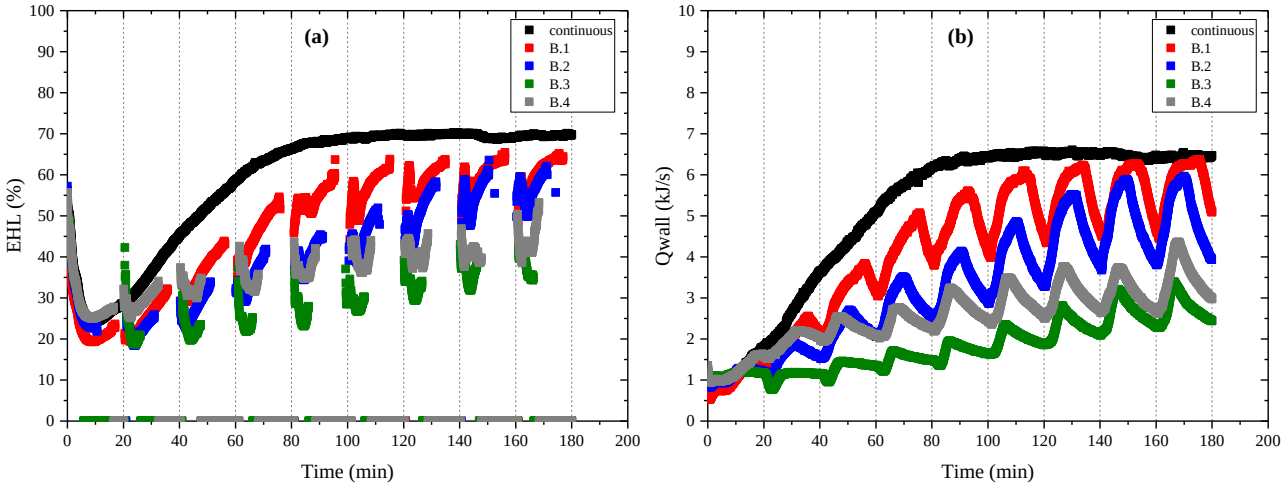

Figure 3.8. (a) Exhaust heat loss and (b) heat loss on the walls, as a function of time, for the continuous process and the processes performed with periodic interruption of the air flow (intermittency B).

3.4 CONCLUSIONS

The results of this study indicated that the application of both intermittent processes led to improved energy performance, compared to conventional spouted bed drying (continuous process). The energy efficiency curves showed that better use of the energy supplied was achieved for both intermittent processes. Furthermore, significant decreases of energy consumption were obtained, relative to the continuous process. Likewise, intermittent drying using the spouted bed also decreased

the energy lost both in the exhaust and to the walls.

In the intermittency with periodic reductions of air flow (intermittency A), an increase of the intermittency ratio resulted in higher energy efficiency and lower energy consumption. However, processes A.1 (α=1/4) and A.4 (time-variant intermittency ratio) were found to be most suitable for the operating conditions of intermittency A. This conclusion was reached due to operational problems indicated by the drying curves, such as the possible existence of heterogeneous drying. In the case of intermittency with periodic interruptions of air flow (intermittency B), increase of the intermittency ratio also provided higher energy efficiency and lower energy consumption. The improvement of energy performance was more significant for intermittency B than for intermittency A.

The findings reported in this work showed that from the energy perspective, the application of intermittency is a promising alternative for use in spouted bed drying. Furthermore, short periods of reduced air flow at the beginning, followed by longer periods of interrupted air flow, could provide more suitable operating conditions in future applications employing the spouted bed.

NOMENCLATURE

A_c	area of conical region	[m^2]
c_p	specific heat of air	[kJ kg^{-1} K^{-1}]
EE	energy efficiency	[-]
EHL	exhaust heat loss	[-]
g	acceleration due to gravity	[m s^{-2}]
Gr	Grashof number	[-]

h	heat transfer coefficient	[W m^{-2} K^{-1}]
$\Delta H_{v,s}$	latent heat of vaporization of sorghum	[kJ kg^{-1}]
$\dot{m}$	mass flow rate of air (dry basis)	[kg s^{-1}]
m_{ds}	mass of dry solids	[kg]
Nu	Nusselt number	[-]
ΔP	pressure drop	[Pa]
Q_{in}	thermal energy supplied	[kJ s^{-1}]
Q_{out}	energy lost in the exhaust	[kJ s^{-1}]
Q_w	energy required to evaporate the water	[kJ]
Q_{wall}	energy lost on the walls	[kJ s^{-1}]
SEC	specific energy consumption	[kJ kg^{-1}]
t	Time	[s]
T	Temperature	[K]
T_{wall}	wall temperature of the conical region	[K]
u_{mj}	minimum spout velocity	[m s^{-1}]
Δv	variation of air velocity	[m s^{-1}]
W_m	mechanical energy	[kJ s^{-1}]
X^*	dimensionless moisture	[-]
x^*	characteristic length of the vertical frustum of the cone	[-]
$\bar{X}$	mean moisture (dry basis)	[kg kg^{-1}]
$\bar{X}_i$	mean initial moisture (dry basis)	[kg kg^{-1}]
Y	absolute air humidity	[kg kg^{-1}]

Subscripts

A	Ambient
G	Gas
i	Initial
in	Inlet
out	Outlet
on	period of drying
off	period of reduction or interruption
end	end of drying
s	Solid
t	Time
v	Vapor

Greek symbols

α	intermittency ratio	[-]
β	volume expansion coefficient	[K^{-1}]
ρ	specific mass of air	[kg m^{-3}]
τ	intermittency time	[s]
γ	cone angle	[degree]
ν	kinematic viscosity	[m^2 s^{-1}]

ACKNOWLEDGEMENTS

The authors appreciate the financial support provided by Coordination for the Improvement of Higher Education Personnel (CAPES) and the São Paulo State Research Foundation (FAPESP, grant #2017/01856-7).

REFERENCES

[1] Liu, Z.; Lv, C. Fast synthesis of mesoporous γ-alumina assisted by a room temperature ionic liquid and its use as a support for the promotional catalytic performance of dibenzothiophene hydrodesulfurization. *RSC Adv.* **2014,** *4,* 10221–10227. DOI: 10.1039/c3ra45185b.

[2] Forman, E. M.; Trujillo, M. A.; Ziegler, K. J.; Bradley, S. A.; Wang, H.; Prabhakar, S.; Vasenkov, S. Self-diffusion of heptane inside aggregates of porous alumina particles by pulsed field gradient NMR. *Microporous Mesoporous Mater.* **2016,** *229,* 117–123. DOI: 10.1016/j.micromeso.2016.04.027.

[3] Xu, B.; Xiao, T.; Yan, Z.; Sun, X.; Sloan, J.; González-Cortés, S. L.; Alshahrani, F.; Green, M. L. H. Synthesis of mesoporous alumina with highly thermal stability using glucose template in aqueous system. *Microporous Mesoporous Mater.* **2006,** *91,* 293–295. DOI: 10.1016/j.micromeso.2005.12.007.

[4] Xiao, Z. L.; Han, C. Y.; Welp, U.; Wang, H. H.; Kwok, W. K.; Willing, G. A.; Hiller, J. M.; Cook, R. E.; Miller, D. J.; Crabtree, G. W. Fabrication of Alumina Nanotubes and Nanowires by Etching Porous Alumina Membranes. *Nano Lett.* **2002,** *11,* 1293–1297. DOI: 10.1021/nl025758q.

[5] Pourcel, F.; Jomaa, W.; Puiggali, J. R.; Rouleau, L. Crack appearance during drying of an alumina gel: Thermo-hydro-mechanical properties. *Dry. Technol.* **2007,** *25,* 759–766. DOI:

10.1080/07373930701370134.

[6] Kudra, T. Energy aspects in drying. *Dry. Technol.* **2004,** *22,* 917–932. DOI: 10.1081/DRT-120038572.

[7] Kudra, T. Energy Performance of Convective Dryers. *Dry. Technol.* **2012,** *30,* 1190–1198. DOI: 10.1080/07373937.2012.690803.

[8] Kumar, C.; Karim, M. A.; Joardder, M. U. H. Intermittent drying of food products: A critical review. *J. Food Eng.* **2014,** *121,* 48–57. DOI: 10.1016/j.jfoodeng.2013.08.014.

[9] Chua, K. J.; Mujumdar, A. S.; Chou, S. K. Intermittent drying of bioproducts - An overview. *Bioresour. Technol.* **2003,** *90,* 285–295. DOI: 10.1016/S0960-8524(03)00133-0.

[10] Filippin, A. P.; Molina Filho, L.; Fadel, V.; Mauro, M. A. Thermal intermittent drying of apples and its effects on energy consumption. *Dry. Technol.* **2018,** *0,* 1–16. DOI: 10.1080/07373937.2017.1421549.

[11] Zhu, Z.; Yang, Z.; Wang, F. Experimental research on intermittent heat pump drying with constant and time-variant intermittency ratio. *Dry. Technol.* **2016,** *34,* 1630–1640. DOI: 10.1080/07373937.2016.1138966.

[12] San José, M. J.; Alvarez, S.; López, R. Drying of industrial sludge waste in a conical spouted bed dryer. Effect of air temperature and air velocity. *Dry. Technol.* **2018,** *0,* 1–11. DOI: 10.1080/07373937.2018.1441155.

[13] Freire, F. B.; Atxutegi, A.; Freire, F. B.; Freire, J. T.; Aguado, R.; Olazar, M. An adaptive lumped parameter cascade model for orange juice solid waste drying in spouted bed. *Dry. Technol.* **2017,** *35,* 577–584. DOI:10.1080/07373937.2016.1190937.

[14] Mathur, K. B.; Epstein, N. *Spouted Beds*; Academic Press: New York, 1974.

[15] Passos, M. L.; Mujumdar, A. S.; Vijaya, G.; Raghavan, V. G. S. Spouted and Spout-Fluidized

Beds for Gram Drying. *Dry. Technol.* **1989,** *7*, 663–696. DOI: 10.1080/07373938908916621.

[16] Oliveira, C.; Rocha, S. Intermittent drying of beans in a spouted bed. *Brazilian J. Chem. Eng.* **2007,** *24*, 571–585. DOI: 10.1590/S0104-66322007000400010.

[17] Bon, J.; Kudra, T. Enthalpy-Driven Optimization of Intermittent Drying. *Dry. Technol.* **2007,** *25*, 523–532. DOI: 10.1080/07373930701226880.

[18] Brito, R. C.; Pádua, T. F.; Freire, J. T.; Béttega, R. Effect of mechanical energy on the energy efficiency of spouted beds applied on drying of sorghum [Sorghum bicolor (L) Moench]. *Chem. Eng. Process. Process Intensif.* **2017,** *117*, 95–105. DOI: 10.1016/j.cep.2017.03.021.

[19] Vieira, M. G. A.; Estrella, L.; Rocha, S. C. S. Energy Efficiency and Drying Kinetics of Recycled Paper Pulp. *Dry. Technol.* **2007,** *25*, 1639–1648. DOI: 10.1080/07373930701590806.

[20] Muthu, V. P.; Chattopadhyay, P. K. Prediction of Heat of Vapourization of Moisture from Cereal Grains - A Modelling Approach. *Dry. Technol.* **1993,** *11*, 1855–1862. DOI: 10.1080/07373939308916931.

[21] Borgnakke, C.; Sonntag, R. E. *Fundamentals of thermodynamics*; John Wiley & Sons: New Jersey, 2009.

[22] Na, T. Y.; Chiou, J. P. Laminar natural convection over a frustum of a cone. *Appl. Sci. Res.* **1979,** *35*, 409–421. DOI: https://doi.org/10.1007/BF00420389.

[23] Calçada, L. A.; Mancini, M. C.; Wildhagen, G. R. S. Drying of inorganic particulate compounds. *Dry. Technol.* **2006,** *24*, 349–358. DOI: 10.1080/07373930600564407.

[24] Perazzini, H.; Freire, F. B.; Freire, J. T. The influence of vibrational acceleration on drying kinetics in vibro-fluidized bed. *Chem. Eng. Process. Process Intensif.* **2017,** *118*, 124–130. DOI: 10.1016/j.cep.2017.04.009.

[25] Malek, M. A.; Lu, B. C. Y. Pressure drop and spoutable bed height in spouted beds. *Ind. Eng.*

Chem. Process Des. Dev. **1965,** *4,* 123–128. DOI: 10.1021/i260013a027.

[26] Souza, G. F. M. V.; Miranda, R. F.; Barrozo, M. A. S. Soybean (*Glycine max* L. Merrill) Seed Drying in Fixed Bed: Process Heterogeneity and Seed Quality. *Dry. Technol.* **2015,** *33,* 1779–1787. DOI: 10.1080/07373937.2015.1039542.

[27] Nishiyama, Y.; Cao, W.; Li, B. Grain intermittent drying characteristics analyzed by a simplified model. *J. Food Eng.* **2006,** *76,* 272–279. DOI: 10.1016/j.jfoodeng.2005.04.059.

[28] Defraeye, T. Towards more efficient intermittent drying of fruit: Insights from combined hygrothermal-quality modelling. *Innov. Food Sci. Emerg. Technol.* **2016,** *38,* 262–271. DOI: 10.1016/j.ifset.2016.10.003.

[29] Zhao, H.; Yang, Z.; Tao, Z. Drying Kinetics of Continuous and Intermittent Heat Pump Drying of Green Soybean Seeds. *Int. J. Food Eng.* **2017,** *13,* 1–15. DOI: 10.1515/ijfe-2017-0182.

[30] Kudra, T.; Ratti, C. Foam-mat drying: Energy and cost analyses. *Can. Biosyst. Eng.* **2006,** *48,* 27–32.

[31] Nazghelichi, T.; Kianmehr, M. H.; Aghbashlo, M. Thermodynamic analysis of fluidized bed drying of carrot cubes. *Energy.* **2010,** *35,* 4679–4684. DOI: 10.1016/j.energy.2010.09.036.

[32] Defendi, R. O.; Paraíso, P. R.; Jorge, L. M. M. Optimization study of soybean intermittent drying in fixed-bed drying technology. *Dry. Technol.* **2017,** *35,* 125–137. DOI: 10.1080/07373937.2016.1162171.

[33] Golmohammadi, M.; Assar, M.; Rajabi-Hamaneh, M.; Hashemi, S. J. Energy efficiency investigation of intermittent paddy rice dryer: Modeling and experimental study. *Food Bioprod. Process.* **2015,** *94,* 275–283. DOI: 10.1016/j.fbp.2014.03.004.

[34] Yang, Z.; Zhu, E.; Zhu, Z.; Wang, J.; Li, S. A comparative study on intermittent heat pump drying process of Chinese cabbage (Brassica campestris L.ssp) seeds. *Food Bioprod. Process.* **2013,** *91,*

381–388. DOI: 10.1016/j.fbp.2013.02.006.

[35] Jokiniemi, H. T.; Ahokas, J. M. Drying process optimisation in a mixed-flow batch grain dryer. *Biosyst. Eng.* **2014,** *121,* 209–220. DOI: 10.1016/j.biosystemseng.2014.01.002.

[36] Darvishi, H.; Azadbakht, M.; Noralahi, B. Experimental performance of mushroom fluidized-bed drying: Effect of osmotic pretreatment and air recirculation. *Renew. Energy.* **2018,** *120,* 201–208. DOI: 10.1016/j.renene.2017.12.068.

[37] Golman, B.; Julklang, W. Analysis of heat recovery from a spray dryer by recirculation of exhaust air. *Energy Convers. Manag.* **2014,** *88,* 641–649. DOI: 10.1016/j.enconman.2014.09.012.

CHAPTER 4

QUALITY ANALISYS OF INTERMITTENT DRYING

This chapter describes the analysis of the intermittent methodology in spouted beds considering quality aspects, which refers to specific objective (2) of this thesis. Thus, the paper described in this chapter aimed to perform the physical and physiological quality analysis of intermittent soybean seeds drying in the spouted bed. Mechanical damages and physiological properties were evaluated by tests of germination, first germination count, seedling length, tetrazolium, sodium hypochlorite, and X-Ray. Five different intermittency profiles and two different intermittency methodologies with periodic reduction and interruption of the air flow were employed. Continuous and intermittent processes with shorter periods of reduced air flow (A.1) provided a lower degree of seed deterioration, considering both physiological and physical aspects. The findings of this study contributed to identify the distinct trend of intermittency application in the spouted bed in relation to other dryers when seed quality attributes are demanded, highlighting as a promising field for further studies.

This chapter is based on:

R. C. Brito, M. B. Zacharias, V. A. Forti & J. T. Freire (2021) Physical and physiological quality of intermittent soybean seeds drying in the spouted bed, Drying Technology, 39:6, 820-833, DOI: 10.1080/07373937.2020.1725544.

4.1 INTRODUCTION

Drying is one of the oldest preservation methods for engineering and/or biological materials, playing a fundamental role in several processing steps and being widely employed in various industrial sectors. Unsuitable drying methods usually led to several problems providing undesired results, mainly relate to quality deterioration. Typical problems of grain and seed drying are the occurrence of mechanical damages, as cracks and fissures due to drying-induced stresses relate to temperature and moisture gradients [1–3]. Processes with high degree of agitation, as moving bed dryers (i.e., spouted bed, fluidized bed, rotatory dryers), can lead to higher mechanical damages. Further market values, such problems can provide physiological potential loss due to microbial attack [4–6].

Several studies have described the influence of drying on quality. Barrozo et al. [4] and Felipe and Barrozo [7] performed soybean drying in moving beds and observed lower damaged seeds indexes for processes with lower temperatures and air flows. Wiriyaumpaiwong et al. [8], in the two-dimensional spouted bed, associated the most of mechanical damages from processes with higher air flows to the combined effects of the high degree of particle agitation and drying rate, which are considered the main factors related to mechanical damages in moving beds [5, 9]. To overcome these difficulties, several technologies and hybrid methodologies, such as intermittent drying, have emerged as promising alternatives.

Intermittency consists basically of alternating between active and passive drying periods, which can be incorporated into the process by periodically changing of operational conditions, such as temperature and air flow, utilization of different sources and mode of energy input (e. g. convection, conduction, radiation, or microwave), operating pressure, among others described in

details by Kumar et al. [10] and Chua et al. [11]. Further energy advantages, intermittent drying can provide benefits for better quality products, minimizing degradation of various quality attributes of dried material, which are inevitable during the drying process [10, 12, 13]. As highlighted by Nishiyama et al. [14], intermittent drying provided to material a tempering period which is usually used between drying periods. This tempering period allows the decrease of moisture gradients that produce tensile stress at the surface and compressive stress in the interior of the grain, providing a product with better quality. Hence, several researchers have studied intermittent drying and found advantages as shorter effective drying time, lower product surface temperature, and higher product quality [15].

Ghasemi et al. [2] performed the multi-stage intermittent drying of rough rice based on stress cracking, tempering period, and total drying duration. The authors verified that the amount of fissures grains increased for longer drying durations in each drying stage. Xu et al. [16] also obtained similar results in the intermittent microwave drying of rice, verifying the decrease of physical degradation with the increase of passive period due to lower internal gradients. Jung and Yoon [17] and Dondee et al. [18] carried out different intermittent drying of soybeans, considering cracking and breakage of grains. Jung and Yoon [17] applied convective drying and observed the decrease of cracked grains by decreasing the duration of the drying period and increasing the passive period. Dondee et al. [18] combined near-infrared radiation with fluidized-bed drying and obtained the reduction of cracking and breaking of soybean beans, which were negligible when compared with individual hot-air fluidized-bed drying. Both studies highlighted the soybean as a well-valuable resource due to healthy nutrients (high-quality protein, oil, and phytochemicals) and wide application in the animal feed and human food industry (grains and processed foods like tofu, soybean sauce, and soymilks). The importance of more efficient soybean seeds drying methods

increases when agricultural aspects are considered since the vital parts of the embryonic axis (radicle, hypocotyl and cotyledon) lie under a thin seed coat. Thus, soybean seeds are more susceptible to mechanical damage, which can lead to reduction in quality and seed lot rejection [19].

Despite the advantages aforementioned, few studies have investigated intermittent drying in the spouted bed, which can provide benefits related to high degrees of agitation and mixing between the phases [20, 21]. The characteristic fluid dynamics of the spouted bed provide an efficient fluid-particle contact, enhancing the rates of heat and mass transfer even at low temperatures. Moreover, the cyclic movement of the solids in the spouted bed allows shorter periods of direct contact of the material with the drying air [22, 23]. These features are advantageous and interesting for the processing of thermosensitive materials such as seeds, since these materials may have their physiological and nutrition properties compromised when directly exposed to high temperature. Thus, despite the higher mechanical damages provide by moving bed dryers, as mentioned previously, the spouted bed stands out against other moving dryers for sensitive materials due to the features described. Given the aforementioned, the spouted bed has been widely studied and applied in several chemical and physical processes, including the drying of pastes and particulate solids [24–28], processing of fine particles [29–32], coating [33–35], and operations of combustion and pyrolysis [36–39].

Energy advantages of intermittency in the spouted bed have been found in previous studies [40]. However, there is still a gap regarding the quality analysis of intermittent drying in the spouted bed, mainly considering mechanical damages on the processing of important grains, such as soybeans. Based on the advantages of the intermittent drying and the spouted bed described previously, the combination of these methodologies could be promising for material quality.

Likewise, further studies are required in order to improve understanding the influence of the mechanical damages from spouted bed drying on seeds physiological properties (viability and vigor), since they are fundamental quality attributes when considering the agricultural aspects.

Thus, the aim of this study was to perform the physical and physiological quality analysis of intermittent soybean seeds drying in the spouted bed. For this purpose, mechanical damages and physiological properties (viability and vigor) were evaluated for the continuous process, four different intermittency profiles, and two different intermittency methodologies. The continuous process was performed with air flow constant throughout the drying process. The different intermittency profiles were based on intermittency ratio, being employed three different conditions with fixed intermittency ratio and one condition with time-variant intermittency ratio. The intermittency methodologies consisted of processes with periodic reductions and interruptions of air flow throughout the drying process.

4.2 MATERIALS AND METHODS

4.2.1 Materials and equipment

Batches of 2 kg of Soybean seeds Intacta RR2 PRO^{TM} (mean diameter of 6.6 ± 0.3 mm) [*Glycine max* (L.) Merrill] were used in drying experiments with conical configuration. The bed mass used corresponded to a static bed height (H_0) of 0.17 m. Before each drying process, the seeds were maintained in an environment saturated with water vapor for 48 h to reach the moisture desired (0.20 ± 0.01 dry basis). Figure 4.1a shows the equipment used for drying experiments and Figure 4.1b shows the geometric factors of conical contactor made of stainless steel.

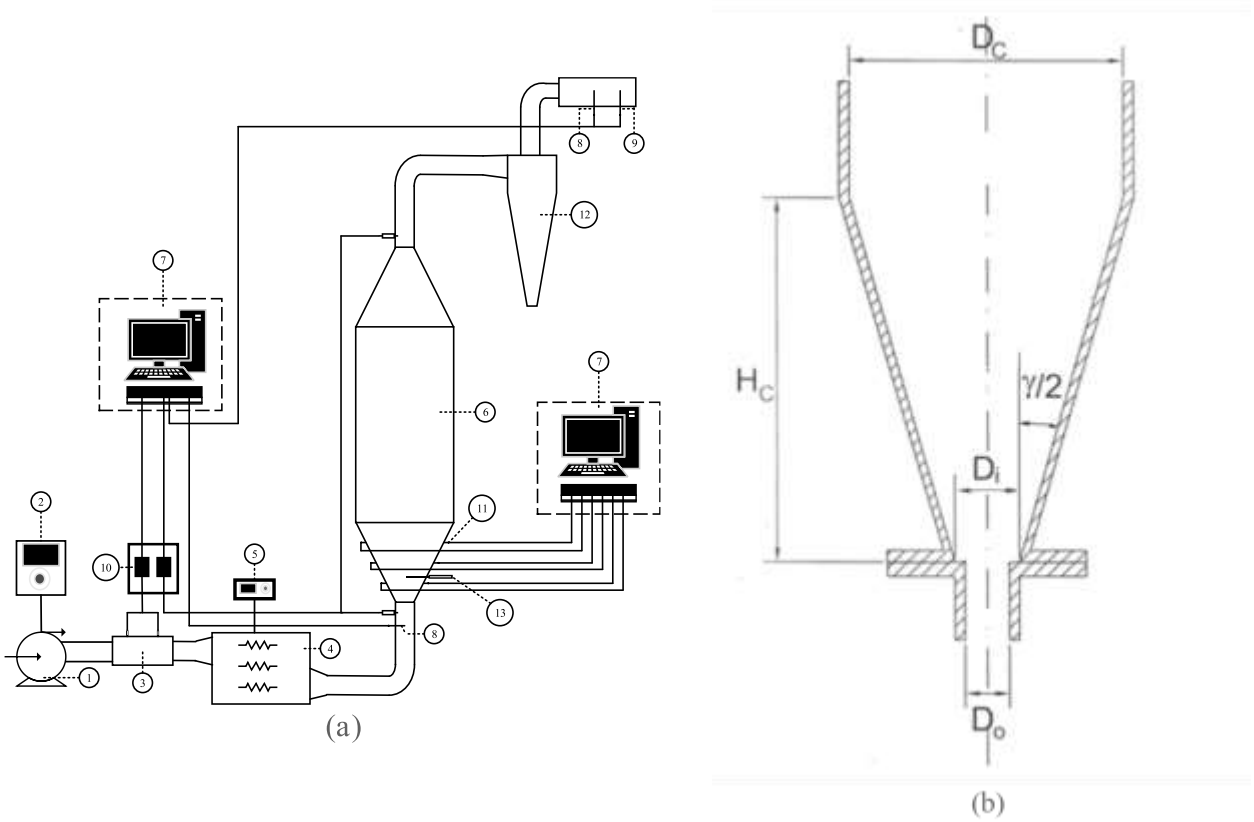

Figure 4.1. (a) Components of the experimental unit used for the drying experiments: (1) blower; (2) frequency inverter; (3) Venturi flow meter; (4) heater; (5) temperature controller; (6) drying chamber; (7) data acquisition system; (8) T type thermocouple; (9) T type wet-bulb thermocouple; (10) pressure transducers; (11) K type thermocouple; (12) cyclone; (13) sampler. (b) Geometric factors of the conical contactor.

As presented in Figure 4.1a, the air providing was performed by a 7.5 HP blower (1) controlled by a frequency inverter (2). A Venturi meter (3) was used to measure the air flow, which was heated by an electric heater with four series resistances (4), being the temperature air controlled by a Flyever FE50SN temperature controller (5). The drying chamber (6) consisted of a cylindrical stainless-steel vessel (0.60 m height, 0.30 m diameter) with two conical contactors at

bottom and top, being the last one connected to a cyclone (7) for collection of the powder produced from friction and the drying process. A small visor made by transparent acrylic was also placed in the cylindrical vessel for visualization of the fluid dynamic. Type T thermocouples (8) were employed to measure the temperature, which were positioned in the inlet and outlet of the drying chamber. The pressure drops at the Venturi meter and in the drying chamber were measured using 0-5 psi pressure transducers (10). All the temperature and pressure drop data were acquired by the data acquisition system (7), employing a Lynx ADS0500 board. The data were acquired at intervals of 3 s, with a frequency of 500 Hz, and the values provided by the data acquisition system were the average of 1024 measurements. Geometric factors of the conical contactors (Figure 4.1b) were as follows: upper diameter (D_c), 0.30 m; contactor angle (γ), 60°; height of the conical section (H_c), 0.23 m; and bottom diameter (D_i), 0.055 m. The gas inlet diameter (D_0) was 0.03 m with a Venturi air distributor, which provide higher stability and homogenous distribution of air at the bed entrance [41].

4.2.2 Experimental procedure

Both continuous and intermittent drying were performed at 50 °C, 60 °C, and 70 °C, being 50 °C the minimum possible temperature to be reached in the experimental unit used. This minimum temperature was a limitation found in the experimental unit since air drying left the blower with temperatures higher than 40 °C due to the environmental conditions and air flow employed. Air flows of 1.25 times the minimum spouting velocity ($u_{ms} = 39.20 \pm 0.08$ m s^{-1}) were used in the continuous condition. The minimum spouting velocity was estimated by both visual and the fluid dynamic characterization, which was performed according to the methodology

described by Mathur and Epstein [42]. This methodology was based on a plot of the bed pressure drop as a function of air velocity (calculated using D_0) by increasing and decreasing the air flow rate. Thus, the minimum spouting velocity was obtained in the collapse of the spouting regime on decreasing the air flow, which was visually observed by both the small visor and the fluid dynamic curves since the pressure drop increases suddenly in the spout collapse. In the intermittent processes, two different intermittencies were employed: periodic reduction (intermittency **A**) and periodic interruption (intermittency **B**) of air flow. Intermittency **A** was carried out varying air flow between $0.85u_{ms}$ and $1.25u_{ms}$, ensuring the drying process between static and spouting regimes. Both methodologies were performed according to the intermittent drying described by Brito et al. [40], being intermittency intervals based on cycles and on the intermittency ratio (α). After preliminary tests, each cycle was set at 20 min and the different intermittent conditions were employed according to Table 4.1. Intermittency ratio was defined as the ratio of the passive drying period under reduced or interrupted air flow (τ_{off}) to the total drying time ($\tau_{off} + \tau_{on}$), as follows:

$$\alpha = \frac{\tau_{off}}{\tau_{off} + \tau_{on}} \quad (1)$$

As summarized in Table 4.1, the continuous process and intermittent process with fixed and time-variant intermittency ratios were employed. The continuous process was performed with air flow constant of $1.25u_{ms}$ throughout the drying process, being $\alpha = 0$. Three different conditions with fixed intermittency ratio were used: **A1** and **B1** with air flow of $1.25u_{ms}$ for 15 min and $0.85u_{ms}$ (or air flow interrupted in condition **B**) for 5 min, being $\alpha = 1/4$; **A2** and **B2** with air flow of $1.25u_{ms}$ for 10 min and $0.85u_{ms}$ (or air flow interrupted in condition **B**) for 10 min, being

$\alpha = 1/2$; **A3** and **B3** with air flow of $1.25u_{ms}$ for 5 min and $0.85u_{ms}$ (or air flow interrupted in condition **B**) for 15 min, being $\alpha = 3/4$. In the conditions with fixed intermittency ratio, the intervals described were employed in all the cycles. The conditions with time-variant intermittency ratios were used because, theoretically, the time required for redistribution of the internal moisture of the material, with movement of the moisture towards the surface, varies throughout the process as the moisture content decreases, as mentioned by Zhu et al. [15] and Brito et al. [40]. Thus, follows the methodology adopted for such conditions (**A4** and **B4**): drying process with air flow of $1.25u_{ms}$ for 15 min and $0.85u_{ms}$ (or air flow interrupted in condition **B**) for 5 min, in the first cycle; air flow of $1.25u_{ms}$ for 10 min and $0.85u_{ms}$ (or air flow interrupted in condition **B**) for 10 min, in the second cycle; air flow of $1.25u_{ms}$ for 5 min and $0.85u_{ms}$ (or air flow interrupted in condition **B**) for 15 min, until the end of drying process.

After ensuring the stability of the process under the air temperature and operating conditions shown in Table 4.1, the airflow was stopped and the spouted bed was loaded with 2 kg of Soybean seeds. The air was then supplied again and the drying process was initiated. Samples were regularly collected from the conical region for determination of the moisture content by measuring the weight loss after heating at 105 °C for 24 h (gravimetric method). The sampling intervals for both intermittent and continuous processes were 5 min up to 60 min of drying. Thereafter, the sampling intervals were 15 min for the continuous process and at each instant of air flow change for the intermittent processes. All the experiments were carried out in duplicate. For each condition, the first experiment was carried out for 4 h and the second experiment was performed until seeds reached moisture in the range from 12% to 13% (wet basis), based on drying curves of the first experiment, which is considered adequate for safe seed storage [5]. Quality analysis was performed

only on the seeds from the second experiment of each condition. All the drying curves were expressed in terms of dimensionless moisture (X^*), as follows:

$$X^* = \frac{\bar{X}(t)}{\bar{X}_i} \tag{2}$$

where $\bar{X}(t)$ is the average moisture in instant t and $\overline{X_i}$ is the initial average moisture, both on dry basis.

Table 4.1. Intermittency ratios used to evaluate the application of intermittency with periodic reduction (intermittency A) and periodic interruption (intermittency B) of the air flow during the drying of soybean in the spouted bed.

Intermittency ratio		***α=1/4***		***α=1/2***		***α=3/4***		***α=time-variant***		***α=0***
Run		***A.1**	***B.1**	**A.2**	**B.2**	**A.3**	**B.3**	**A.4**	**B.4**	**Continuous**
1st cycle	τ_{on} ***(min)***	15		10		5		15		20
	τ_{off} ***(min)***	5		10		15		5		0
2nd cycle	τ_{on} ***(min)***	15		10		5		10		20
	τ_{off} ***(min)***	5		10		15		10		0
3rd – 12th cycle	τ_{on} ***(min)***	15		10		5		5		20
	τ_{off} ***(min)***	5		10		15		15		0

*A and B indicate intermittency with periodic reduction and interruption of the air flow, respectively.

4.2.3 Seed Quality analysis

Both physiological (viability and vigor) and physical (mechanical damages) attributes were considered for seed quality analysis, in which tests of germination, first germination count, seedling length, tetrazolium, sodium hypochlorite, and X-Ray were performed.

According to Rules for Seed Analysis (RSA) [43], the germination tests were performed with four samples of 50 seeds per treatment (Table 4.1), which were distributed on germination paper towel (Germitest) moistened with an amount of water equivalent 2.5 times the weight of the dry substrate and placed to germinate at 25ºC in a germination chamber. Five days after sowing, the first germination count was carried out considering the normal seedlings and dead seeds, while abnormal seedlings were kept until the eighth day when the final count of germination tests was performed. The total average length of seedlings was also obtained on the eighth day (seedling length). First germination count and seedling length results were employed to evaluate seeds vigor, as well as tetrazolium tests, since the Association of Official Seed Analysts (AOSA, 1983) define vigor as the total sum of all seeds properties which result in uniform and fast production of healthy seedlings under a wide range of environmental conditions.

Tetrazolium tests were performed according to França-Neto et al. [44], who established criteria of classification based on the seed vigor: Class 1 (highest vigor), Class 2 (high vigor), Class 3 (medium vigor), Class 4 (low vigor), Class 5 (very low vigor), Class ≥6 (dead seeds with severe damages). Hence, seeds were classified as viable (classes 1-5) and non-viable (classes 6-8). Four repetitions of 50 seeds per treatment were preconditioned on a paper towel moistened with an amount of water equivalent to 2.5 times the weight of the dry substrate, for a period of 16 h at 25 °C in a germination chamber. Afterward, seeds were immersed in a 2,3,5-triphenyl

tetrazolium chloride solution (0.075 %) for 2 h at 40 °C in a germination chamber, being sectioned lengthwise and examined individually after this period, according to the criteria described by França-Neto et al. [44]. Results of germination, first germination count, seedling length (Table 4.3), and tetrazolium tests (Table 4.4) were expressed as dimensionless indexes in relation to the initial condition (before the drying process). Tetrazolium tests were also used to evaluate the mechanical damages of seeds, along with sodium hypochlorite and X-Ray tests. In the sodium hypochlorite tests, four samples of 50 seeds per treatment were immersed in a sodium hypochlorite solution (2.5%) for 10 min according to Krzyzanowski et al. [45], being the fissured seeds counted after this period.

X-Ray analysis was performed employing the MultiFocus Digital Radiography System (MDRS) (FAPESP, grant # 2018/03807-6). Four samples of twenty-five seeds per treatment were placed in individual wells on an acrylic plate and fixed with transparent adhesive tape to keep the embryonic axis parallel to the plate, similar to Pinto et al. [19] and Melo et al. [46]. Seeds were exposed to the X-Ray emission source using an intensity of 25 kV. As well as tetrazolium tests, images from X-Ray were treated and the seeds were classified according to mechanical damages observed: class 1 (intact seeds), class 2E (non-severe damages in embryonic axis), class 2T (non-severe damages on tegument), and class 3 (severe damages). In the mechanical damage analysis, results from tetrazolium tests, sodium hypochlorite, and X-Ray were expressed in percentage of damaged seeds.

4.2.4 Statistical analysis

After checked the assumptions required for parametric methods according to Montgomery [47], results of the quality analysis were submitted to analysis of variance (ANOVA) and the means were compared by Tukey test (5%) using STATISTICA®.

4.3 RESULTS AND DISCUSSION

4.3.1 Drying curves

The drying results were presented as average values between the first and second experiments. As mentioned previously, the first experiment was performed for 4 h and the second experiment was performed until seeds reached moisture in the range from 12% to 13% (wet basis), which is considered adequate for safe seed storage [5]. This procedure was adopted in order to minimize the effect of different final moisture on quality. Thus, only the seeds from the second experiment were submitted to the quality analysis. Figure 4.2 presents the dimensionless moisture, as a function of drying time, for the continuous processes.

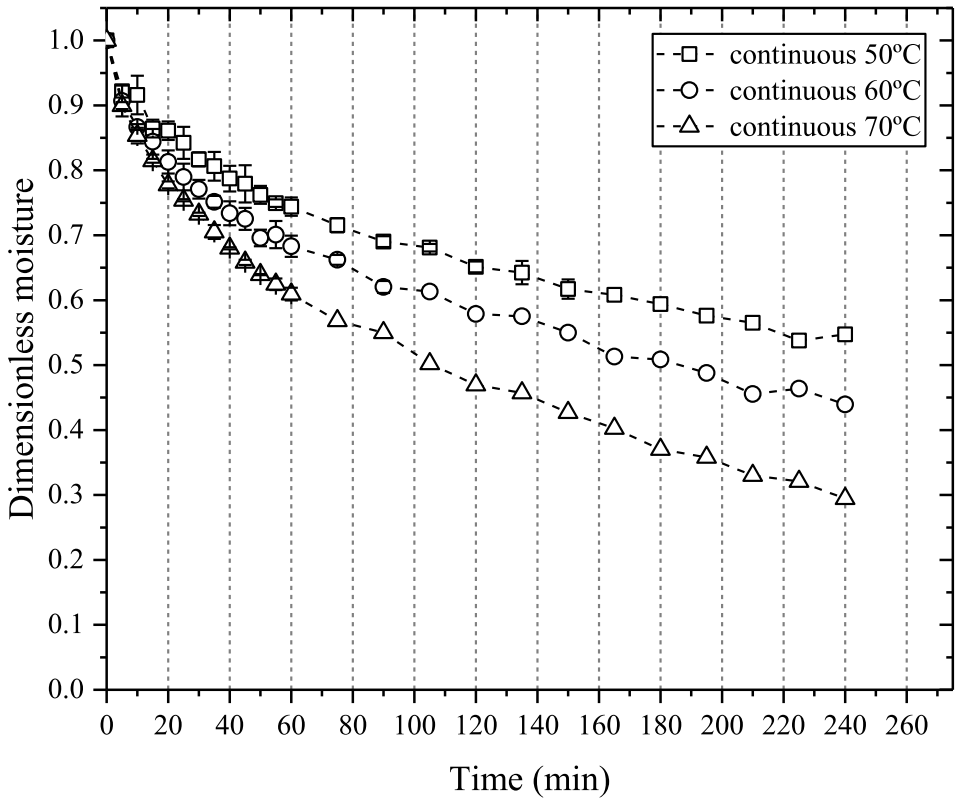

Figure 4.2. Dimensionless moisture, as a function of drying time, for (a) the processes with reduction of the air flow (intermittency A) and (b) the processes with interruption of the air flow (intermittency B).

Expected results were observed since increasing temperature caused the decrease of time drying to reach analogous dimensionless moisture. These results can be explained by the higher amount of thermal energy provided to the system. This trend was also observed for all intermittent conditions. In addition to thermal energy, higher saturation vapor pressure is obtained with the increase of air inlet temperature, which means higher driving force for mass transfer. Thus, a shorter drying time at 70°C was required to reach the same moisture content in comparison with conditions at 50°C and 60°C. Similar results were also obtained by Olazar et al. [48], who

performed the drying of biomass in a conical spouted bed and observed a significant reduction in the final sawdust moisture content with the increase of air inlet temperature. The authors attributed such findings as an additional advantage for the processing of biomass.

Figure 4.3 presents the dimensionless moisture, as a function of drying time, for the processes with reduction (4.3a) and interruption (4.3b) of the air flow.

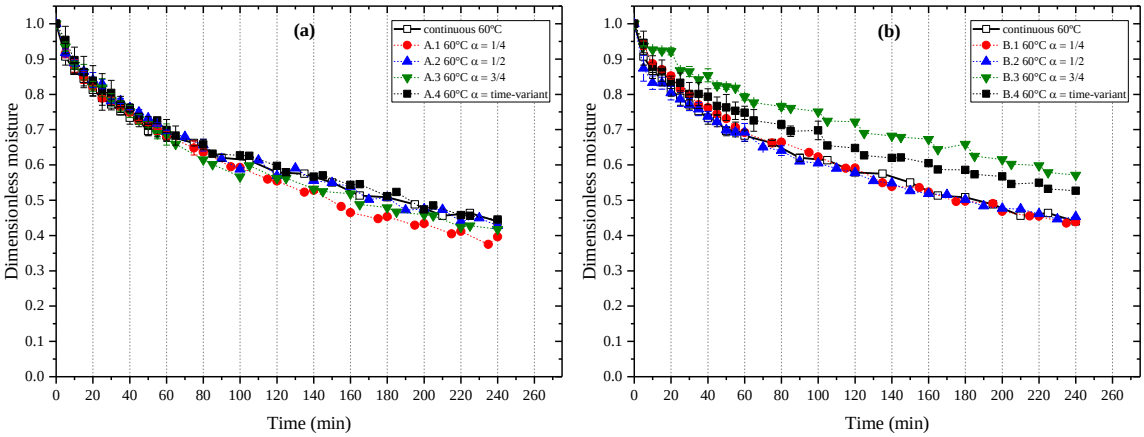

Figure 4.3. Dimensionless moisture, as a function of drying time, for (a) the processes with reduction of the air flow (intermittency A) and (b) the processes with interruption of the air flow (intermittency B) at 60°C.

No significant differences were observed in the processes with periodic reduction of the air flow (Figure 4.3a) and the data almost overlapped the continuous condition. Such results can be attributed to predominant mass transfer mechanisms involved in soybean drying. The behavior of continuous processes consists of an exponential decrease of dimensionless moisture approaching a condition of dynamic equilibrium in the final instants, suggesting the predominance of internal mass transfer resistances with falling drying rates throughout the process. Under such conditions,

the influence of external drying conditions is minimized and the process becomes less susceptible to air flow reductions, unlike the results obtained with alumina by Brito et al. [40] in which the reduction of air flow provided a more heterogeneous drying. These findings highlighted one of the main advantages of the methodology over the fixed bed and the continuous spouted bed process since the drying could be performed such as the conventional spouted bed process with lower air flow.

In the processes with periodic interruption of the air flow (Figure 4.3b), the overlapping with continuous drying also was observed for the conditions B.1 and B.2. These findings suggest that the tempering periods adopted in these conditions probably were insufficient to allow the redistribution of the internal moisture, which is one of the advantages of intermittency from the quality point of view (refreshing effect). Such results can be attributed to the dimensions and structural features of soybean, which probably demanded a higher tempering time. Higher temperatures could provide faster migration of water from the interior to the external surface of kernels soybean due to higher drying constant as observed by Nishiyama et al. [14]. However, the same trend was observed for 50°C and 70°C.

Conditions B.3 and B.4 presented periods of stabilization when the dimensionless moisture of the solids remained approximately constant and the decrease occurred in a stepwise way. Typical of processes employing intermittent drying with air flow interruption, these periods of stabilization corresponded to the air flow interruption intervals. As previously mentioned, this stepwise decrease can contribute to a better-quality product due to the redistribution of the internal moisture in the tempering period. Such redistribution causes a decrease of moisture and temperature gradients, providing the reduction of surface tensions that result in damages and cracking. Furthermore, the removal of moisture is favored after the tempering period due to

constant transfer towards the surface and greater vapor pressure difference between the interface and the air flow, enhancing the drying rate and providing similar final moisture content with shorter effective drying time [10, 49, 50]. Table 4.2 presents the effective drying time and the final dimensionless moisture values of the first experiment, which was performed for 4 h, for the processes with periodic interruption of the air flow at 60°C. As described previously, even with the shorter effective drying time, processes B.1 and B.2 presented final dimensionless moisture similar to the continuous process. However, the decrease of effective drying time of processes B.3 and B.4 in relation to the continuous process, which were of 75% and 69%, respectively, were significant and sufficient to provide higher final dimensionless moisture than continuous process.

Table 4.2. Effective drying time and final dimensionless moisture for different operating conditions at 60°C in the soybean drying process with interruption of the air flow (intermittency B).

Operating condition	Effective drying time (min)	Final dimensionless moisture
Continuous	240	0.44
B.1	180	0.44
B.2	120	0.45
B.3	60	0.57
B.4	75	0.53

The drying results evidenced the advantages of intermittency A (reduction of air flow) in relation to continuous processes, due to lower air flow, and suggested that tempering times adopted in B.1 and B.2 were insufficient to ensure the refreshing effect. However, an important issue remaining is to evaluate if better quality products were also obtained with the intermittency in the

spouted bed as in other dryers, mainly in processes B.3 and B.4 which probably provided the desired refreshing effect.

4.3.2 Quality analysis

4.3.2.1 Germination

Figure 4.4 presents the results of the germination index in function of temperature for intermittent conditions analogous. Germination obtained for the initial sample was 82.7 ± 3.8 %.

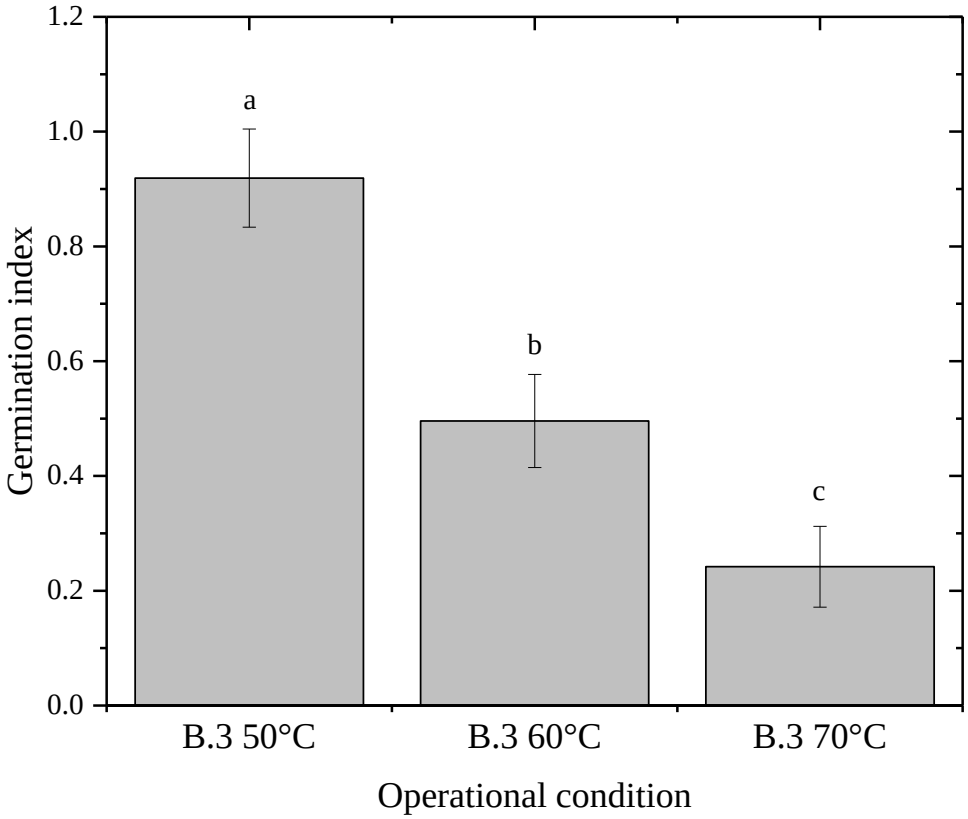

Figure 4.4. Germination index in function of temperature for intermittent conditions B.3. *Means followed by a different letter at a given graph are significantly different at p<.05 by Tukey test.

The decrease of germination index was observed increasing temperature, indicating higher

degradation of material viability. Such behavior was also observed for all other continuous and intermittent conditions employed in this work, as well as in several other studies performed with similar materials [4, 9, 51]. Among the various thermal damages bound to loss of seed viability, the disruption of cell membranes and protein denaturation are some related to seed structure [52].

Figure 4.5 presents the results of germination index in function of intermittent conditions for the temperature of 50°C, which provided a higher germination index than 60°C and 70°C.

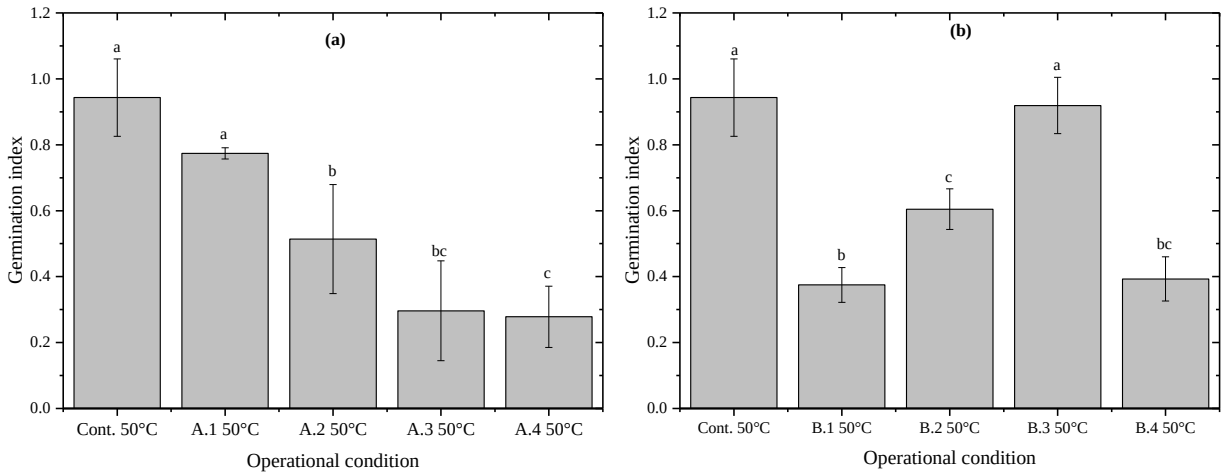

Figure 4.5. Germination index, as a function of intermittent conditions, for (a) the processes with reduction of the air flow (intermittency A) and (b) the processes with interruption of the air flow (intermittency B) at 50°C. *Means followed by a different letter at a given graph are significantly different at $p<.05$ by Tukey test.

In relation to intermittency **A**, the decrease of germination index was observed with the increase of ratio intermittency, being the higher germination index represented by the A.1 and continuous process. Considering means values, the reductions in relation to continuous process were 18.0%, 45.5%, 68.6%, and 70.5% for the conditions A.1, A.2, A.3, and A.4, respectively.

Thus, the processes with shorter drying time under lower air flows provided seeds with greater viability. These findings suggest that longer times of reduced air flow and direct air contact with the seeds contribute to greater viability loss. The reduction of the air flow led to longer residence time and confinement of most of the drying air in an internal spout, which is inherent to the mechanism of transition from a static to a spouting condition [53]. Thus, besides temperature, the exposure time of seeds to drying conditions was also an important variable for the material viability, as similarly verified in other studies [54, 55].

Exposure time can also support the influence of intermittency **B** (interruptions of air flow) in which an increase of intermittency ratio contributed to the increase of germination index whether constant intermittency ratios are considered. A higher germination index was obtained for condition B.3, providing germination even at 70°C (Figure 4.4), temperature at which there was no germination for any other intermittent conditions. These results can be attributed to the shorter effective drying time obtained with the periodic interruption of air flow, also enabling the refreshing effect described previously and the decrease of kernel temperature. Thus, higher the intermittency rate and interrupted air flow period provide lower viability loss. Interestingly, the values of germination index obtained for other intermittent conditions (B.1, B.2, and B.4) were lower than the value obtained for continuous process. This finding suggests a gap regarding the application of the intermittency with interruption of air flow in the spouted bed, since, despite its advantages, the methodology was insufficient to provide a product with better viability. These results can be bound to tempering periods adopted, demanding the analysis of the other properties of soybean seeds such as vigor and mechanical damage.

4.3.2.2 First count and seedling length

Table 4.3 and Figure 4.6 present the results of seedling total length index and first germination count index, respectively, in function of intermittent conditions for the temperature of 50°C, since processes at 60°C and 70°C provided greater vigor reduction with a tendency similar to the germination index. The first count and seedling length obtained for the initial sample were 74.7 ± 1.8 % and 15.1 ± 0.2 cm, respectively.

Table 4.3. Seedling total length for the different intermittent conditions employed at 50°C.

Run	Seedling total length index
Cont. 50°C	0.94 ± 0.07 [a*]
A.1 50°C	0.84 ± 0.08 [ac]
A.2 50°C	0.81 ± 0.05 [ac]
A.3 50°C	0.48 ± 0.05 [b]
A.4 50°C	0.45 ± 0.13 [b]
B.1 50°C	0.53 ± 0.02 [b]
B.2 50°C	0.72 ± 0.04 [c]
B.3 50°C	0.72 ± 0.08 [c]
B.4 50°C	0.47 ± 0.04 [b]

*Means followed by a different letter at a given column are significantly different at p<.05 by Tukey test.

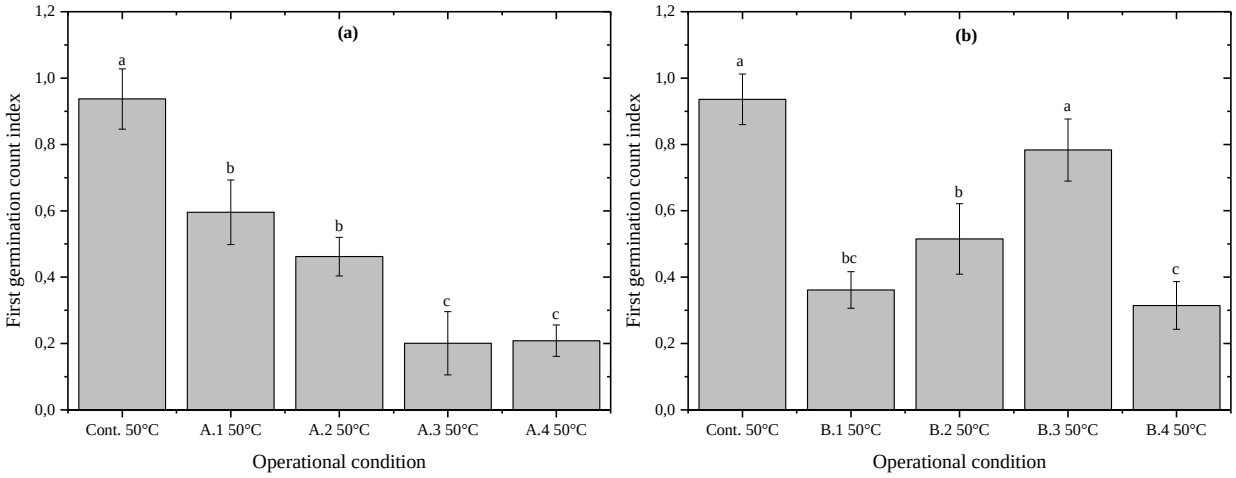

Figure 4.6. First Germination Count Index, as a function of intermittent conditions, for (a) the processes with reduction of the air flow (intermittency A) and (b) the processes with interruption of the air flow (intermittency B) at 50°C. *Means followed by a different letter at a given graph are significantly different at p<.05.

Regarding First Germination Count Index (Figure 4.6), behaviors and trends similar to the germination index (Figure 4.5) were observed, being the higher value obtained for continuous process followed by conditions A.1 and B.3. However, unlike the germination index, condition A.1 presented statistically significant differences in relation to the continuous process, suggesting the vigor loss. Likewise, Table 4.3 presented a lower distinction of the condition B.3 in relation to the other intermittent conditions. Despite the greater viability, these findings suggested lower vigor for both conditions (A.1 and B.3) indicating the latent effect on seeds of most of the damage in these conditions. Considering such results, the physiological properties were also analyzed by tetrazolium tests, which could contribute significantly enabling the identification of possible causes for the physiological potential reduction.

4.3.2.3 Tetrazolium Tests

As described previously, the classification of seeds was performed as described by França-Neto et al. [44], according to vigor: Class 1 (highest vigor), Class 2 (high vigor), Class 3 (medium vigor), Class 4 (low vigor), Class 5 (very low vigor), Class ≥6 (dead seeds). Thus, Table 4.4 presents the tetrazolium index obtained for all operational conditions employed and Figure 4.7 presents the tetrazolium classification (%) for continuous and intermittent drying at 50°C. Tetrazolium percentages obtained for initial sample were 46.8 ± 4.6 % (class 1), 44.3 ± 4.5 % (class 2-3), 6.6 ± 0.9 % (class 4-5), and 4.2 ± 1.0 % (class 6).

Table 4.4. Soybean seed vigor classification obtained in tetrazolium tests for the different operating conditions employed.

Run	TETRAZOLIUM INDEX			
	Classification			
	1	2-3	4-5	≥ 6
Cont.50°C	0.45 ± 0.10	1.22 ± 0.27	2.35 ± 1.01	2.14 ± 1.04
A.1 50°C	0.52 ± 0.18	1.02 ± 0.07	2.65 ± 0.99	3.33 ± 0.82
A.2 50°C	0.31 ± 0.11	1.09 ± 0.18	2.88 ± 0.55	4.17 ± 1.59
A.3 50°C	0.21 ± 0.18	1.05 ± 0.33	3.33 ± 0.64	5.12 ± 2.03
A.4 50°C	0.07 ± 0.09	0.49 ± 0.24	2.95 ± 1.36	12.74 ± 2.24
B.1 50°C	0.00 ± 0.00	0.11 ± 0.13	1.74 ± 1.44	19.88 ± 3.24
B.2 50°C	0.02 ± 0.02	0.54 ± 0.23	2.27 ± 0.82	14.17 ± 5.15
B.3 50°C	0.12 ± 0.07	0.84 ± 0.20	1.59 ± 0.58	11.19 ± 2.09
B.4 50°C	0.03 ± 0.04	0.17 ± 0.11	2.88 ± 1.14	17.50 ± 3.27
Cont. 60°C	0.17 ± 0.03	1.08 ± 0.13	3.86 ± 0.13	4.40 ± 1.36
A.1 60°C	0.15 ± 0.06	1.11 ± 0.24	3.64 ± 1.01	4.40 ± 1.56
A.2 60°C	0.03 ± 0.04	0.91 ± 0.24	4.17 ± 0.39	7.38 ± 2.58
A.3 60°C	0.12 ± 0.10	0.86 ± 0.14	4.17 ± 1.27	6.90 ± 1.09
A.4 60°C	0.00 ± 0.00	0.15 ± 0.15	2.27 ± 0.76	18.45 ± 3.02
B.1 60°C	0.00 ± 0.00	0.08 ± 0.07	2.12 ± 0,74	19.64 ± 1.86
B.2 60°C	0.02 ± 0.02	0.23 ± 0.25	1.82 ± 0.64	18.21 ± 3.89
B.3 60°C	0.07 ± 0.08	0.26 ± 0.17	1.97 ± 1.18	17.14 ± 5.21
B.4 60°C	0.00 ± 0.00	0.07 ± 0.07	0.98 ± 0.45	21.43 ± 1.30
Cont. 70°C	0.00 ± 0.00	0.05 ± 0.06	2.58 ± 1.40	19.29 ± 1.83
A.1 70°C	0.02 ± 0.04	0.05 ± 0.06	0.83 ± 0.58	22.02 ± 1.32
A.2 70°C	0.00 ± 0.00	0.05 ± 0.03	0.98 ± 0.87	21.55 ± 1.70
A.3 70°C	0.01 ± 0.02	0.20 ± 0.15	2.27 ± 0.97	18.10 ± 2.26
A.4 70°C	0.00 ± 0.00	0.00 ± 0.00	0.15 ± 0.15	23.21 ± 0.52
B.1 70°C	0.00 ± 0.00	0.02 ± 0.02	0.30 ± 0.30	23.10 ± 0.71
B.2 70°C	0.00 ± 0.00	0.00 ± 0.00	0.38 ± 0.50	23.10 ± 0.79
B.3 70°C	0.00 ± 0.00	0.30 ± 0.15	2.27 ± 0.69	17.26 ± 2.22
B.4 70°C	0.00 ± 0.00	0.01 ± 0.02	0.15 ± 0.26	23.33 ± 0.58

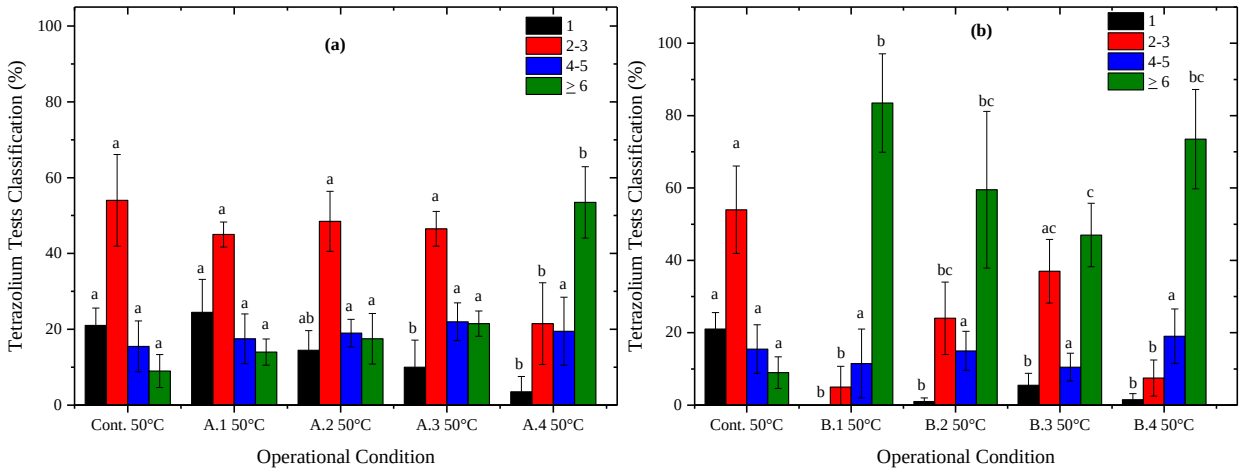

Figure 4.7. Soybean seed classification obtained in tetrazolium tests, as a function of intermittent conditions, for (a) the processes with reduction of the air flow (intermittency A) and (b) the processes with interruption of the air flow (intermittency B) at 50°C. *Means followed by a different letter at a given column are significantly different at p<.05 by Tukey test.

Table 4.4 showed the increase of seeds classified as 4-5 and ≥6 with the increase of temperature, evidencing the greater vigor loss, as also observed for seedling length and first germination index. These findings suggested that temperatures above 50°C are inadequate for seeds drying in the spouted bed when physiological parameters are required even considering intermittent conditions. At 50°C, the highest percentages of seeds classified as 2 and 3 were obtained in the processes continuous, A.1, A.2, and A.3, since no statistically significant differences were observed between the means (Figure 4.7). Likewise, no statistically significant differences were observed in these conditions between the means of classifications 4-5 and ≥6. For the other intermittent conditions, with both reduction and interruption of air flow, there was a sharp increase in the percentage of seeds classified in 6-8. These findings agreed with the results of the seedling total length index (Table 4.3), indicating that condition B.3 at 50°C, despite the

greater viability, provided the lower vigor in the spouted bed. Therefore, considering the physiological aspects, the processes continuous and A.1, both at 50°C, provided a lower degree of seed deterioration.

These findings were contrary to previous studies which have highlighted the advantages of intermittent drying for quality, mainly in relation to processes with periodic interruption of air flow because of the refreshing effect mentioned previously [11, 14, 49, 56]. Thus, it can be assumed that the trends of intermittency in the spouted bed are significantly different than other dryers. A possible explanation for this contradiction can be based on the analysis of the mechanical damage of the seeds processing in the spouted bed.

4.3.2.4 Analysis of mechanical damage

Figure 4.8 presents the results of mechanical damage obtained in the sodium hypochlorite tests for processes at 50°C since greater physiological potential loss were obtained at 60°C and 70°C, as previously presented and mentioned.

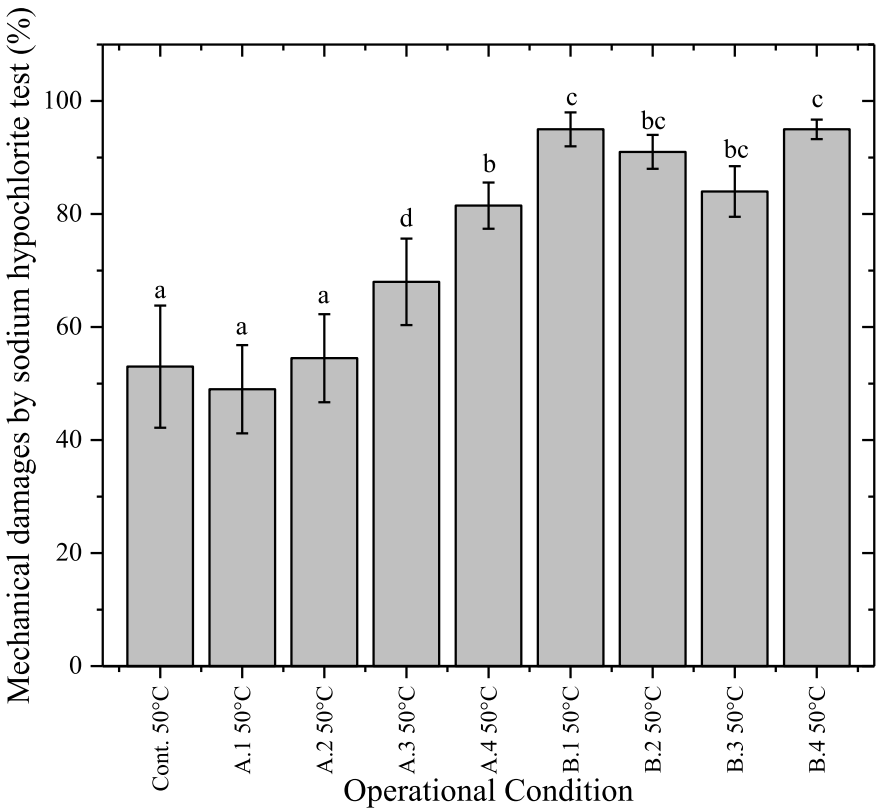

Figure 4.8. Results of mechanical damage by sodium hypochlorite in function of continuous and intermittent conditions for processes at 50°C. *Means followed by a different letter at a given column are significantly different at p<.05 by Tukey test.

The increase of intermittency ratio **A** caused the increase of damaged seeds, presenting a clear trend. No statistically significant differences were observed between processes continuous, A.1, and A.2. These findings can be attributed to the longer time under lower air flows (static bed) with the increase of intermittency ratio **A**, providing a longer exposure period of seeds in direct contact with air heated. Thus, seeds were more susceptible to cracks and fissures due to higher surface tensions with the heating and higher temperature and concentration gradients, which are harmful to quality seeds as described by Barrozo et al. [9]. Furthermore, the high degree of

agitation provided by spouted bed leads to a high percentage of damaged seeds.

In the intermittency **B**, there was a tendency to decrease mechanical damage with increasing intermittency ratio **B**, although no significant statistical differences were observed between different intermittent conditions employed. This trend can be attributed to the longer passive period of drying with increasing intermittency ratio **B**, as well as the refreshing effect with the interruption of air flow and the decrease of seed temperature. However, the mechanical damages observed in the continuous condition were lower than the intermittent conditions with interruption of air flow. This result can be justified considering the fluid dynamic regime of spouted bed, since the periodic interruptions of air flow successively submitted the seeds to a condition of maximum pressure drop, providing higher drag and buoyancy forces on the particles required to establish the spouting regime. Hence, the application of intermittency with periodic interruption of air flow in the spouted bed contributed to obtaining a more intense seed friction condition than continuous process, providing greater mechanical damages. Contrary results have been obtained applying similar intermittent methodology for drying of soybeans in different dryers as Jung and Yoon [17], who verified the decrease of damaged seeds with the application of intermittency. It's worth mentioning that the sodium hypochlorite tests provide only information about total damage, providing general information about mechanical damages without classifying such damages.

Thus, as performed in the vigor analysis, the mechanical damages were classified by tetrazolium tests, considering superficial damage in tegument (classes 1-3), damage to the embryonic axis and cotyledon (classes 4-5), and inviable seeds (class 6). Figure 4.9 presents the results obtained in the classification of mechanical damage.

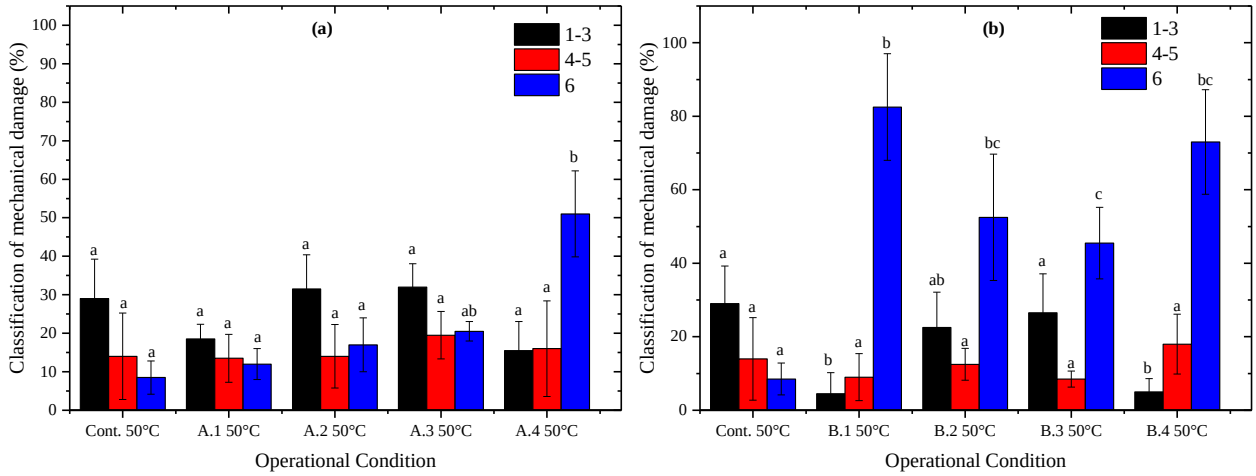

Figure 4.9. Mechanical damage classification of soybean seeds obtained in tetrazolium tests, as a function of intermittent conditions, for (a) the processes with reduction of the air flow (intermittency A) and (b) the processes with interruption of the air flow (intermittency B) at 50°C. *Means followed by a different letter at a given column are significantly different at p<.05 by Tukey test.

In Figure 4.9a, processes continuous, A.1, A.2, and A.3 presented a higher percentage of superficial damage in tegument (classes 1-3), and no significant statistical differences were observed between such conditions. All other conditions, including intermittency **B**, presented a sharper increase of seeds classified as non-viable (class 6), corroborating with the physiological and mechanical results presented and discussed previously. These findings suggested that the mechanical damages provided by intermittency **B** were more harmful to seed quality than continuous and intermittency **A** processes, indicating the unfeasibility of such methodology in the spouted bed when better quality products are required.

Figure 4.10 presents the results obtained in the X-Ray tests.

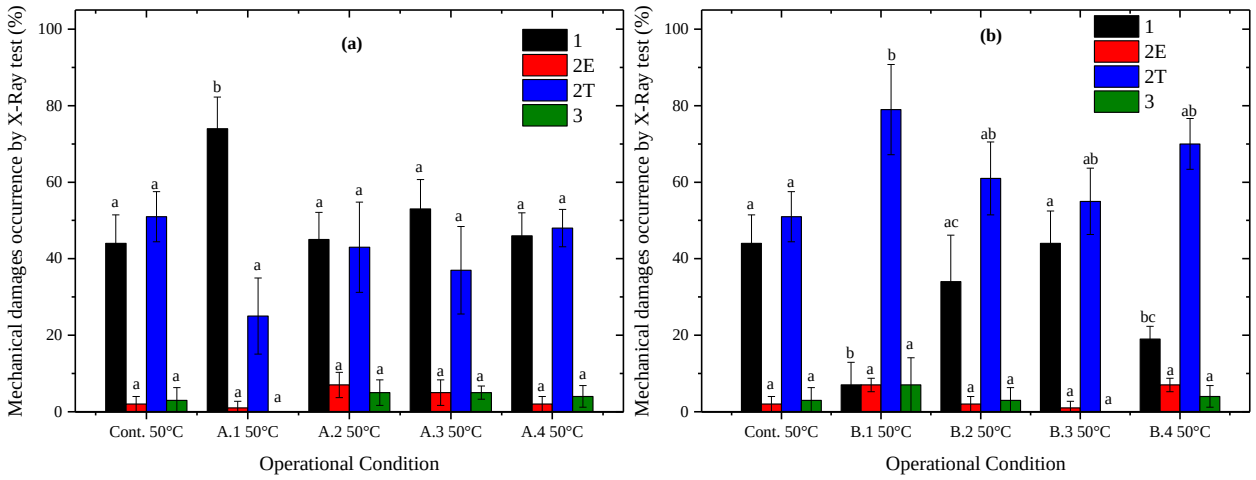

Figure 4.10. Mechanical damage classification of soybean seeds obtained in X-Ray tests, as a function of intermittent conditions, for (a) the processes with reduction of the air flow (intermittency A) and (b) the processes with interruption of the air flow (intermittency B) at 50°C. *Means followed by a different letter at a given column are significantly different at p<.05 by Tukey test. *1 = intact seeds; 2E = non-severe damage to the embryo; 2T = non-severe damage to the tegument; 3 = severe damage.

In Figure 4.10a, process **A.1** presented a higher percentage of intact seeds (class 1) comparing with continuous and other intermittent processes **A**. In relation to non-severe (class 2) and severe (class 3) damages, no significant statistical differences were observed between the different intermittent ratio **A**, similarly to tetrazolium tests results. These findings, together with sodium hypochlorite and tetrazolium tests, suggested that most of both viability and vigor loss were due to damages (imminent and latent) caused by the higher heating with the reduction of the air flow as described previously. Regarding intermittency **B (**Figure 4.10b), condition **B.1** presented a higher percentage of tegument damage and a lower percentage of intact seeds. Likewise, intermittency **B** overall presented both a higher percentage of tegument damages and a

lower percentage of intact seeds than to the other conditions (continuous and intermittent **A**). Results of condition **B.1** suggested the greater mechanical damage of seeds in conditions with larger effective drying periods followed by shorter interruption periods, probably due to the combined effect of insufficient tempering time and more intense seed friction condition.

4.4 CONCLUSIONS

The processes continuous and A.1, both at 50°C, provided the lower degree of seed deterioration, considering both physiological and physical aspects. Processes A.1 and B.3 provided higher viabilities than other conditions, presenting a minor distinction in relation to vigor loss. The results obtained in the analysis of mechanical damage indicated that mechanical damages of seeds caused by methodology **B** were more harmful to physiological properties than damages caused by intermittency **A**, in which heating was more determinant for such properties. Furthermore, mechanical damages of continuous condition in the spouted bed due to high degree agitation were not as harmful to physiological properties as heating damages, suggesting that further studies under lower temperatures can provide good quality results. Therefore, the findings of this study contributed to identifying the distinct trend of intermittency application in the spouted bed in relation to other dryers when seed quality attributes are demanded.

ACKNOWLEDGEMENTS

The authors appreciate the financial support provided by Coordination for the Improvement of Higher Education Personnel (CAPES), the São Paulo State Research Foundation (FAPESP, grant #2017/01856-7), and FAPESP/ESALQ/USP (grant #2018/03807-6).

REFERENCES

[1] Kowalski, S. J.; Pawłowski, A. Energy Consumption and Quality Aspect by Intermittent Drying. *Chem. Eng. Process. Process Intensif.*, **2011**, *50* (4), 384–390. https://doi.org/10.1016/j.cep.2011.02.012.

[2] Ghasemi, A.; Sadeghi, M.; Mireei, S. A. Multi-Stage Intermittent Drying of Rough Rice in Terms of Tempering and Stress Cracking Indices and Moisture Gradients Interpretation. *Dry. Technol.*, **2018**, *36* (1), 109–117. https://doi.org/10.1080/07373937.2017.1303777.

[3] Kudra, T.; Niewczas, I.; Szot, B.; Raghavan, G. S. V. Stress Cracking During High-Intensity Drying and Its Effect on Grain Quality. *Dry. Technol.*, **1996**, *14* (2), 367–380. https://doi.org/10.1080/07373939608917102.

[4] Barrozo, M. A. S.; Felipe, C. A. S.; Sartori, D. J. M.; Freire, J. T. Quality of Soybean Seeds Undergoing Moving Bed Drying: Countercurrent and Crosscurrent Flows. *Dry. Technol.*, **2006**, *24* (4), 415–422. https://doi.org/10.1080/07373930600611638.

[5] Souza, G. F. M. V; Miranda, R. F.; Barrozo, M. A. S. Soybean (Glycine Max L. Merrill) Seed Drying in Fixed Bed: Process Heterogeneity and Seed Quality. *Dry. Technol.*, **2015**, *33* (14), 1779–1787. https://doi.org/10.1080/07373937.2015.1039542.

[6] Suzy Zeng, X.; Roger Ruan, R.; Fulcher, R. G.; Chen, P. Evaluation of Soybean Seedcoat Cracking during Drying: Part II. Using MRI. *Dry. Technol.*, **1996**, *14* (7–8), 1595–1623. https://doi.org/10.1080/07373939608917165.

[7] Felipe, C. A. S.; Barrozo, M. A. S. Drying of Soybean Seeds in a Concurrent Moving Bed: Heat and Mass Transfer and Quality Analysis. *Dry. Technol.*, **2003**, *21* (3), 439–456. https://doi.org/10.1081/DRT-120018456.

[8] Wiriyaumpaiwong, S.; Soponronnarit, S.; Prachayawarakorn, S. Soybean Drying by Two-Dimensional Spouted Bed. *Dry. Technol.*, **2003**, *21* (9), 1735–1757. https://doi.org/10.1081/DRT-120025506.

[9] Barrozo, M. A. S.; Mujumdar, A.; Freire, J. T. Air-Drying of Seeds: A Review. *Dry. Technol.*, **2014**, *32* (10), 1127–1141. https://doi.org/10.1080/07373937.2014.915220.

[10] Kumar, C.; Karim, M. A.; Joardder, M. U. H. Intermittent Drying of Food Products: A Critical Review. *J. Food Eng.*, **2014**, *121* (1), 48–57. https://doi.org/10.1016/j.jfoodeng.2013.08.014.

[11] Chua, K. J.; Mujumdar, A. S.; Chou, S. K. Intermittent Drying of Bioproducts - An Overview. *Bioresour. Technol.*, **2003**, *90* (3), 285–295. https://doi.org/10.1016/S0960-8524(03)00133-0.

[12] Mierzwa, D.; Szadzińska, J.; Pawłowski, A.; Pashminehazar, R.; Kharaghani, A. Nonstationary Convective Drying of Raspberries, Assisted by Microwaves and Ultrasound. *Dry. Technol.*, **2019**, *0* (0), 1–14. https://doi.org/10.1080/07373937.2018.1481087.

[13] Ju, H. Y.; Zhao, S. H.; Mujumdar, A. S.; Zhao, H. Y.; Duan, X.; Zheng, Z. A.; Gao, Z. J.; Xiao, H. W. Step-down Relative Humidity Convective Air Drying Strategy to Enhance Drying Kinetics, Efficiency, and Quality of American Ginseng Root (Panax Quinquefolium). *Dry. Technol.*, **2019**, *3937*. https://doi.org/10.1080/07373937.2019.1597373.

[14] Nishiyama, Y.; Cao, W.; Li, B. Grain Intermittent Drying Characteristics Analyzed by a Simplified Model. *J. Food Eng.*, **2006**, *76* (3), 272–279. https://doi.org/10.1016/j.jfoodeng.2005.04.059.

[15] Zhu, Z.; Yang, Z.; Wang, F. Experimental Research on Intermittent Heat Pump Drying with

Constant and Time-Variant Intermittency Ratio. *Dry. Technol.*, **2016**, *34* (13), 1630–1640. https://doi.org/10.1080/07373937.2016.1138966.

[16] Xu, F.; Chen, Z.; Huang, M.; Li, C.; Zhou, W. Effect of Intermittent Microwave Drying on Biophysical Characteristics of Rice. *J. Food Process Eng.*, **2017**, *40* (6). https://doi.org/10.1111/jfpe.12590.

[17] Jung, H.; Yoon, W. B. The Effect of Intermittent Drying on the Cracking Ratio of Soybeans (Glycine Max) at Different Relative Humidity Using Reaction Engineering Approach Modeling. *Food Sci. Nutr.*, **2018**, *6* (6), 1492–1500. https://doi.org/10.1002/fsn3.709.

[18] Dondee, S.; Meeso, N.; Soponronnarit, S.; Siriamornpun, S. Reducing Cracking and Breakage of Soybean Grains under Combined Near-Infrared Radiation and Fluidized-Bed Drying. *J. Food Eng.*, **2011**, *104* (1), 6–13. https://doi.org/10.1016/j.jfoodeng.2010.11.018.

[19] Pinto, T. L. F.; Cicero, S. M.; França-Neto, J. B.; Forti, V. A. An Assessment of Mechanical and Stink Bug Damage in Soybean Seed Using X-Ray Analysis Test. *Seed Sci. Technol.*, **2009**, *37* (1), 110–120. https://doi.org/10.15258/sst.2009.37.1.13.

[20] Oliveira, C.; Rocha, S. Intermittent Drying of Beans in a Spouted Bed. *Brazilian J. Chem. Eng.*, **2007**, *24* (04), 571–585. https://doi.org/10.1590/S0104-66322007000400010.

[21] Bon, J.; Kudra, T. Enthalpy-Driven Optimization of Intermittent Drying. *Dry. Technol.*, **2007**, *25* (4), 523–532. https://doi.org/10.1080/07373930701226880.

[22] Passos, M. L.; Mujumdar, A. S.; Vijaya, G.; Raghavan, V. G. S. Spouted and Spout-Fluidized Beds for Gram Drying. *Dry. Technol.*, **1989**, *7* (4), 663–696. https://doi.org/10.1080/07373938908916621.

[23] Peterson, W. S. Spouted Bed Drier. *Can. J. Chem. Eng.*, **1962**, *40* (5), 226–230. https://doi.org/10.1002/cjce.5450400512.

[24] Vieira, G. N. A.; Olazar, M.; Freire, J. T.; Freire, F. B. Real-Time Monitoring of Milk Powder Moisture Content during Drying in a Spouted Bed Dryer Using a Hybrid Neural Soft Sensor. *Dry. Technol.*, **2019**, *37* (9), 1184–1190. https://doi.org/10.1080/07373937.2018.1492614.

[25] Jayatunga, G. K.; Amarasinghe, B. M. W. P. K. Drying Kinetics, Quality and Moisture Diffusivity of Spouted Bed Dried Sri Lankan Black Pepper. *J. Food Eng.*, **2019**, *263*, 38–45. https://doi.org/10.1016/j.jfoodeng.2019.05.023.

[26] Dantas, S. C. de M.; Pontes Júnior, S. M. de; Medeiros, F. G. M. de; Santos Júnior, L. C.; Alsina, O. L. S. de; Medeiros, M. de F. D. de. Spouted-bed Drying of Acerola Pulp (Malpighia Emarginata DC): Effects of Adding Milk and Milk Protein on Process Performance and Characterization of Dried Fruit Powders. *J. Food Process Eng.*, **2019**, 1–13. https://doi.org/10.1111/jfpe.13205.

[27] Brito, R. C.; Sousa, R. C.; Béttega, R.; Freire, F. B.; Freire, J. T. Analysis of the Energy Performance of a Modified Mechanically Spouted Bed Applied in the Drying of Alumina and Skimmed Milk. *Chem. Eng. Process. Process Intensif.*, **2018**, *130*, 1–10. https://doi.org/10.1016/j.cep.2018.05.014.

[28] Barros, J. P. A. A.; Ferreira, M. C.; Freire, J. T. Spouted Bed Drying on Inert Particles: Evaluation of Particle Size Distribution of Recovered, Accumulated and Elutriated Powders. *Dry. Technol.*, **2019**, *0* (0), 1–12. https://doi.org/10.1080/07373937.2019.1656644.

[29] Tellabide, M.; Estiati, I.; Pablos, A.; Altzibar, H.; Aguado, R.; Olazar, M. New Operation Regimes in Fountain Confined Conical Spouted Beds. *Chem. Eng. Sci.*, **2019**, *211*, 115255. https://doi.org/10.1016/j.ces.2019.115255.

[30] Estiati, I.; Altzibar, H.; Tellabide, M.; Olazar, M. A New Method to Measure Fine Particle Circulation Rates in Draft Tube Conical Spouted Beds. *Powder Technol.*, **2017**, *316*, 87–91. https://doi.org/10.1016/j.powtec.2017.01.040.

[31] Estiati, I.; Tellabide, M.; Saldarriaga, J. F.; Altzibar, H.; Olazar, M. Fine Particle Entrainment in Fountain Confined Conical Spouted Beds. *Powder Technol.*, **2019**, *344*, 278–285. https://doi.org/10.1016/j.powtec.2018.12.035.

[32] Pablos, A.; Aguado, R.; Vicente, J.; Altzibar, H.; Bilbao, J.; Olazar, M. Effect of Operating Conditions on the Drying of Fine and Ultrafine Sand in a Fountain Confined Conical Spouted Bed. *Dry. Technol.*, **2019**, *0* (0), 1–16. https://doi.org/10.1080/07373937.2019.1645684.

[33] Rocha, A. P. T.; Lisboa, H. M.; Alsina, O. L. S.; Silva, O. S. Coating Process of Phyllanthus Niruri Linn Granules Using Spouted Bed. *Powder Technol.*, **2018**, *336*, 85–91. https://doi.org/10.1016/j.powtec.2018.05.052.

[34] Liu, M.; Chen, M.; Liu, R.; Chang, J.; Shao, Y.; Liu, B.; Tang, Y. Scale-up Strategy Study of Coating Furnace for TRISO Particle Fabrication Based on Numerical Simulations. *Nucl. Eng. Des.*, **2018**, *357*, 110413. https://doi.org/10.1016/j.nucengdes.2019.110413.

[35] Pietsch, S.; Peter, A.; Wahl, P.; Khinast, J.; Heinrich, S. Measurement of Granule Layer Thickness in a Spouted Bed Coating Process via Optical Coherence Tomography. *Powder Technol.*, **2019**, *356*, 139–147. https://doi.org/10.1016/j.powtec.2019.08.022.

[36] Niksiar, A.; Nasernejad, B. Modeling of Gasification Reaction to Produce Activated Carbon from Pistachio Shells in a Spouted Bed. *Biomass and Bioenergy*, **2018**, *119*, 97–108. https://doi.org/10.1016/j.biombioe.2018.09.008.

[37] Lopez, G.; Alvarez, J.; Amutio, M.; Hooshdaran, B.; Cortazar, M.; Haghshenasfard, M.;

Hosseini, S. H.; Olazar, M. Kinetic Modeling and Experimental Validation of Biomass Fast Pyrolysis in a Conical Spouted Bed Reactor. *Chem. Eng. J.*, **2019**, *373*, 677–686. https://doi.org/10.1016/j.cej.2019.05.072.

[38] Saldarriaga, J. F.; Estiati, I.; Atxutegi, A.; Aguado, R.; Bilbao, J.; Olazar, M. Distribution of Cycle Times in Sawdust Conical Spouted Bed Equipped with Fountain Confiner and Draft Tube. *Ind. Eng. Chem. Res.*, **2019**, *58* (5), 1932–1940. https://doi.org/10.1021/acs.iecr.8b03451.

[39] Boujjat, H.; Rodat, S.; Chuayboon, S.; Abanades, S. Experimental and Numerical Study of a Directly Irradiated Hybrid Solar/Combustion Spouted Bed Reactor for Continuous Steam Gasification of Biomass. *Energy*, **2019**, *189*, 116118. https://doi.org/10.1016/j.energy.2019.116118.

[40] Brito, R. C.; Béttega, R.; Freire, J. T. Energy Analysis of Intermittent Drying in the Spouted Bed. *Dry. Technol.*, **2019**, *37* (12), 1498–1510. https://doi.org/10.1080/07373937.2018.1512503.

[41] Batista, J. N. M.; Brito, R. C.; Béttega, R. Influence of Inlet Air Distributor Geometry on the Fluid Dynamics of Conical Spouted Beds: A Cfd Study. *Chem. Ind. Chem. Eng. Q.*, **2018**, *24* (4), 369–378. https://doi.org/10.2298/CICEQ171011009B.

[42] MATHUR, K. B.; EPSTEIN, N. *Spouted Beds*; Academic Press: New York, 1974.

[43] BRASIL. *Ministério Da Agricultura, Pecuária e Abastecimento. Regras Para Análise de Sementes*; MAPA/ACS: Brasília, 2009.

[44] França Neto, J.; Krzyzanowski, F.; da Costa, N. *O Teste de Tetrazólio Em Sementes de Soja*; EMBRAPA-CNPSo: Londrina, 1998.

[45] Krzyzanowski, F. C.; França-Neto, J. de B.; Costa, N. P. da. Teste Do Hipoclorito de Sódio

Para Semente de Soja. *Circ. Técnica/Embrapa Soja*, **2004**, No. 37, 1–4.

[46] Melo, R. de A.; Forti, V. A.; Cicero, S. M.; Novembre, A. D.; Melo, P. C. T. de. Use of X-Ray to Evaluate Damage Caused by Weevils in Cowpea Seeds. *Hortic. Bras.*, **2010**, *28* (4), 472–476. https://doi.org/10.1590/S0102-05362010000400016.

[47] Montgomery, D. *Design and Analysis of Experiments*, eighth.; John Wiley & Sons, 2013.

[48] Olazar, M.; Lopez, G.; Altzibar, H.; Amutio, M.; Bilbao, J. Drying of Biomass in a Conical Spouted Bed with Different Types of Internal Devices. *Dry. Technol.*, **2012**, *30*, 207–216. https://doi.org/10.1080/07373937.2011.633194.

[49] Defraeye, T. Towards More Efficient Intermittent Drying of Fruit: Insights from Combined Hygrothermal-Quality Modelling. *Innov. Food Sci. Emerg. Technol.*, **2016**. https://doi.org/10.1016/j.ifset.2016.10.003.

[50] Jumah, R.; Al-Kteimat, E.; Al-Hamad, A.; Telfah, E. Constant and Intermittent Drying Characteristics of Olive Cake. *Dry. Technol.*, **2007**, *25* (9), 1417–1422. https://doi.org/10.1080/07373930701536668.

[51] Laoretani, D.; Gely, M. C.; Nolasco, S. Effect of Two Drying Processes about Soybean Seed Quality. *Agric. Eng. Int. CIGR J.*, **2017**, *19* (4), 124–132.

[52] Daniell, J. W.; Chappell, W. E.; Couch, H. B. Effect of Sublethal and Lethal Temperature on Plant Cells. *Plant Physiol.*, **1969**, *44* (12), 1684–1689. https://doi.org/10.1104/pp.44.12.1684.

[53] Malek, M. A.; Lu, B. C. Y. Pressure Drop and Spoutable Bed Height in Spouted Beds. *Ind. Eng. Chem. Process Des. Dev.*, **1965**, *4* (1), 123–128. https://doi.org/10.1021/i260013a027.

[54] Herter, U.; Burris, J. S. Changes in Moisture, Temperature, and Quality of Corn Seed during High-Temperature Drying. *Can. J. Plant Sci.*, **1989**, *69* (3), 749–761.

[55] Herter, U.; Burris, J. S. Effect of Drying Rate and Temperature on Drying Injury of Corn Seed. *Can. J. Plant Sci.*, **1989**, *69* (3), 763–774. https://doi.org/10.4141/cjps89-092.

[56] Filippin, A. P.; Molina Filho, L.; Fadel, V.; Mauro, M. A. Thermal Intermittent Drying of Apples and Its Effects on Energy Consumption. *Dry. Technol.*, **2018**, 1–16. https://doi.org/10.1080/07373937.2017.1421549.

CHAPTER 5

MATHEMATICAL MODELLING OF INTERMITTENT DRYING

In this chapter, which is focused on specific objective (3) of this thesis, the model proposed for intermittent drying is described. The mathematical modelling of this technique remains a challenging task, especially in spouted bed dryers. Thus, the paper described in this chapter aims to propose a fully predictive model for intermittent drying in a conical spouted bed dryer. A single-phase model is used to represent mass and heat transfer at the surface and inside of single particles, and the predictions are compared with experimental results of both continuous and intermittent soybean drying in a spouted bed. The model proposed provides physically consistent results and good agreement with experimental measurements, mainly for drying conditions under moderate air temperature with medium and long resting periods. The internal gradients of moisture and temperature are also well represented by the model in both continuous and intermittent processes. Therefore, this study describes the successful application of a phenomenological and fully predictive model for continuous and intermittent drying. In this way, this study contributes to obtaining effective and optimized drying processes, mainly when energy costs and product quality should be considered.

5.1 INTRODUCTION

Intermittent drying is a promising and alternative methodology to conventional drying in steady-state conditions, whereas the latter is widely recognized as an ineffective and energy-intensive process. Recognized as one of the most energy-efficient drying processes, intermittency consists basically of alternating between active and passive drying periods, leading to the implementation of a process with drying conditions varying in space and/or time (mainly temperature, air flow, and chamber pressure). Thus, this drying technique offers benefits related to energy costs and better-quality products, mainly due to reduced energy supply, shorter effective drying time, lower material temperature, and decreasing drying-induced stresses related to temperature and moisture internal gradients [1,2]. However, the mathematical modelling of intermittent drying remains a challenging task as involves simultaneous heat and mass transfer with drying and resting periods. Although the average moisture content remains constant in the resting period, the redistribution of the internal moisture is continuous [2–4]. The mathematical modelling is fundamental to obtain an effective, safe, controlled, and efficient intermittent drying process.

In this sense, several drying models have been proposed and developed for intermittent drying. Kumar et al. [5] summarize the categories of modelling approaches for intermittent drying, namely, empirical and fundamental models, which are further subdivided into single phase, two phases, multiphase, and reaction engineering approaches. Empirical models, of which Page and Exponential models are most commonly used, usually have simple mathematical formulation and involve uncomplicated computational implementation [5,6]. However, these models are unable to represent the physics of the process, the whole period of intermittent drying, and predict the variation of internal moisture and temperature gradients, as they normally include lumped

parameter models [7]. In contrast to these models, the fundamental models are generally based on the phenomena of heat and mass transfer during drying and, thereby, provide physical meaning in the consideration of the limiting mechanisms and material structure [8]. In this context, the single-phase models are very popular and most commonly used in intermittent drying modelling due to predictive capability and their simplicity, as these models consider only one phase [5]. Nishiyama et al. [2], Váquiro et al. [9], and Kowalski and Pawlowski [10] are some of the authors who have employed such models to represent intermittent drying.

Nishiyama et al. [2] have applied a sphere drying model in the intermittent drying of rice and wheat grains. Good agreement has been obtained by these authors, with a standard error of less than 0.47%, and a surface mass transfer coefficient has been proposed and successfully employed to simulate resting period. Váquiro et al. [9] have obtained a suitable mathematical model to address the heat and mass transfer phenomena in continuous and intermittent drying processes of mango for a differential element of cubic geometry. In addition, the authors have optimized intermittent drying based on enthalpy as an objective function. Kowalski and Pawlowski [10] have developed a mathematical model based on the partial pressure of vapor to describe the drying kinetics in both continuous and intermittent processes. These authors have also shown minimized cracks when the drying is conducted under constant external conditions during the constant rate period, followed by periodically changed drying air temperature and humidity in the falling rate period.

Despite being successfully applied in several dryers, the intermittent drying models aforementioned have been hardly used in spouted bed dryers, which are recognized as versatile multiphase systems and offer benefits related to high degrees of agitation and mixing between phases. Jumah et al. [11] and Bon and Kudra [1] have developed and optimized a general model

for the batch drying of grains in a rotating jet spouted bed, which is an inherently intermittent dryer. Jumah et al. [11] have compared the model predictions with experimental results obtained for yellow dent corn drying using both continuous and intermittent drying. However, there is still a remarkable gap regarding the modelling of spouted bed intermittent drying and few studies are found in the literature.

Therefore, the objective of this study is to propose a fully predictive mathematical model for intermittent drying in a conical spouted bed dryer. Accordingly, soybeans particles have been used due to their healthy nutrients and wide application in the animal feed and the human food industry. Thus, a single-phase model is proposed for a single particle, and then, the assumptions usually adopted in spouted bed systems to represent the whole bed are evaluated in both continuous and intermittent processes. The present study represents a continuity of our previous studies that deal with spouted bed intermittent drying from energy and quality aspects [12,13].

5.2 MATERIALS AND METHODS

5.2.1 Materials and Equipment

Batches of 2 kg of soybean seeds Intacta RR2 PRO™ [Glycine max (L.) Merril] have been used in all drying experiments with a conical configuration. The apparent density ($\rho_{ds} = 1210$ kg m^{-3}) and the mean diameter ($d_{pe} = 6.6 \pm 0.3$ mm) of the seeds have been determined by displacement method using toluene and image processing, respectively. Such batches correspond to a static bed height (H0) of 0.17 m. Figure 5.1 shows the experimental unit used, which has been described in detail in a previous paper [14].

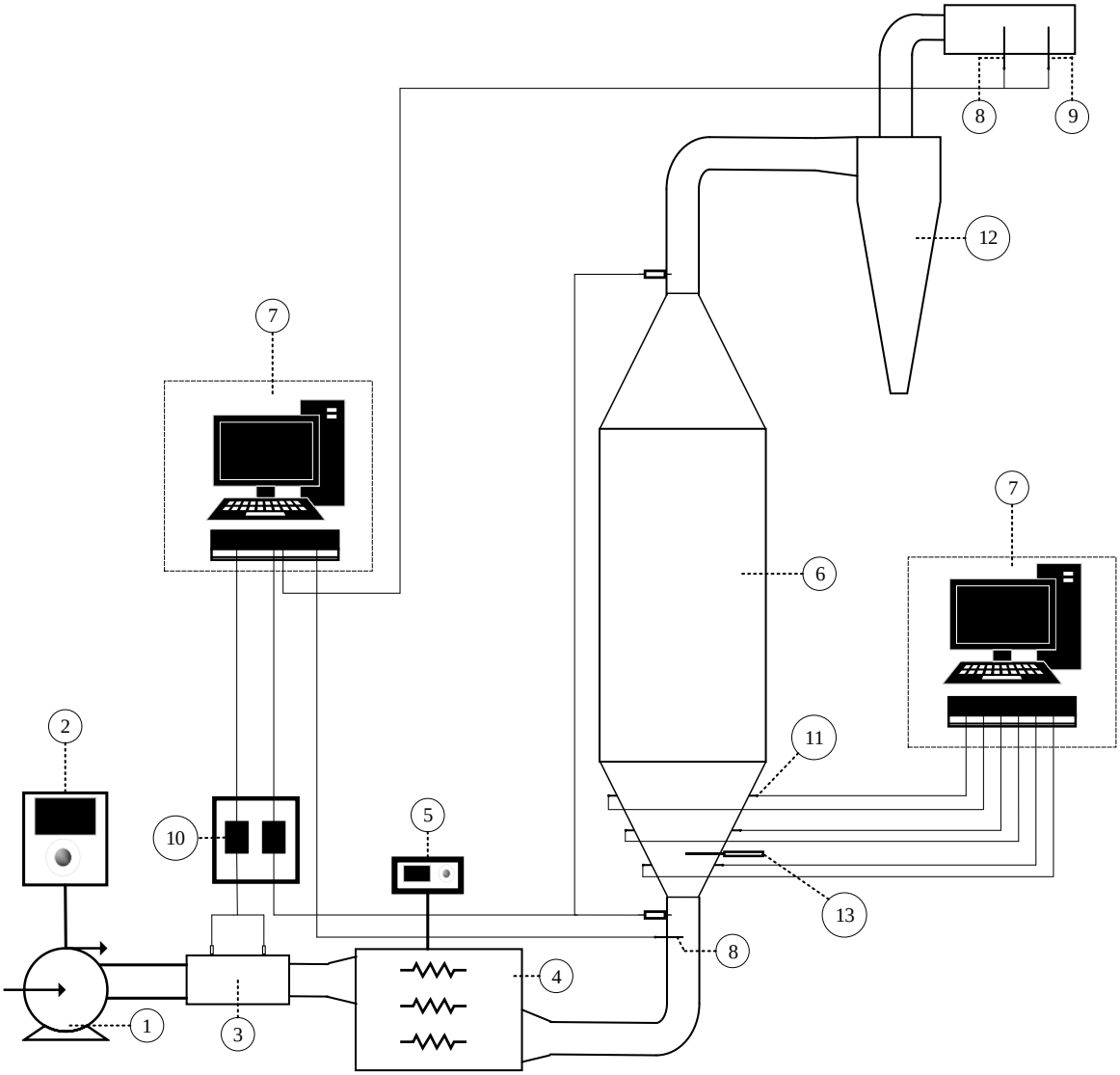

Figure 5.1. Components of the experimental unit used for the drying experiments: (1) blower; (2) frequency inverter; (3) Venturi flow meter; (4) heater; (5) temperature controller; (6) drying chamber; (7) data acquisition system; (8) T type thermocouple; (9) T type wet bulb thermocouple; (10) pressure transducers; (11) K type thermocouple; (12) cyclone; (13) sampler.

5.2.2 Experimental Procedure

To validate the model proposed, experimental drying results from a previous paper [14] have been used. Before each drying process, the seeds have been maintained in an environment saturated with water vapor for 48 h to reach the moisture content desired (0.20 ± 0.01 dry basis). The inlet air temperature in both continuous and intermittent drying have been kept constant at 50 °C, 60 °C, and 70 °C. Based on the minimum spouting velocity (u_{ms}), which have been estimated by both visual and the fluid dynamic characterization [15], inlet air velocities in the $1.25u_{ms}$ - $1.30u_{ms}$ range have been used in all drying conditions. The drying runs have been carried out for 5 h (continuous drying) and for 4 h (intermittent drying). Intermittent drying with periodic interruption of air flow (on/off spouting-heating) have been employed in all the different intermittent conditions evaluated, which are defined based on the intermittency ratios described in Table 5.1. In this study, the intermittency ratio is defined as the ratio of the resting period (τ_{off}) to the total drying time ($\tau_{off} + \tau_{on}$) of each cycle of 20 min. More details about the experimental procedure are given in a previous paper [14].

Table 5.1. Intermittency ratios used to evaluate the application of intermittency with periodic interruption of the air flow during the drying of soybean in the spouted bed.

Intermittency ratio		***alpha=1/4***	***alpha=1/2***	***alpha=3/4***	***alpha=0 (continuous drying)***
1st cycle	τ_{on} ***(min)***	15	10	5	20
	τ_{off} ***(min)***	5	10	15	0
2nd cycle	τ_{on} ***(min)***	15	10	5	20
	τ_{off} ***(min)***	5	10	15	0
3rd – 12th cycle	τ_{on} ***(min)***	15	10	5	20
	τ_{off} ***(min)***	5	10	15	0

5.2.3 Mathematical Modelling

The model is developed from those used by Jumah et al. [11], Bon and Kudra [1], and Váquiro et al. [9]. Thus, the following assumptions are adopted to address the heat and mass transfer phenomena in continuous and intermittent drying processes.

- The soybean particles are uniform in size, homogeneous, and can be approximated as isotropic spheres.
- The particles are perfectly mixed and all particles within the bed are at the same temperature and have the same moisture content at any instant during the drying process.

- The effect of particle shrinkage on transfer processes is negligible.
- Heat and mass transfer between particles in the bed and heat losses to the ambient are negligible.
- Inside the solid, the transfer of liquid moisture occurs by diffusion and governs the drying rate, whereas the moisture transfer in the vapor phase is negligible compared to that in the liquid phase due to the low-temperature drying. Thus, there is no phase change within the particle and evaporation occurs only at the particle surface.

Based on such assumptions, the equations governing the coupled heat and mass mechanisms are as follows:

Governing equations

$$\frac{\partial X}{\partial t} = \frac{1}{r^2}\frac{\partial}{\partial r}\left(D_{eff}\, r^2 \frac{\partial X}{\partial r}\right) \tag{1}$$

$$\rho_{ds}\left(C_{ps} + XC_{pw}\right)\frac{\partial T}{\partial t} = \frac{1}{r^2}\frac{\partial}{\partial r}\left(k\, r^2 \frac{\partial T}{\partial r}\right) + D_{eff}\, \rho_{ds}\, C_{pw} \frac{\partial X}{\partial r}\frac{\partial T}{\partial r} \tag{2}$$

Initial conditions

$$t = 0 \rightarrow X(r,0) = X_0 \quad \Lambda \quad T(r,0) = T_0 \tag{3}$$

Boundary conditions (at heating period)

$$t > 0 \rightarrow \frac{\partial X(0,t)}{\partial r} = 0 \quad \Lambda \quad \frac{\partial T(0,t)}{\partial r} = 0 \tag{4}$$

$$t > 0 \rightarrow -D_{eff}\rho_{ds}\frac{\partial X\left(R_{pe},t\right)}{\partial r} = \frac{h_m MM}{R_g}\left[\frac{\varphi\left(R_{pe},t\right)P_s\left(R_{pe},t\right)}{T_{abs}\left(R_{pe},t\right)} - \frac{\varphi_\infty P_{s_\infty}}{T_{\infty_{abs}}}\right] \tag{5}$$

$$t > 0 \rightarrow -k\frac{\partial T\left(R_{pe},t\right)}{\partial r} = h\left[T\left(R_{pe},t\right) - T_\infty\right] - D_{eff}\, \rho_{ds}\, \frac{\partial X\left(R_{pe},t\right)}{\partial r}\lambda \tag{6}$$

Boundary conditions (at resting period)

$$t > 0 \rightarrow -D_{eff}\rho_{ds}\frac{\partial X(R_{pe},t)}{\partial r} = 0 \quad (7)$$

$$t > 0 \rightarrow -k\frac{\partial T(R_{pe},t)}{\partial r} = 0 \quad (8)$$

The following equations have been used to estimate physical and thermal properties of the product (Equations (9)-(11)) [16–20], psychometric data (Equation (14)) [1], convection mass and heat transfer coefficients (Equations (21)-(22)) [21], and air properties (Equations (15)-(20)) [1,9].

$$\frac{D_{eff}}{{R_{pe}}^2} = 8.64\exp\left(\frac{-4848.5}{T_{abs}}\right)\exp(3.8\,X) \quad (9)$$

$$k = 0.602\,X_{(wet\ basis)} + 0.259\left(1 - X_{(wet\ basis)}\right) \quad (10)$$

$$C_{ps} = 1.296 + \left(7.5\,X_{(wet\ basis)}\right) - 0.0016\left(100\,X_{(wet\ basis)}\right)^2 \quad (11)$$

$$C_{pw} = 1005.3 + 0.01782\,T + 4.7047\,10^{-4}\,{T_{abs}}^2 - 1.9275\,10^{-7}\,{T_{abs}}^3 \quad (11)$$

$$\varphi = \exp\left(-exp(-0.00672\,T + 3.02)(100\,X)^{-1.508}\right) \quad (12)$$

$$\lambda = Rv\,{T_{abs}}^2\left\{\frac{6887}{{T_{abs}}^2} - \frac{5.31}{T_{abs}} - \frac{\frac{0.00672}{(100\,X)^{1.508}}\exp\left[\frac{-exp(-0.00672\,T + 3.02)}{(100\,X)^{1.508}} + 0.00672\,T + 3.02\right]}{\varphi}\right\} \quad (13)$$

$$P_s = M\exp\left(\frac{A + B\,T_{abs} + C\,{T_{abs}}^2 + J\,{T_{abs}}^3 + E\,{T_{abs}}^4}{F\,T_{abs} - G\,{T_{abs}}^2}\right), \qquad 273.16 \leq T_{abs} \leq 533.16 \quad (14)$$

$$M = 22105649.25; A = -27405.526; B = 97.5413; C = -0.146244;$$

$$J = 1.2558\,10^{-4}; E = -4.8502\,10^{-8}; F = 4.34903; G = 3.9381\,10^{-3};$$

$$D_a = \frac{0.0118\,10^{-7}\,{T_{abs}}^{1.75}}{P} \quad (15)$$

$$\rho_a = \frac{0.0289\ P}{R_g T_{abs}} \tag{16}$$

$$\mu_a = 1.7243\ 10^{-5} + 4.581\ 10^{-8}\ T \tag{17}$$

$$k_a = 0.024204 + 7.5793\ 10^{-5}\ T \tag{18}$$

$$C_{pv} = 10384.59 - 50.37\ T_{abs} + 0.074\ {T_{abs}}^2 \tag{19}$$

$$C_{pg} = 974.74 + 0.127\ T_{abs} \tag{20}$$

$$h_m = \frac{D_a}{d_{pe}} 0.829 Re^{0.687} Sc^{0.333} Ar^{0.031} \left(tan\ \frac{\gamma}{2}\right)^{-0.915} \left(\frac{H_o}{d_{pe}}\right)^{-1.227} \phi^{2.304} \tag{21}$$

$$h = \frac{k_a}{d_{pe}} 0.897 Re^{0.464} Pr^{0.333} Ar^{0.116} \left(tan\ \frac{\gamma}{2}\right)^{-0.813} \left(\frac{H_o}{d_{pe}}\right)^{-1.19} \phi^{2.261} \tag{22}$$

Besides the boundary conditions given by Equations (7) and (8), a natural convection boundary condition has also been evaluated in the resting period of the intermittent drying. Thus, the following equations have been used to estimate the mass and heat transfer coefficients in the boundary conditions given by Equations (5) and (6):

$$h_m = \frac{D_a}{d_{pe}} \left\{ 2 + \frac{0.589\ (Gr\ Sc)^{\frac{1}{4}}}{\left[1 + \left(\frac{0.46}{Sc}\right)^{\frac{9}{16}}\right]^{\frac{4}{9}}} \right\} \tag{23}$$

$$h = \frac{k_a}{d_{pe}} \left\{ 2 + \frac{0.589\ (Gr\ Pr)^{\frac{1}{4}}}{\left[1 + \left(\frac{0.46}{Pr}\right)^{\frac{9}{16}}\right]^{\frac{4}{9}}} \right\} \tag{24}$$

5.2.4 Numerical solution

As the diffusivity and thermal conductivity are both moisture-temperature dependent, the nonlinear partial differential equations (1) and (2), with their initial and boundary conditions, have been solved using a finite difference approximation, based on Sincovec and Madsen [22] and Jumah et al. [11]. Thus, Equations (1) and (2) have been re-written in the following general form:

$$\frac{\partial u_j}{\partial t} = f_j \left[\frac{1}{r^2} \frac{\partial}{\partial r} \left(r^2 D_j \frac{\partial u_j}{\partial r} \right) \right] \tag{25}$$

where *j=1,2* representing *X* and *T*.

Likewise, the boundary conditions given by Equations (4)-(8) have also been re-written as:

$$\alpha_j u_j + \beta_j \frac{\partial u_j}{\partial r} = \gamma_j \tag{27}$$

Thus, the following discretized equations are obtained by centered difference approximation:

$$\frac{1}{r^2}\frac{\partial}{\partial r}\left(r^2 D_j(u_j) \frac{\partial u_j(t,r)}{\partial r} \right) = \frac{3}{\left(r_{i+1/2}\right)^3 - \left(r_{i-1/2}\right)^3} \left[\left(r_{i+1/2}\right)^2 D_{j,i+1/2} \left(\frac{u_{j,i+1} - u_{j,i}}{h_i} \right) - \left(r_{i-1/2}\right)^2 D_{j,i-1/2} \left(\frac{u_{j,i} - u_{j,i-1}}{h_{i-1}} \right) \right] \tag{28}$$

where $r_{i\pm\frac{1}{2}} = \frac{r_{i\pm1} + r_i}{2}$; $D_{j,i\pm\frac{1}{2}} = D_j \left(r_{i\pm\frac{1}{2}}, \boldsymbol{u}_{i\pm\frac{1}{2}} \right)$; $\boldsymbol{u}_{i\pm\frac{1}{2}} = \left(\frac{\boldsymbol{u}_{1,i\pm1} + \boldsymbol{u}_{1,i}}{2}, \frac{\boldsymbol{u}_{2,i\pm1} + \boldsymbol{u}_{2,i}}{2} \right)$; $h_i = r_{i+1} - r_i$

Finally, the boundary conditions are re-defined as follows:

- At the boundary where $r = r_1$, they are approximated by:

$$\frac{\partial u_j}{\partial r} \cong \begin{cases} \dfrac{u_{j,2} - u_{j,1}}{h_1} & if\ \beta_j = 0 \\ \dfrac{\gamma_j - \alpha_j u_{j,1}}{\beta_j} & if\ \beta_j \neq 0 \end{cases} \tag{29}$$

$$\frac{1}{r^2}\frac{\partial}{\partial r}\left(r^2 D_j(r,\boldsymbol{u})\frac{\partial u_j(t,r)}{\partial r}\right) = \left\{\begin{array}{l} \dfrac{3}{\left(r_{1+\frac{1}{2}}\right)^3 - (r_1)^3}\left[\left({r_{1+\frac{1}{2}}}^2 D_{j,1+\frac{1}{2}} - {r_1}^2 D_{j,1}\right)\left(\dfrac{u_{j,2}-u_{j,1}}{h_1}\right)\right] \quad if\ \beta_j = 0 \\ \dfrac{3}{\left(r_{1+\frac{1}{2}}\right)^3 - (r_1)^3}\left[{r_{1+\frac{1}{2}}}^2 D_{j,1+\frac{1}{2}}\left(\dfrac{u_{j,2}-u_{j,1}}{h_1}\right) - {r_1}^2 D_{j,1}\left(\dfrac{\gamma_j - \alpha_j u_{j,1}}{\beta_j}\right)\right] \quad if\ \beta_j \neq 0 \end{array}\right\} \tag{30}$$

- At the boundary where $r = r_N$ (N is the spatial mesh), they are approximated by:

$$\frac{\partial u_j}{\partial r} \cong \left\{\begin{array}{l} \dfrac{u_{j,N} - u_{j,N-1}}{h_{N-1}} \quad if\ \beta_j = 0 \\ \dfrac{\gamma_j - \alpha_j u_{j,N}}{\beta_j} \quad if\ \beta_j \neq 0 \end{array}\right\} \tag{31}$$

$$\frac{1}{r^2}\frac{\partial}{\partial r}\left(r^2 D_j(r,\boldsymbol{u})\frac{\partial u_j(t,r)}{\partial r}\right) = \left\{\begin{array}{l} \dfrac{3}{(r_N)^3 - \left(r_{N-\frac{1}{2}}\right)^3}\left[\left({r_N}^2 D_{j,N} - {r_{N-\frac{1}{2}}}^2 D_{j,N-\frac{1}{2}}\right)\left(\dfrac{u_{j,N}-u_{j,N-1}}{h_N}\right)\right] \quad if\ \beta_j = 0 \\ \dfrac{3}{(r_N)^3 - \left(r_{N-\frac{1}{2}}\right)^3}\left[{r_N}^2 D_{j,N}\left(\dfrac{\gamma_j - \alpha_j u_{j,N}}{\beta_j}\right) - {r_{N-\frac{1}{2}}}^2 D_{j,N-\frac{1}{2}}\left(\dfrac{u_{j,N}-u_{j,N-1}}{h_N}\right)\right] \quad if\ \beta_j \neq 0 \end{array}\right\} \tag{32}$$

Thus, the system of equations obtained has been solved in MATLAB R2017a, with a uniform mesh of 40 points in the spatial discretization.

5.3 RESULTS AND DISCUSSION

5.3.1 Continuous Drying

Figure 5.2 shows predicted and experimental results of both the dimensionless moisture, based on the average moisture content, and the solid temperature.

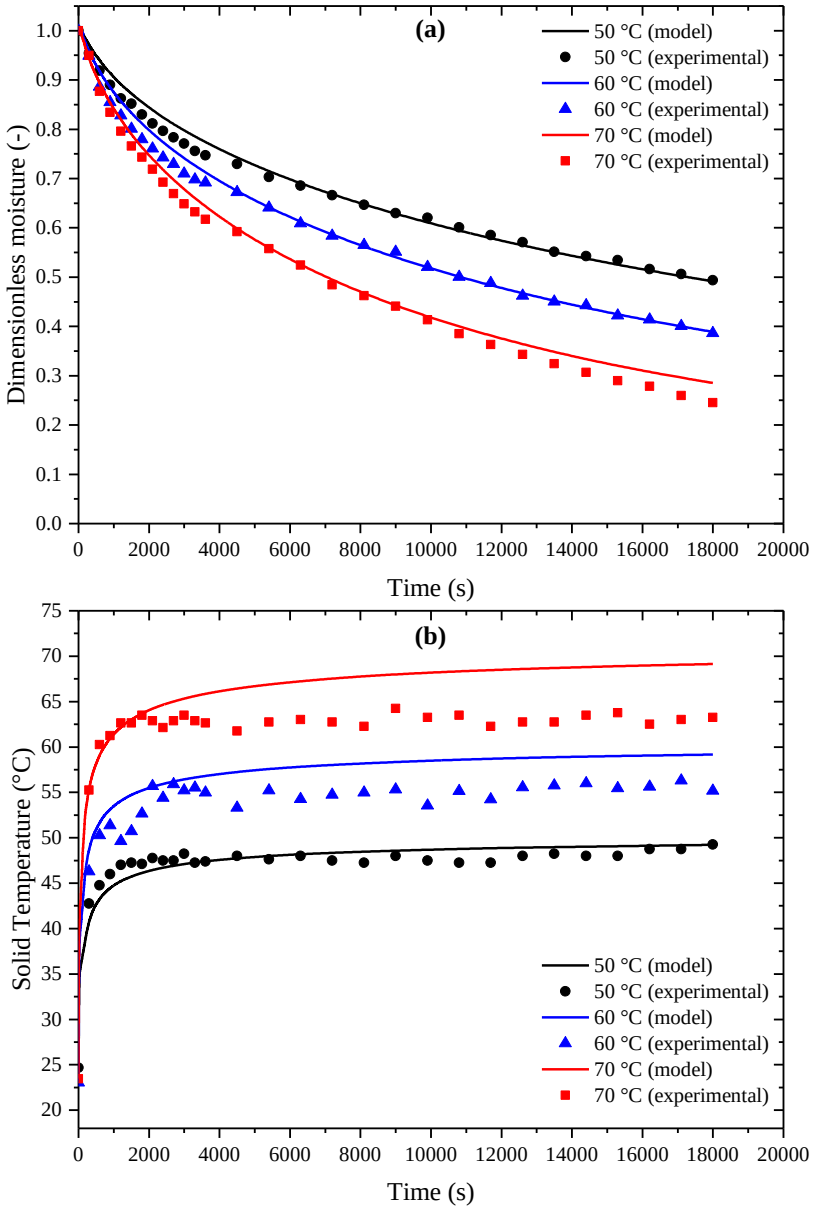

Figure 5.2. (a) Dimensionless moisture and (b) average solid temperature (predicted and measured experimentally), as a function of drying time, for continuous drying at 50 °C, 60 °C, and 70 °C.

The behaviors observed in the dimensionless moisture curves (Figure 5.2a) are typical for soybean particles, which are represented by a continuous and exponential decrease in dimensionless moisture over time. Such behaviors suggest the internal mass transfer resistance as

the controlling step throughout the drying process. This hypothesis is confirmed by the mass transfer Biot number (Bi_m ranges from 138 to 829 in this study). Likewise, the solids temperature results (Figure 5.2b) also indicate the internal mass transfer resistance control, as most of the energy supplied is used as sensible heat and a sharp increase in the solid temperature is observed at the beginning, followed by an apparent stabilization over time. These results are in agreement with most studies presented in the literature [23,24].

Good agreement is observed between the measured and predicted dimensionless moisture (Figure 5.2a) for all the air inlet temperatures evaluated. A discrepancy is observed in the energy model, as the values of solid temperature for the conditions are overestimated as the air inlet temperature increases (60 °C and 70 °C). This finding can be attributed to the heat losses from the dryer, which is neglected in the model. As the inlet air temperature increases, the heat lost from the dryer also increases due to the temperature gradient between the air and the wall of the equipment, and, thereby, this term tends to be more significant in the model. Moreover, the experimental methodology adopted to obtain the solids temperature may also have contributed to this discrepancy observed, because samples are regularly collected from the conical region. Despite the thermally insulated containers employed, the heat losses in the measurement are inevitable, mainly for higher solid temperatures.

Nevertheless, the good results obtained demonstrate the reliability and robustness of the model, which is phenomenological and fully predictive without parameter fitting and adjustment. Thus, the single-particle model and the assumptions adopted are suitable for continuous drying on the spouted bed under moderate air temperatures. Similar results have been obtained by Jumah et al. [11] in a Rotating Jet Spouted Bed. Based on the predictions obtained for the continuous conditions, the results for the intermittent conditions at 50 °C are presented in the next sections.

5.3.2 Intermittent Drying

Figure 5.3 shows predicted and experimental results of both the dimensionless moisture, based on the average moisture content, and the solid temperature for the intermittent conditions.

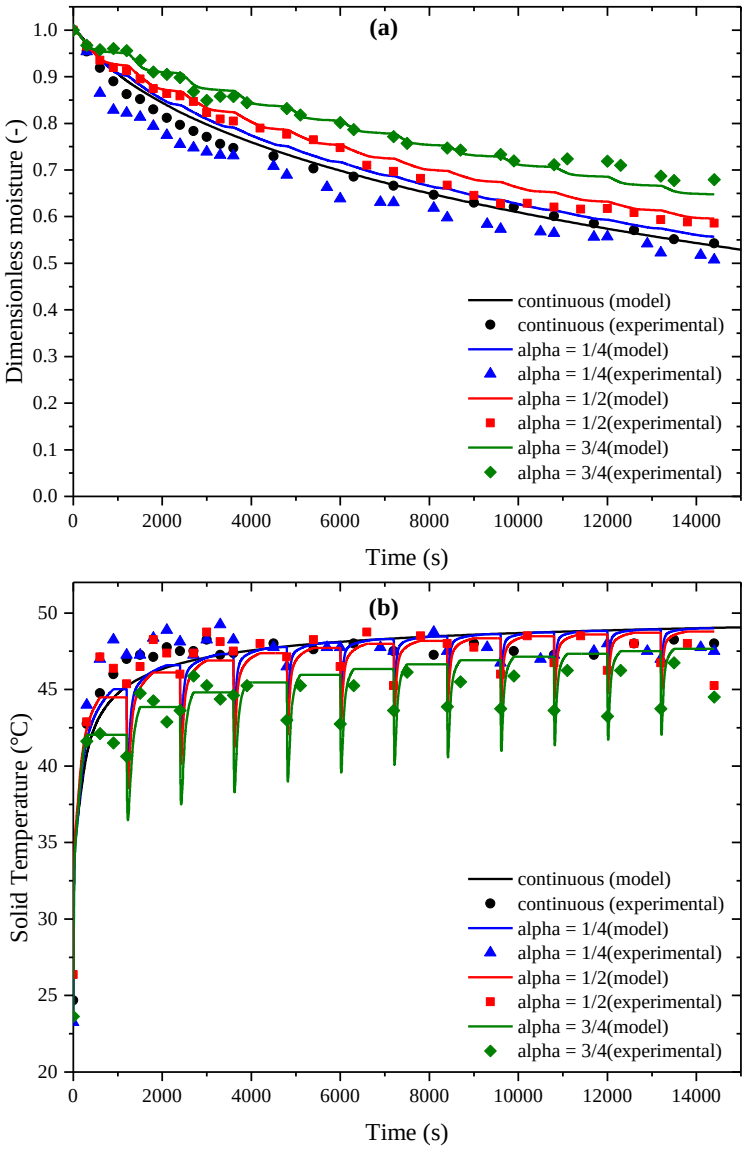

Figure 5.3. (a) Dimensionless moisture and (b) average solid temperature (predicted and measured experimentally), as a function of drying time, for intermittent drying conditions at 50 °C.

According to Figure 5.3a, a decrease in the dimensionless moisture in a stepwise way is predicted by the model in all the intermittent conditions evaluated. Such behavior is typical of intermittent drying under an on/off spouting-heating regime and has been obtained by several authors [2,25]. The effect of the intermittency ratio is also well represented by the model, i.e., as the intermittency ratio increases, the dimensionless moisture also increases due to the longer resting period. Besides the physically consistent response of the model, good agreement is observed between the measured and predicted dimensionless moisture for the medium (alpha = 1/2) and longest (alpha = 3/4) resting periods. The worst prediction of the model corresponds to the condition with the shortest resting period (alpha = 1/4), which unexpectedly provides measured dimensionless moisture values even lower than the continuous condition. This result can be attributed to the particle-particle interaction and short resting period that allows better use of the heat stored in the annular region during the drying period. These justifications can also be attributed to the results obtained for the average solid temperature (Figure 5.3b).

Overall, the model provides good agreement for the average solid temperature with the experimental data for all the intermittent conditions employed. However, an inconsistent behavior is observed in which a constant solid temperature is predicted by the model during the resting period, followed by a sharp drop at the beginning of each spouting period. As also mentioned by Jumah et al. [11], this inconsistency may partly be explained by an inappropriate heat transfer boundary condition at the surface of the particle, as a condition of zero temperature gradient is adopted in the energy model. In fact, the particle gradually cools in the resting period according to the average solid temperature measured. Thus, a natural convection boundary condition is evaluated and the results are shown in Figure 5.4 for the intermittent condition with the shortest resting period (alpha = 1/4), which provides the worst predictions.

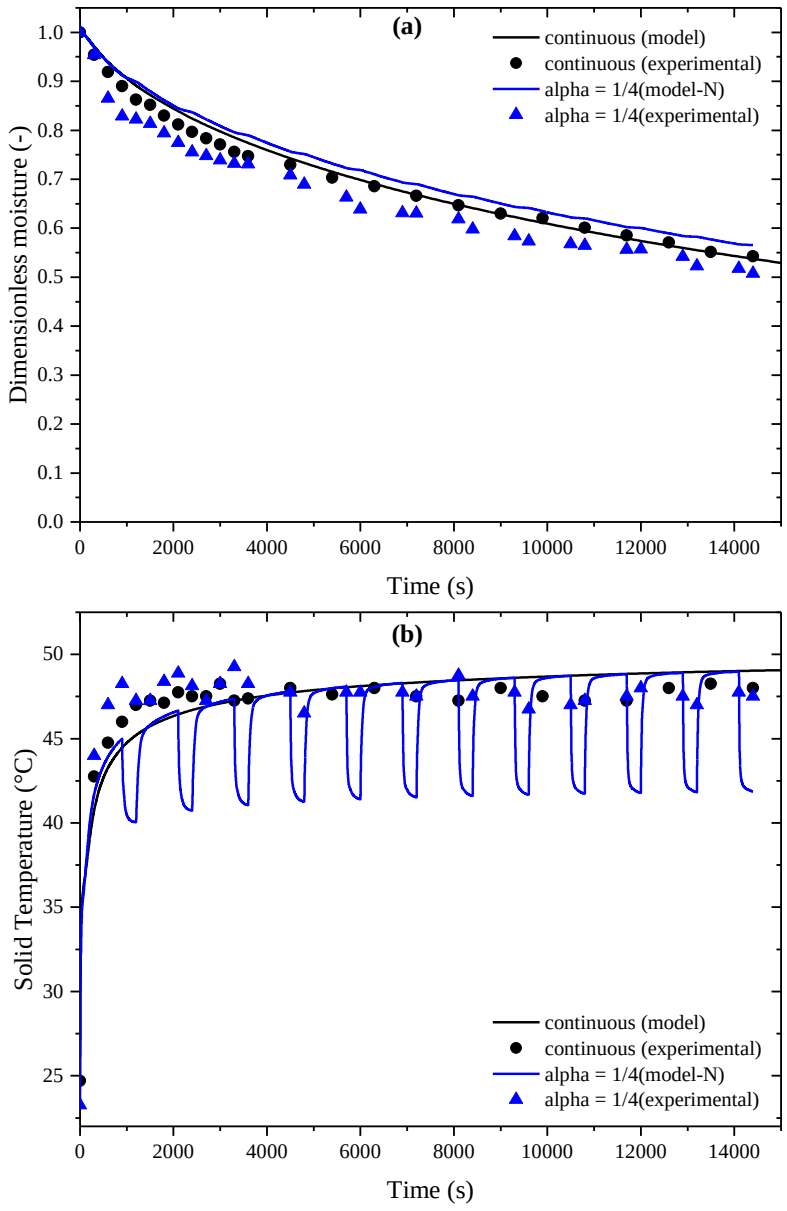

Figure 5.4. (a) Dimensionless moisture and (b) average solid temperature (predicted and measured experimentally), as a function of drying time, for intermittent drying condition at 50 °C and natural convection boundary condition.

As observed in Figure 5.4a, there is no significant effect of the boundary condition on the dimensionless moisture prediction, providing poor predictions. This finding implies that both boundary conditions at the particle surface, i.e., zero concentration gradient and natural mass

convection, are inadequate to provide good predictions in the spouted bed for intermittent drying with short resting periods. In these cases, particle-particle interactions must be considered and an empirical or a lumped parameter model for spouted bed should provide better results, as presented in a previous study [26]. Regarding the average solid temperature predictions, Figure 5.4b shows a significantly distinct trend represented by a gradual cooling in the resting period, which is physically more consistent than that obtained with a condition of zero temperature gradient. Similar behavior is presented by Defraeye [27] in the intermittent drying of fruit tissue. Nonetheless, the minimum average solid temperature reached by the model in the resting period is much less than the minimum experimental value. This result is related to the assumptions adopted for the modeling, where the particles are considered perfectly mixed and a single particle model is employed to represent the whole bed behavior. In the resting period, the particle-particle interactions prevent the sharp cooling of the particles commonly observed in the drying of single and isolated particles.

Therefore, the good results obtained in the continuous drying demonstrate the reliability and robustness of the model for this condition, as well as for intermittent drying with medium and long resting periods. However, the model and the assumptions adopted are less accurate for high air temperatures and short resting periods, mainly due to the heat loss and particle-particle interactions. Nevertheless, the model can still be used to predict the internal gradients of moisture and temperature, which is difficult to be measured experimentally. The temperature and moisture spatial distribution inside the particle are fundamental analyzes in the intermittent drying, especially aiming the product quality and the energy optimization, such as performed by Bon and Kudra [1].

5.3.3 Spatial Profiles

Figure 5.5 shows the moisture and temperature profiles inside the particle predicted by the model.

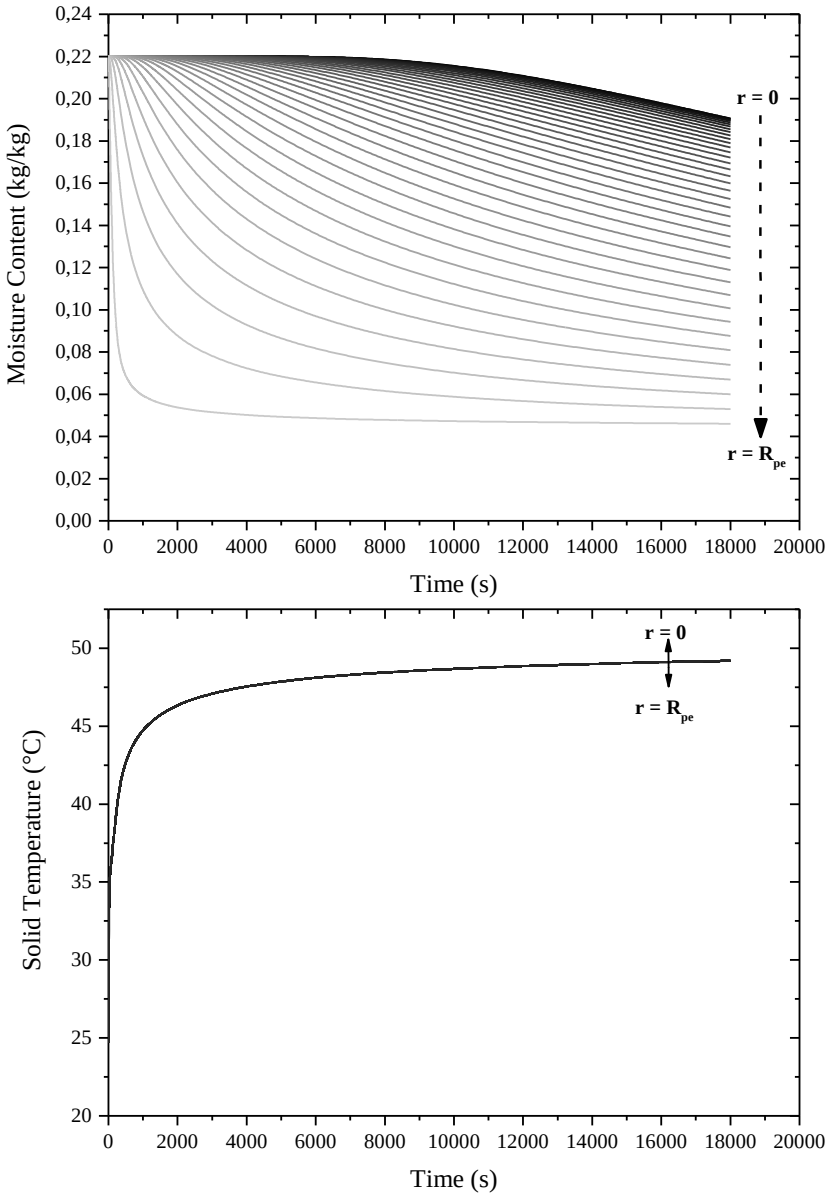

Figure 5.5. (a) Moisture content and (b) solid temperature spatial distribution inside the particle, as a function of time, for continuous drying at 50 °C.

As observed, moisture gradients inside the particle are substantial, whereas the internal temperature gradient is negligible. This result is expected and might be explained based on the Lewis Number obtained in this study (Le>>>1), which implies that the rate of internal heat transfer is faster than the rate of mass transfer [28]. Furthermore, the heat transfer Biot number estimated in this study (Bi<0.2) suggests a negligible internal heat transfer resistance and, therefore, a uniform internal temperature distribution, such as presented in Figure 5.5b. Thus, a lumped temperature model would provide similar results for the spouted bed drying, as demonstrated by Robbins and Fryer [29].

The key role of intermittent drying can be highlighted through the moisture gradient profiles observed in Figure 5.5a, in which high moisture contents are observed at the internal layers of the particle and a sharp decrease in surface moisture content to dynamic equilibrium value is observed. As mentioned before, intermittent drying allows the decrease of moisture gradients due to the resting period, providing a better-quality product. Thus, the internal moisture gradient profiles for the intermittent conditions are presented in Figure 5.6, as well as the surface moisture content.

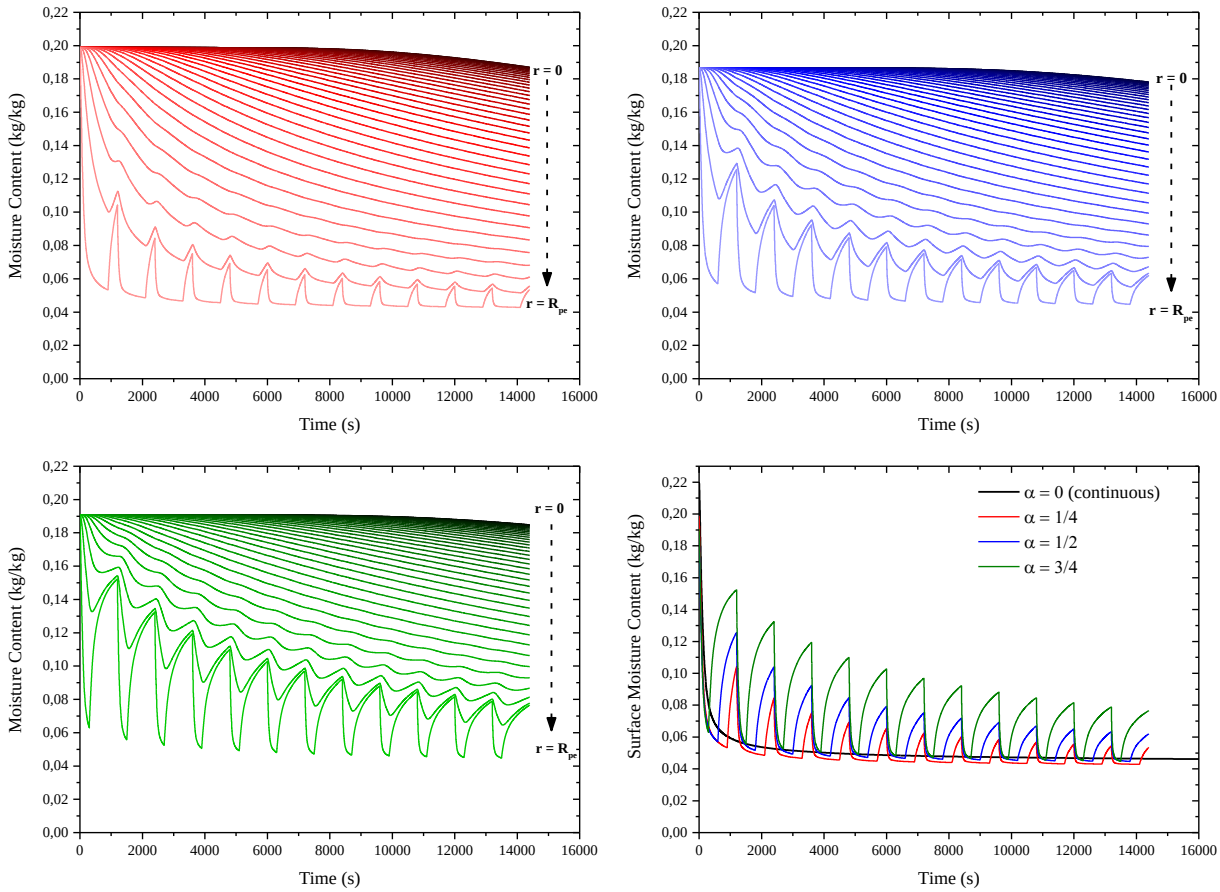

Figure 5.6. Moisture content spatial distribution inside the particle and surface moisture content profiles, as a function of time, for all intermittent conditions at 50 °C.

Similar behavior is obtained for all the intermittent conditions evaluated, which is represented by periodic increases in moisture content at the outer layers of the particles. Consequently, a peak of moisture content is reached in the resting period due to the migration of water from the interior to the external surface of soybean particles. The effect of the intermittency ratio is better observed by the surface moisture content. As the intermittency ratio increases, the peak of moisture content observed also increases because the long resting periods provide more time for internal moisture redistribution. Therefore, the model employed provides predictions

physically consistent of the internal gradients of moisture and temperature, which are essential results in the intermittent drying for product quality and energy optimization.

5.4 CONCLUSIONS

A fully predictive mathematical model for continuous and intermittent drying is proposed in this study. The predictions of the proposed single-phase model for a single particle are compared with experimental results obtained from the spouted bed drying of soybean particles. Good agreement between predicted and experimental results are obtained for continuous drying under moderate air temperature, as well as for intermittent drying with medium and long resting periods. Poor predictions are obtained for high air temperatures and short resting periods, mainly due to heat loss and particle-particle interactions. Thus, the assumptions adopted are less accurate for such conditions in the spouted bed, and, thereby, different terms should be implemented in the model. Nevertheless, the model employed provides predictions physically consistent of the internal gradients of moisture and temperature, which are essential results in the intermittent drying for product quality and energy optimization. Therefore, this study describes the successful application of a reliable and robust model for continuous and intermittent drying, which is phenomenological and fully predictive without parameter fitting and adjustment.

NOMENCLATURE

Ar	Archimedes number	[-]
C_p	specific heat	[kJ kg^{-1} K^{-1}]

D	diffusive coefficients in the general form	[-]
D_{eff}	effective moisture diffusivity in solid	[m^2 s^{-1}]
D_a	molecular diffusivity water–air	[m^2 s^{-1}]
d_{pe}	particle diameter	[m]
Gr	Grashof number	[-]
h	convective heat transfer coefficient	[W $m^{-2}K^{-1}$]
h_m	convective mass transfer coefficient	[m s^{-1}]
H_o	static bed height	[m]
k	thermal conductivity of the product	[W m K^{-1}]
k_a	thermal conductivity of the air	[W m^{-1} K^{-1}]
MM	molar mass of air	[kg mol^{-1}]
P	pressure	[Pa]
P_s	saturation vapor pressure	[Pa]
Pr	Prandtl number	[-]
r	radial distance from center of sphere	[m]
R_g	universal gas constant	[J mol^{-1} K^{-1}]
R_v	$R_g/molar\ mass\ of\ water$	[J kg^{-1} K^{-1}]
R_{pe}	particle radius	[m]
Re	Reynolds number	[-]
Sc	Schmidt number	[-]
t	time	[s]
T	temperature	[ºC]

T_{abs}	absolute temperature	[K]
u_{ms}	minimum spouting velocity	[m s^{-1}]
X	solid moisture content	[kg kg^{-1}]

Subscripts

a	air
ds	dry solid
g	gas
p	particle
s	solid
v	vapor
w	water

Greek symbols

ϕ	sphericity	[-]
μ	dynamic viscosity	[kg m^{-1} s^{-1}]
ρ	specific mass	[kg m^{-3}]
φ	water activity	[-]
γ	cone angle	[degree]
λ	latent heat	[kJ kg^{-1}]

ACKNOWLEDGEMENTS

The authors appreciate the financial support provided by Coordination for the Improvement of Higher Education Personnel (CAPES), the São Paulo State Research Foundation (FAPESP, grant #2017/01856-7 and grant #2018/22655-2), the Spain's Ministry of Science and Innovation (PID2019-107357RB-I00 (AEI/FEDER, UE)), and the European Commission (HORIZON H2020-MSCA RISE-2018. Contract No.: 823745). I. Estiati thanks the University of the Basque Country for her postgraduate grant (ESPDOC18/14).

REFERENCES

[1] J. Bon, T. Kudra, Enthalpy-driven optimization of intermittent drying, Dry. Technol. 25 (2007) 523–532. doi:10.1080/07373930701226880.

[2] Y. Nishiyama, W. Cao, B. Li, Grain intermittent drying characteristics analyzed by a simplified model, J. Food Eng. 76 (2006) 272–279. doi:10.1016/j.jfoodeng.2005.04.059.

[3] W. Cao, Y. Nishiyama, S. Koide, Thin-layer drying of Maitake mushroom analysed with a simplified model, Biosyst. Eng. 85 (2003) 331–337. doi:10.1016/S1537-5110(03)00061-8.

[4] W. Cao, Y. Nishiyama, S. Koide, Simulation of intermittent drying of Maitake mushroom by a simplified model, Biosyst. Eng. 87 (2004) 325–331. doi:10.1016/j.biosystemseng.2003.12.003.

[5] C. Kumar, A. Putranto, M. Mahiuddin, S.C. Saha, Y.T. Gu, M.A. Karim, Mathematical Modelling of Intermittent Drying, in: M.A. Karim, C.L. Law (Eds.), Intermittent Nonstationary Dry. Technol. Princ. Appl., Taylor & Francis Group, LLC, 2017: pp. 163–191.

[6] A. Putranto, X.D. Chen, S. Devahastin, Z. Xiao, P.A. Webley, Application of the reaction

engineering approach (REA) for modeling intermittent drying under time-varying humidity and temperature, Chem. Eng. Sci. 66 (2011) 2149–2156. doi:10.1016/j.ces.2011.02.025.

[7] R. Baini, T.A.G. Langrish, Choosing an appropriate drying model for intermittent and continuous drying of bananas, J. Food Eng. 79 (2007) 330–343. doi:10.1016/j.jfoodeng.2006.01.068.

[8] X. Gao, J. Wang, S. Wang, Z. Li, Modeling of drying kinetics of green peas by reaction engineering approach, Dry. Technol. 34 (2016) 437–442. doi:10.1080/07373937.2015.1060491.

[9] H.A. Váquiro, G. Clemente, J. V. García-Pérez, A. Mulet, J. Bon, Enthalpy-driven optimization of intermittent drying of Mangifera indica L., Chem. Eng. Res. Des. 87 (2009) 885–898. doi:10.1016/j.cherd.2008.12.002.

[10] S.J. Kowalski, A. Pawłowski, Modeling of kinetics in stationary and intermittent drying, Dry. Technol. 28 (2010) 1023–1031. doi:10.1080/07373937.2010.497095.

[11] R.Y. Jumah, A.S. Mujumdar, G.S.V. Raghavan, A Mathematical Model for Constant and Intermittent Batch Drying of Grains in a Novel Rotating Jet Spouted bed, Dry. Technol. 14 (1996) 765–802. doi:10.1080/07373939608917124.

[12] R.C. Brito, R. Béttega, J.T. Freire, Energy analysis of intermittent drying in the spouted bed, Dry. Technol. 37 (2019). doi:10.1080/07373937.2018.1512503.

[13] R.C. Brito, M.B. Zacharias, V.A. Forti, J.T. Freire, Physical and physiological quality of intermittent soybean seeds drying in the spouted bed, Dry. Technol. 0 (2020) 1–14. doi:10.1080/07373937.2020.1725544.

[14] R.C. Brito, M.B. Zacharias, V.A. Forti, J.T. Freire, Physical and physiological quality of intermittent soybean seeds drying in the spouted bed, Dry. Technol. (2020).

doi:10.1080/07373937.2020.1725544.

[15] K.B. Mathur, N. Epstein, Spouted Beds, Academic Press, New York, 1974.

[16] M.A.S. Barrozo, H.M. Henrique, D.J.M. Sartori, J.T. Freire, The use of the orthogonal collocation method on the study of the drying kinetics of soybean seeds, J. Stored Prod. Res. 42 (2006) 348–356. doi:10.1016/j.jspr.2005.06.002.

[17] M. Hemis, G.S.V. Raghavan, Effect of Convective Air Attributes with Microwave Drying of Soybean: Model Prediction and Experimental Validation, Dry. Technol. 32 (2014) 543–549. doi:10.1080/07373937.2013.843189.

[18] L. Otten, G. Samaan, Determination of the specific heat of agricultural materials: Part II. Experimental Results, Can. Agric. Eng. 22 (1980) 25–27.

[19] M.A.S. Barrozo, D.J.M. Sartori, J.T. Freire, J.A. Achcar, Discrimination of Equilibrium Moisture Equations for Soybean Using Nonlinearity Measures, Dry. Technol. 14 (1996) 1779–1794. doi:10.1080/07373939608917173.

[20] A.H. Zahed, N. Epstein, Batch and continuous spouted bed drying of cereal grains: The thermal equilibrium model, Can. J. Chem. Eng. 70 (1992) 945–953. doi:10.1002/cjce.5450700517.

[21] A. Kmiec, Simultaneous heat and mass transfer in spouted beds, Can. J. Chem. Eng. 53 (1975) 18–24. doi:10.1002/cjce.5450530103.

[22] R.F. Sincovec, N.K. Madsen, Software for Nonlinear Partial Differential Equations, ACM Trans. Math. Softw. 1 (1975) 232–260. doi:10.1145/355644.355649.

[23] Z. Yang, E. Zhu, Z. Zhu, Water desorption isotherm and drying characteristics of green soybean, J. Stored Prod. Res. 60 (2015) 25–30. doi:10.1016/j.jspr.2014.10.006.

[24] M. a. S. Barrozo, V. V. Murata, a. J. Assis, J.T. Freire, Modeling of Drying in Moving Bed,

Dry. Technol. 24 (2006) 269–279. doi:10.1080/07373930600564530.

[25] A. Putranto, X.D. Chen, Z. Xiao, P.A. Webley, Mathematical modeling of intermittent and convective drying of rice and coffee using the reaction engineering approach (REA), J. Food Eng. 105 (2011) 638–646. doi:10.1016/j.jfoodeng.2011.03.036.

[26] E.R. Paula, R.C. Brito, J.T. Freire, F.B. Freire, Soft sensor based on a lumped parameter model of solids drying in a spouted bed, Dry. Technol. (2020). doi:10.1080/07373937.2019.1709198.

[27] T. Defraeye, Towards more efficient intermittent drying of fruit: Insights from combined hygrothermal-quality modelling, Innov. Food Sci. Emerg. Technol. 38 (2016) 262–271. doi:10.1016/j.ifset.2016.10.003.

[28] X.D. Chen, Lewis number in the context of air-drying of hygroscopic materials, Sep. Purif. Technol. 48 (2006) 121–132. doi:10.1016/j.seppur.2005.07.002.

[29] P.T. Robbins, P.J. Fryer, The spouted-bed roasting of barley: Development of a predictive model for moisture and temperature, J. Food Eng. 59 (2003) 199–208. doi:10.1016/S0260-8774(02)00459-4.

CHAPTER 6

HYDRODYNAMIC ANALYSIS OF DRAFT TUBE SPOUTED BEDS

As part of the draft tube design, this chapter describes the hydrodynamic analysis of spouted bed with different types of draft tubes, which refers to specific objective (4) of this thesis. Besides the methodologies usually employed for hydrodynamic characterization in spouted beds, pressure fluctuation analysis has also been used to identify different gas-solid flow patterns. Thus, the paper described in this chapter aimed to apply pressure fluctuation analysis to spouted beds operating with fine and irregular particles, either without tube or equipped with draft tube. The minimum spouting velocities estimated by the spectral analysis in systems without tubes differ from those obtained based on the characteristic curves in the range from 10.60% (sand) to 3.50% (glass beads). Thus, the main novelty of this study lies in the application of pressure fluctuation and spectral analyses in spouted beds operating with fine and irregular particles by considering the influence of the internal devices. Therefore, the methodology proposed based on both hydrodynamic and spectral analyses is a feasible and promising alternative for delimiting the minimum spouting velocity and stable operating conditions in industrial processes, especially when the aim is process control and scaling up.

This chapter is based on:

R.C. de Brito, M. Tellabide, I. Estiati, J.T. Freire, M. Olazar, Estimation of the minimum spouting velocity based on pressure fluctuation analysis, J. Taiwan Inst. Chem. Eng. 113 (2020) 56–65. doi:10.1016/j.jtice.2020.08.022.

6.1 INTRODUCTION

Spouted beds are recognized as an efficient gas-solid contact method, as under suitable conditions they are versatile multiphase systems with a high degree of agitation and mixing between the phases due to their peculiar hydrodynamic behavior. These properties significantly improve heat and mass transfer rates, which are essential requirements in many processes in chemical industry. Thus, the spouted bed has been applied in a wide range of chemical and physical operations, such as biomass pyrolysis [1,2], coating [3,4], gasification [5,6], torrefaction [7], chemical vapor deposition [8,9], drying [10], and elutriation [11], among others. As a result, the variety of processed materials has also expanded significantly since the original design of the spouted bed, which was specifically proposed for coarse particles corresponding to group D of Geldart classification [12,13]. Currently, new internal devices have allowed the operation with fine, irregular, and sticky particles [14–17]. These devices are specifically a variety of draft tubes and the fountain confiner [18–20].

Despite these recent developments, most of the aforementioned spouted bed applications are usually restricted to laboratory scale and pilot plants, with scaling up being already a challenging task [21]. Accordingly, characterization of their hydrodynamic behavior is fundamental for design, operation, control, and scale up purposes. Several studies have been performed to provide tools to step forward on the knowledge of hydrodynamic characteristics. Thus, Atxutegi et al. [16] have developed a methodology based on a borescopic technique for the monitoring of solid flow in conical spouted beds operating with fine and coarse particles under a wide range of conditions. Yang et al. [22] have investigated the fountain height behavior in a rectangular spouted bed operating with particles corresponding to both groups D and B of Geldart classification by using

Fast Fourier Transform (FFT) to characterize the periodical fountain variation. Both studies are based on image recording and processing, which involves difficulties in the spouted bed, mainly due to the spouting regime demanding a robust algorithm. Otherwise, most of the studies involving spouted bed regimes are based on pressure drop monitoring and visual observation. Nevertheless, the latter is unfeasible when scaling-up or in industrial processes, in which contactors are usually made of opaque materials and may also involve high temperatures [23].

Within this context, the analysis of pressure fluctuations has emerged as a promising alternative to characterize gas-solid flow systems. This technology lies in a non-intrusive method allowing simple measurements that provide a meaningful understanding of the dynamic behavior [24,25]. Pressure fluctuations are related to gas flow through the bed, movement of solids, particle-particle and gas-particle interactions, particle-wall collisions, formation, rise and eruption of bubbles, and unit features (line configuration, air supply and so on) [26,27]. Such numerous sources may complicate the interpretation of time-series signals. Thus, several algorithms have been proposed to obtain useful information from pressure fluctuation data. These algorithms are classified as time-domain analysis (standard deviation, cycle frequency and Hurst exponent), frequency-domain analysis (power spectral density and wavelet coefficients), and state-space analysis (entropy analysis and attractor reconstruction) [24]. Frequency-domain analysis is the usual one to obtain dominant frequencies of the flow pattern and is typically based on Fourier transform, which consists in converting time-series signals into frequency spectra [26,28].

Although consolidated in fluidized beds, pressure fluctuation analysis has been used in spouted beds only in the last few years [26,29–34]. Mollick and Sathiyamoorthy [33] have identified stable spouting regimes in both two-dimensional and three-dimensional spouted beds by evaluating the average pressure drop across the bed and standard deviation of pressure fluctuations

with Archimedes number. Mostoufi et al. [30] have employed the power spectral density function of pressure fluctuations in a conical spouted bed to obtain more detailed insight into the hydrodynamic regimes. Piskova and Mörl [26] have characterized spouted bed regimes in different pieces of equipment by comparing time, frequency and phase space analyses of pressure fluctuation signals. These authors have been able to identify different flow regimes in spouted beds based on pressure fluctuation analysis, presenting this method as a promising cost-effective tool for process control.

However, there is still a gap regarding the application of this technique in a spouted bed operating with fine and irregular particles, especially, considering the influence of the internal devices that are usually required with these materials. Furthermore, the estimation of hydrodynamics parameters by pressure fluctuation analysis is essential in industrial processes. Thus, the minimum spouting velocity is a key parameter for appropriate design, scale up, and operation in industrial applications [35,36]. Therefore, the aim of this paper is to perform the pressure fluctuation analysis in draft tube conical spouted beds operating with fine and irregular particles. Accordingly, hydrodynamic and pressure fluctuation analyses were performed for sand, glass beads, and soybean in three different configurations: without tube and with nonporous and open-sided ones. Thus, this study proposes an alternative methodology based on both hydrodynamic and spectral analyses to estimate the minimum spouting velocity in such configurations operating with fine and irregular particles, which are usually characterized by unstable and pulsating regimes.

6.2 MATERIALS AND METHODS

6.2.1 Materials and equipment

Figure 6.1 presents the experimental unit used, which is described in a previous paper [14]. The runs have been performed using contactors made of polyethylene terephthalate. The geometric factors of the conical contactors are as follows: column diameter (D_c), 0.36 m; contactor angle (γ), 36°; height of the conical section (H_c), 0.45 m; and base diameter (D_i), 0.06 m. The gas inlet diameter (D_0) is 0.04 m. The static bed height (H_0) used in all runs is 0.17 m. The experiments have been carried out without draft tube and with nonporous and open-sided draft tubes. The dimensions of the draft tubes, which were described in detail by Tellabide et al. [14], are as follows: length of the tube (L_T), 0.17 m; height of the entrainment zone, i.e., distance between the gas inlet nozzle and bottom of the draft tube (L_H), 0.07 m; diameter of the tube (D_T), 0.04 m; and aperture ratio of the open-sided draft tube, 57%.

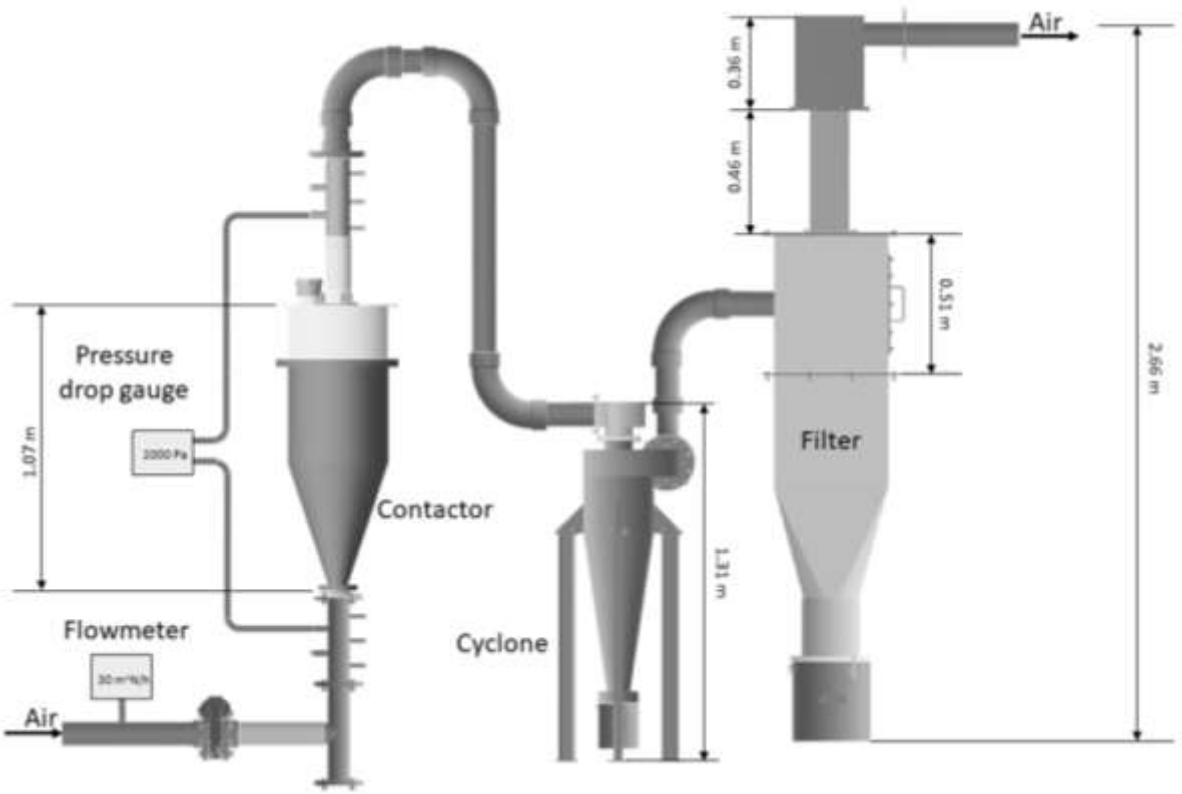

Figure 6.1. Schematic diagram of the experimental unit used (Tellabide et al. [14]).

Sand, glass, and soybean particles have been used in this study, with average particle sizes (d_p) of 0.25, 1, and 6 mm, respectively. These materials have been chosen to allow comparisons between fine and coarse particles, as well as between spherical and irregular particles. Thus, a wide range of solid flow patterns and features have been evaluated. The average particle size has been obtained by sieving (CISA RP 200N sieve shaker), caliper, and image analysis (Image-Pro Plus®). The density of sand, glass beads, and soybean are 2390, 2420, and 1210 kg m^{-3}, respectively, which have been determined based on the displacement method using water and toluene.

For the runs with sand particles, a fountain confiner made of polyethylene terephthalate has been used. This device is a cylindrical tube with the upper end closed to avoid gas and solid leaving

the contactor and has a cone shaped top to avoid the deposition of the solid from the feed on the outside of the device, and force it to describe a downward trajectory. More details about this device can be found in Tellabide et al. [14]. The dimensions of the fountain confiner are as follows: length of the confiner, 0.50 m; diameter of the confiner (D_F), 0.20 m; and the distance between bed surface and the lower end of the confiner (H_F), 0.06 m.

6.2.2 Experimental procedure and analysis methods

The hydrodynamic characterization of the systems has been performed according to the methodology described by Mathur and Epstein [13], which is based on a plot of bed pressure drop versus the air velocity (based on D_0) by increasing and decreasing the air flow rate. Pressure has been measured (±0.05% of accuracy) using differential pressure sensors inserted at the contactor input and output. All the runs have been repeated at least two times in order to obtain reliable results. As described previously, many approaches have been used to identify the flow regimes in gas-solid spouted beds. In this paper, the analysis of pressure fluctuation signals (PFS) and spectral analysis (Power Spectral Density, PSD) have been carried out to describe the dynamical behavior of the different systems. Pressure fluctuation signals have been measured at a sampling rate of 1 kHz by absolute pressure sensors (type PD23, Keller) inserted at the contactor input and output. Data acquisition has been carried out by decreasing the air flow rate for a time of 10 s, which has been proven suitable for most spouted bed systems [26]. Runs have been carried out in triplicate in order to ensure reproducibility of results. As mentioned above, there are several methods based on frequency-domain analysis, which are often used to obtain dominant frequencies and to characterize the hydrodynamic regimes in different frequency bands, namely, power spectral and

wavelet analyses [26,28]. In addition, Telgarsky [37] mentions several standard tools to analyse time series and detect dominant frequencies, such as fast Fourier transform, short-time Fourier transform, periodogram, and scalogram of various wavelets. In this study, the power spectral analysis (PSD) is the method adopted to obtain dominant frequencies in the system and has been performed by fast Fourier transformation (FFT) of pressure fluctuation signals using the Signal Processing Toolbox code in MATLAB.

6.3 RESULTS AND DISCUSSION

6.3.1 Characteristic curves

Figure 6.2 shows as an example the characteristic curves (pressure drop vs. air velocity) for certain systems analyzed. Thus, Figure 6.2a shows the curves for the three materials when no draft is used and Figure 6.2b the curves for the three configurations of soybean beds, i.e., without draft tube, and with nonporous and open-sided draft tubes.

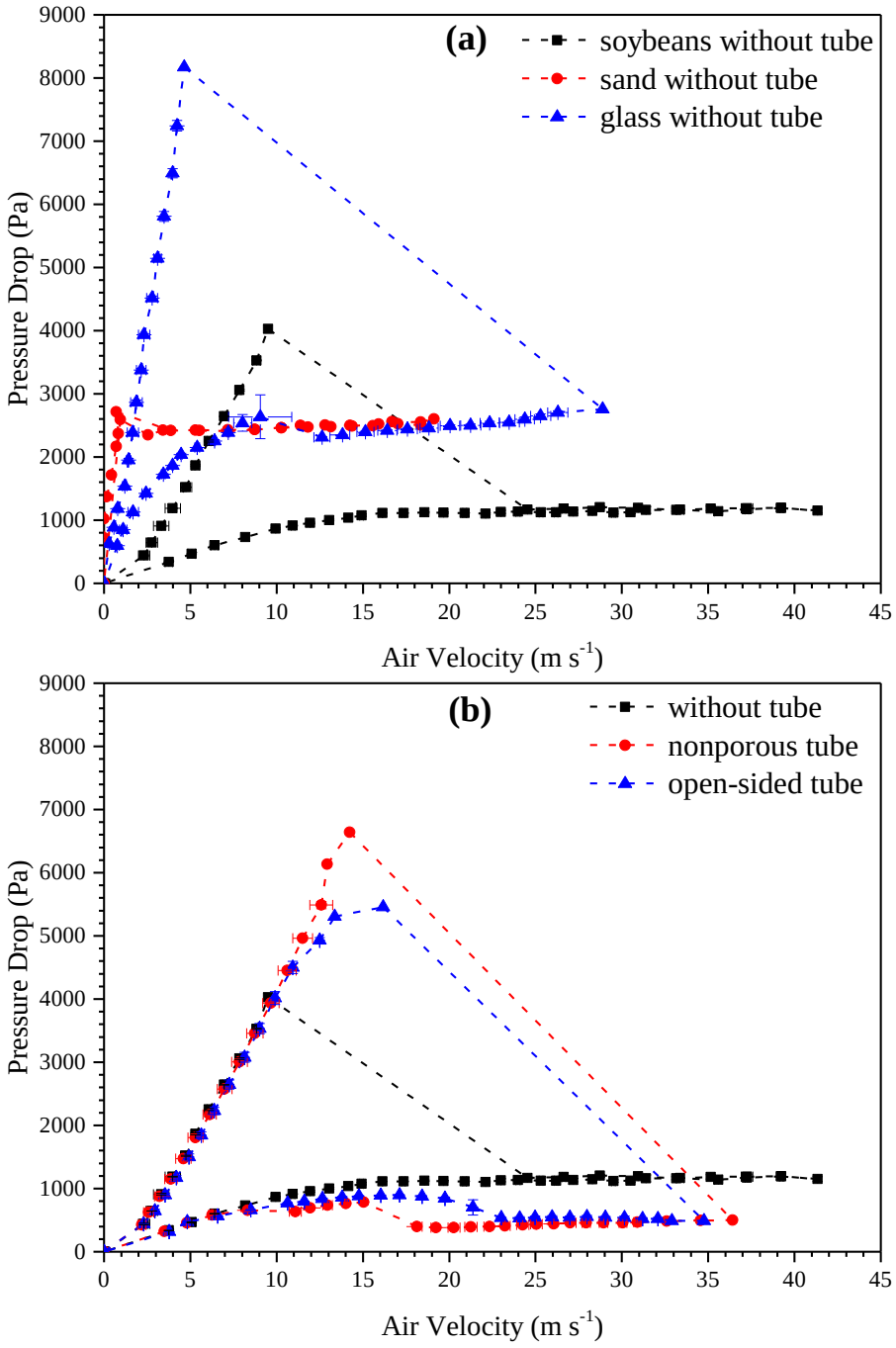

Figure 6.2. Pressure drop evolution with air velocity for (a) soybean, glass and sand beds without tube and for (b) soybean beds without tubes, and with nonporous and open-sided tubes.

As observed in Figure 6.2a, typical characteristic curves, such as those described by Mathur and Epstein [13], are obtained for glass particles. As mentioned previously, these curves show the

evolution when the air flow rate is increased and decreased. Initially, pressure drop increases almost linearly when air flow rate is increased until a peak value, i.e., the peak pressure drop (ΔP_m), in which the transition from an inner cavity to an internal spout occurs. With further increase in air flow rate, the internal spout breaks through the bed surface and the solids concentration in the region just above the internal spout decreases abruptly. Consequently, a sharp decrease in pressure drop occurs until an approximately constant value, i.e., the operating pressure drop (ΔP_s) is attained and the spouting regime is established. As air flow rate is decreased, there is a point in which the spouting regime ceases, and the corresponding velocity is termed minimum spouting velocity (u_{ms}), which is clearly detected by both the contactor transparent wall and the characteristic curve, as there is an increase in pressure drop when the spout collapses.

Nevertheless, this increase in pressure drop when the spout collapses is not observed with sand and soybean beds. Unlike glass beads, the fountain collapse with sand particles is characterized by a slight decrease in pressure drop, Figure 6.2a. This behavior is typical of fine particles (Geldart B particles), which is described in detail by Tellabide et al. [14]. These authors have also identified different spouting regimes for this kind of material by decreasing the air velocity from very high velocities to those of the static bed. According to Tellabide et al. [14], the characteristic curves of fine particles and the transitional points between different spouting regimes depend on the type of configuration used (without draft tubes or with open-sided or nonporous draft tubes).

Regarding soybean particles, pressure drop remains approximately constant when the spout collapse occurs. Such behavior can be attributed to the nature of particle-particle and gas-particle interactions in the case of coarse particles. High air percolation in the annulus is observed in soybean beds due to the size of this grain ($d_p = 6\ mm$) compared to sand particles ($d_p = 0.25\ mm$)

and glass beads ($d_p = 1\ mm$). Furthermore, a high agitation degree of soybean particles can still be visually observed on decreasing air flow rate after the fountain collapse, i.e., the bed remains unpacked for a while. Therefore, due to the air percolation and unrestricted particle movement, the increase in pressure drop is not observed with soybean particles. However, Figure 6.2b shows an increase in pressure drop at the point the spout collapses when both nonporous and open-sided tubes are employed. These results are explained by the limitation in particle movement in the bed when these internal devices are used.

Therefore, difficulties arise in delimiting the minimum spouting velocity for sand and soybean beds by using the evolution of pressure drop with air velocity. Therefore, the need of an alternative methodology to estimate the minimum spouting velocity for these materials is evident, which is specifically the aim of this study. Sari et al. [32] have found similar difficulties in a conical spouted bed operating with heavy particles. Thus, the authors have obtained the minimum spouting velocity from bed pressure drop data and monitoring the upper layer of the particle bed through the cylindrical acrylic part of the equipment (transparent wall). However, visual methodology can involve inaccuracies when fine and irregular materials are handled, as they undergo unstable regimes, or it may be even unfeasible for industrial-scale equipment, which is generally made of opaque materials. Therefore, methodologies based on pressure fluctuation and spectral analyses may be helpful to overcome these limitations.

6.3.2 Pressure Fluctuation Signals and Spectral Analysis

Pressure fluctuation signals (PFS) and spectral analysis (Power Spectral Density, PSD) are used to describe the dynamical behavior of the different systems. As shown above, not only the

material, but also the configuration (without draft tubes or with open-sided or nonporous draft tubes) significantly influences the results. Thus, PFS and PSD results for the different materials used are separately analyzed for each configuration. These analyses have been performed on decreasing air flow rate.

6.3.2.1 Without draft tubes

Figure 6.3 shows as an example the results for the evolution of pressure fluctuations with time and the power spectral density with frequency for sand (graphs 6.3a and 6.3b), glass beads (graphs 6.3c and 6.3d), and soybean (graphs 6.3e and 6.3f). These results correspond to given spouting velocities, which are higher than the minimum one for each material in order to ensure stable spouting. Thus, according to certain authors, stable spouting regime is attained when air velocity is in the range from $1.2u_{ms}$ to $2.1u_{ms}$ [23,32]. In the example shown in Figure 6.3, the velocity used for sand beds is $1.5u_{ms}$ and for the other materials $1.3u_{ms}$. Nevertheless, pressure fluctuation signals have been obtained and analyzed in a wide range of velocities, from below the minimum spouting velocity to well above this one.

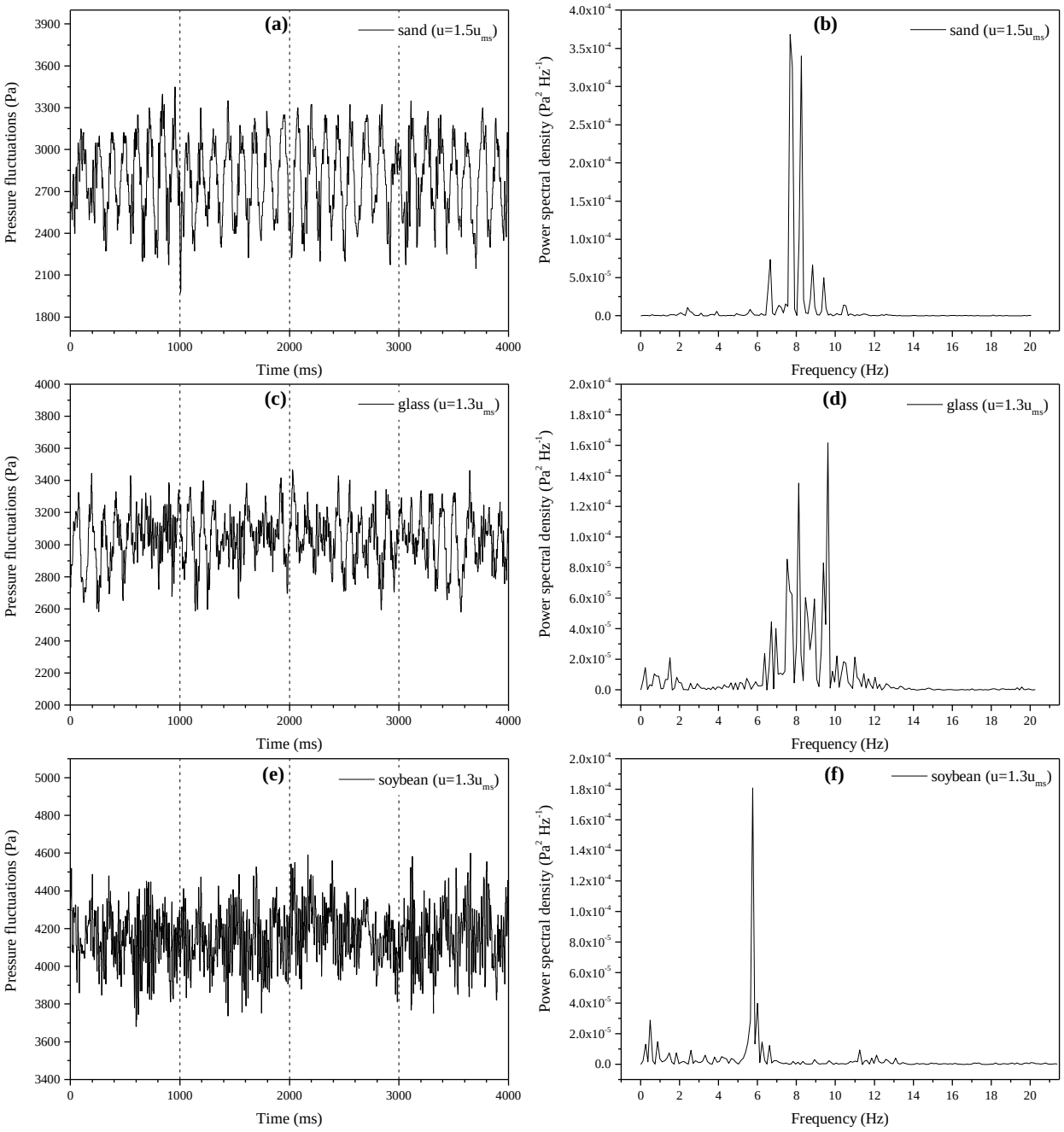

Figure 6.3. Evolution of pressure fluctuation with time and power spectral density with frequency for (a, b) sand, (c, d) glass beads and (e, f) soybean, for air velocities above that of minimum spouting.

The pressure fluctuation signals obtained for the materials studied are typical to spouted beds. Qualitatively, all the materials follow a similar behavior with cyclic fluctuations in pressure drop. Such behavior can be attributed to the vigorous and cyclic movement of the particles when the spouting regime is established. Several authors have obtained similar results [26,29,31].

Nevertheless, a detailed analysis shows significant differences in the signals corresponding to the different materials. Thus, the most evident and clear signals of pressure fluctuations are those corresponding to sand particles. The pressure fluctuations obtained for soybean beds are significantly less evident than for the other material beds, which is partially explained by their high degree of agitation and particle movement at different frequencies. Despite the good stability provided by the fountain confiner, sand particles move in clusters due to their small size and particle-particle interactions (Geldart B). Thus, a pulsating spouting regime due mainly to pulsating particle movement in the spout is observed. This behavior may be clearly observed through the contactor transparent wall. Thus, the spout is almost collapsed but suddenly it is wide open, with these phenomena occurring at a given frequency. Likewise, the pulsating motion has also been observed by Mostoufi et al. [30], who have attributed this phenomenon to the flow of solids from the bulk of the annulus into the spout. These authors have observed that small particles provide stronger pulsation at the annulus-spout interface than large particles, suggesting a higher solid transfer rate from the annulus into the spout in the case of small particles.

Although glass and soybean particles are larger than those of sand, and so lead to more stable beds than those of sand particles, pulsating spouting regimes are visually observed. This finding is consistent with that by Olazar et al. [38], who have found a similar behavior for 1-8 mm glass beads in conical spouted beds. Furthermore, they observed that stable spouting was not formed for the smallest particles ($d_p = 1\ mm$), but a transition from fixed bed to an unstable state, which was

evidenced by bubble formation. For the largest particles ($d_p = 8\,mm$), stable spouting was only reached for shallow beds ($H_0 < 8\,cm$). For static bed heights above this value ($H_0 > 8\,cm$), Olazar et al. [38] observed a transition from fixed bed to a slugging regime with bubbles from wall to wall. This study reveals these pulsating spouting regimes which are evidenced by the PSD results, since dominant frequencies are obtained for all materials (Figures 6.3b, 6.3d, and 6.3f).

The dominant frequencies obtained are 7-9 Hz, 8-10 Hz, and 6 Hz, for sand, glass, and soybean particles, respectively. These values are within the range of the main frequencies reported for most spouted bed systems, i.e., on the order of 1-10 Hz [26]. These dominant frequencies are related to the periodic pulsation inside the spout. As stated by Mollick and Sathiyamoorthy [33], dominant frequencies indicate the repeatability of specific pressure fluctuation values at these frequencies. The mentioned authors performed similar analyses with zirconia spherical particles. Despite the different particles and conditions, Mollick and Sathiyamoorthy [33] observed dominant frequencies in the transition from one hydrodynamic regime to the other. During regime transition, the whole system was generally unstable and pulsating, which applies also to the systems analyzed in this study. As mentioned previously, these pulsating spouting regimes were visually observed in this study for all the particles used without draft tubes.

Such dominant frequencies are hardly observed at air velocities lower than the minimum spouting one, as shown in Figure 6.4 for u = 0.6 u_{ms}, where low intensity dominant frequencies are observed for all the materials. Furthermore, the amplitude of the pressure fluctuation signals is also much shorter than above minimum spouting for all the materials. The low power spectral density and short amplitude of the peaks are related to the air percolation through the bed without causing significant particle movement. Thus, pressure fluctuations are reduced under low air velocities. Several authors have obtained similar results under packed bed conditions [29,31].

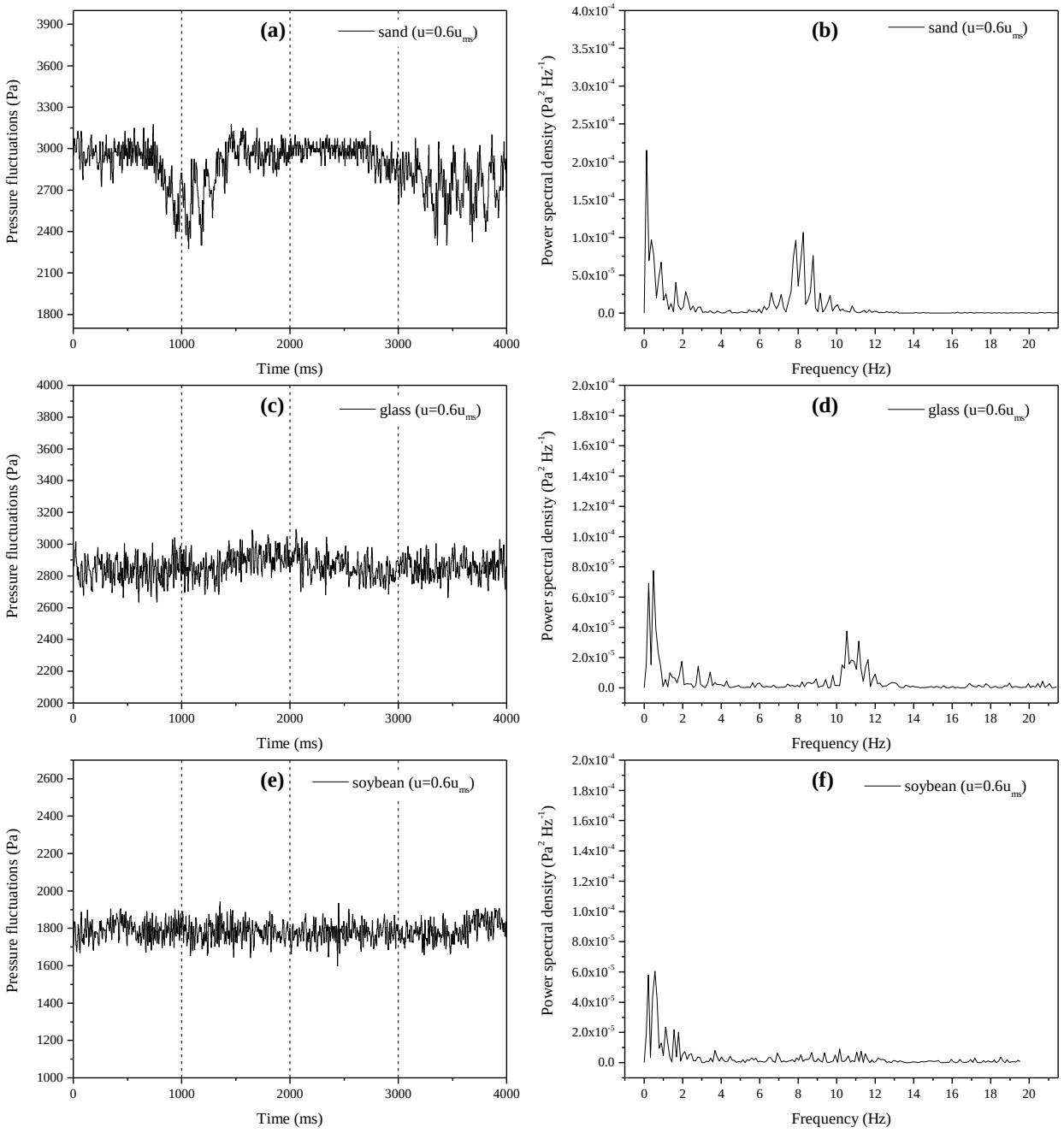

Figure 6.4. Evolution of pressure fluctuation with time and power spectral density with frequency for (a, b) sand, (c, d) glass beads and (e, f) soybean, for air velocities below that of minimum spouting

Therefore, monitoring the evolution of dominant frequencies in a wide range of air velocities from well above that of minimum spouting to below this one may shed light on the transition from the spouting regime to the fixed bed. This spectral analysis can be even more useful when combined with the characteristic curves (pressure drop vs. air velocity), which are the basis of the conventional method proposed by Mathur and Epstein [13] to identify spouting regimes. Figure 6.5 shows the evolution of pressure drop and dominant frequencies with air velocity for the runs without draft tube. As observed, overall there is a similar trend for all the materials on decreasing air velocity, i.e., dominant frequencies remain approximately constant when air velocity is decreased, until a sharp and very pronounced drop in frequency occurs at a certain velocity. This sharp drop in the dominant frequency occurs at the same range of velocities as a slight decrease in pressure drop for sand particle beds (Figure 6.5a) or an increase in pressure drop for glass particle beds (Figure 6.5b) in the characteristic curves when air velocity is decreased. The sharp drop in dominant frequency occurs at $u = 3.76\, m\, s^{-1}$ for sand particles, and $at\ u = 13.04\, m\, s^{-1}$ for glass particles, whereas the minimum spouting velocity obtained for these materials in the characteristic curves are $u = 3.40\, m\, s^{-1}$ and $u = 12.60\, m\, s^{-1}$ for sand and glass, respectively. Thus, this sharp drop in dominant frequency corresponds to the minimum spouting velocity, as indicated in Figure 6.5. As described previously, the minimum spouting velocity can be obtained from the characteristic curves when the pressure drop changes by spout collapse on decreasing air velocity. Regarding soybean, the sharp drop in dominant frequency occurs at $u = 26.10\, m\, s^{-1}$, but there is no change in pressure drop, i.e., pressure drop remains approximately constant when the spout collapses. However, the value of $u = 26.10\, m\, s^{-1}$ coincides with the minimum spouting velocity obtained by monitoring the upper layer of the particle bed (fountain collapse) through the contactor transparent wall.

Therefore, these results suggest that the minimum spouting velocity can be estimated based on the sharp drop in dominant frequencies when decreasing air velocity, with the differences between these values and those obtained based on the characteristic curves being in the range from 10.60% to 3.50% for sand and glass particles, respectively. As mentioned above, the materials studied may lead to slugging and pulsating spouting regimes at air velocities higher than the minimum spouting velocity. Nevertheless, the methodology proposed is suitable for fine and coarse particles, either they are irregular or spherical. However, fine materials, and even the coarse ones in large units, require internal devices, such as draft tubes and/or fountain confiners to improve and overcome the limitations related to stability and scaling up. As mentioned previously, there is hardly any study in the literature regarding the influence of such internal devices on pressure fluctuations.

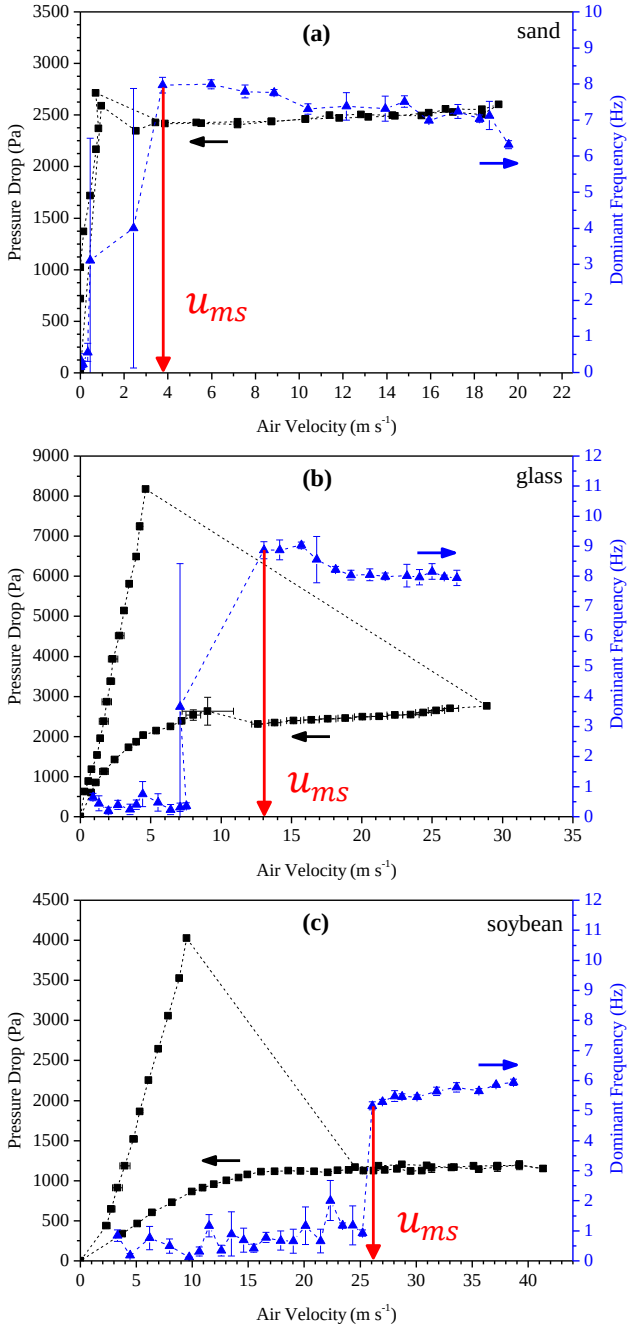

Figure 6.5. Evolution of pressure drop and dominant frequency with air velocity for the systems without draft tube and beds of (a) sand, (b) glass beads, and (c) soybeans.

6.3.2.2 Nonporous tubes

Figure 6.6 shows the pressure drop and dominant frequency versus the air velocity for systems with a nonporous draft tube. Similarly to the process without a draft tube, both sand and glass particle beds with a nonporous tube also undergo a sharp decrease in frequency when the minimum spouting velocity is approached by decreasing air velocity. Even with a nonporous tube, sand particles have a visible pulsating spout regime, which is responsible for the dominant frequencies observed. However, this pulsating spout regime is not visually observed with glass particles due to the high stability provided by the nonporous tubes. However, pressure fluctuations clearly show that there is a dominant frequency at spouting velocity. In fact, the dominant frequency is approximately the same until the minimum spouting velocity is reached. It seems that the dominant frequencies observed with these small glass beads are related to their small size ($d_p = 1\ mm$), as air percolation through the annular region with small particles is lower than with coarse particles. Such air percolation is even lower with the nonporous tube. Thus, the particle-gas interactions are concentrated in the spout channel, in which the solid input is limited to the entrainment zone and all the particles travel upwards the fountain due to the nonporous tube. Therefore, this internal device hampers solid cross-flow from the annulus into the spout at any level in the bed [19,39]. Consequently, the dominant frequency is attributed to the system for this type of gas-solid interaction. This discussion is also applicable to sand particles. In these cases, the alternative methodology proposed based on both hydrodynamic and spectral analyses is suitable to estimate the minimum spouting velocity, as dominant frequencies and/or sharp drops in operating pressure are observed for these materials in the nonporous configuration.

Regarding soybean particles, unlike the systems without tubes, dominant frequency peaks are not observed. This result is a consequence of the very stable spouting regime attained in the spouting of these coarse particle beds with nonporous tube, as neither pulsating movement nor slugging effect is observed. Consequently, both bed and fountain heights remain almost constant without periodic variations in the spouting regime. Thus, when the whole bed exhibits vigorous circulation under stable spouting at any frequency, pressure fluctuations become less evident (no changing trend), as also observed by Leu and Lo [31]. Consequently, there is no clearly dominant frequency, i.e., there is stable spouting regime with low frequencies in the bed pressure fluctuation. Furthermore, the porous soybean bed allows more air percolation into the annulus region than the other smaller particles, as previously described. Thus, gas-particle interaction is not limited to the spout channel, but occurs in the whole bed. This fact related to the effect of air percolation suggests that packing density and specific surface area are relevant parameters to be considered in such analysis.

These results are supported by Figure 6.7, which shows the pressure fluctuation signals versus time and the power spectral density versus frequency for soybean beds with nonporous tubes, when operation is carried out at air velocities higher than the minimum spouting one. Similarly, as described for packed bed conditions (Figure 6.4), pressure fluctuations of short amplitude and low dominant frequency are observed. These features suggest a very stable spouting regime. Similar results have been reported by Piskova and Mörl [26] and Mollick and Sathiyamoorthy [33]. Furthermore, Mollick and Sathiyamoorthy [33] have found several low intensity peaks under stable spouting conditions.

These findings reveal that PSD analysis is able to clearly delimit the minimum spouting velocity in nonporous draft tube configurations when fine and small particles are used, represented

in this study by sand and glass particles, respectively. In relation to very stable spouting regimes, i.e., soybean with a nonporous tube, the methodology is ineffective due to the difficulty in selecting dominant frequencies. For this type of material, both visual observation and characteristic curves are more efficient than PSD analysis. Nevertheless, these findings contribute to providing new understanding related to the application of pressure fluctuation analysis to conical spouted beds equipped with nonporous tube and operating with fine and irregular particles, whose hydrodynamic behaviour is very different to that reported by several authors [26,30,33], in which either other configurations or larger particles have been used.

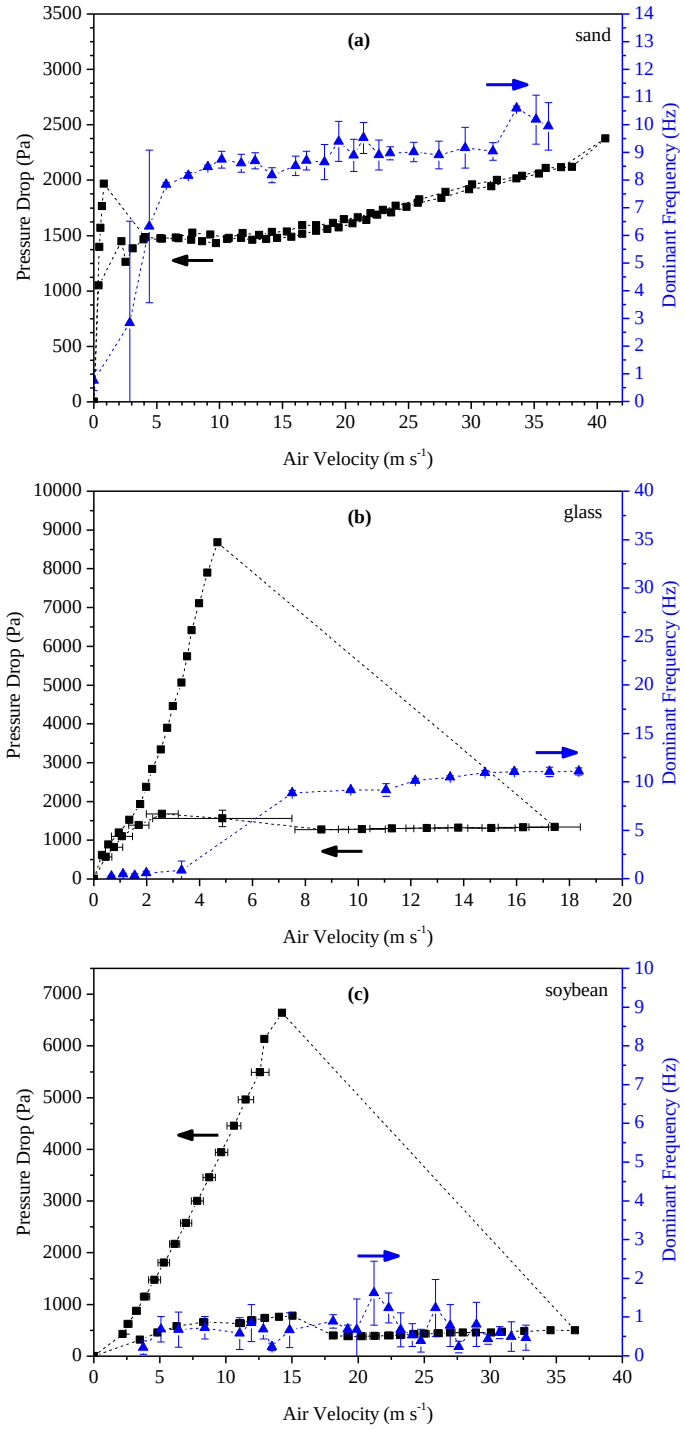

Figure 6.6. Evolution of pressure drop and dominant frequency with air velocity for the systems with nonporous operated and beds of (a) sand, (b) glass beads, and (c) soybeans.

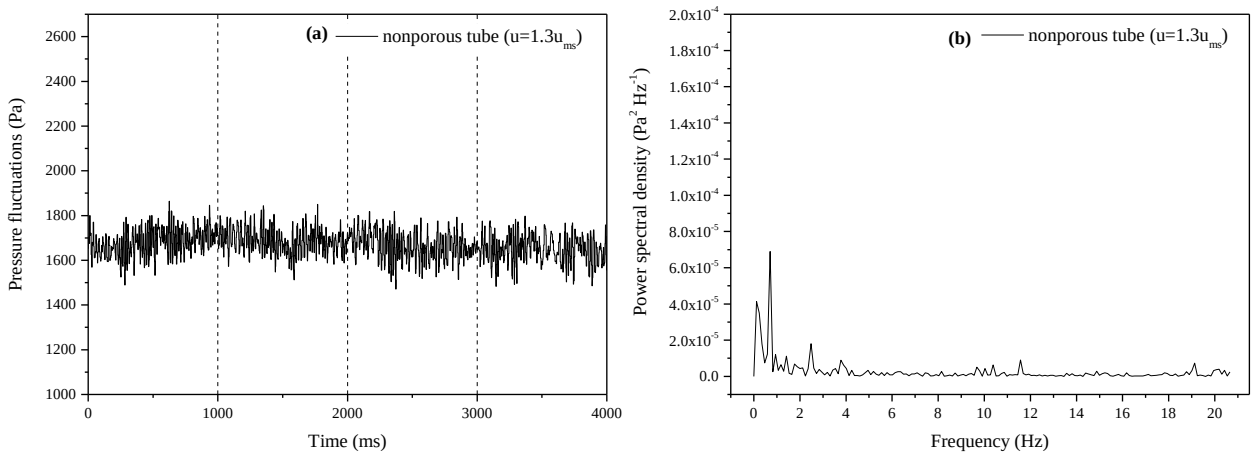

Figure 6.7. Evolution of (a) pressure fluctuations with time and (b) power spectral density with frequency for soybean beds with nonporous tubes.

6.3.2.3 Open-sided tubes

Figure 6.8 shows the evolution of pressure drop and dominant frequency with air velocity for systems operating with open-sided draft tubes.

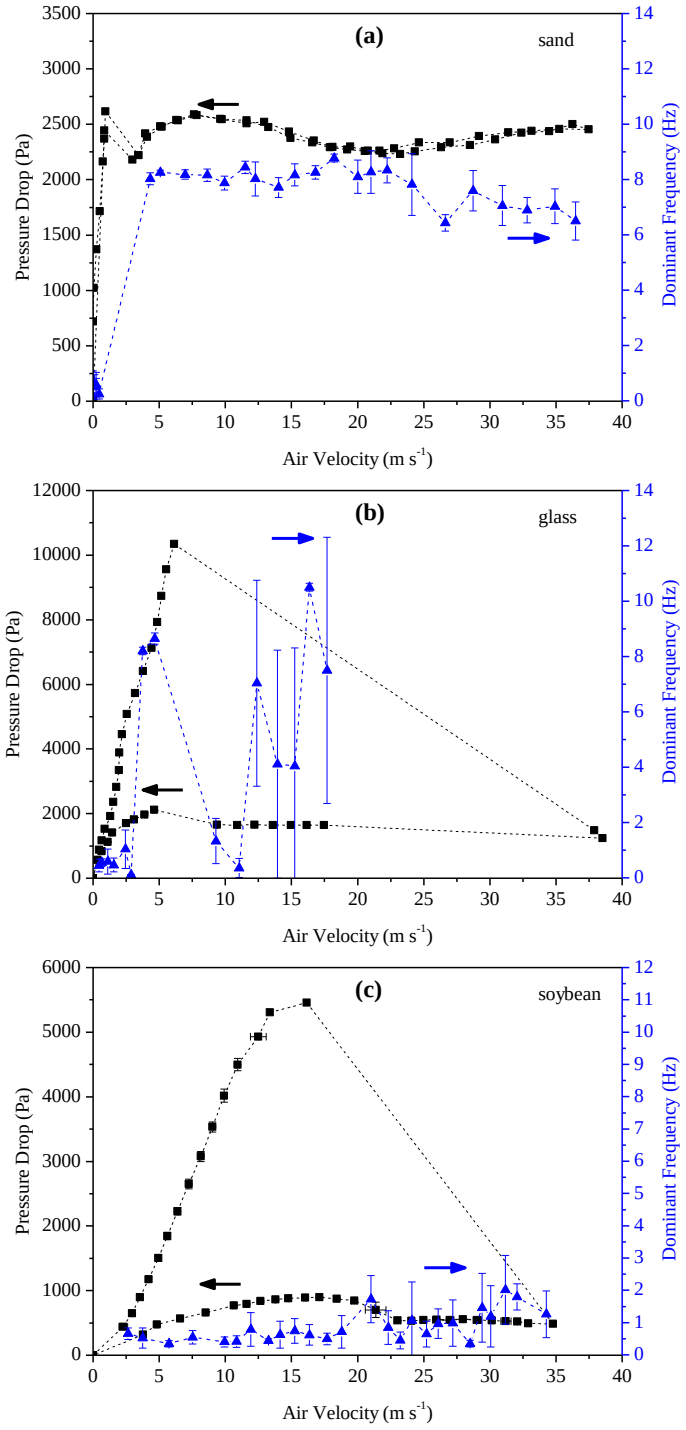

Figure 6.8. Evolution of pressure drop and dominant frequency with air velocity for the systems with open-sided draft tube and beds of (a) sand, (b) glass beads, and (c) soybeans.

The results obtained with sand particles follow a similar trend as those for the other two configurations, i.e., without tubes and with nonporous tubes. Therefore, a discussion similar to those made for sand particles apply to this case. This finding is evidence that the methodology proposed in this study is a promising and suitable alternative to delimit the minimum spouting velocity for these materials, which are characterized by pulsating and slugging regimes. Likewise, the results for soybean beds with open-sided tubes are consistent with those obtained with nonporous tubes, since both configurations are characterized by very stable spouting regimes. However, glass particles with these tubes show a different behavior from the other two configurations, as the dominant frequency is highly fluctuating with air velocity. This behavior suggests the existence of multiple dominant frequencies at different air velocities. In order to confirm this fact, Figure 6.9 shows the power spectral density versus frequency for glass bead beds with open-sided draft tubes at different air velocities.

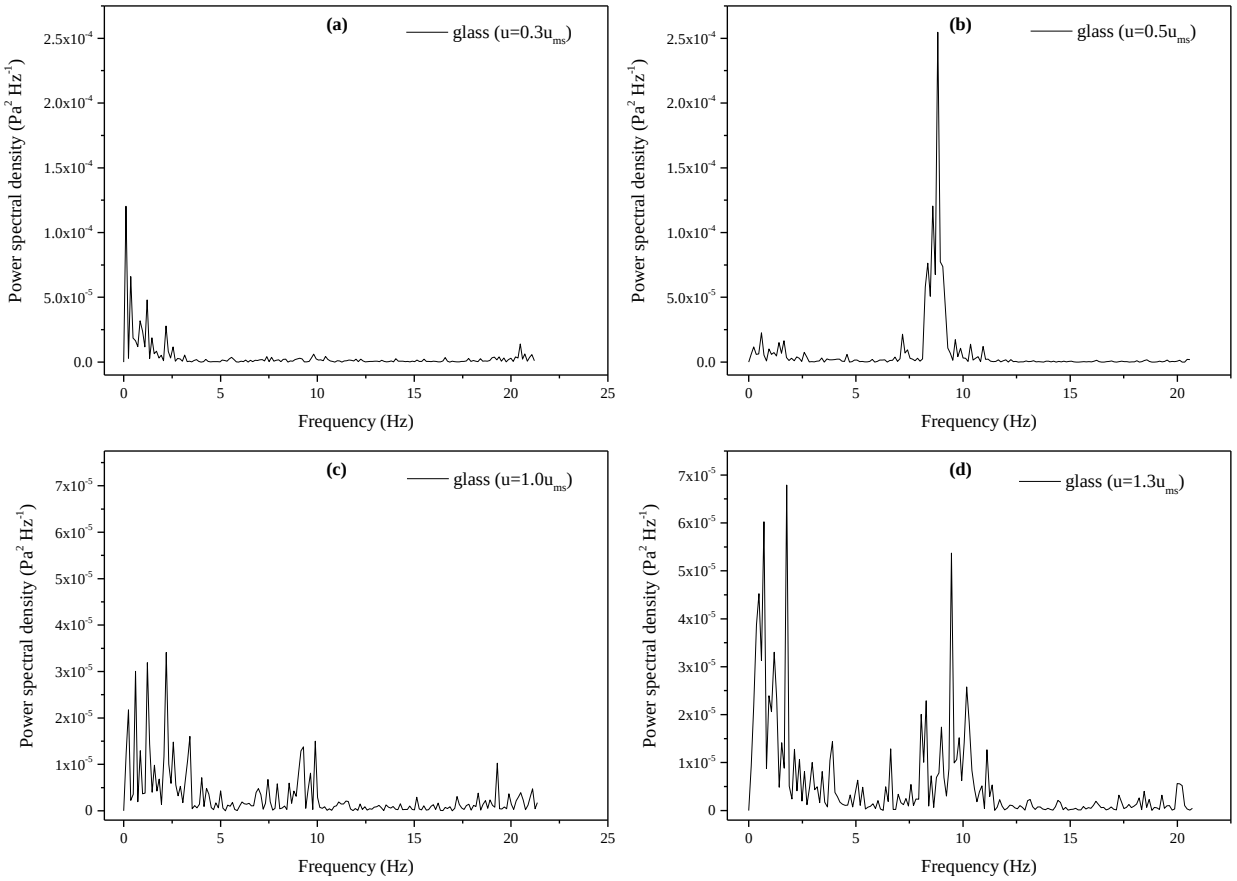

Figure 6.9. Power spectral density versus frequency for glass bead beds with open-sided draft tube operating at (a) $u = 0.3u_{ms}$, (b) $u = 0.5u_{ms}$, (c) $u = 1.0u_{ms}$, and (d) $u = 1.3u_{ms}$.

At $u = 0.3u_{ms}$ (packed bed), peaks at low dominant frequency are observed, which is consistent with the results shown above (Figure 6.4). A sharp peak near 10 Hz appears at $u = 0.5u_{ms}$, which corresponds to the air velocity following the sudden increase in pressure drop on decreasing air velocity observed in the characteristic curve (pressure drop versus air velocity). This peak is attributed to the high energy required by the particles in the regime transition. When the spouting regime is established (Figure 6.9c), such peak loses intensity due to continuous spouting of particles once the spout is open. An increase in air velocity when the spouting regime is well

established leads to an increase in the peak at 10 Hz, as well as the appearance of multiple peaks. This result is consistent with the findings reported by Mollick and Sathiyamoorthy [33].

The behaviour observed for glass particles in this study is related to the combined effect of the solid cross-flow from the annulus into the spout at any level in the bed and the higher air percolation in the annulus provided by the open-sided tubes. In addition to these aspects, a more stable regime than without tube is also observed for glass beads with an open-sided tube, i.e., similar to the stability attained for soybeans operating with internal devices. This fact explains the highly fluctuating behaviour of the dominant frequency in this configuration, as shown in Figure 6.8b. Nevertheless, PSD analysis is still able to characterize and identify different flow regimes by monitoring the qualitative behaviour at different air velocities, as also reported by several authors [26,29,33]. Therefore, this study confirms that spectral analysis is a promising alternative to determine quantitatively the value of relevant hydrodynamic parameters, especially when combined with characteristic curves.

6.4 CONCLUSIONS

The methodology proposed in this study allows estimating the minimum spouting velocity for fine and irregular particles, represented by sand particles, in systems without and with draft tubes. In all the conditions evaluated, this material presents sharp drops of dominant frequencies on decreasing air velocity. Accordingly, the methodology proposed proves to be especially suitable for these types of particles that leak to pulsating spouting. Thus, fine and irregular particles are characterized by circulation in clusters due to their small size and particle-particle interactions (Geldart B). Consequently, the spout is almost collapsed and suddenly wide open, with these

phenomena occurring at a given frequency, even with internal devices. Concerning small spherical particles (glass beads) the spectral analysis is still able to provide the minimum spouting velocity for both without and with nonporous draft tubes. In the process with open-sided draft tubes, the methodology has presented some limitations for glass particles due to multiple dominant frequencies at different air velocities. In this case, the PSD analysis monitoring the qualitative behavior at different air velocities is still able to identify the different flow regimes. Regarding soybean particles, the spectral analysis has also provided the minimum spouting velocities in the systems without tubes, which is also characterized by a pulsating spouting regime. In this configuration with soybean particles, the conventional method for obtaining the minimum spouting velocity (characteristic curve) has not been feasible since the pressure drop remains approximately constant in the spout collapse. However, due to the high stability, the spectral analysis is not efficient to provide the minimum spouting velocity for processes with internal devices operating with coarse spherical particles, as soybean grains. In these cases, the characteristic curve is more adequate than the PSD analysis to estimate the minimum spouting velocity. Therefore, the findings of this study provide a new understanding related to the application of pressure fluctuation analysis in draft tube conical spouted beds operating with fine and irregular particles, as well as for coarse and spherical particles, which are characterized by unstable and pulsating regimes. Furthermore, the alternative methodology proposed in this study based on both hydrodynamic and spectral analysis to estimate the minimum spouting velocity is a promising tool for industrial processes, mainly for the processing of fine and irregular particles, as they lead to unstable and pulsating regimes. These aspects are even more relevant when the aim is process control and scaling up, as the application of spectral analysis is more feasible than visual methodologies. Thus, further research should be undertaken to explore the effect different

geometric factors and materials have on the methodology proposed to identify more applications and limitations in the spouted bed.

ACKNOWLEDGEMENTS

The authors appreciate the financial support provided by Coordination for the Improvement of Higher Education Personnel (CAPES), the São Paulo State Research Foundation (FAPESP, grant #2017/01856-7 and grant #2018/22655-2), the Spain's Ministry of Economy and Competitiveness (CTQ2016-75535-R (AEI/FEDER, UE)) and the European Commission (HORIZON H2020-MSCA RISE-2018. Contract No.: 823745). I. Estiati thanks the University of the Basque Country for her postgraduate grant (ESPDOC18/14). M. Tellabide thanks the Spain's Ministry of Education, Culture and Sport for his Ph.D. grant (FPU14/05814).

REFERENCES

[1] Santamaria L, Arregi A, Lopez G, Artetxe M, Amutio M, Bilbao J, et al. Effect of La2O3 promotion on a Ni/Al2O3 catalyst for H2 production in the in-line biomass pyrolysis-reforming. Fuel 2020;262:116593. doi:10.1016/j.fuel.2019.116593.

[2] Lopez G, Alvarez J, Amutio M, Hooshdaran B, Cortazar M, Haghshenasfard M, et al. Kinetic modeling and experimental validation of biomass fast pyrolysis in a conical spouted bed reactor. Chem Eng J 2019;373:677–86. doi:10.1016/j.cej.2019.05.072.

[3] Liu M, Chen Z, Chen M, Shao Y, Liu B, Tang Y. Scale-up strategy study of coating furnace for TRISO particle fabrication based on numerical simulations. Nucl Eng Des

2020;357:110413. doi:10.1016/j.nucengdes.2019.110413.

[4] Pietsch S, Peter A, Wahl P, Khinast J, Heinrich S. Measurement of granule layer thickness in a spouted bed coating process via optical coherence tomography. Powder Technol 2019;356:139–47. doi:10.1016/j.powtec.2019.08.022.

[5] Spiegl N, Berrueco C, Long X, Paterson N, Millan M. Production of a fuel gas by fluidised bed coal gasification compatible with CO2 capture. Fuel 2020;259:116242. doi:10.1016/j.fuel.2019.116242.

[6] Niksiar A, Nasernejad B. Modeling of gasification reaction to produce activated carbon from pistachio shells in a spouted bed. Biomass and Bioenergy 2018;119:97–108. doi:10.1016/j.biombioe.2018.09.008.

[7] Wang Z, Lim CJ, Grace JR. A comprehensive study of sawdust torrefaction in a dual-compartment slot-rectangular spouted bed reactor. Energy 2019;189:116306. doi:10.1016/j.energy.2019.116306.

[8] Mollick PK, Venugopalan R, Roy M, Rao PT, Sathiyamoorthy D, Sengupta P, et al. Deposition of diversely textured buffer pyrolytic carbon layer in TRISO coated particle by controlled manipulation of spouted bed hydrodynamics. Chem Eng Sci 2015;128:44–53. doi:10.1016/j.ces.2015.01.065.

[9] Yang X, Zhang F, Guo M, Zhong Y, Wang P, Lin J, et al. Preparation of SiC layer with sub-micro grain structure in TRISO particles by spouted bed CVD. J Eur Ceram Soc 2019;39:2839–45. doi:10.1016/j.jeurceramsoc.2019.02.005.

[10] Moradi M, Azizi S, Niakousari M, Kamgar S, Mousavi Khaneghah A. Drying of green bell pepper slices using an IR-assisted Spouted Bed Dryer: An assessment of drying kinetics and energy consumption. Innov Food Sci Emerg Technol 2020;60:102280.

doi:10.1016/j.ifset.2019.102280.

[11] Tanabe EH, Silva RM, Oliveira Júnior DL, Bertuol DA. Recovery of valuable metals from waste cables by employing mechanical processing followed by spouted bed elutriation. Particuology 2019;45:74–80. doi:10.1016/j.partic.2018.12.002.

[12] Geldart D. Types of gas fluidization. Powder Technol 1973;7:285–92. doi:10.1016/0032-5910(73)80037-3.

[13] Mathur KB, Epstein N. Spouted Beds. New York: Academic Press; 1974.

[14] Tellabide M, Estiati I, Pablos A, Altzibar H, Aguado R, Olazar M. New operation regimes in fountain confined conical spouted beds. Chem Eng Sci 2020;211:115255. doi:10.1016/j.ces.2019.115255.

[15] Saldarriaga JF, Estiati I, Atxutegi A, Aguado R, Bilbao J, Olazar M. Distribution of Cycle Times in Sawdust Conical Spouted Bed Equipped with Fountain Confiner and Draft Tube. Ind Eng Chem Res 2019;58:1932–40. doi:10.1021/acs.iecr.8b03451.

[16] Atxutegi A, Tellabide M, Lopez G, Aguado R, Bilbao J, Olazar M. Implementation of a borescopic technique in a conical spouted bed for tracking spherical and irregular particles. Chem Eng J 2019;374:39–48. doi:10.1016/j.cej.2019.05.143.

[17] Al-Juwaya T, Ali N, Al-Dahhan M. Investigation of hydrodynamics of binary solids mixture spouted beds using radioactive particle tracking (RPT) technique. Chem Eng Res Des 2019;148:21–44. doi:10.1016/j.cherd.2019.05.051.

[18] Estiati I, Tellabide M, Saldarriaga JF, Altzibar H, Olazar M. Fine particle entrainment in fountain confined conical spouted beds. Powder Technol 2019;344:278–85. doi:10.1016/j.powtec.2018.12.035.

[19] Olazar M, Lopez G, Altzibar H, Amutio M, Bilbao J. Drying of Biomass in a Conical

Spouted Bed with Different Types of Internal Devices. Dry Technol 2012;30:207–16. doi:Doi 10.1080/07373937.2011.633194.

[20] Pablos A, Aguado R, Vicente J, Altzibar H, Bilbao J, Olazar M. Effect of operating conditions on the drying of fine and ultrafine sand in a fountain confined conical spouted bed. Dry Technol 2019;0:1–16. doi:10.1080/07373937.2019.1645684.

[21] Moliner C, Marchelli F, Bosio B, Arato E. Modelling of spouted and spout-fluid beds: Key for their successful scale up. Energies 2017;10. doi:10.3390/en10111729.

[22] Yang J, Breault RW, Rowan SL. Experimental investigation of fountain height in a shallow rectangular spouted bed using digital image analysis. Chem Eng J 2020;380:122467. doi:10.1016/j.cej.2019.122467.

[23] Foroughi-Dahr M, Sotudeh-Gharebagh R, Mostoufi N. Characterization of flow properties of pharmaceutical pellets in draft tube conical spout-fluid beds. J Ind Eng Chem 2018;68:274–81. doi:10.1016/j.jiec.2018.07.054.

[24] Ma J, van Ommen JR, Liu D, Mudde RF, Chen X, Pan S, et al. Fluidization dynamics of cohesive Geldart B particles. Part II: Pressure fluctuation analysis. Chem Eng J 2019;368:627–38. doi:10.1016/j.cej.2019.02.187.

[25] Bi HT. A critical review of the complex pressure fluctuation phenomenon in gas-solids fluidized beds. Chem Eng Sci 2007;62:3473–93. doi:10.1016/j.ces.2006.12.092.

[26] Piskova E, Mörl L. Characterization of spouted bed regimes using pressure fluctuation signals. Chem Eng Sci 2008;63:2307–16. doi:10.1016/j.ces.2006.05.005.

[27] Van Der Schaaf J, Schouten JC, Van Den Bleek CM. Origin, propagation and attenuation of pressure waves in gas-solid fluidized beds. Powder Technol 1998;95:220–33. doi:10.1016/S0032-5910(97)03341-X.

[28] Jaiboon OA, Chalermsinsuwan B, Mekasut L, Piumsomboon P. Effect of flow pattern on power spectral density of pressure fluctuation in various fluidization regimes. Powder Technol 2013;233:215–26. doi:10.1016/j.powtec.2012.09.014.

[29] Xu J, Bao X, Wei W, Shi G, Shen S, Bi HT, et al. Statistical and frequency analysis of pressure fluctuations in spouted beds. Powder Technol 2004;140:141–54. doi:10.1016/j.powtec.2004.02.003.

[30] Mostoufi N, Kulah G, Koksal M. Flow structure characterization in conical spouted beds using pressure fluctuation signals. Powder Technol 2015;269:392–400. doi:10.1016/j.powtec.2014.09.028.

[31] Leu LP, Lo MC. Pressure fluctuations in spouted beds. J Chinese Inst Chem Eng 2005;36:391–8. doi:10.6967/JCICE.200507.0391.

[32] Sari S, Kulah G, Koksal M. Characterization of gas-solid flow in conical spouted beds operating with heavy particles. Exp Therm Fluid Sci 2012;40:132–9. doi:10.1016/j.expthermflusci.2012.02.008.

[33] Mollick PK, Sathiyamoorthy D. Assessment of stability of spouted bed using pressure fluctuation analysis. Ind Eng Chem Res 2012;51:12117–25. doi:10.1021/ie300950p.

[34] Zhang H, Liu M, Li T, Huang Z, Sun X, Bo H, et al. Experimental investigation on gas-solid hydrodynamics of coarse particles in a two-dimensional spouted bed. Powder Technol 2017;307:175–83. doi:10.1016/j.powtec.2016.11.024.

[35] Hosseini SH, Karami M, Altzibar H, Olazar M. Prediction of pressure drop and minimum spouting velocity in draft tube conical spouted beds using genetic programming approach. Can J Chem Eng 2019;2019:583–9. doi:10.1002/cjce.23590.

[36] Marchelli F, Hou Q, Bosio B, Arato E, Yu A. Comparison of different drag models in CFD-

DEM simulations of spouted beds. Powder Technol 2020;360:1253–70. doi:10.1016/j.powtec.2019.10.058.

[37] Telgarsky R. Dominant Frequency Extraction. Eprint ArXiv: 13060103 2013;1:1–12.

[38] Olazar M, San José MJ, Aguayo AT, Arandes JM, Bilbao J. Stable operation conditions for gas-solid contact regimes in conical spouted beds. Ind Eng Chem Res 1992;31:1784–92. doi:10.1021/ie00007a025.

[39] Altzibar H, Lopez G, Aguado R, Alvarez S, San Jose MJ, Olazar M. Hydrodynamics of conical spouted beds using different types of internal devices. Chem Eng Technol 2009;32:463–9. doi:10.1002/ceat.200800605.

CHAPTER 7

DRYING IN DRAFT TUBE CONICAL SPOUTED BEDS

This chapter describes the analysis of the drying of particulate solids in draft tube spouted beds, which refers to specific objective (5) of this thesis. Drying is a highly energy-intensive process and dryers are considered one of the most energy-consuming industrial equipment. Nevertheless, the energy contribution of the draft tube in the spouted bed has hardly been studied. Thus, the paper described in this chapter aimed to perform an energy analysis of a draft tube conical spouted bed for particulate materials. Drying of alumina, soybean, and barley has been performed with three different configurations: without tube and with nonporous and open-sided tubes. Energy Efficiency, Drying Efficiency, and Specific Energy Consumption have been the parameters considered for energy analysis. The nonporous tube provided the best energy performance for diffusive materials, such as barley and soybean particles, with reductions in the energy consumption in the range from 31.60% to 42.40% in relation to configuration without tube. The configurations with open-sided tube and without tube provided similar energy performance for all materials. Therefore, this study contributes to support that the draft tubes are promising devices for improving energy issues in the spouted bed, mainly in the processing of low moisture materials.

This chapter is based on:

R.C. de Brito, M. Tellabide, I. Estiati, J.T. Freire, M. Olazar, Drying of particulate materials in draft tube conical spouted beds: Energy analysis, Powder Technol. 388 (2021) 110–121. doi:10.1016/j.powtec.2021.04.074.

7.1 INTRODUCTION

Drying is used in a wide range of industry sectors and processing stages, such as those involving chemicals, foodstuffs, textiles, and so on. This operation is essential in order to provide materials with suitable levels of moisture content either for preservation and storage in their final form or as an intermediate step prior to other ones, such as pyrolysis and gasification [1–3]. When handling biological materials, such as barley and soybean, which are valuable resources due to their healthy nutrients for animal and human food, drying plays an important role in their quality and preservation [4,5]. Additionally, in the processing of alumina (Al_2O_3), a particulate material with several industrial applications (catalyst, catalyst support, adsorbent, and fabrication of nanomaterials), drying is essential to ensure a satisfactory mechanical strength in the final product [6–8].

However, drying is a highly energy-intensive process and dryers are considered one of the most energy-consuming industrial equipment. These energy issues are mainly attributed to the latent heat of evaporation, heat losses through the dryer body, inefficient operation, heat losses through the exhaust gases, and inefficient air-material heat transfer, which are inherent to convective dryers [9,10]. Although issues related to methodology and source data hinder the attainment of a reliable current energy statistics [2], some authors have mentioned that drying may account for about 10-20% of the total energy used by industry in most developed countries and this percentage is still increasing [10,11].

The energy issues have motivated several researchers to develop novel drying technologies, efficient methodologies, and effective analyses of energy use. In this context, Mehran et al. [12] have employed a solar-assisted fluidized-bed drying system for the processing of paddy grains.

The dryer consists of a solar water heater and solar-powered infrared lamp to reduce fossil fuel consumption. Esmailie et al. [13] have analysed four challenges and their solutions related to the solar fluidized bed dyer, namely, the thermal energy required to dry grains, the pressure drop in the system, the electric energy required to fluidized grains, and the geometry of dryng bed. Yu et al. [14] have evaluated the concept of relative humidity control strategy in the convective drying of carrot cubes to enhance the energy and exergy efficiency in the drying process. Mondal et al. [15] have performed the energy and exergy analysis for a mixed flow dryer in the drying of high moisture maize grains. They identified the efficiency variation as a function of drying temperature and proposed a model equation for energy and exergy parameters.

Among the dryers currently available, spouted beds are recognized as an efficient gas-solid contact method and a versatile multiphase system, with a high degree of agitation and mixture between phases due to their distinct hydrodynamic behaviour [16,17]. Thus, this technology has been applied in a wide range of chemical and physical operations, such as biomass pyrolysis [18,19], gasification [20,21], feeding [22,23], chemical vapour deposition [24,25], coating [26], drying [27–29], among others. However, the spouted bed has several limitations that restrain an effective industrial application. In addition to the energy issues described above, scaling up and processing of large amounts of material are some of these limitations [9,30]. Thus, different methodologies have been proposed in the literature to overcome these problems and ensure a feasible industrial application for this versatile equipment. Accordingly, draft tubes have been widely employed in the spouted bed as an alternative to overcome the limitations related to scaling up and stability [3,31]. Despite the good gas-solid contact, Olazar et al. [3] have observed that a dryer without a draft tube is limited to bench-scale applications, and they have demonstrated that the open-sided draft tube is a better option for drying purposes than both nonporous and without

draft tube configurations, as it improves gas percolation and stability. Nagashima et al. [31] and Altzibar et al. [32,33] have reported the influence of draft tubes on the minimum spouting velocity and bed pressure drop. These findings suggest that the application of draft tubes is a promising alternative for improving energy issues, since they significantly affect the minimum spouting velocity and the operating pressure drop, and therefore the energy performance of the spouted bed. Draft tubes have also been applied in other configurations of spouted beds, such as the one by Esmailie et al. [34], who have studied and simulated a solar spouted bed dryer with draft tube. These authors have also mentioned that the draft tube inside a spouted bed can decrease the electric energy required to move the particles. Despite the importance of energy aspects, there is still a remarkable gap regarding the energy contribution of the draft tube in the spouted bed. As mentioned by Kemp [10], an effective energy analysis is a vital first step in identifying opportunities to save energy and acquire a better understanding of energy involving aspects in any design and practical application.

Within this context, the objective of this study is to perform an energy analysis of draft tube conical spouted beds for the drying of particulate materials. Accordingly, three different particles have been used (alumina, barley, and soybean) in three unit configurations, namely, without draft tube and with nonporous and open-sided ones. Thus, the energy contribution of the internal devices has been evaluated for materials with different properties and drying mechanisms. Besides, a simple energy analysis (based on drying and hydrodynamic curves) has been described, which can be easily applied to spouted beds when the aim is their design or any practical application.

7.2 MATERIALS AND METHODS

7.2.1 Materials, Equipment, and Experimental Procedure

The experimental unit used has been described in a previous paper [30]. Hydrodynamic characterization and drying runs have been performed using contactors made of polyethylene terephthalate. The geometric factors of the conical contactors are as follows: column diameter (D_c), 0.36 m; contactor angle (γ), 60°; height of the conical section (H_c), 0.26 m; and contactor base diameter (D_i), 0.063 m. The gas inlet diameter (D_0) is 0.04 m. The runs have been carried out without draft tube and with nonporous and open-sided ones. The dimensions of the draft tubes, which are described in detail by Tellabide et al. [30], are as follows: length of the tube (L_T), 0.17 m; height of the entrainment zone, i.e., distance between the gas inlet nozzle and the bottom of the draft tube (L_H), 0.07 m; diameter of the tube (D_T), 0.04 m; and aperture ratio (AR) of the open-sided draft tube, 57%.

Alumina, barley, and soybean particles have been used in this study, with average sizes of 3.50, 5.04, and 6.60 mm, respectively, which have been determined by sieving and image processing (*Image Pró Plus*®). The apparent density of alumina, barley, and soybean particles are 700, 1270, and 1210 kg m^{-3}, respectively, which have been determined based on the displacement method using toluene. The static bed height (H_0) used in all the runs was 0.17 m, corresponding to dry bed masses of 2.70, 2.00, and 2.50 kg for alumina, barley, and soybean particles, respectively.

The hydrodynamic characterization has been performed according to Mathur and Epstein [17], which allowed determining the minimum spouting velocity (u_{ms}) and the operating pressure drop (ΔP_s). In the drying runs, the inlet air velocity used in the three configurations and for all the

materials was within the $1.25u_{ms}$ - $1.30u_{ms}$ range. Likewise, the inlet air temperature was maintained constant at 20 °C, for alumina particles, and 50 °C, for both barley and soybean particles. Before each drying process, the alumina particles were saturated with water by soaking for 24 h, reaching a moisture content of 0.47 ± 0.01 (dry basis, d. b.). To obtain the initial moisture content desired for barley and soybean, pre-determined amounts of water were added to 200 g samples of barley and soybean particles. These samples were placed inside polyethylene containers and kept refrigerated at 4 °C for 24 h. Thus, initial moisture contents of 22.4 ± 0.6 d. b. and 20.4 ± 0.9 d. b. for barley and soybean, respectively, were reached. The drying runs were carried out for 180 min (alumina particles) and for 240 min (barley and soybean particles). During the drying process, samples of particles were regularly collected from the bed in order to determine their moisture content, which was measured based on the weight loss by heating them at 105 °C for 24 h (gravimetric method). For all the particles used, samples were taken every 5 min up to 60 min operation, and every 15 min from 60 min until the end of the process. All the runs were replicated twice. Both hydrodynamic and drying runs have been monitored by a data acquisition system, which has been used to acquire the inlet and outlet drying air temperature and humidity, average solid temperature, pressure drop in the bed, and air flow rate.

7.2.2 Energy Analysis

Energy analysis involving drying processes is a difficult issue because the energy performance of a dryer can be characterized by several indices including volumetric evaporation rate, evaporation efficiency, surface heat loss, steam consumption, unit heat consumption, energy efficiency, thermal efficiency, and others [2,35]. Although most of these indices are used to

consider the particularities of various drying processes, they can also lead to misuse and misinterpretation. Thus, the dryer design, operating parameters and material properties are some of the essential factors to be considered in order to define the most suitable indices to evaluate energy performance and so analyse effectively energy use, which according to Kemp [10] is a vital first step to identify opportunities for energy-saving. In this study, the energy analysis has been performed considering a theoretical dryer similar to that described by Kudra [9], which has been applied in several studies in the literature [36–39]. Therefore, the following indices have been adopted: energy efficiency, drying efficiency, and specific energy consumption.

The energy efficiency has been obtained for all the particles and is usually considered as the ratio of the energy required to evaporate the water (Q_w) over the total energy supplied to the system, i.e., thermal (Q_{in}) and mechanical energy (W_m). Regarding diffusive materials, such as barley, soybean, and most food products, another energy term should be considered in the energy analysis, as the drying of these materials usually occurs in the falling drying rate. Thus, the assumption of evaporation from a free water surface does not hold in the energy analysis, as it leads to low and meaningless efficiency values. Some authors [36,39] define drying efficiency as the amount of energy required to heat the grain (Q_m) and evaporate the water over the total energy input in the operation, whereas Kudra [2] define it as the ratio of the energy required to evaporate the water and the total energy supplied to the system, i.e., enthalpy of the inlet air stream (Q_{in}) minus the enthalpy of the exhaust air (Q_{out}). According to Kudra [2], the latter is a better measure of the quality of a drying process (the drying Q-factor) than conventional parameters, as it gives an indication of the heat wasted, and therefore the amount of sensible heat provided by the drying agent that is used for evaporation. Thus, for barley and soybean, both drying efficiencies have been used, but with different nomenclature to avoid misuse of terminology. Both energy and drying

efficiencies have been calculated as instantaneous indices, which are especially useful parameters when analysing dryer configurations in the design stage [2,40]. The specific energy consumption was defined as the ratio between the total energy supplied to the system and the amount of water removed from the particles. This parameter is widely used in industry and is known as a well-defined benchmark value for an adiabatic dryer [9,41]. Based on the definitions described above, the following equations have been employed to obtain these energy indices:

Energy efficiency (EE)

$$EE\ (t) = \frac{Q_w(t)}{\int_0^t (Q_{in} + W_m)dt} \quad (1)$$

Drying efficiency (DE)

$$DE\ (t) = \frac{Q_w(t) + Q_m(t)}{\int_0^t (Q_{in} + W_m)dt} \quad (2)$$

Drying efficiency proposed by Kudra [2] *(DE_K)*

$$DE_K\ (t) = \frac{Q_w(t)}{\int_0^t [(Q_{in} - Q_{out}) + W_m]dt} \quad (3)$$

Specific energy consumption (SEC)

$$SEC = \frac{\int_0^t (Q_{in} + W_m)dt}{m_{ds}\left(\bar{X}_{t,end} - X_i\right)} \quad (4)$$

An energy balance has been performed to quantify the terms required to obtain the energy parameters. The control volume adopted for the energy balance is shown in Figure 7.1 and accounts for the particles and air in that region. The energy balance has been performed according to Baker and Mckenzie [41] and Keey [42], except for the inclusion of the mechanical energy, which is required to maintain the spouting regime characteristic of the spouted bed.

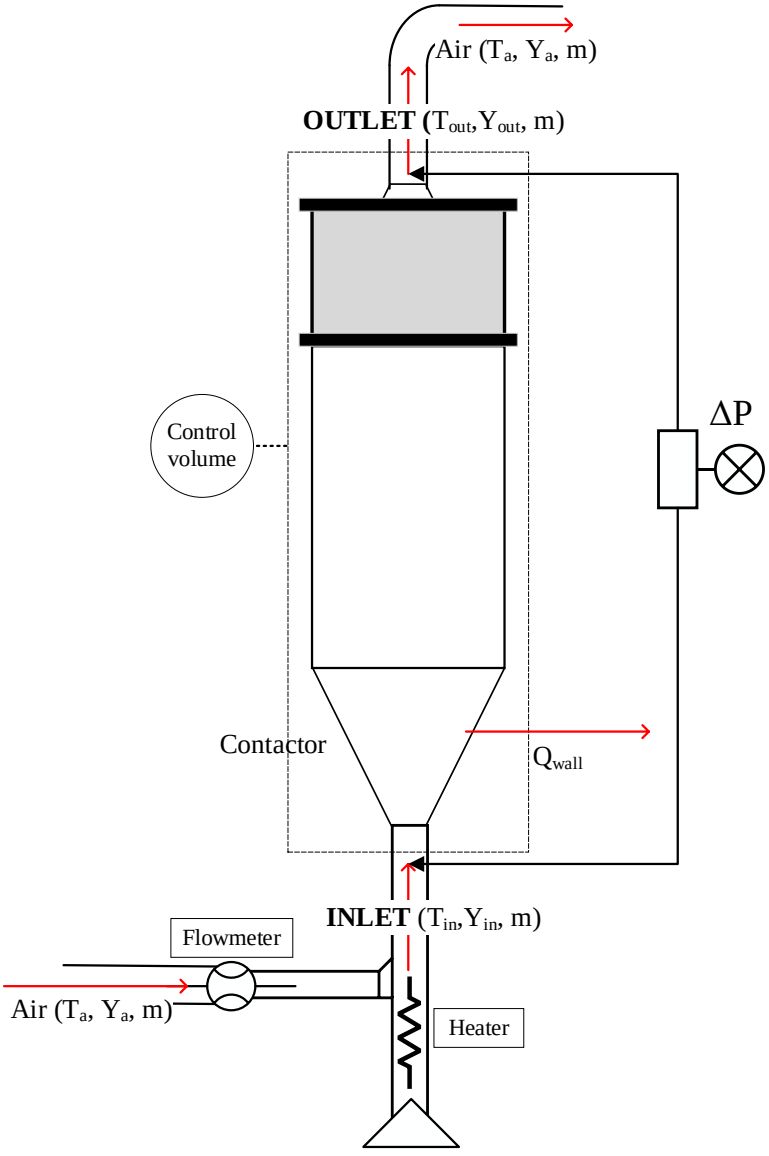

Figure 7.1. Schematic diagram of the control volume adopted for the energy analysis (adapted from Brito et al. [41]).

A full description of the procedure adopted for the energy balance, as well as all the parameters and equations required, are detailed in Brito et al. [43]. Based on the energy balance in the control volume represented in Figure 7.1, the following equations for the terms required have been obtained:

Thermal energy at the inlet and outlet

$$Q_{in} = \dot{m} \int_{T_a}^{T_{in}} c_p dT \quad (5)$$

$$Q_{out} = \dot{m} \int_{T_a}^{T_{out}} c_p dT \quad (6)$$

where $\dot{m}$ and c_p are the mass flow rate of the air (kg s^{-1}) and its specific heat (kJ kg^{-1} K^{-1}), and T_{in}, T_{out}, and T_a represent the air temperatures at the inlet, outlet, and that adopted as reference, respectively.

Mechanical energy required for spouting regime

$$W_m = \dot{m} \left(\frac{\Delta v^2}{2} + \frac{\Delta P}{\rho} \right) \quad (7)$$

where Δv is the difference between the air velocities at the inlet and outlet positions (m s^{-1}), ΔP is the pressure drop in the bed (Pa), and ρ is the specific mass of the air (kg m^{-3}).

Energy required for water evaporation

$$Q_w = \Delta H_{v,s} m_{ds} (\bar{X}_t - \bar{X}_i) \quad (8)$$

where $\Delta H_{v,s}$ is the latent heat of vaporization (kJ kg^{-1}), m_{ds} is the mass of dry solids (kg), and $\bar{X}_t$ and $\bar{X}_i$ are the average moisture contents (dry basis) at instant t and the initial one, respectively.

Energy required for heating the processes with barley and soybeans

$$Q_m = \ m_{ws} c_{ps} (\bar{T}_{m,t} - \bar{T}_{m,i}) \quad (9)$$

where m_{ws} is the mass of wet solids (kg), c_{ps} is the specific heat of wet solids (kJ kg^{-1} K^{-1}), and $\bar{T}_{m,t}$ and $\bar{T}_{m,i}$ are the average solid temperatures (K) at instant t and the initial one, respectively.

Finally, the following correlations have been used to estimate the parameters required:

Latent heat of vaporization for alumina beads [44]

$$\Delta H_{v,s} = 2502.535259 - 2.38576424\ \bar{T}_{m,t}(°C) \quad (10)$$

Latent heat of vaporization for barley and soybean particles [44,45]

$$\Delta H_{v,s} = \left[2502{,}535259 - 2{,}38576424 \bar{T}_{m,t}(°C)\right][1 + a exp(b\bar{X}_t)] \quad (11)$$

Parameters in the latent heat of vaporization for barley particles [45]

$a = 1.0;\ b = -19.9$

Parameters in the latent heat of vaporization for soybean particles [45]

$a = 0.4; b = -13.9$

Specific heat of air [46]

$$c_p = c_{p,g} + c_{p,v}Y \quad (12)$$

$$c_{p,g} = 1.05 - 0.365\left(\frac{T(K)}{1000}\right) + 0.85\left(\frac{T(K)}{1000}\right)^2 - 0.39\left(\frac{T(K)}{1000}\right)^3 \quad (13)$$

$$c_{p,v} = 1.79 + 0.107\left(\frac{T(K)}{1000}\right) + 0.586\left(\frac{T(K)}{1000}\right)^2 - 0.20\left(\frac{T(K)}{1000}\right)^3 \quad (14)$$

Specific mass of air [47]

$$\rho = 2.2538 - 0.003588\,T(K) \quad (15)$$

Specific heat of solids [48]

$$c_{ps} = A + B\bar{X}_t + C\bar{X}_t{}^2 \quad (16)$$

Parameters in the specific heat for barley particles [48]

$A = 1.186; B = -0.000128; C = 0.0023$

Parameters in the specific heat for soybean particles [48]

$A = 1.296; B = 0.075; C = -0.0016$

7.3 RESULTS AND DISCUSSION

7.3.1 Energy Efficiency, Drying Efficiency, and Specific Energy Consumption

Figure 7.2 shows the instantaneous energy efficiencies, as a function of time, for the processes without draft tube and with nonporous and open-sided ones. The energy efficiency was determined throughout the drying process, based on the average drying profile for each configuration.

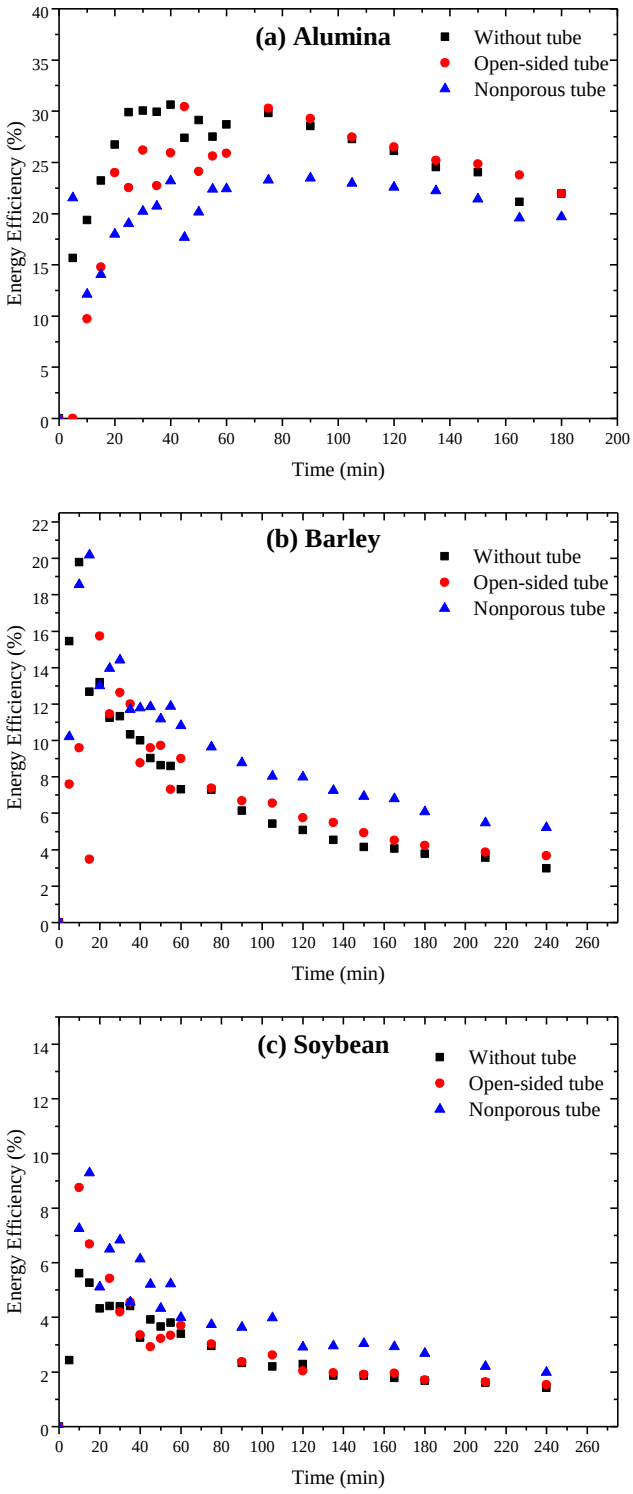

Figure 7.2. Evolution of energy efficiency with time for the processes without draft tube and with nonporous and open-sided ones: (a) alumina beads, (b) barley, and (c) soybean.

Figure 7.2a shows similar trends for alumina particles under all conditions, with a sharp increase in energy efficiency at the beginning of the process up to 60 min, followed by a slight decrease over time. Nevertheless, the trend for barley and soybean particles differs, Figures 7.2b and 7.2c, since the energy efficiency decreases exponentially over time. During the starting stage, great amounts of energy are required due to the high moisture content of the materials. Accordingly, the energy supplied is effectively used to remove moisture, and high energy efficiency values are therefore attained. Similar results and behaviours have been reported by several authors [14,38,49,50].

The dependency between energy efficiency and moisture content is evident, with the latter being influenced by the porous structure and drying mechanism of the material. According to Kudra [2], the behaviour observed for alumina particles is typical in the literature. Thus, he states that these particles are capillary-porous materials with negligible internal mass transfer resistance. The different drying mechanism of barley and soybean particles, which is discussed in detail in the next section, explains both their lower energy efficiency and different drying trend compared to alumina beads. When the internal mass transfer resistance prevails, more energy is required to remove the bound moisture content, which is intimately associated with the porous structure of the material. Kudra [35] and Strumillo et al. [51] have described that the bound water moisture content of grains is of about 22% (wet basis, w. b.), which is higher than the average initial moisture content of the barley and soybean particles used in this study, 18.3 ± 0.6% w. b. and 17.0 ± 0.6% w. b., respectively. Thus, more energy is required for breaking the material-moisture bonds, removal of microcapillary water, and overheating the already dry surface layers. Likewise, a high amount of the energy supplied is used as sensible heat to maintain the required temperature gradient for the heat and mass transfer rates, significantly influencing the diffusivity of the

material. Even lower energy efficiencies are obtained for these types of materials dried in the spouted bed, in which the air-flow rate needed for the spouting regime is significantly higher than that required to supply heat for the drying, as mentioned by Kudra [35]. Thus, in order to evaluate the quality of the drying processes with these types of materials and allow a suitable comparison between different configurations, drying efficiency is a more suitable parameter.

Figures 7.3 and 7.4 show the drying efficiencies for barley and soybean particles.

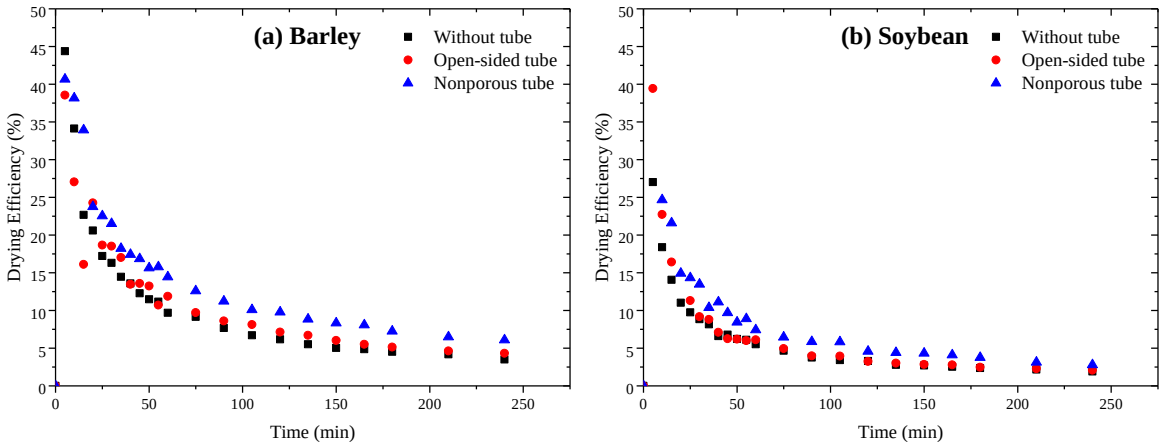

Figure 7.3. Evolution of drying efficiency with time for the processes without draft tube and with nonporous and open-sided ones: (a) barley and (b) soybean.

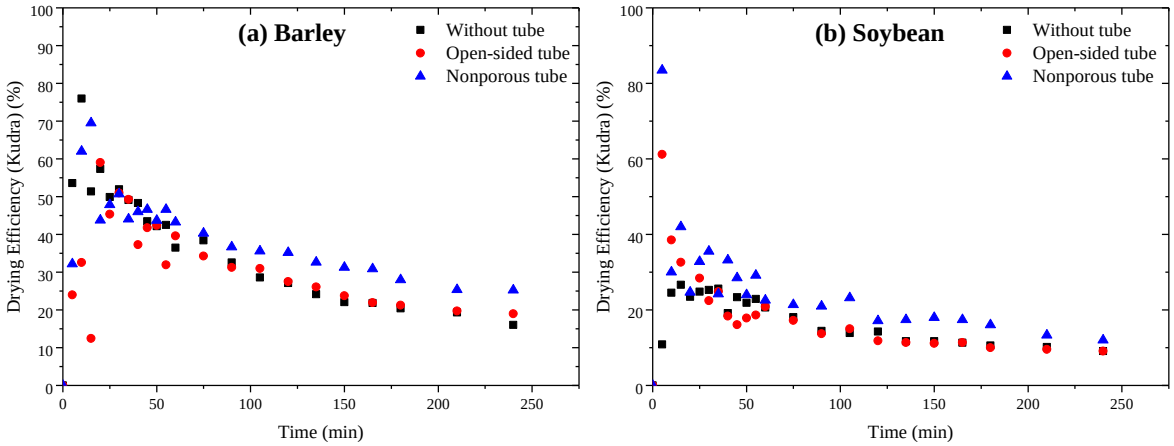

Figure 7.4. Evolution of the drying efficiency proposed by Kudra [2] with time for the processes without draft tube and with nonporous and open-sided ones: (a) barley and (b) soybeans.

As expected, Figures 7.3 and 7.4 show higher drying efficiencies than those observed in Figures 7.2b and 7.2c, mainly in the initial drying period. This fact can be attributed to the energy used as sensible heat in the drying process, which is considered in the drying efficiency parameter. In the initial drying period, a significant fraction of the energy supplied is used for material heating. As drying proceeds, the energy used as sensible heat still plays an important role in maintaining the temperature gradient for heat transfer and internal moisture migration, directly influencing the diffusivity in the material. Therefore, neglecting this energy term as useful in the energy analysis can lead to low and meaningless efficiency values, especially when processing diffusive materials, such as barley and soybeans, which was also mentioned by Kudra [35].

Furthermore, qualitatively similar results are obtained for both drying efficiency parameters (the standard and that defined by Kudra), i.e., continuous and exponential decrease over time. The evolution of the drying efficiency defined by Kudra (DE_K) shows a weak peak at a very short time, which should be attributed to material heating in the initial drying period and the low initial

moisture content, suggesting that the internal mass transfer resistance prevails throughout the entire process. Similar results with different materials can be found in the literature [2,52,53]. Besides, DE_K parameter provides higher values than the other two parameters evaluated (DE and EE). This result is explained by the energy lost by the exhaust air, which in the definition of DE_K is not considered as lost energy. Therefore, this component of energy represents one of the main causes of the high energy consumption and inefficiencies in the convective drying. Yu et al. [14] have estimated an average energy loss rate caused by exhaust air 6.13 and 151.85 times the heat transfer rate for water evaporation and material heating, respectively.

The results of all the energy parameters presented, as well as the understanding of their qualitative behaviour, allow analysing the energy contribution provided by the draft tubes in the drying process. For alumina particles (Figure 7.2a), higher energy efficiencies are observed in the process without a draft tube for drying times lower than 60 min. Thereafter, the energy efficiencies of the processes without and with open-sided draft tubes overlap. The lowest energy efficiency is obtained with the nonporous draft tube in the entire drying process. For barley and soybean particles, the highest energy efficiency (Figures 7.2b and 7.2c) and drying efficiency (Figures 7.3 and 7.4) are obtained with the nonporous draft tube, whereas the processes without tube and with open-sided one present similar energy performances, but lower efficiencies than in the nonporous configuration. These trends are also observed in Figure 7.5, which shows the specific energy consumption for the processes without draft tube and with nonporous and open-sided ones.

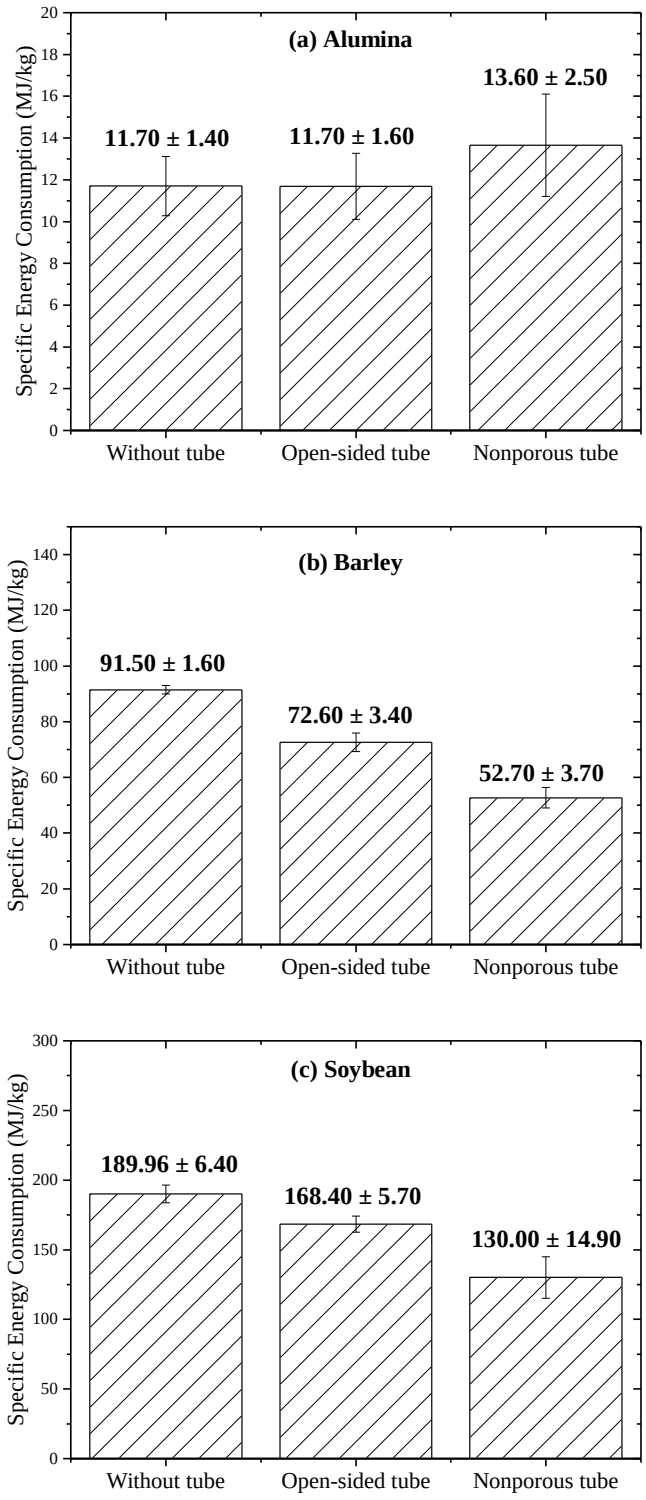

Figure 7.5. Specific energy consumption for the processes without draft tube and with nonporous and open-sided ones: (a) alumina beads, (b) barley, and (c) soybean.

Regarding alumina particles, although differences are not significant, the highest specific energy consumption is obtained with the nonporous draft tube. However, for barley and soybean particles, the system with the nonporous tube is the one of lowest specific energy consumption. Thus, the nonporous draft tube provided reductions in energy consumption of 42.40% for barley particles and 31.60% for soybean particles compared to the configuration without tube. Likewise, the open-sided draft tube provided reductions of 20.70% and 11.30% for barley and soybean particles, respectively, compared to the configuration without tube. Given the lack of previous studies evaluating the energy aspects of draft tubes, both the drying and the hydrodynamic curves allow clarifying and explaining the results described.

7.3.2 Dimensionless Moisture and Drying Rate

Figures 7.6, 7.7, and 7.8 show the drying curves obtained without draft tube and with nonporous and open-sided ones for alumina, barley, and soybean particles, respectively. The drying curves are plotted in terms of dimensionless moisture content (ratio between the average moisture content at an instant t and the initial average moisture content, both on a dry basis).

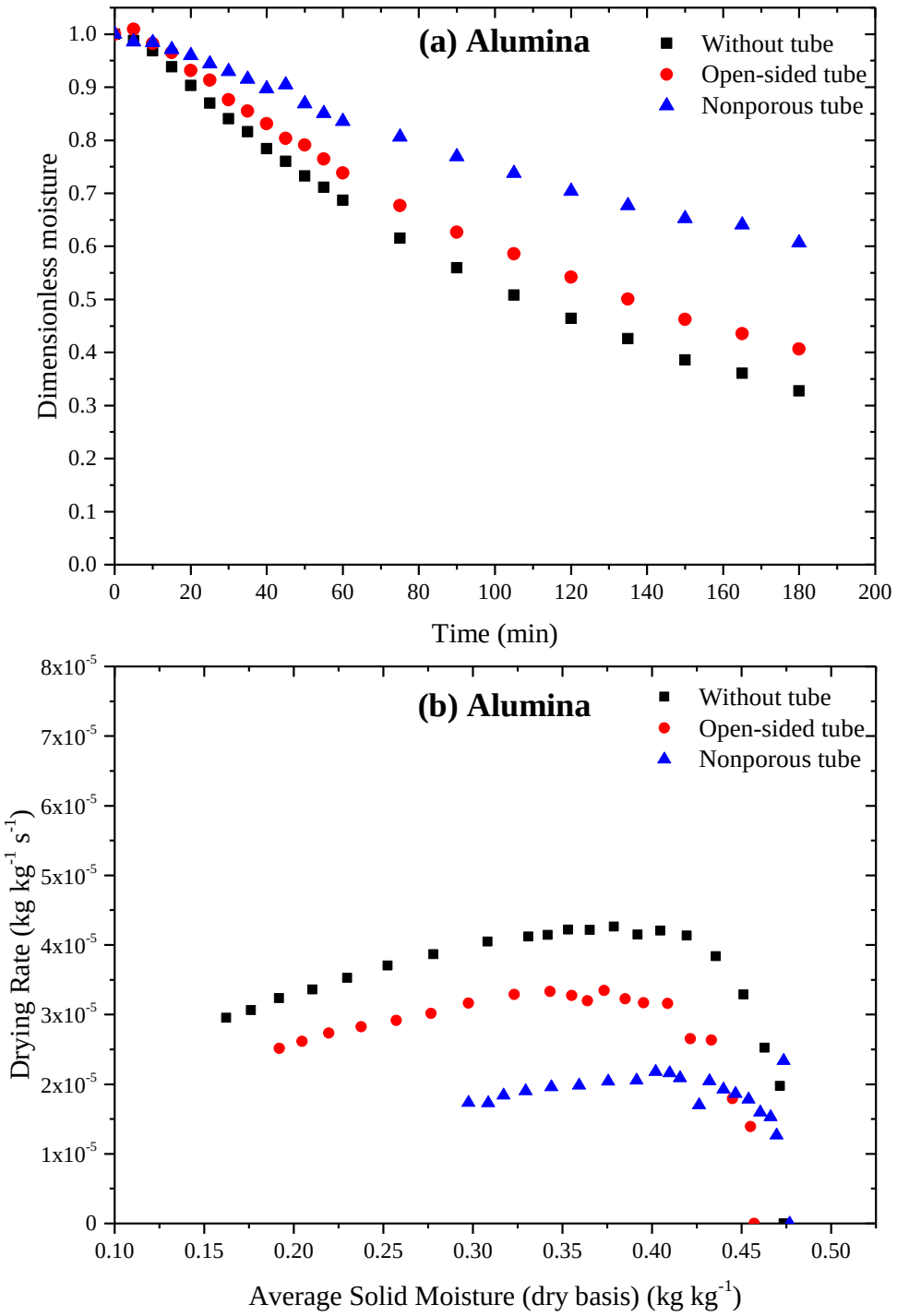

Figure 7.6. (a) Evolution of the dimensionless moisture content with drying time, and (b) drying rate vs. average solid moisture content, for alumina beads in the systems without draft tube and with nonporous and open-sided ones.

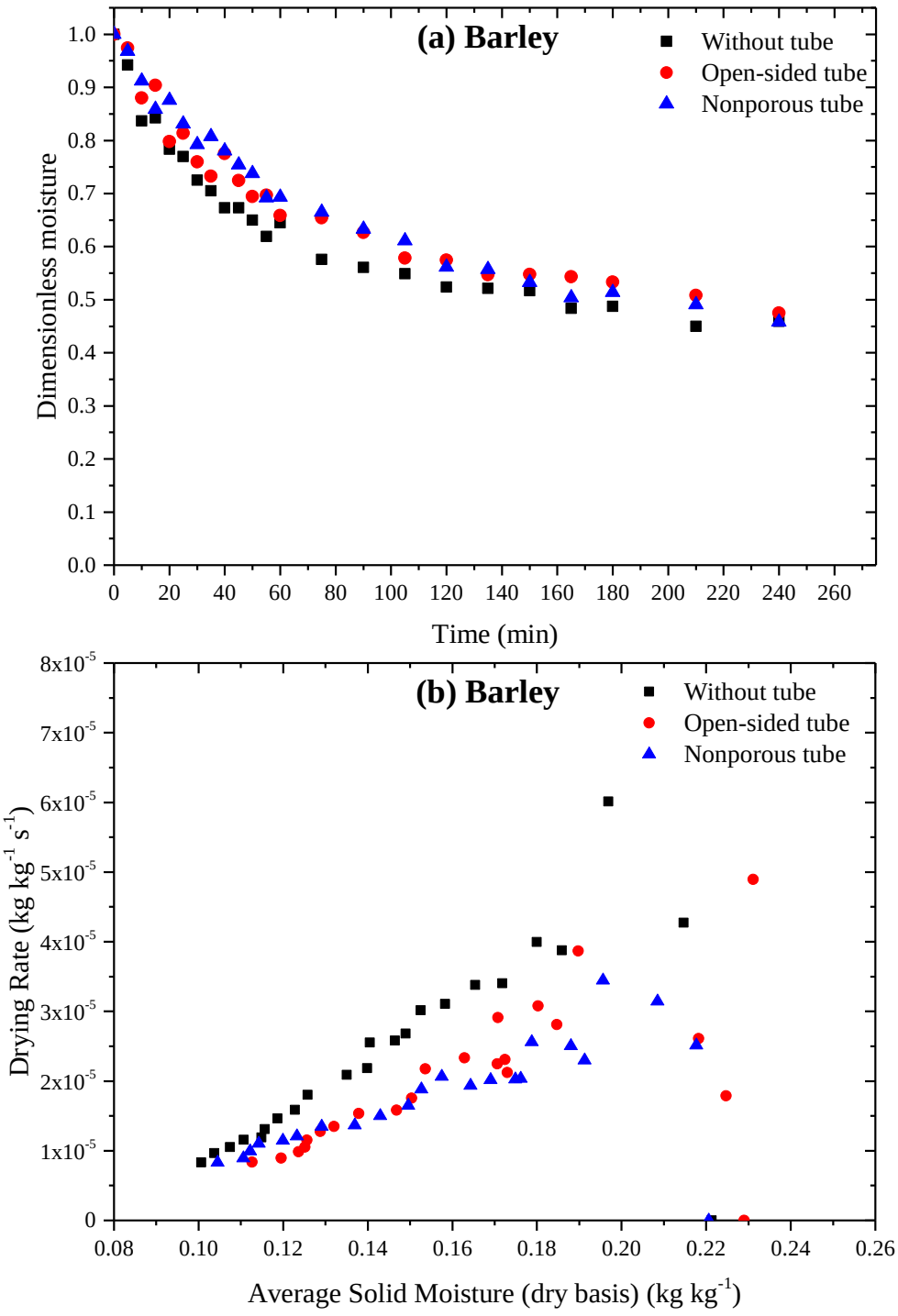

Figure 7.7. (a) Evolution of the dimensionless moisture content with drying time, and (b) drying rate vs. average solid moisture content, for barley in the systems without draft tube and with nonporous and open-sided ones.

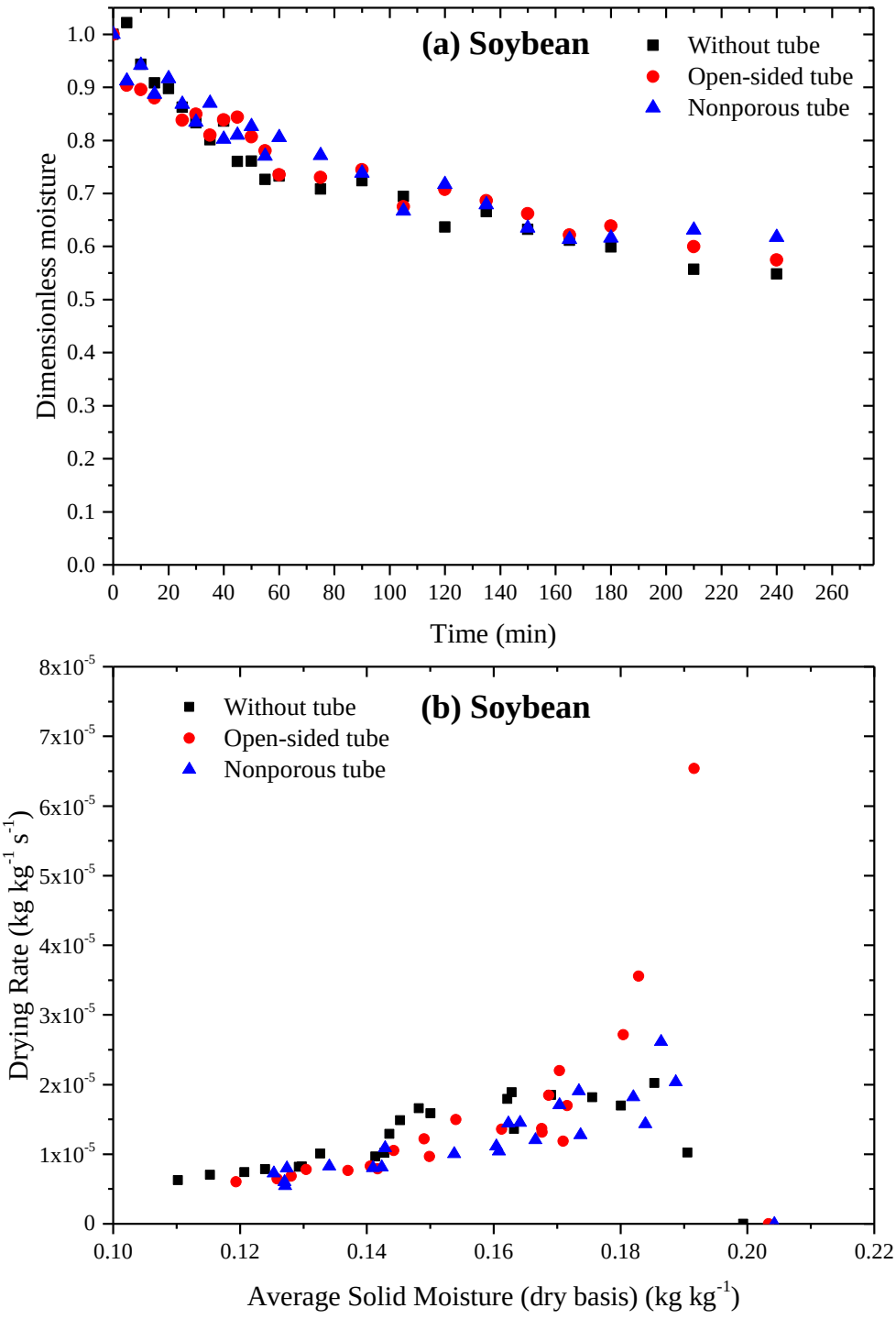

Figure 7.8. (a) Evolution of the dimensionless moisture content with drying time, and (b) drying rate vs. average solid moisture content, for soybean in the systems without draft tubes and with nonporous and open-sided ones.

As observed in Figure 7.6a, the drying curves obtained are typical of alumina particles in all cases, with an approximately linear decrease in the dimensionless moisture over time up to approximately 60 min [2,38]. This behaviour suggests that the external mass transfer resistance controls the drying process, indicating that the drying conditions are insufficient to reach a dynamic equilibrium condition. This result is also consistent with the increase observed in the energy efficiency up to 60 min for the alumina particles (Figure 7.2a), suggesting that the energy supplied during this period is effectively employed to remove moisture. Figure 7.6b supports the hypothesis that external mass transfer resistance is the controlling step, as the drying rate remains almost constant throughout the drying process for both open-sided and nonporous tubes. Similarly, the system without a draft tube also shows a constant drying rate, followed by a falling drying rate from the average solid moisture of approximately 0.40 (dry basis). A higher amount of moisture was removed in the systems without a draft tube, followed by the systems with open-sided and nonporous draft tubes, respectively. These results are explained by the reduced air percolation and poor gas-solid contact in the annulus of systems with internal devices, compromising the moisture removal. Furthermore, the control of the external mass transfer resistance makes the drying process more susceptible to external conditions, such as air flow rate and hydrodynamic features. Similar conclusions were also obtained by Olazar et al. [3] and Estiati et al. [54] with biomass and fine sand particles, respectively, in the spouted bed with draft tubes.

Based on the drying mechanism and the influence of the draft tube on the drying process, the good energy results obtained in the system without draft tube using alumina particles are due to the excellent gas-solid contact, which leads to a better energy utilization, and therefore higher moisture removal. However, as mentioned previously, the energy efficiency of the system with open-sided tube (Figure 7.2a) overlaps the one without tube from 60 min operation to the end of

the drying process. Therefore, higher energy efficiencies are attained in the systems with internal devices when materials with low moisture content are dried under conditions in which the internal mass transfer resistance is the rate-controlling step. This trend is observed with barley and soybean particles (Figures 7.2a and 7.2b), as discussed above.

Unlike alumina beads, both barley (Figure 7.7a) and soybean (Figure 7.8a) particles follow a continuous and exponential decrease in the dimensionless moisture over time. Furthermore, falling drying rates are observed throughout the drying process for both barley (Figure 7.7b) and soybean (Figure 7.8b) in all the configurations evaluated. These results reinforce the hypothesis that internal mass transfer resistance is the controlling step in the drying of these materials, as has also been observed by several authors [5,55–57]. Regarding the influence of the internal devices on the drying of barley, the system without draft tube presents a slightly higher drying rate than both open-sided and nonporous configurations. Similar behaviour has been also observed for soybean particles, although there are no significant differences between the configurations studied. Despite these findings, the effect of the internal devices on the drying of both barley and soybean is less significant than on the drying of alumina. These results are explained by the drying mechanism involving both barley and soybean particles because under the conditions used the influence of external drying parameters is minimized. Thus, the lower air percolation and poorer gas-solid contact provided by the internal devices are less significant in moisture removal. These facts explain the energy results obtained with these particles, where the nonporous tube provides the best energy performance.

These findings lead to conclude that the use of internal devices to improve the energy performance of the process is highly conditioned by the drying mechanism of the particulate material. Therefore, the internal devices tend to provide better energy results with diffusive

materials because the removal of moisture from these materials is less affected by the reduced air percolation and poorer gas-solid contact obtained with draft tubes. Nonetheless, even for convective materials, the internal devices can provide interesting energy results, as shown above for alumina particles, i.e., the configurations without and with open-sided configurations present similar energy performances. In fact, the air percolation and gas-solid contact provided by the open-sided tubes is higher than the nonporous one, and therefore the hydrodynamic features conferred by the draft tubes upon the spouted bed may improve the energy aspects of the drying processes.

7.3.3 Hydrodynamic curves

Figure 7.9 shows the evolutions of pressure drop vs. air velocity (characteristic curves) and Table 7.1 sets out the hydrodynamic parameters for all the particles used in the systems without draft tube and with nonporous and open-sided ones.

Table 7.1. Hydrodynamic parameters for alumina, barley, and soybean particles for the systems without draft tube and with nonporous and open-sided ones.

Material	Configuration	ΔP_S (Pa)	u_{ms} (m/s)
Alumina	Without tube	633.40±33.00	21.30±0.60
	Open-sided tube	514.70±30.30	17.40±0.30
	Nonporous tube	315.00±12.40	14.20±0.10
Barley	Without tube	426.90±57.20	16.90±0.90
	Open-sided tube	216.60±5.10	13.20±0.10
	Nonporous tube	133.40±2.20	9.60±0.02
Soybean	Without tube	853.70±79.00	31.10±0.60
	Open-sided tube	410.60±17.30	26.80±0.10
	Nonporous tube	268.40±15.50	19.20±0.10

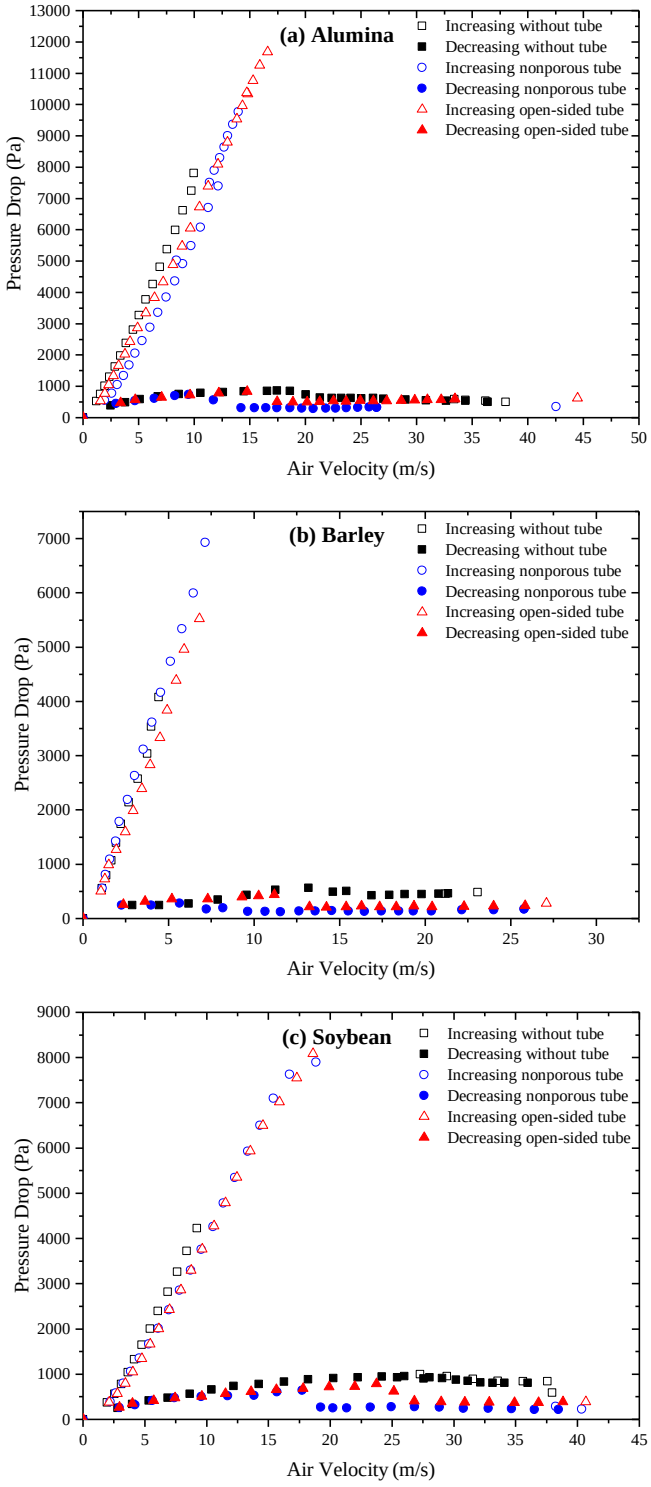

Figure 7.9. Evolution of pressure drop with air velocity for the systems without draft tube and with nonporous and open-sided ones: (a) alumina beads, (b) barley, and (c) soybean.

Characteristic curves of spouted beds similar to those described by Mathur and Epstein [17] are obtained for all the particles used. As expected, the internal device leads to a decrease in minimum spouting velocity (u_{ms}) and operating pressure drop (ΔP_S), with the lowest value corresponding to the nonporous draft tube. These results have already been reported by several authors [3,32,33,58].

These findings support the energy results obtained with the internal devices because the lower minimum spouting velocity provided by the draft tubes compared to the configuration without tube implies a decrease in both thermal and mechanical energy supplied to the system. The lower operating pressure drop contributes also to the latter. Figure 7.10 shows the thermal and mechanical energy supplied in all the configurations studied and Table 7.2 shows the reduction in both thermal and mechanical energy in the systems with nonporous and open-sided draft tubes compared to the one without draft tube.

Table 7.2. Reduction in thermal and mechanical energy for alumina, barley, and soybean in the systems with nonporous and open-sided draft tubes compared to that without draft tube.

Material	Configuration	Thermal Energy	Mechanical Energy
Alumina	Nonporous tube	27.3%	72.1%
	Open-sided tube	10.5%	46.7%
Barley	Nonporous tube	41.4%	78.3%
	Open-sided tube	19.3%	54.3%
Soybean	Nonporous tube	38.1%	76.2%
	Open-sided tube	12.9%	38.5%

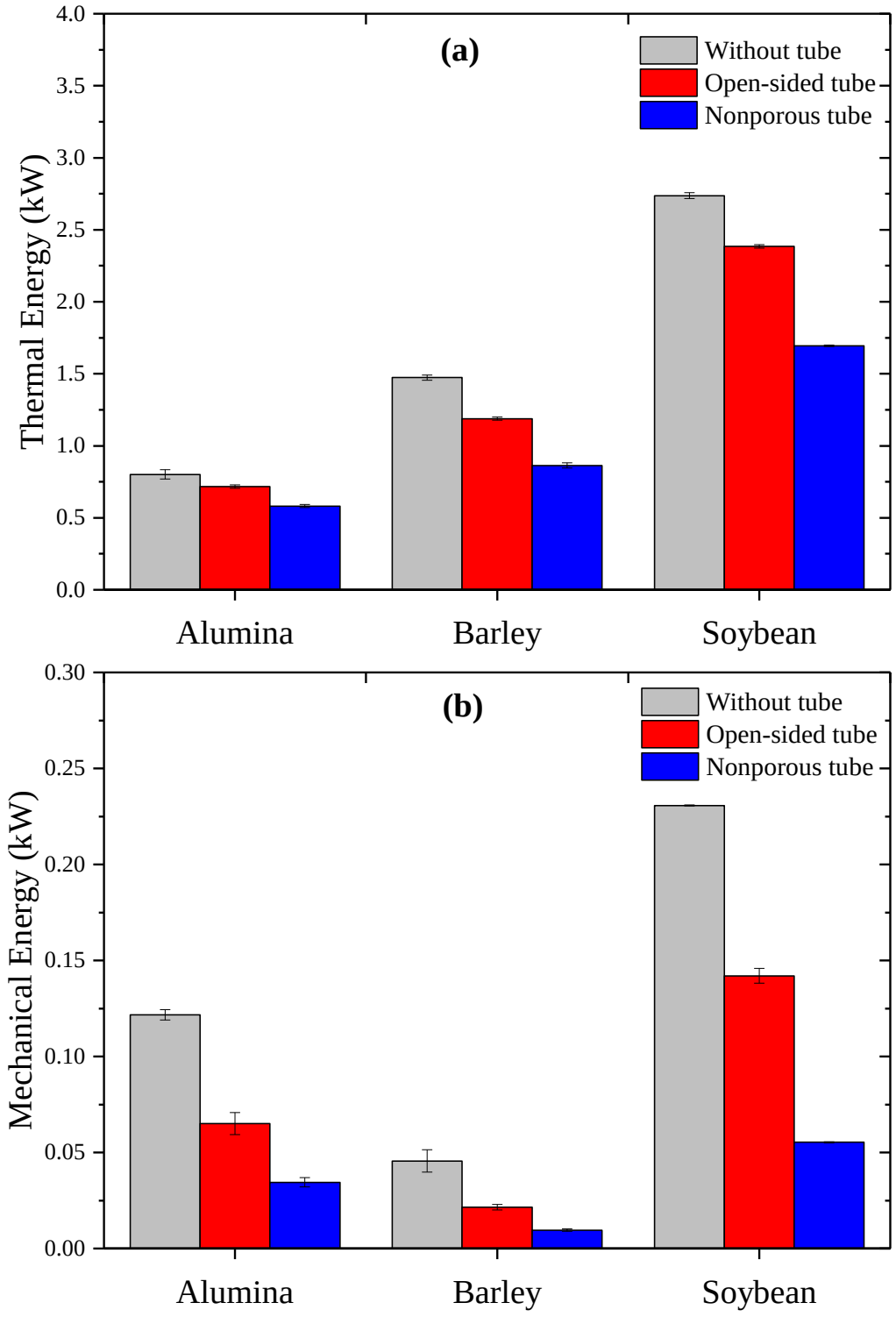

Figure 7.10. (a) Thermal and (b) Mechanical Energy required in the drying of alumina, barley, and soybean drying in the systems without draft tube and with nonporous and open-sided ones.

As observed in Figure 7.10, the internal devices reduce both the thermal and the mechanical energy required for the drying process, so that the nonporous tube demands the lowest amount of energy in all particulate materials used. As observed in Table 7.2, both nonporous and open-sided tubes cause a significant reduction in mechanical energy, which can be attributed to the lower operating pressure drop required. This is a highly relevant result, especially regarding the spouted bed dryer, in which the air flow needed for spouting is significantly higher than that required in the drying process [35]. Therefore, the drying and hydrodynamic results support the best energy performance of the nonporous tube for barley and soybean, as well as the similar energy performance of the configurations without tube and open-sided configurations, mainly in the systems with alumina particles. The latter finding suggests that the configuration with the open-sided draft tube is the best alternative for convective materials due to the additional advantages provided by this internal device related to scaling up and stability [3,32,33,58].

Therefore, despite the smaller amount of moisture removed compared to the configuration without tube, the draft tube involves a better energy utilization due to the smaller amount of total energy supplied to the system, mainly in processes involving materials in which the internal mass transfer resistance is the rate limiting step, such as barley and soybean particles.

7.4 CONCLUSIONS

An energy study has been carried out for the drying of alumina, barley, and soybean particles in draft tube conical spouted beds. For alumina particles, the open-sided draft tube provided the best energy utilization due to the decrease in minimum spouting velocity and operating pressure drop compared to the configuration without tube. Thus, a smaller amount of energy was required

to perform the drying process. The nonporous draft tube allowed a further decrease in the mentioned hydrodynamic parameters. However, this decrease occurs at the expense of poor air percolation into the annulus, and therefore this configuration performs worse than the other ones. Nevertheless, in the case of barley and soybean particles, the nonporous tube provided the best energy performance with the highest efficiency and lowest energy consumption. Therefore, although the configurations with draft tube supply less energy than the conventional configuration without tube, the type of draft tube that optimizes energy performance is highly dependent on the particulate material to be dried. Thus, the relationship between air percolation and drying mechanism is a key aspect to be considered in the design and application of draft tubes in spouted beds, mainly from an energy aspect. Additionally, the findings of this study contribute to support that draft tubes are promising devices for improving energy issues in spouted beds, mainly in the processing of low moisture materials.

ACKNOWLEDGEMENTS

The authors appreciate the financial support provided by Coordination for the Improvement of Higher Education Personnel (CAPES), the São Paulo State Research Foundation (FAPESP, grant #2017/01856-7 and grant #2018/22655-2), the Spain's Ministries of Economy and Competitiveness (CTQ2016-75535-R (AEI/FEDER, UE)) and Science and Innovation (PID2019-107357RB-I00 (AEI/FEDER, UE)), and the European Commission (HORIZON H2020-MSCA RISE-2018. Contract No.: 823745). I. Estiati thanks the University of the Basque Country for her postgraduate grant (ESPDOC18/14).

REFERENCES

[1] T. Nazghelichi, M.H. Kianmehr, M. Aghbashlo, Thermodynamic analysis of fluidized bed drying of carrot cubes, Energy. 35 (2010) 4679–4684. doi:10.1016/j.energy.2010.09.036.

[2] T. Kudra, Energy aspects in drying, Dry. Technol. 22 (2004) 917–932. doi:10.1081/DRT-120038572.

[3] M. Olazar, G. Lopez, H. Altzibar, M. Amutio, J. Bilbao, Drying of Biomass in a Conical Spouted Bed with Different Types of Internal Devices, Dry. Technol. 30 (2012) 207–216. doi:Doi 10.1080/07373937.2011.633194.

[4] T.L.F. Pinto, S.M. Cicero, J.B. França-Neto, V.A. Forti, An assessment of mechanical and stink bug damage in soybean seed using X-ray analysis test, Seed Sci. Technol. 37 (2009) 110–120. doi:10.15258/sst.2009.37.1.13.

[5] M. Markowski, I. Białobrzewski, A. Modrzewska, Kinetics of spouted-bed drying of barley: Diffusivities for sphere and ellipsoid, J. Food Eng. 96 (2010) 380–387. doi:10.1016/j.jfoodeng.2009.08.011.

[6] F. Pourcel, W. Jomaa, J.R. Puiggali, L. Rouleau, Crack appearance during drying of an alumina gel: Thermo-hydro-mechanical properties, Dry. Technol. 25 (2007) 759–766. doi:10.1080/07373930701370134.

[7] Z. Liu, C. Lv, Fast synthesis of mesoporous γ-alumina assisted by a room temperature ionic liquid and its use as a support for the promotional catalytic performance of dibenzothiophene hydrodesulfurization, RSC Adv. 4 (2014) 10221–10227. doi:10.1039/c3ra45185b.

[8] Z.L. Xiao, C.Y. Han, U. Welp, H.H. Wang, W.K. Kwok, G.A. Willing, J.M. Hiller, R.E.

Cook, D.J. Miller, G.W. Crabtree, Fabrication of Alumina Nanotubes and Nanowires by Etching Porous Alumina Membranes, Nano Lett. 2 (2002) 1293–1297. doi:10.1021/nl025758q.

[9] T. Kudra, Energy Performance of Convective Dryers, Dry. Technol. 30 (2012) 1190–1198. doi:10.1080/07373937.2012.690803.

[10] I.C. Kemp, Fundamentals of Energy Analysis of Dryers, Mod. Dry. Technol. 4–4 (2014) 1–45. doi:10.1002/9783527631728.ch21.

[11] C.G.J. Baker, Energy efficient dryer operation - An update on developments, Dry. Technol. 23 (2005) 2071–2087. doi:10.1080/07373930500210556.

[12] S. Mehran, M. Nikian, M. Ghazi, H. Zareiforoush, I. Bagheri, Experimental investigation and energy analysis of a solar-assisted fluidized-bed dryer including solar water heater and solar-powered infrared lamp for paddy grains drying, Sol. Energy. 190 (2019) 167–184. doi:10.1016/j.solener.2019.08.002.

[13] F. Esmailie, M. Aminy, H. Ghadamian, Energy Intensity Diagnostics Contributed to Solar Dryers Energy Challenges, J. Clean Energy Technol. 3 (2015) 388–392. doi:10.7763/jocet.2015.v3.229.

[14] X.L. Yu, M. Zielinska, H.Y. Ju, A.S. Mujumdar, X. Duan, Z.J. Gao, H.W. Xiao, Multistage relative humidity control strategy enhances energy and exergy efficiency of convective drying of carrot cubes, Int. J. Heat Mass Transf. 149 (2020). doi:10.1016/j.ijheatmasstransfer.2019.119231.

[15] M.H.T. Mondal, M.A. Hossain, M.A.M. Sheikh, Md. Akhtaruzzaman, M.S.H. Sarker, Energetic and exergetic investigation of a mixed flow dryer: A case study of maize grain drying, Dry. Technol. 0 (2020) 1–15. doi:10.1080/07373937.2019.1709077.

[16] M. Olazar, M.J. San José, A.T. Aguayo, J.M. Arandes, J. Bilbao, Stable operation conditions for gas-solid contact regimes in conical spouted beds, Ind. Eng. Chem. Res. 31 (1992) 1784–1792. doi:10.1021/ie00007a025.

[17] K.B. Mathur, N. Epstein, Spouted Beds, Academic Press, New York, 1974.

[18] K. Azizi, M. Keshavarz Moraveji, A. Arregi, M. Amutio, G. Lopez, M. Olazar, On the pyrolysis of different microalgae species in a conical spouted bed reactor: Bio-fuel yields and characterization, Bioresour. Technol. 311 (2020). doi:10.1016/j.biortech.2020.123561.

[19] K.M. Barcelos, P.S. Almeida, M.S. Araujo, T.P. Xavier, K.G. Santos, M.S. Bacelos, T.S. Lira, Particle segregation in spouted bed pyrolysis reactor: Sand-coconut shell and sand-cocoa shell mixtures, Biomass and Bioenergy. 138 (2020) 105592. doi:10.1016/j.biombioe.2020.105592.

[20] N. Spiegl, C. Berrueco, X. Long, N. Paterson, M. Millan, Production of a fuel gas by fluidised bed coal gasification compatible with CO2 capture, Fuel. 259 (2020) 116242. doi:10.1016/j.fuel.2019.116242.

[21] A. Niksiar, B. Nasernejad, Modeling of gasification reaction to produce activated carbon from pistachio shells in a spouted bed, Biomass and Bioenergy. 119 (2018) 97–108. doi:10.1016/j.biombioe.2018.09.008.

[22] L. Massaro Sousa, M.C. Ferreira, On the performance of a spouted bed type device for feeding spent coffee grounds to a circulating fluidized bed reactor, Chem. Eng. Res. Des. 160 (2020) 31–38. doi:10.1016/j.cherd.2020.05.002.

[23] L. Massaro Sousa, M.C. Ferreira, Q.F. Hou, A.B. Yu, Feeding spent coffee grounds into reactors: TFM simulation of a non-mechanical spouted bed type feeder, Waste Manag. 109 (2020) 161–170. doi:10.1016/j.wasman.2020.04.056.

[24] P.K. Mollick, R. Venugopalan, M. Roy, P.T. Rao, D. Sathiyamoorthy, P. Sengupta, G. Sharma, C.B. Basak, J.K. Chakravartty, Deposition of diversely textured buffer pyrolytic carbon layer in TRISO coated particle by controlled manipulation of spouted bed hydrodynamics, Chem. Eng. Sci. 128 (2015) 44–53. doi:10.1016/j.ces.2015.01.065.

[25] X. Yang, F. Zhang, M. Guo, Y. Zhong, P. Wang, J. Lin, Z. Zhu, Preparation of SiC layer with sub-micro grain structure in TRISO particles by spouted bed CVD, J. Eur. Ceram. Soc. 39 (2019) 2839–2845. doi:10.1016/j.jeurceramsoc.2019.02.005.

[26] D. Peshev, E. Eichner, M. Goslinska, S. Pietsch, Y. Trambabova, T. Terzieva, N. Georgieva, S. Heinrich, Particle formulation of hydroalcoholic rosemary (Rosmarinus officinalis L.) extracts using a spouted bed, Particuology. 51 (2020) 26–34. doi:10.1016/j.partic.2019.10.002.

[27] M. Moradi, S. Azizi, M. Niakousari, S. Kamgar, A. Mousavi Khaneghah, Drying of green bell pepper slices using an IR-assisted Spouted Bed Dryer: An assessment of drying kinetics and energy consumption, Innov. Food Sci. Emerg. Technol. 60 (2020) 102280. doi:10.1016/j.ifset.2019.102280.

[28] S. Rajashekhara, D.V.R. Murthy, Drying of Agricultural Grains in a Multiple Porous Draft Tube Spouted Bed, Chem. Eng. Commun. 204 (2017) 942–950. doi:10.1080/00986445.2017.1328412.

[29] G.K.K. Jayatunga, B.M.W.P.K.M.W.P.K. Amarasinghe, Drying kinetics, quality and moisture diffusivity of spouted bed dried Sri Lankan black pepper, J. Food Eng. 263 (2019) 38–45. doi:10.1016/j.jfoodeng.2019.05.023.

[30] M. Tellabide, I. Estiati, A. Pablos, H. Altzibar, R. Aguado, M. Olazar, New operation regimes in fountain confined conical spouted beds, Chem. Eng. Sci. 211 (2020) 115255.

doi:10.1016/j.ces.2019.115255.

[31] H. Nagashima, K. Suzukawa, T. Ishikura, Hydrodynamic performance of spouted beds with different types of draft tubes, Particuology. 11 (2013) 475–482. doi:10.1016/j.partic.2013.01.007.

[32] H. Altzibar, G. Lopez, J. Bilbao, M. Olazar, Minimum Spouting Velocity of Conical Spouted Beds Equipped with Draft Tubes of Different Configuration, Ind. Eng. Chem. Res. 52 (2013) 2995–3006. doi:10.1021/ie302407f.

[33] H. Altzibar, G. Lopez, J. Bilbao, M. Olazar, Effect of draft tube geometry on pressure drop in draft tube conical spouted beds, Can. J. Chem. Eng. 91 (2013) 1865–1870. doi:10.1002/cjce.21913.

[34] F. Esmailie, H. Ghadamian, M. Aminy, Transport phenomena study in a solar spouted bed dryer within a draft tube, Environ. Prog. Sustain. Energy. 37 (2018) 488–497. doi:10.1002/ep.12670.

[35] T. Kudra, Energy Aspects in Food Dehydration, in: C. Ratti (Ed.), Adv. Food Dehydration, Taylor & Francis Group, LLC, 2009: pp. 423–445.

[36] M.L. Passos, A.S. Mujumdar, G. Vijaya, V.G.S. Raghavan, Spouted and Spout-Fluidized Beds for Gram Drying, Dry. Technol. 7 (1989) 663–696. doi:10.1080/07373938908916621.

[37] C. Oliveira, S. Rocha, Intermittent drying of beans in a spouted bed, Brazilian J. Chem. Eng. 24 (2007) 571–585. doi:10.1590/S0104-66322007000400010.

[38] R.C. Brito, R. Béttega, J.T. Freire, Energy analysis of intermittent drying in the spouted bed, Dry. Technol. 37 (2019) 1498–1510. doi:10.1080/07373937.2018.1512503.

[39] M.G.A. Vieira, L. Estrella, S.C.S. Rocha, Energy Efficiency and Drying Kinetics of Recycled Paper Pulp, Dry. Technol. 25 (2007) 1639–1648.

doi:10.1080/07373930701590806.

[40] T. Kudra, C. Ratti, Foam-mat drying : Energy and cost analyses, Can. Biosyst. Eng. 48 (2006) 27–32.

[41] C.G.J. Baker, K.A. McKenzie, Energy consumption of industrial spray dryers, Dry. Technol. 23 (2005) 365–386. doi:10.1081/DRT-200047665.

[42] R.B. Keey, Drying of Loose and Particulate Materials, Hemisphere Publishing Corporation, New York, 1992.

[43] R.C. Brito, R. Bettega, J.T. Freire, Intermittent Drying: Principles and Fundamentals, in: G. Albini, J.T. Freire (Eds.), Spec. Top. Part. Syst. v.5 (in Port., 1st ed., São Carlos, 2019: pp. 205–231.

[44] V.P. Muthu, P.K. Chattopadhyay, Prediction of Heat of Vapourization of Moisture from Cereal Grains - A Modelling Approach, Dry. Technol. 11 (1993) 1855–1862. doi:10.1080/07373939308916931.

[45] S. Cenkowski, D.S. Jayas, D. Hao, Latent heat of vaporization for selected foods and crops, Can. Agric. Eng. 34 (1992).

[46] C. Borgnakke, R.E. Sonntag, Fundamentals of thermodynamics, 7th ed., John Wiley & Sons, 2009.

[47] F.B. Freire, A. Atxutegi, F.B. Freire, J.T. Freire, R. Aguado, M. Olazar, An adaptive lumped parameter cascade model for orange juice solid waste drying in spouted bed, Dry. Technol. 35 (2017) 577–584. doi:10.1080/07373937.2016.1190937.

[48] L. Otten, G. Samaan, Determination of the specific heat of agricultural materials: Part II. Experimental Results, Can. Agric. Eng. 22 (1980) 25–27.

[49] G. Albini, F.B. Freire, J.T. Freire, Barley: Effect of airflow reversal on fixed bed drying,

Chem. Eng. Process. - Process Intensif. 134 (2018) 97–104. doi:10.1016/j.cep.2018.11.001.

[50] S. Hatami, G. Payganeh, A. Mehrpanahi, Energy and exergy analysis of an indirect solar dryer based on a dynamic model, J. Clean. Prod. 244 (2020) 118809. doi:10.1016/j.jclepro.2019.118809.

[51] C. Strumiłło, P.L. Jones, R. Żyłła, Energy aspects in drying, in: A.S. Mujumdar (Ed.), Handb. Ind. Dry., Fourth, Taylor & Francis Group, LLC, 2014: pp. 1077–1100. doi:10.1201/b17208.

[52] N. V. Men'shutina, M.G. Gordienko, A.A. Voinovskii, T. Kudra, Dynamic criteria for evaluating the energy consumption efficiency of drying equipment, Theor. Found. Chem. Eng. 39 (2005) 158–162. doi:10.1007/s11236-005-0057-9.

[53] T. Kudra, C. Ratti, Foam-mat drying: Energy and cost analyses, Can. Biosyst. Eng. / Le Genie Des Biosyst. Au Canada. 48 (2006).

[54] I. Estiati, M. Tellabide, J.F. Saldarriaga, H. Altzibar, M. Olazar, Influence of the fountain confiner in a conical spouted bed dryer, Powder Technol. 356 (2019) 193–199. doi:10.1016/j.powtec.2019.08.005.

[55] P.T. Robbins, P.J. Fryer, The spouted-bed roasting of barley: Development of a predictive model for moisture and temperature, J. Food Eng. 59 (2003) 199–208. doi:10.1016/S0260-8774(02)00459-4.

[56] H. Zhao, Z. Yang, Z. Tao, Drying Kinetics of Continuous and Intermittent Heat Pump Drying of Green Soybean Seeds, Int. J. Food Eng. 13 (2017) 1–15. doi:10.1515/ijfe-2017-0182.

[57] R.C. Brito, M.B. Zacharias, V.A. Forti, J.T. Freire, Physical and physiological quality of intermittent soybean seeds drying in the spouted bed, Dry. Technol. 0 (2020) 1–14.

doi:10.1080/07373937.2020.1725544.

[58] H. Altzibar, G. Lopez, R. Aguado, S. Alvarez, M.J. San Jose, M. Olazar, Hydrodynamics of conical spouted beds using different types of internal devices, Chem. Eng. Technol. 32 (2009) 463–469. doi:10.1002/ceat.200800605.

CHAPTER 8

DRAFT TUBE DESIGN

This chapter describes the methodology proposed for the development of draft tubes to be used in spouted beds, which refers to specific objective (6) of this thesis. Although only a few parameters define draft tubes, the design of these devices is complex and remains a challenging task. Therefore, the paper described in this chapter proposed a new criterion for the design of draft tubes (nonporous and open-sided) based on the average spout diameter measured by a borescopic technique in conical spouted beds without draft tube. Based on the radial and axial particle velocity profiles, hydrodynamic analysis, and cycle time distributions, the new configurations are compared with those without tube and with conventional draft tubes. The new open-sided tube provides maximum particle velocities of 480.90±14.60 mm/s in the spout and 90.10±4.40 mm/s in the annulus. These values are lower and higher than the particle velocities obtained without draft tube in the spout and annulus regions, respectively, which means it modifies particle residence time in these regions. The new open-sided tube provides a more efficient gas-solid contact than any conventional one, with spouting behaviour being very similar to the configuration without tube (differences in the minimum spouting velocity being in the 2-6% range), which is a key aspect for scale up purposes.

This chapter is based on:

R.C. de Brito, M. Tellabide, A. Atxutegi, I. Estiati, J.T. Freire, M. Olazar, Draft tube design based on a borescopic technique in conical spouted beds, Adv. Powder Technol. (2021).

doi:10.1016/j.apt.2021.10.004.

8.1 INTRODUCTION

Although spouted beds have been developed as an alternative to fixed and fluidized beds for handling coarse particles, they are recognised as an efficient gas-solid contact method for a wide range of particle sizes, with a high degree of agitation and mixing between phases due to their distinct hydrodynamic behaviour [1–3]. As these features are essential to achieve high heat, mass, and momentum transfer rates, spouted beds have found applications in many physical and chemical processes, such as biomass pyrolysis [4,5], gasification [6,7], feeding [8,9], chemical vapour deposition [10,11], coating [12,13] and drying [14–16], among others. Despite the versatility of this multiphase reactor, the spouted bed has several limitations that restrain an effective industrial application. The maximum spoutable bed height and the ratio between the inlet diameter and particle diameter are the main limitations of the conventional spouted beds hindering their application in large-scale industrial processes [1,2]. In fact, stable operation with conical vessels is only attained when the ratio between the inlet diameter and particle diameter ranges between 2 and 60 [17,18]. Thus, most of the aforementioned spouted bed applications are usually restricted to bench scale.

Accordingly, different configurations and new internal devices have been proposed and studied to overcome such limitations. Compared to the conventional spouted bed, the conical configuration enables higher operation stability over a wider range of gas flow rates, as highlighted by Olazar et al. [1,19], who have defined stable operation conditions for gas-solid contact regimes and performed the drying of pinewood sawdust in conical spouted beds. Among the internal devices, fountain confiners [3] and draft tubes [20,21] are worth noting, as they significantly modify the solid flow pattern and increase the contactor operating range. A suitable design and use of the draft tubes in the conical spouted bed leads to significant improvements in the

performance and stability of this contactor, as these tubes reduce the minimum spouting velocity and operating pressure drop, as well as allow controlling the solid circulation pattern and the overall solid circulation flow rate [22,23]. Furthermore, the draft tubes avoid the maximum spoutable bed height of the conventional spouted bed by supporting the surrounding annular bed and avoiding the spouting collapse in deep beds [24,25]. Therefore, the draft tube is a key device to overcome the scale up limitations of the spouted beds.

Karimi et al. [22] developed a multi-layer perceptron neural network for the design and scale up of conical spouted beds with open-sided draft tubes, as they allow a better air percolation than the traditional nonporous ones. Mollick et al. [26] proposed a novel porous draft tube to both stabilize the spouting regime and promote air percolation from the spout into the annulus. Makibar et al. [27] studied the draft tube selection and evaluated the performance of these internal devices in a pilot-scale conical spouted bed. These authors made use of the length of the tube, its diameter and the height of the entrainment zone as the main defining parameters for the draft tubes. Nevertheless, the design of these devices remains a challenging task that requires knowledge regarding their influence on the gas-solid flow pattern [20]. Therefore, there is still a gap in the literature regarding the design of draft tubes, especially concerning the type of tube and its diameter. According to Makibar et al. [27], the draft tube diameter must be approximately the diameter of the spout under stable conditions, as draft tubes with diameters smaller than that of the spout cause deviation of the flow through the outside of the tube and related instability problems. In addition to the poor percolation, an unsuitable design of the tube diameter compromises the cross-flow of solid particles from the annulus into the spout, which worsens the gas-solid contact and bed hydrodynamics. Both aspects are essential for the scaling up of the reactor, as they

condition heat and mass transfer rates, which are crucial parameters that must be carefully tailored for each application.

The experimental complexity involved in obtaining the spout diameter (due to the oscillatory nature of pressure drop and solid flow) has led authors to use either the inlet diameter [19] or measurements obtained in half-column spouted beds as a reference [27] for both the selection and the design of draft tubes. Although they have shed some light on the fundamental hydrodynamic characteristics involving the design of draft tubes, recent technological advances in particle tracking and monitoring of the internal hydrodynamic behaviour reduce some of the shortcomings of previous techniques, as they allow obtaining dynamic data of the internal solid flow. Rahimir-Ahar and Hatamipour [28] described and discussed in detail the application of most of these techniques in spouted beds. Qian et al. [29] developed a novel endoscopic photography technique by coupling a high-speed CCD camera to an intrusive fiber-optic endoscope in order to investigate the solid flow pattern inside a 3D spouted bed. Atxutegi et al. [30] implemented a similar borescopic high-speed particle tracking velocimetry (PTV) technique in a conical spouted bed for tracking spherical and irregular particles. These authors highlighted the flexibility and the advantages of this technique, as it does not require any modification for high volume systems and allows obtaining local flow properties with sampling frequencies well above the natural oscillation frequency characteristic of spouted beds (4-8 Hz). Tellabide et al. [31] applied this borescopic technique to characterize solid flow and track fine particles in a fountain confined conical spouted bed. Compared to the traditional external PTV method, which is limited to 2D or half-column spouted beds, the use of a borescope is more advantageous for industrial applications, in which the units are usually made of opaque materials. Therefore, the borescopic technique is more flexible

than other techniques for scale up purposes, as it allows real time monitoring of the flow inside the bed, and therefore full understanding of the hydrodynamic behaviour in such contactors.

Based on the aforementioned background, this study aims to propose a new design criterion based on a borescopic technique for the development of draft tubes to be used in conical spouted beds. Accordingly, the hydrodynamics of the configuration without tube is analyzed, by paying special attention to the spout zone, and two types of draft tubes are proposed based on the spout equivalent diameter, namely, nonporous and open-sided tubes. The influence of the new draft tubes on bed hydrodynamics is compared with that of the conventional ones, and relevant information is discussed on the behavior of the new devices in the scaling up of these units.

8.2 MATERIALS AND METHODS

8.2.1 Materials and Equipment

The experimental unit has been described in detail in a previous paper [3]. All the experiments have been performed using a contactor made of polyethylene terephthalate. The geometric factors of the conical contactor are shown in Table 8.1 and schematized in Figure 8.1a. The geometric factors of the conical contactor have been based on Olazar et al. [1,17]. Alumina has been used as the particulate material, with an average size of 3.50 mm, which has been determined by sieving and image processing (*Image Pró Plus*®). A static bed height (H_0) of 0.15 m was used in all the experimental runs, which corresponds to a bed mass of 2.70 kg.

Table 8.1. Geometric factors of the contactor used in all the configurations.

Geometric Factors	Dimensions
Column diameter (m), D_c	0.36
Contactor angle (°), γ	60
Height of the conical section (m), H_c	0.23
Contactor base diameter (m), D_i	0.063
Inlet diameter (m), D_0	0.040

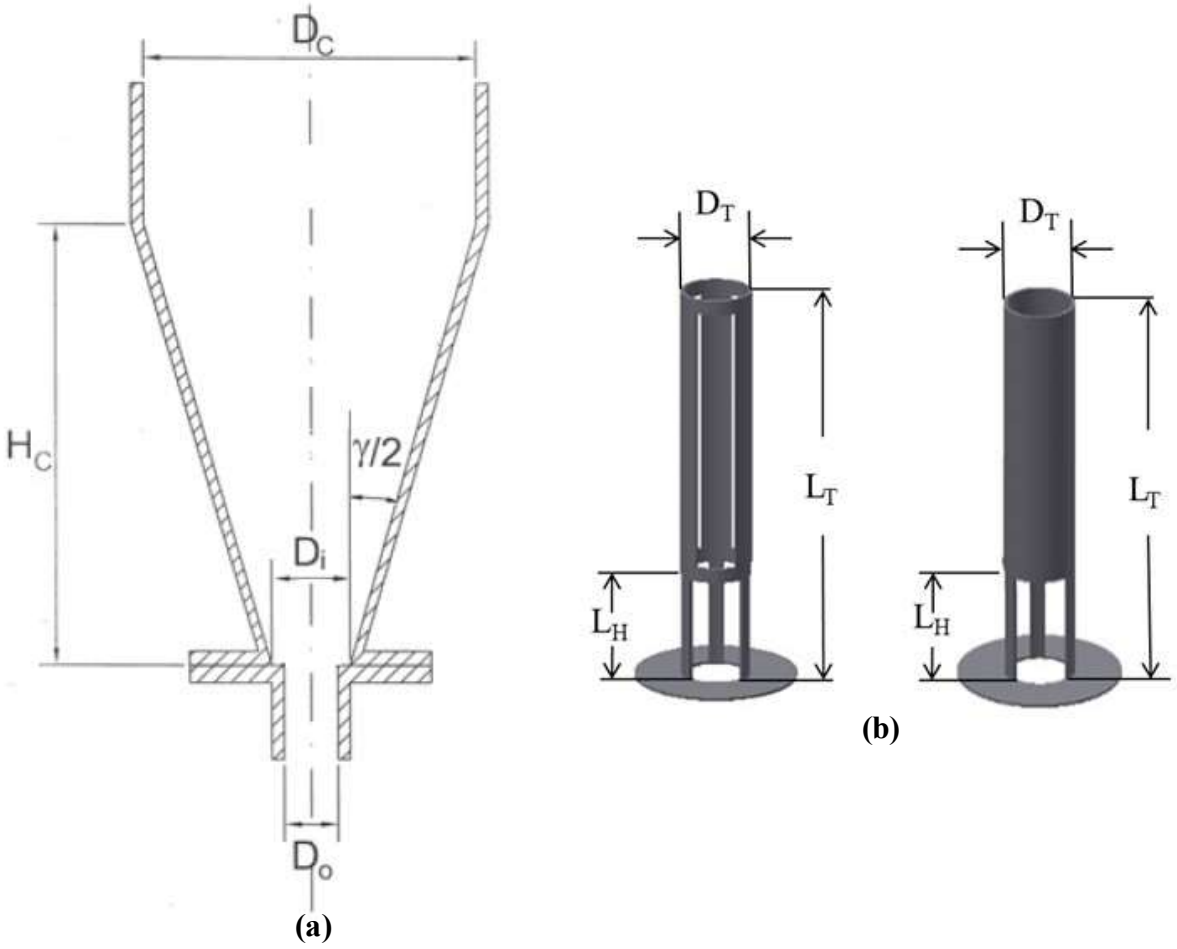

Figure 8.1. Geometric factors of (a) the conical contactor and (b) the open-sided and nonporous draft tubes.

The runs have been carried out without draft tube (WO) and with nonporous (NP) and open-sided (OS) ones. As mentioned before, two draft tubes differing in diameter have been used in each configuration (nonporous and open-sided), i.e., one with the diameter equal to the inlet diameter and the other one with the diameter equal to the average spout diameter obtained from the experimentation without draft tube. Hereinafter, the former types are referred as conventional draft tubes and the latter as new draft tubes. The dimensions of the conventional draft tubes (Figure 8.1b), which are described in detail by Tellabide et al. [3], are as follows: length of the tube (L_T), 0.17 m; height of the entrainment zone, i.e., distance between the gas inlet nozzle and the bottom of the draft tube (L_H), 0.07 m; diameter of the tube (D_T), 0.04 m; aperture ratio (AR) of the open-sided draft tube, 57% (with 0% being the nonporous draft tube). The dimensions of the new devices are the same, except the tube diameter, which has been determined based on the borescopic technique described below.

The experimental set-up of both the optical and the borescopic systems is shown in Figure 8.2. The image recording system, Figure 8.2a, is integrated into the contactor (1) and consists of a borescope (2), a light source, and a camera displacement system (3) composed of straight and circular sliders. This set-up allows the insertion of the borescope at any axial and radial position in the contactor. The borescope assembly (Figure 8.2b) is composed of a protector cartridge (1), a borescope (2), an optical adapter (3), and a high-speed camera (4), which is an *AOS S-PRI* (AOS Technologies AG) with a maximum recording resolution of 900 x 700 pixels and a maximum frame rate of 16500 fps with reduced resolution. More details about the optical and the borescopic systems are given in a previous paper [30]. According to Atxutegi et al. [30], such procedure has provided an error below 10%.

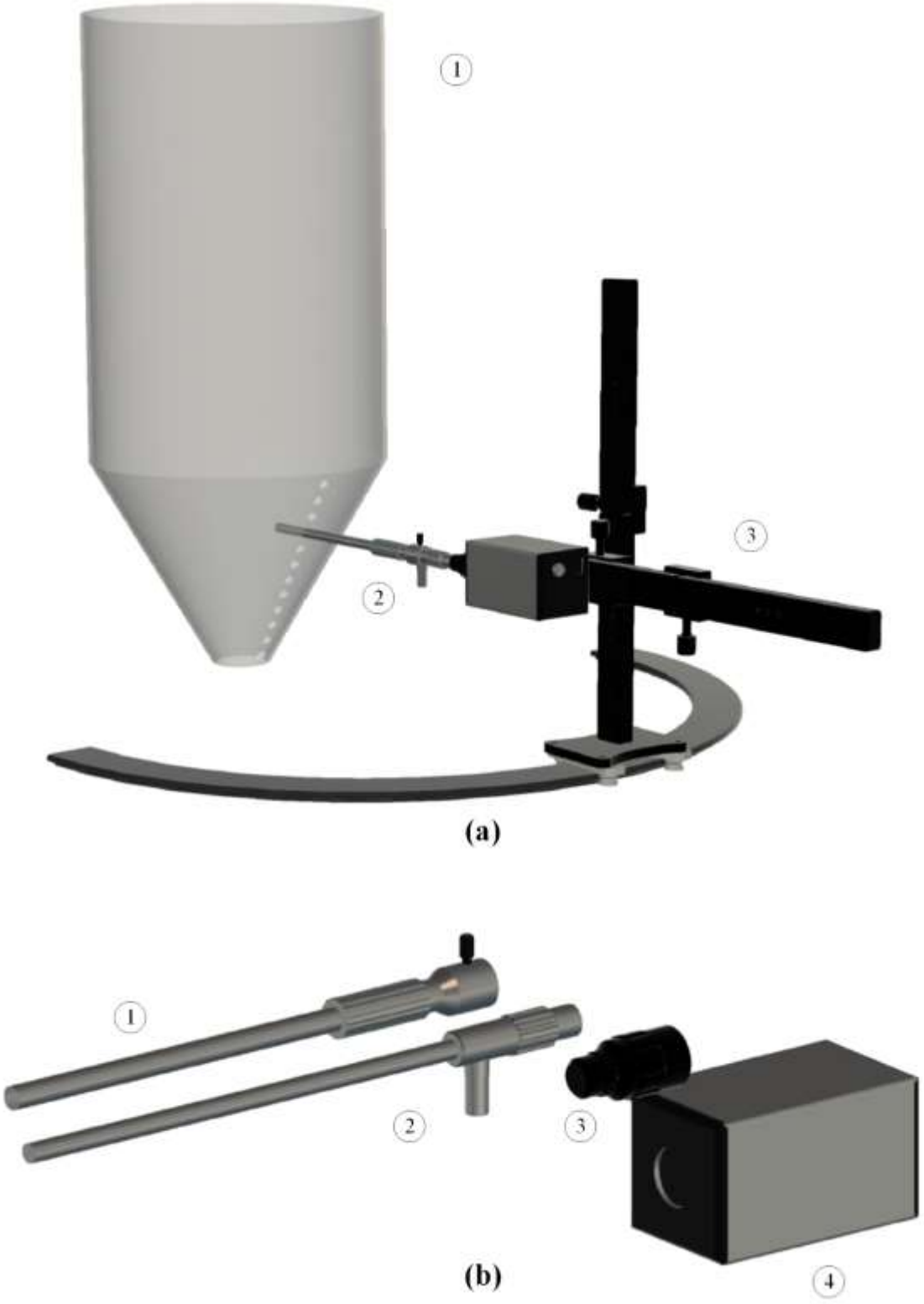

Figure 8.2. Experimental setup of (a) the optical system and (b) the borescope assembly.

8.2.2 Experimental Procedure

As previously mentioned, the design of the new draft tubes has been performed applying a borescopic technique, which enables the capture of particle velocity. Thus, the measurements have been carried out by progressively moving the tip of the borescope along the radial direction every centimeter from the contactor wall to the center of the contactor. This procedure has been conducted at five bed levels from the bed bottom to the bed surface: 0.02, 0.05, 0.08, 0.11, and 0.14 m. Four recordings for 2.5 seconds each have been taken at each measurement position.

The particle velocities have been obtained by an image processing algorithm developed in Matlab® 2017b. Some modifications have been done to the algorithm to account for the reflective nature of the material under study, Figure 8.3. Thus, given the spherical shape of these particles, the images captured by the optical system are processed with a canny edge detector combined with a Hough circle detection algorithm, which allows detecting particle centroids and particle radii. As shown in Figure 8.3, a particle close to the sapphire glass (protector at the tip of the endoscope) may take a big portion of the recording plane, which hinders detection and increases the noise in the final solid velocity signal. This problem has been solved by enlarging the frame, i.e., adding black pixel rows and columns around the frame. This algorithm finds spheres based on a specified range of radii and provides the centroid location with the radius in each detection. Subsequently, particles are paired in consecutive frames and the net displacement in the direction parallel to the measuring plane is obtained. The net particle displacement is related to the optical displacement by means of pixel distances and recording frame rates. The procedure described is applied to every frame and pairs of frames, which allows tracking particles and measuring their velocity in both spout and annulus. It is assumed that the vertical solid displacement is the main velocity

component in all regions in the spouted bed, as the solid displacement is mainly ascending in the spout and descending in the annulus. Accordingly, the spout limits have been determined based on the points where particle movement changes from upward to downward.

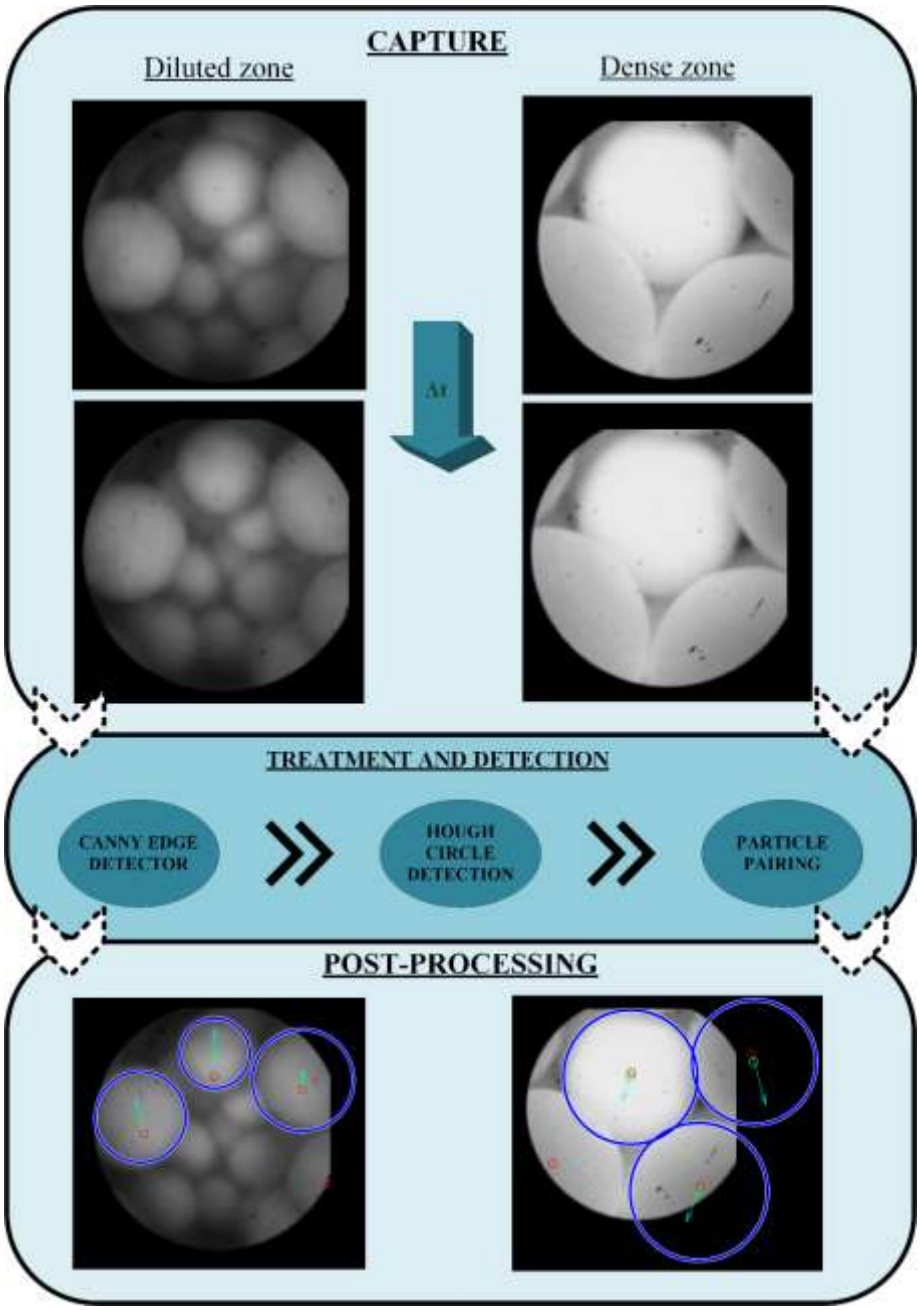

Figure 8.3. Schematic representation of the methodology used for the particle velocity estimation.

In addition to particle velocity profiles and spout geometry, the hydrodynamics has been characterized and cycle time distributions determined for all the configurations in order attain the best knowledge of the new draft tubes. The hydrodynamic characterization has been performed according to the procedure presented by Mathur and Epstein [2]. This methodology has been carried out in triplicate and has provided the minimum spouting velocity (u_{ms}) and the operating pressure drop (ΔP_s) for each configuration. The hydrodynamic characterization has been performed by a data acquisition system, which has been used to acquire pressure drop in the bed and air flow rate. Pressure measurements (±0.055% of accuracy) have been performed by means of two taps inserted into the contactor input and output, and the air flow rate has been measured by means of a thermal mass flowmeter, which allow an accurate measurement with an error below 2% (including linearity of 0.5% + 0.05% / °C). Based on this information, an inlet air velocity in the $1.25u_{ms}$ - $1.30u_{ms}$ range has been used in all cases, as this is a reasonable range for most practical applications.

As reported by several authors [32–35], cycle times have been measured by visual monitoring of a marked (painted) alumina particle through the transparent wall and from the top of the bed. This particle is placed on the surface of the annular zone and the time taken to reappear on the fountain is measured successively. For each configuration, a minimum of 100 measurements have been taken to determine the average and the minimum cycle times with enough statistical significance. The maximum cycle time has been measured by monitoring the particle trajectory along the contactor wall, as this is longest path for the particle to travel. In fact, the wall surface provides significant friction to the particle movement, and therefore the particles following this path have the lowest downward velocity.

8.3 RESULTS AND DISCUSSION

8.3.1 Draft tube design

Figure 8.4 shows the spout shape for the configuration without draft tube. The geometry has been defined by the isovalue lines of null velocity at the five bed levels measured with the borescopic technique.

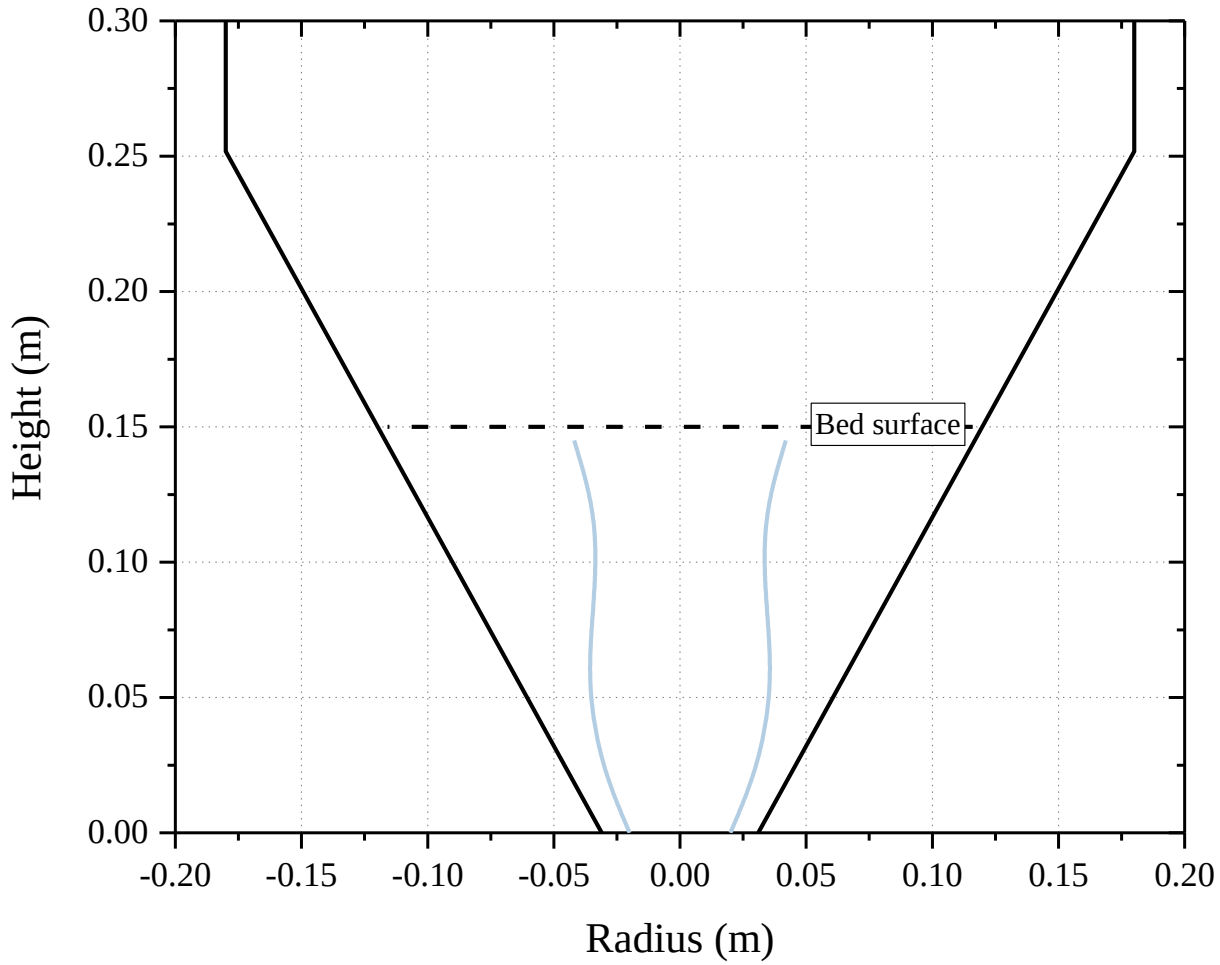

Figure 8.4. Spout shape obtained by PTV methodology for the configuration without draft tube (WO).

As observed in Figure 8.4, the spout expands significantly in the region immediately above the gas entrance orifice. It then narrows slightly in the height range between 0.05 m and 0.10 m, and finally expands again near the bed surface. The spout shape is heavily influenced by the type of solid and particular configuration. Thus, Olazar et al. [36] analysed the spout geometry for coarse particles in conical spouted beds using an optical fibre, and they report a sudden expansion and a subsequent neck close to the bottom, followed by steady expansion to the bed surface. Nevertheless, the results by Mukhlenov and Gorshtein [37] for fine particles show the spout always expands from the inlet to the bed surface. This difference in the shape is explained by two simultaneous facts. On the one hand, small particles are pushed aside more easily than coarse ones due to their lower mass, which avoids spout necking. On the other hand, air percolation from the spout into the annulus is worse as particles are smaller, which also contributes to expanding the neck and leading to a fully diverging spout. Therefore, it is of outermost importance to know the spout shape and diameter for the material to be treated, as it will heavily influence the spout volume and the gas-solid contact performance. The spout shape shown in Figure 8.4 is similar to that obtained by Olazar et al. [36] in a conical spouted bed with glass beads, which is consistent with most of the results reported in the literature, in which the average spout diameter is found to be much greater than the contactor inlet diameter [38,39].

As mentioned by Mathur and Epstein [40] and Bridgwater and Mathur [41], the balance of forces acting on the spout-annulus interface controls the spout shape, suggesting a state of dynamic equilibrium between these forces when the spout attains a stable shape. However, such forces on the spout-annulus interface arise from both the gas and solids flow patterns, which depend on phase properties and bed geometry. Likewise, the spout oscillates around the contactor axis, with its diameter changing from the bottom to the top of the bed, as shown in Figure 8.4. Furthermore,

this variation does not necessarily follow any general pattern. In this study, the spout volume (Figure 8.4) has been determined from the experimental data by a Matlab® code and, assuming an equivalent volume cylinder of 0.15 m in length, an equivalent diameter, $D_{s,eq}$, of 0.070±0.007 m has been estimated. Given the spout oscillations and the detection error of the methodology [30], the error in the calculation of average spout diameter is in the 8-10% range. Thus, as the ratio between the equivalent spout diameter and the inlet diameter ($D_{s,eq}/D_0$) obtained for the experimental conditions employed is 1.75, a ratio between the tube diameter and the inlet diameter (D_T/D_0) of 2 has been adopted for the design of the new draft tubes. The new draft tubes based on the equivalent spout diameter of the configuration without draft tube have been designed and built, as they are shown in Figure 8.5.

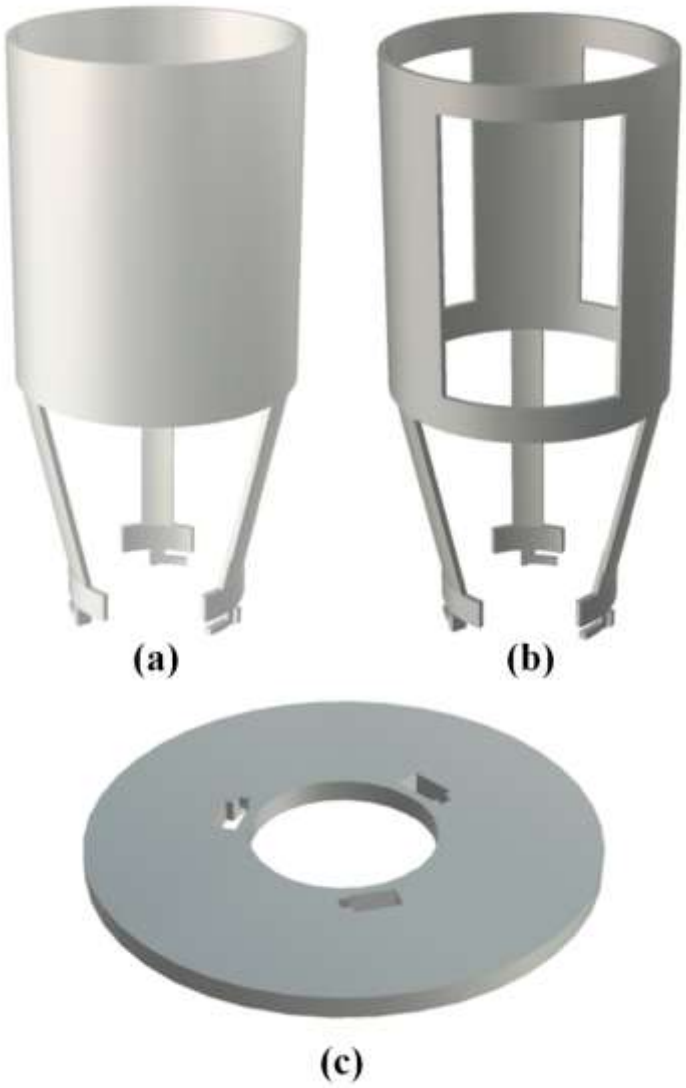

Figure 8.5. Schematic representation of the draft tubes designed based on the spout diameter: (a) nonporous draft tube (DT = 0.076 m), (b) open-sided draft tube (DT = 0.076 m), and (c) draft tube base (D0 = 0.040 m).

As presented in Figure 8.5, the diameter of the new draft tubes (D_T = 0.076 m) is almost twice the inlet diameter (D_0 = 0.040 m) and larger than the base diameter (D_i =0.063 m). Furthermore, a removable base (Figure 8.5c) has been designed to allow the insertion of the new draft tubes from the top of the contactor.

8.3.2 Hydrodynamic curves

The hydrodynamics of the configurations equipped with the new draft tubes was studied based on their characteristic curves. Thus, Figure 8.6, shows the evolution of pressure drop vs. air velocity (characteristic curves).

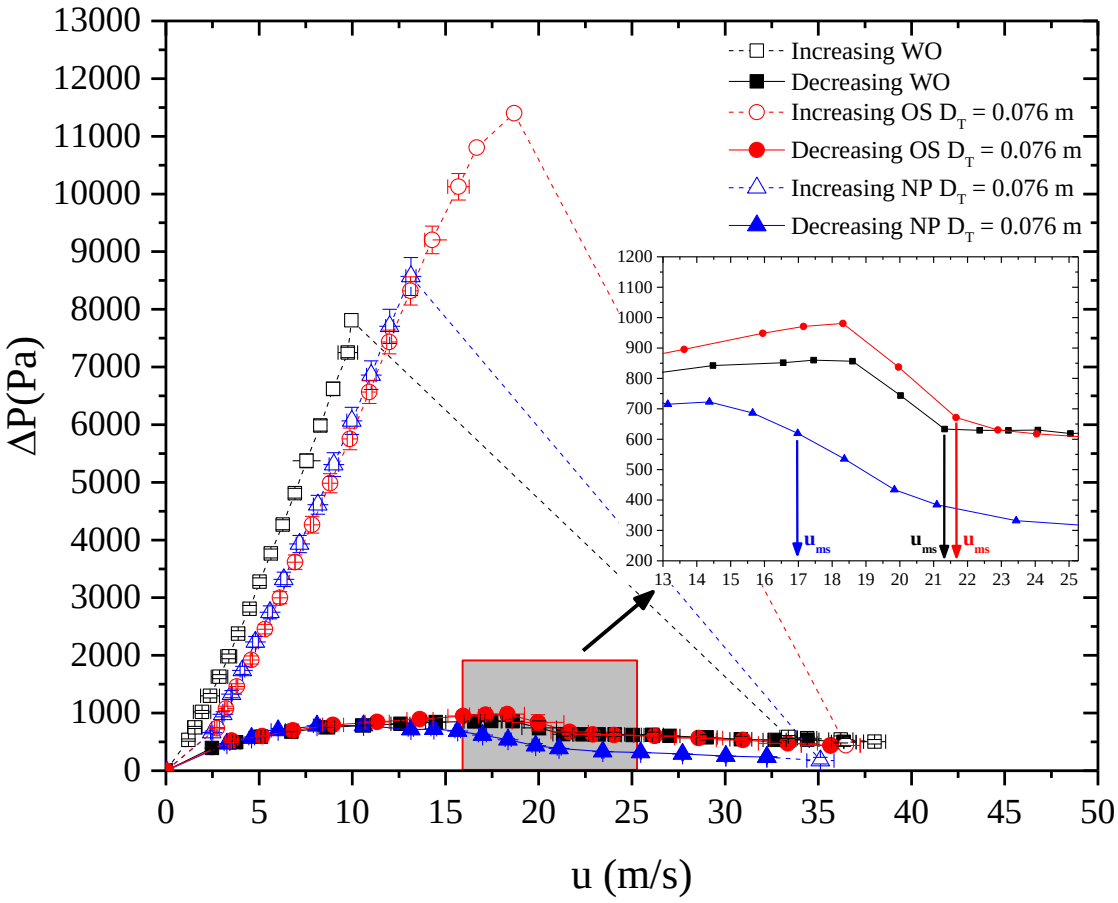

Figure 8.6. Evolution of pressure drop with air velocity for the configurations without draft tube and with the new nonporous and open-sided ones.

All the configurations used in this study follow the typical characteristic curves of spouted beds [2]. As reported by several authors [19–21,42–44], the use of conventional draft tubes leads to a decrease in the minimum spouting velocity and operating pressure drop. Table 8.2 compares

the values of these hydrodynamic parameters for the configurations without tube, and with the conventional and new draft tubes. As observed, the smallest values are those corresponding to the conventional nonporous tube.

Table 8.2. Hydrodynamic parameters of the configurations under study.

Configuration	ΔP_S **(Pa)**	u_{ms} **(m/s)**
Without tube	633.40±33.00	21.30±0.60
Open-sided tube (D_T = 0.040 m)	514.70±30.30	17.40±0.30
Nonporous tube (D_T = 0.040 m)	315.00±12.40	14.20±0.10
Open-sided tube (D_T = 0.076 m)	671.50±19.10	21.70±1.00
Nonporous tube (D_T = 0.076 m)	619.30±13.30	17.00±0.20

The new draft tubes require higher minimum spouting velocities and lead to higher operating pressure drops than their conventional counterparts, as an increase in the spout diameter requires higher momentum to start particle movement. Consequently, the new open-sided tube requires a minimum spouting velocity that is approximately 25% higher than the conventional one and the new nonporous one requires a minimum spouting velocity 20% higher than the conventional one. Thus, the minimum flow rate required in the configuration with the new open-sided draft tube is approximately the same as in the one without draft tube, whereas in the configuration with the new nonporous draft tube the minimum flow rate is similar to the one with the conventional open-sided draft tube. Although a larger diameter means an increase in the operational costs, the use of these devices allows for stable spouting with an accurate control of particle cycle times.

8.3.3 Spout Geometry

The delimitation of the spout-annulus interface has been conducted in the configurations with all the draft tubes (conventional and new ones), apart from that in the configuration without tube described above. The spout shapes for all the cases are shown in Figure 8.7.

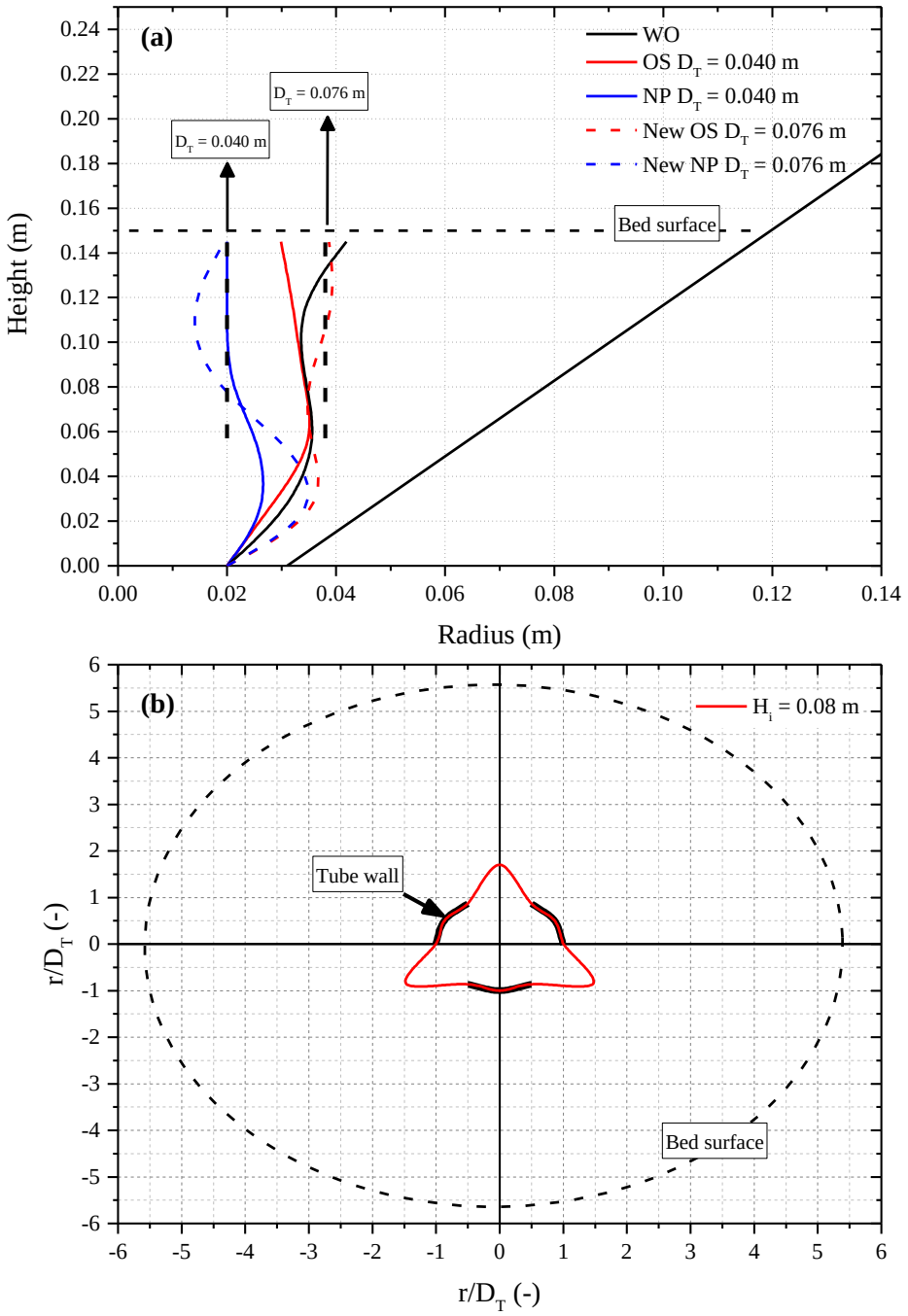

Figure 8.7. (a) Spout shapes obtained by PTV methodology for all configurations studied, i.e., without tube (WO), conventional and new open-sided tubes (OS), and conventional and new nonporous tubes (NP); and (b) Cross-sectional spout shape in the configuration with the conventional open-sided draft tube.

As observed in Figure 8.7a, the spout geometry is significantly influenced by the draft tubes. In the configuration with the conventional nonporous tube, i.e., a tube diameter equal to the inlet diameter (D_T = 0.040 m), the spout shape is delimited by the tube wall in the upper half of the bed. Nevertheless, a slight spout expansion is observed at the bottom section before the air enters the tube, which can be attributed to particle incorporation into the spout and their change in velocity from downwards to upwards in this entrainment zone. Consequently, as the draft tube delimits the spout in this configuration, the average spout diameter is lower than that of the configuration without draft tube. The reduced spout volume in this configuration, along with the low solid cross-flow rate from the annulus into the spout (only in the entrainment zone) [19,21], results in a significantly lower solid circulation flow rate than in the configuration without draft tube. Therefore, the gas-solid interactions and the rate of transfer phenomena are compromised with the insertion of the conventional nonporous tube.

The spout geometry in the configuration with the conventional open-sided tube, Figure 8.7a, is similar to that of the configuration without tube, as it has a sharp expansion in the entrainment zone (between the inlet and the lower end of the tube) followed by a steady narrowing of the spout until the bed surface. It should be noted that this shape corresponds to the open fraction of the tube, in which the spout diameter is even larger than the tube diameter. In the closed fraction, the spout diameter is the tube diameter itself. The geometry of the cross-section of the spout has been delineated according to the methodology by Tellabide et al. [31], Figure 8.7b, who also observed a three-pointed star spout shape when they used an open-sided draft tube. In view of Figure 8.7b, the average spout diameter with this device is slightly higher than the inlet diameter.

Regarding the new draft tubes (D_T = 0.076 m), the open-sided one leads to a spout shape similar to the configuration without draft tube, except for a more pronounced spout expansion in

the entrainment zone and a diameter equal to the tube one in the remaining section of the bed. The former is related to the increase in the tube diameter, which has an influence on the particle cross-flow from the annulus into the spout at the bottom and on the particle velocity profile in the annular region. Thus, an increase in tube diameter increases the particle flow rate through the spout region, leading to a more effective gas-solid interaction than in the configurations with the conventional open-sided draft tube. Furthermore, an increase in tube diameter also leads to a decrease in the air velocity through the spout, and therefore to an increase in the residence time of the gas phase in this region. Nevertheless, unlike the conventional open-sided draft tube, the new ones do not cause any expansion of the spout in the opened fraction of the tube (the shape shown in Figure 8.7a corresponds to the interface in the opened fraction). As observed in Figure 8.7a, the outer surface of the spout in the opened fraction of the tube is approximately the same as the tube diameter, as the gas phase does not have enough pressure to permeate into the annulus due to the lower air velocity than in the conventional open-sided tube. These findings suggest that an open-sided draft tube designed based on these premises is a promising device in processes demanding effective gas-solid contact (drying, pyrolysis, coating, and so on), as well as in the scaling-up of these units. As mentioned above, the spout geometry of the configuration with the new open-sided tube is similar to that without the draft tube (Figure 8.7a), which is evidence of their hydrodynamic similarities. According to Aradhya et al. [45], the hydrodynamic similarity means that the values of the hydrodynamic parameters are similar in both cases. Thus, the results set out in Table 8.2 for the operating pressure drop and the minimum spouting velocity differ in the range from 2% to 6% in the configurations without draft tube and with the new open-sided tube. Although their hydrodynamics are similar, the great advantage of the new open-sided draft tube lies in the stabilization of the spouting regime by avoiding the maximum spoutable bed height, as well as the

inlet restrictions (the ratio of the inlet diameter to particle diameter), which are key aspects to overcome the scaling up of the spouted bed.

Concerning the average spout diameter for the configuration with the new nonporous draft tube, Figure 8.7a, it is even smaller than the tube diameter. Thus, the spout in this configuration has a sharp expansion in the entrainment zone, but subsequently undergoes a great contraction with a neck halfway between the upper and lower end of the tube. This result is evidence of a downward trajectory of the particles within the draft tube close to the inner wall. This unexpected finding is explained based on the particle velocity profiles shown and discussed in the next section.

8.3.4 Particle Velocity Profiles

As previously mentioned, the inlet air velocity has been set relative to the minimum spouting velocity, u_{ms}, in order to operate at the same hydrodynamic regime, with air velocities ranging between $1.25u_{ms}$ and $1.30u_{ms}$ for all the runs. Therefore, the inlet air velocity differs depending on the configuration, which leads to differences in solid velocities. An analysis of these velocities based only on absolute values may come to misleading conclusions, as the momentum available to drag particles differs in each case. This is especially apparent in the analysis of the longitudinal profiles along the spout axis, in which the drag force provided by the gas phase is the dominant factor affecting particle flow. Thus, Figure 8.8 shows the longitudinal profiles of particle velocity in terms of both the absolute values and the dimensionless values defined as the ratio between particle velocity and inlet air velocity.

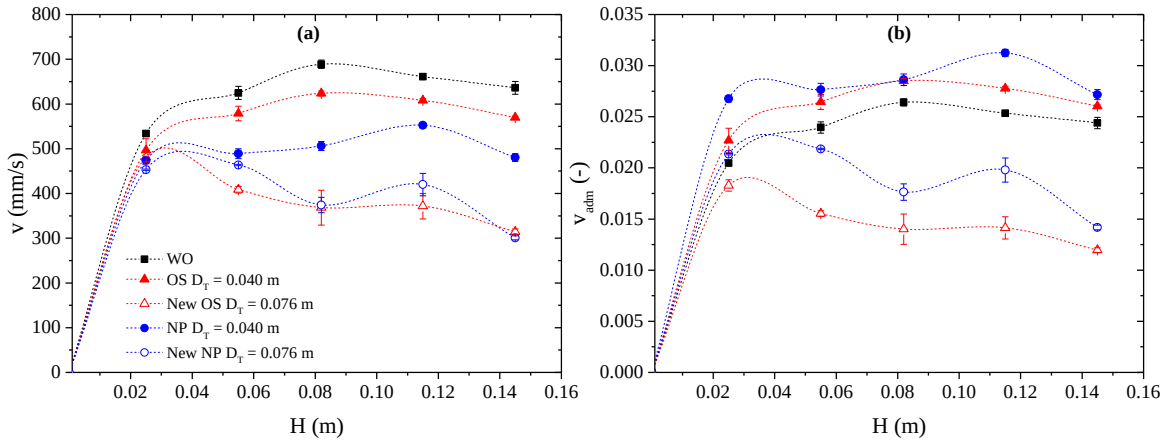

Figure 8.8. Longitudinal profiles of the vertical component of particle velocity along the spout axis in the configurations studied. (a) absolute particle velocity and (b) dimensionless particle velocity.

As presented in Figure 8.8a, the longitudinal profiles observed are qualitatively similar in the configurations without tube and with the conventional draft tubes. Thus, as the air is fed into the system, the particles are rapidly accelerated up to approximately 2 cm. Above this level, velocity increases smoothly until it peaks at a given longitudinal position, and then decreases as the particles are approaching again the bed surface due to the air momentum drainage. This behaviour is typical and has been also described by several authors [46–49]. In the configurations without tube and with the conventional open-sided tube, the maximum particle velocities are attained at an intermediate bed level. However, in the configuration with the conventional nonporous tube, the maximum particle velocity is attained in the upper zone near the bed surface. The high air velocity through the spout region explains this trend observed with the nonporous draft tube, as this internal device avoids air percolation into the annulus and entails a low solid flow rate through the spout. Both facts affect significantly the gas-particle momentum transfer in this configuration. Zhao et al. [25] have reported a similar trend in the particle acceleration through

the tube in a draft tube spouted bed. Furthermore, the facts mentioned are also consistent with the results reported by Zhao et al. [46], who found that the ratio of the spout outlet flow rate to the total flow rate in a two-dimensional spouted bed with draft plates is about 92%.

Regarding the configurations with the new draft tubes, particle velocity peaks at a much lower longitudinal position (approximately at 2 cm from the bottom) than in the other configurations, i.e., without the draft tube and with the conventional ones. Accordingly, the momentum of the inlet air in the new configurations is not enough to maintain the particle accelerating throughout the tube in the upper zone. Such findings suggest an increase in the air flow rate through the annular region, especially when the configurations without tube and with the new open-sided draft tube are compared, as both configurations require a similar minimum spouting velocity. Furthermore, as mentioned above, the new draft tubes lead to an increase in the total particle circulation flow rate through the spout region, enhancing the gas-particle momentum transfer.

Unlike the configuration with the new open-sided tube, in which the particle steadily decelerates towards the bed surface, there are two peaks of particle acceleration in the configuration with the new nonporous tube. As observed in Figure 8.8a, these peaks are located at H_i = 0.02 m and H_i = 0.11 m. The second peak is explained by the neck in the spout shown in Figure 8.7a for this configuration, which causes an increase in the air velocity at this section in the spout. Zhu et al. [50] found similar results in a two-dimensional spouted bed operating with both wet and dry particles. These authors reported a spout width smaller for wet particles than for dry ones, leading to a higher acceleration of wet grains in the spout.

The highest particle velocity is observed for the configuration without tube along the whole length of the spout (Figure 8.8a). Although the configurations with both the conventional open-

sided tube and the conventional nonporous one have lower particle velocities than the configuration without tube, the reverse happens when dimensionless particle velocities are used instead of absolute values, Figure 8.8b. Thus, the lowest particle velocities for the configuration with the conventional nonporous tube, Figure 8.8a, are related to the lowest inlet air velocities required in this configuration for spouting. Nevertheless, the highest values of the dimensionless particle velocity in Figure 8.8b for the same configuration are related to higher fraction of the air being directed through the spout region due to the insertion of the nonporous tube. A similar trend was observed by Ishikura et al. [20], which they also attributed to the lack of gas percolation into the annular zone.

Concerning the particle velocities with the new draft tubes, the trends are similar when either the absolute values (Figure 8.8a) or dimensionless ones (Figure 8.8b) are used, except that the differences are more pronounced. Thus, the configuration with the new open-sided draft tube provided the lowest particle velocities along the whole length of the spout. This particle velocity is explained by the increase in the spout cross section, which leads to a decrease in the air velocity through the spout and to an increase in the total solid flow rate. Compared with the configuration without tube, the lower particle velocities obtained with the new open-sided tube suggest an increase in the air flow rate through the annular region, as both configurations require a similar minimum spouting velocity (a difference within 2%). This hypothesis is also supported by the more pronounced spout expansion in the entrainment zone with the new open-sided tube (Figure 8.7a). Overall, the findings obtained with the new open-sided tube suggest that this internal device can provide longer residence times for the gas and particles in the spout region, which is a highly relevant result in processes in which high heat and mass transfer rates are required. As observed in Figure 8.8a, the peak particle velocity along the axis is 688.90±9.20 mm/s in the configuration

without tube, whereas it is 480.90±14.60 mm/s in the configuration with the new open-sided tube. As stated by Mollick et al. [26], the solid-fluid contact time is a key parameter to be considered in the design of draft tubes. According to these authors, these devices should be designed in order to decrease superficial gas velocities and increase residence times, with high turbulence being ensured.

Although the facts mentioned about air percolation may partially explain the results observed with the new nonporous draft tube, the lower particle velocities obtained with this tube than with the conventional ones are also related to the downward movement of the particles within the draft tube. Such a downward flow of the solids occurs in the region close to the inner wall of the tube, which involve additional resistance to the particle flow in the spout. This downward solid flow inside the draft tube is clearly observed in Figure 8.9, in which the radial profiles of the vertical component of particle velocity are shown at an intermediate longitudinal position (H_i = 0.11 m) for both spout and annular regions.

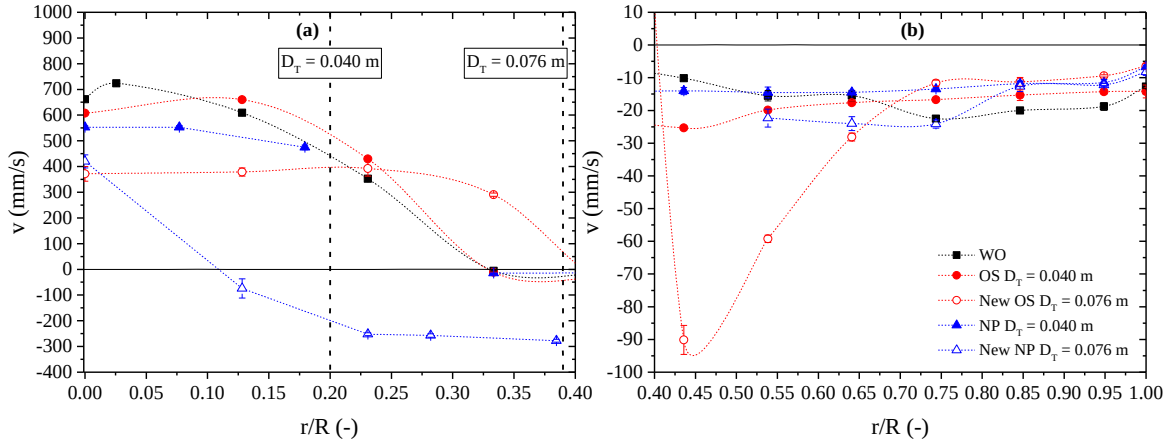

Figure 8.9. Radial profiles of the vertical component of particle velocity in the configurations analyzed. (a) spout region and (b) annular region.

As observed in Figure 8.9a, the particle velocity in the configuration with the new nonporous tube has negative values from approximately $r/R = 0.1$ to the tube wall ($r/R = 0.4$), which confirms the downward particle flow inside the draft tube. The joint effect of low particle velocities on the bed surface, mainly near the contactor wall, and low solid flow rates through the spout region with the nonporous tubes, leads to the formation of a crater on the upper surface of the bed. This crater has been previously described by Saldarriaga et al. [33] and makes particles slide into the draft tube directly from the bed surface, similar to a "cascade flow". This downward movement within the draft tube is a consequence of a too large tube diameter, and therefore too low velocity in the spout region, which, in addition to creating particle back mixing, reduces the natural flow of spouted beds. A similar behaviour has also been reported by Zhang et al. [47] in a two-dimensional spouted bed with coarse particles. These authors have observed coarse particles falling back in the fountain and have attributed this phenomenon to the weak drag force in that region.

Figure 8.9a shows that the radial profiles of both without tube and with the conventional open-sided draft tube configuration present a parabolic shape with the maximum particle velocity slightly displaced from the axis. This displacement can be attributed to the radial movement of particles in the spout region, as also mentioned by Olazar et al. [38]. Thus, the particle velocity decreases from a peak value around the spout axis to zero at about $r/R = 0.33$, which corresponds to the spout-annulus interface in the configurations without tube and with the conventional open-sided tube. This location is a higher radial position than that corresponding to tube wall in the conventional open-sided tube, which is consistent with the spout expansion in the opened fraction of the draft tube.

As observed in Figure 8.9b, the configuration with the conventional nonporous tube has a uniform radial profile in the annulus with the solids moving almost in plug flow. Likewise, the

new nonporous tube also has a similar uniform radial profile from the tube wall to approximately an intermediate position in the annulus (r/R = 0.75), but the downward velocity decreases from this position to the wall of the contactor, especially on the wall itself. Similarly, Zhao et al. [25] found that the average particle velocity in the annulus increases by 28% as the tube diameter is increased from 30 mm to 40 mm. These authors related such results with the solid circulation rate, which is affected by the entrainment area as the tube diameter is increased. The higher air percolation into the annulus provided by the new nonporous tube, especially near the tube wall, also contributes to explaining these results. In all the configurations studied, the lowest particle velocities are observed near the contactor wall due to the wall friction, as also reported by several authors [36,38,48,51].

The configuration with the new open-sided tube provides the highest particle velocities in the annular region at around r/R = 0.65 from the tube wall, with a very pronounced inverse peak of the downward particle velocity at around r/R = 0.44, i.e., near the tube wall. In this radial position, a maximum downward particle velocity of 90.10±4.40 mm/s is observed with the new open-sided tube, whereas the configuration without draft tube leads to a maximum downward particle velocity of 22.50±0.90 mm/s at around r/R = 0.75. This trend is due to the higher air percolation in this configuration than in the other configurations studied, which is a consequence of the opened fraction of the tube. In fact, these opened cross-sectional zones behave like sink points in the spout-annulus interface, similarly to the entrainment zone at the bottom section, as mentioned by Roy et al. [52]. The overall consequence is a higher solid circulation flow rate in the annular region with the new open-sided tube than with the other configurations, especially in the zone between the tube wall and intermediate annular positions. Therefore, the residence time of the particles in the annular region can be reduced in this configuration due to the increase in particle

velocity. The relationship between air percolation in the annulus and the solid circulation flow rate has already been discussed in the literature [48, 50]. Thus, an increase in the spouting gas flow rate leads to an increase in the downward particle velocity.

A slight increase in the downward particle velocity close to the tube wall has also been observed for the conventional open-sided tube, Figure 8.9b, although much less pronounced than that observed for the new open-sided tube, which is consistent with the sink point described above. Concerning the configuration without tube, the radial profile has a parabolic shape with the maximum downward particle velocity at intermediate positions in the annulus. As mentioned above, this maximum value is much smaller than that observed with the new open-sided tube. It should be noted that the studies without tube in the literature report the location of the maximum particle velocity in the annulus at radial positions near the spout-annulus interface [39,53]. Therefore, other variables, such as particle properties and the geometric factors of the contactor, may affect the radial position of the maximum particle velocity in the annulus.

Overall, based on the results and discussion concerning both spout geometry and particle velocity, the new draft tubes proposed are of great interest, with advantages in at least two major aspects, solid-fluid contact and air percolation. Compared to the conventional configuration, the new open-sided tube provides lower particle velocity in the spout and higher particle velocity in the annulus regions, which modifies the particle residence time in these regions. Likewise, the particle recirculation inside the new nonporous tube (upward in the core and downward on the inside wall) contributes to increasing particle residence time in the spout (a region of high gas-solid contact), albeit distorting the natural flow of spouted beds.

The residence time of the solid phase in the three zones of spouted beds is strongly linked to the solid cycle times, and therefore they have been studied with these new devices. Furthermore,

this parameter is a key factor to be considered in any spouted bed application, as the average cycle time is closely related to heat and mass transfer rates and reactor capacity.

8.3.5 Cycle Time Distribution (CTD)

The use of internal devices significantly modifies the cycle time distribution, which is evident in Figure 8.10. As observed, the configuration without draft tube leads to a somehow normal distribution, whereas those with the open-sided and nonporous draft tubes lead to distributions biased towards higher cycles.

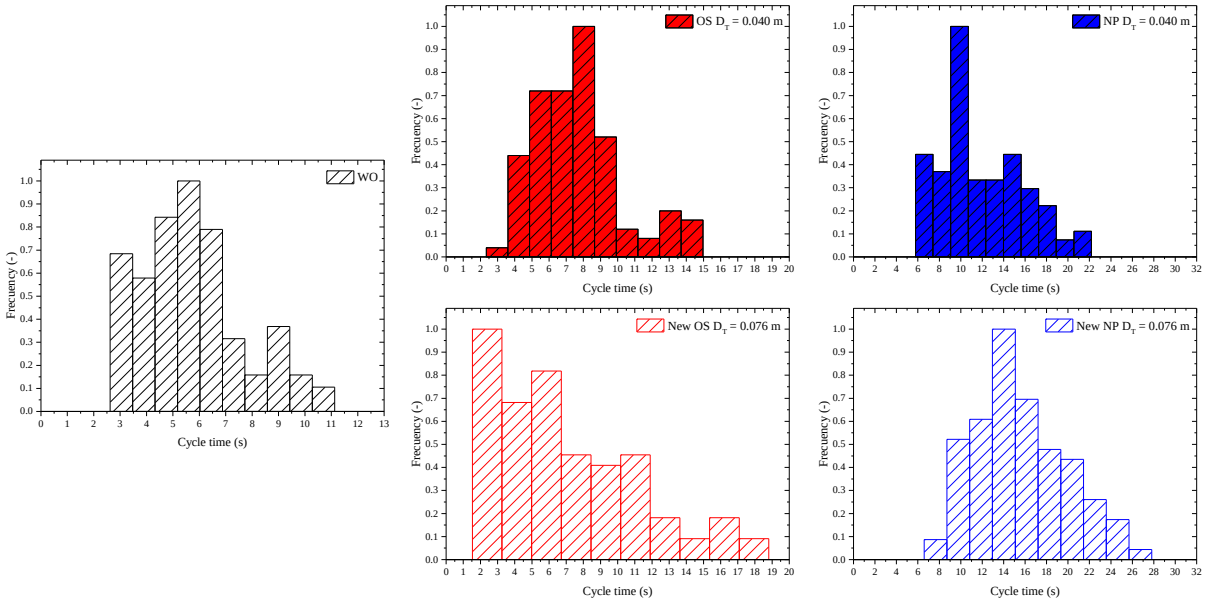

Figure 8.10. Cycle time distributions for the configurations studied.

The distributions for both the configuration without tube and with the conventional open-sided tube are unimodal asymmetric ones, whereas the one for the conventional nonporous tube follows a bimodal distribution. Thus, short cycles prevail in the configurations without tube and the conventional open-sided tube, with average cycle times in the 5-7 s and 6-8 s ranges,

respectively. In the configuration with the nonporous tube, this device does not allow solid cross-flow from the annulus into the spout, except in the entrainment height, which leads to longer cycles. Similarly as obtained by Saldarriaga et al. [33,34] with a conventional open-sided tube in beds of sawdust, the distribution for the new open-sided tube also follows an exponential distribution. Therefore, short cycles (2-6 s) prevail in this configuration, which supports the fact that the new design of the open-sided draft tube leads to higher solid circulation rates. These short cycles correspond to the particles that incorporate into the spout through the opened fraction of the tube in the upper half of the bed. This preferential incorporation is consistent with the high particle velocity in the annulus (especially close to the tube wall) discussed above. However, the cycle time distribution of the new open-sided tube is wider than that obtained without tube. The configurations with the nonporous draft tube, either the conventional or the new one, require a minimum of approximately 4-8 s to complete a cycle. Furthermore, the mean cycle time consistently increases as the opening ratio of the draft tube is reduced, Table 8.3. Thus, the shortest average cycle time corresponds to the configuration without tube (100% aperture ratio) and the longest one to the configuration with the non-porous tube (0% aperture ratio).

Table 8.3. Average, minimum, and maximum cycle times for all the configurations studied.

Configuration	t_c**(s)**	$t_{c,min}$ **(s)**	$t_{c,max}$**(s)**
Without tube	5.72	2.62	11.13
Open-sided tube (D_T = 0.040 m)	7.70	2.34	14.97
Nonporous tube (D_T = 0.040 m)	11.90	5.80	22.20
Open-sided tube (D_T = 0.076 m)	6.98	1.53	18.81
Nonporous tube (D_T = 0.076 m)	15.61	6.59	27.82

As observed in Table 8.3, the new draft tube designs lead to either shortening the average cycle time (open-sided one) of lengthening it (nonporous one). Although an increase in the draft tube diameter reduces the volume of the solid in the annulus, the longest average, minimum, and maximum cycle times are obtained with the new nonporous tube. These values are consistent with the significant particle back-mixing observed in the draft tube, in which particles move downwards in a considerable fraction of the cross-sectional are close to the walls. As the current methodology to measure the cycle time is based on the time that the particle takes to travel from the top of the fountain downwards and back again to the surface [32,54], the particle recirculation inside the new nonporous tube contributes to lengthening the cycle time in this configuration.

8.4 CONCLUSIONS

New open-sided and nonporous draft tubes have been designed based on a borescopic technique and adopting as reference the equivalent spout diameter without tube. The new open-sided tube provides a more efficient gas-solid contact than any conventional one, as it increases the spout volume, as well as the contact time in this zone. Such features are essential to achieve an intensive degree of mixing and high heat and mass transfer rates, which are required in most physical and chemical processes (combustion, pyrolysis, coating and drying, among others). Furthermore, the new open-sided tube has an interesting hydrodynamic similarity with the configuration without tube, which is evidenced by both the spout geometry and hydrodynamic parameters (differences in the range from 2% to 6%). Furthermore, this device ensures high bed stability, which is a key aspect for scale up purposes. The new nonporous tube leads to significant differences in the solid flow pattern and cycle time distribution, with particles moving downwards

within the device, and therefore increasing their cycle time. In spite of this feature, the particle movement and circulation in the spout is much higher than in the annulus, which means high efficiency in the gas-solid contact, and so high heat and mass transfer rates. Therefore, this study means a step further to overcome the spouted bed limitations related to scale up and applications in large-scale industrial processes by using internal devices tailored to the actual spout geometry.

ACKNOWLEDGEMENTS

The authors appreciate the financial support provided by Coordination for the Improvement of Higher Education Personnel (CAPES), the São Paulo State Research Foundation (FAPESP, grant #2017/01856-7 and grant #2018/22655-2), the Spain's Ministry of Science and Innovation (PID2019-107357RB-I00 (AEI/FEDER, UE)), The Basque Government (IT1218-19 and KK-2020/00107), and the European Commission (HORIZON H2020-MSCA RISE-2018. Contract No.: 823745). M. Tellabide thanks Spain’s Ministry of Education, Culture, and Sport for his Ph.D. grant (FPU14/05814). I. Estiati thanks the University of the Basque Country for her postgraduate grant (ESPDOC18/14).

REFERENCES

[1] M. Olazar, M.J. San José, A.T. Aguayo, J.M. Arandes, J. Bilbao, Stable operation conditions for gas-solid contact regimes in conical spouted beds, Ind. Eng. Chem. Res. 31 (1992) 1784–1792. doi:10.1021/ie00007a025.

[2] K.B. Mathur, N. Epstein, Spouted Beds, Academic Press, New York, 1974.

[3] M. Tellabide, I. Estiati, A. Pablos, H. Altzibar, R. Aguado, M. Olazar, New operation

regimes in fountain confined conical spouted beds, Chem. Eng. Sci. 211 (2020) 115255. doi:10.1016/j.ces.2019.115255.

[4] K. Azizi, M. Keshavarz Moraveji, A. Arregi, M. Amutio, G. Lopez, M. Olazar, On the pyrolysis of different microalgae species in a conical spouted bed reactor: Bio-fuel yields and characterization, Bioresour. Technol. 311 (2020). doi:10.1016/j.biortech.2020.123561.

[5] K.M. Barcelos, P.S. Almeida, M.S. Araujo, T.P. Xavier, K.G. Santos, M.S. Bacelos, T.S. Lira, Particle segregation in spouted bed pyrolysis reactor: Sand-coconut shell and sand-cocoa shell mixtures, Biomass and Bioenergy. 138 (2020) 105592. doi:10.1016/j.biombioe.2020.105592.

[6] N. Spiegl, C. Berrueco, X. Long, N. Paterson, M. Millan, Production of a fuel gas by fluidised bed coal gasification compatible with CO2 capture, Fuel. 259 (2020) 116242. doi:10.1016/j.fuel.2019.116242.

[7] A. Niksiar, B. Nasernejad, Modeling of gasification reaction to produce activated carbon from pistachio shells in a spouted bed, Biomass and Bioenergy. 119 (2018) 97–108. doi:10.1016/j.biombioe.2018.09.008.

[8] L. Massaro Sousa, M.C. Ferreira, On the performance of a spouted bed type device for feeding spent coffee grounds to a circulating fluidized bed reactor, Chem. Eng. Res. Des. 160 (2020) 31–38. doi:10.1016/j.cherd.2020.05.002.

[9] L. Massaro Sousa, M.C. Ferreira, Q.F. Hou, A.B. Yu, Feeding spent coffee grounds into reactors: TFM simulation of a non-mechanical spouted bed type feeder, Waste Manag. 109 (2020) 161–170. doi:10.1016/j.wasman.2020.04.056.

[10] P.K. Mollick, R. Venugopalan, M. Roy, P.T. Rao, D. Sathiyamoorthy, P. Sengupta, G. Sharma, C.B. Basak, J.K. Chakravartty, Deposition of diversely textured buffer pyrolytic

carbon layer in TRISO coated particle by controlled manipulation of spouted bed hydrodynamics, Chem. Eng. Sci. 128 (2015) 44–53. doi:10.1016/j.ces.2015.01.065.

[11] X. Yang, F. Zhang, M. Guo, Y. Zhong, P. Wang, J. Lin, Z. Zhu, Preparation of SiC layer with sub-micro grain structure in TRISO particles by spouted bed CVD, J. Eur. Ceram. Soc. 39 (2019) 2839–2845. doi:10.1016/j.jeurceramsoc.2019.02.005.

[12] D. Peshev, E. Eichner, M. Goslinska, S. Pietsch, Y. Trambabova, T. Terzieva, N. Georgieva, S. Heinrich, Particle formulation of hydroalcoholic rosemary (Rosmarinus officinalis L.) extracts using a spouted bed, Particuology. 51 (2020) 26–34. doi:10.1016/j.partic.2019.10.002.

[13] S. Pietsch, A. Peter, P. Wahl, J. Khinast, S. Heinrich, Measurement of granule layer thickness in a spouted bed coating process via optical coherence tomography, Powder Technol. 356 (2019) 139–147. doi:10.1016/j.powtec.2019.08.022.

[14] M. Moradi, S. Azizi, M. Niakousari, S. Kamgar, A. Mousavi Khaneghah, Drying of green bell pepper slices using an IR-assisted Spouted Bed Dryer: An assessment of drying kinetics and energy consumption, Innov. Food Sci. Emerg. Technol. 60 (2020) 102280. doi:10.1016/j.ifset.2019.102280.

[15] S. Rajashekhara, D.V.R. Murthy, Drying of Agricultural Grains in a Multiple Porous Draft Tube Spouted Bed, Chem. Eng. Commun. 204 (2017) 942–950. doi:10.1080/00986445.2017.1328412.

[16] G.K.K. Jayatunga, B.M.W.P.K.M.W.P.K. Amarasinghe, Drying kinetics, quality and moisture diffusivity of spouted bed dried Sri Lankan black pepper, J. Food Eng. 263 (2019) 38–45. doi:10.1016/j.jfoodeng.2019.05.023.

[17] M. Olazar, M.J. San José, J. Bilbao, Conical spouted beds, in: N. Epstein, J.R. Grace (Eds.),

Spouted Spout-Fluid Beds Fundam. Appl., First, Cambridge University Press, New York, 2011: p. 340.

[18] H. Altzibar, G. Lopez, J. Bilbao, M. Olazar, Minimum Spouting Velocity of Conical Spouted Beds Equipped with Draft Tubes of Different Configuration, Ind. Eng. Chem. Res. 52 (2013) 2995–3006. doi:10.1021/ie302407f.

[19] M. Olazar, G. Lopez, H. Altzibar, M. Amutio, J. Bilbao, Drying of Biomass in a Conical Spouted Bed with Different Types of Internal Devices, Dry. Technol. 30 (2012) 207–216. doi:Doi 10.1080/07373937.2011.633194.

[20] T. Ishikura, H. Nagashima, M. Ide, Hydrodynamics of a spouted bed with a porous draft tube containing a small amount of finer particles, Powder Technol. 131 (2003) 56–65. doi:10.1016/S0032-5910(02)00321-2.

[21] H. Altzibar, G. Lopez, R. Aguado, S. Alvarez, M.J. San Jose, M. Olazar, Hydrodynamics of conical spouted beds using different types of internal devices, Chem. Eng. Technol. 32 (2009) 463–469. doi:10.1002/ceat.200800605.

[22] M. Karimi, B. Vaferi, S.H. Hosseini, M. Olazar, S. Rashidi, Smart computing approach for design and scale-up of conical spouted beds with open-sided draft tubes, Particuology. (2020). doi:10.1016/j.partic.2020.09.003.

[23] M.J. San José, M. Olazar, S. Alvarez, M.A. Izquierdo, J. Bilbao, Solid cross-flow into the spout and particle trajectories in conical spouted beds, Chem. Eng. Sci. 53 (1998) 3561–3570. doi:10.1016/S0009-2509(98)00170-5.

[24] J.R. Muir, F. Berrutit, L.A. Behle, Solids Circulation in Spouted and Spout-Fluid Beds with Draft-Tubes, Chem. Eng. Commun. 88 (1990) 153–171. doi:10.1080/00986449008940553.

[25] X.L. Zhao, Q. Yao, S.Q. Li, Effects of draft tubes on particle velocity profiles in spouted

beds, Chem. Eng. Technol. 29 (2006) 875–881. doi:10.1002/ceat.200600087.

[26] P.K. Mollick, A.B. Pandit, T. Mukherjee, P.K. Vijayan, Novel Porous Draft Tube to Manipulate Fluid Throughput from Spout to Annulus in a Spouted Bed, Ind. Eng. Chem. Res. 59 (2020) 3229–3237. doi:10.1021/acs.iecr.9b04035.

[27] J. Makibar, A.R. Fernandez-Akarregi, L. Díaz, G. Lopez, M. Olazar, Pilot scale conical spouted bed pyrolysis reactor: Draft tube selection and hydrodynamic performance, Powder Technol. 219 (2012) 49–58. doi:10.1016/j.powtec.2011.12.008.

[28] Z. Rahimi-Ahar, M.S. Hatamipour, Hydrodynamics, numerical study and application of spouted bed, Rev. Chem. Eng. 34 (2018) 743–766. doi:10.1515/revce-2017-0036.

[29] L. Qian, Y. Lu, W. Zhong, B. Jin, Developing a High Speed Fiber-optic Endoscopic Technique for Measuring Particle Phase Characteristics in a Spouted Bed, Procedia Eng. 102 (2015) 150–158. doi:10.1016/j.proeng.2015.01.118.

[30] A. Atxutegi, M. Tellabide, G. Lopez, R. Aguado, J. Bilbao, M. Olazar, Implementation of a borescopic technique in a conical spouted bed for tracking spherical and irregular particles, Chem. Eng. J. 374 (2019) 39–48. doi:10.1016/j.cej.2019.05.143.

[31] M. Tellabide, I. Estiati, A. Atxutegi, H. Altzibar, R. Aguado, M. Olazar, Fine particle flow pattern and region delimitation in fountain confined conical spouted beds, J. Ind. Eng. Chem. (2021). doi:10.1016/j.jiec.2021.01.006.

[32] I. Estiati, M. Tellabide, J.F. Saldarriaga, H. Altzibar, F.B. Freire, J.T. Freire, M. Olazar, Comparison of artificial neural networks with empirical correlations for estimating the average cycle time in conical spouted beds, Particuology. 42 (2019) 48–57. doi:10.1016/j.partic.2018.03.010.

[33] J.F. Saldarriaga, A. Atxutegi, R. Aguado, H. Altzibar, J. Bilbao, M. Olazar, Influence of

contactor geometry and draft tube configuration on the cycle time distribution in sawdust conical spouted beds, Chem. Eng. Res. Des. 102 (2015) 80–89. doi:10.1016/j.cherd.2015.05.042.

[34] J.F. Saldarriaga, I. Estiati, A. Atxutegi, R. Aguado, J. Bilbao, M. Olazar, Distribution of Cycle Times in Sawdust Conical Spouted Bed Equipped with Fountain Confiner and Draft Tube, Ind. Eng. Chem. Res. 58 (2019) 1932–1940. doi:10.1021/acs.iecr.8b03451.

[35] I. Estiati, H. Altzibar, M. Olazar, Particle cycle times in draft tube conical spouted beds, Chem. Eng. Trans. 39 (2014) 1669–1674. doi:10.3303/CET1439279.

[36] M. Olazar, M.J.S. José, L.L. Ricardo, S. Alvarez, J. Bilbao, Study of Local Properties in Conical Spouted Beds Using an Optical Fiber Probe, Ind. Eng. Chem. Res. 34 (1995) 4033–4039. doi:10.1021/ie00038a044.

[37] I.P. Mukhlenov, A.E. Gorshtein, Investigation of a Spouted Bed, Khim. Prom. 41 (1965) 443–446.

[38] M. Olazar, M.J. San José, S. Alvarez, A. Morales, J. Bilbao, Measurement of Particle Velocities in Conical Spouted Beds Using an Optical Fiber Probe, Ind. Eng. Chem. Res. 37 (1998) 4520–4527. doi:10.1021/ie9800243.

[39] G. Kulah, S. Sari, M. Koksal, Particle Velocity, Solids Hold-Up, and Solids Flux Distributions in Conical Spouted Beds Operating with Heavy Particles, Ind. Eng. Chem. Res. 55 (2016) 3131–3138. doi:10.1021/acs.iecr.5b04496.

[40] H. Littman, Minimum Fluid Flowrate, Pressure Drop and Stability, 70 (1992) 0–6.

[41] J. Bridgwater, K.B. Mathur, Prediction of spout diameter in a spouted bed-A theoretical model, Powder Technol. 6 (1972) 183–187. doi:10.1016/0032-5910(72)83011-0.

[42] H. Altzibar, G. Lopez, J. Bilbao, M. Olazar, Minimum Spouting Velocity of Conical

Spouted Beds Equipped with Draft Tubes of Different Configuration, Ind. Eng. Chem. Res. 52 (2013) 2995–3006. doi:10.1021/ie302407f.

[43] H. Altzibar, G. Lopez, J. Bilbao, M. Olazar, Effect of draft tube geometry on pressure drop in draft tube conical spouted beds, Can. J. Chem. Eng. 91 (2013) 1865–1870. doi:10.1002/cjce.21913.

[44] H. Nagashima, K. Suzukawa, T. Ishikura, Hydrodynamic performance of spouted beds with different types of draft tubes, Particuology. 11 (2013) 475–482. doi:10.1016/j.partic.2013.01.007.

[45] S. Aradhya, H. Taofeeq, M. Al-Dahhan, A new mechanistic scale-up methodology for gas-solid spouted beds, Chem. Eng. Process. Process Intensif. 110 (2016) 146–159. doi:10.1016/j.cep.2016.10.005.

[46] X.L. Zhao, S.Q. Li, G.Q. Liu, Q. Song, Q. Yao, Flow patterns of solids in a two-dimensional spouted bed with draft plates: PIV measurement and DEM simulations, Powder Technol. 183 (2008) 79–87. doi:10.1016/j.powtec.2007.11.021.

[47] H. Zhang, M. Liu, T. Li, Z. Huang, X. Sun, H. Bo, Y. Dong, Experimental investigation on gas-solid hydrodynamics of coarse particles in a two-dimensional spouted bed, Powder Technol. 307 (2017) 175–183. doi:10.1016/j.powtec.2016.11.024.

[48] Y.-L. He, S.-Z. Qin, C.J. Lim, J.R. Grace, Particle velocity profiles and solid flow patterns in spouted beds, Can. J. Chem. Eng. 72 (1994) 561–568. doi:10.1002/cjce.5450720402.

[49] T. Djeridane, F. Larachi, D. Roy, J. Chaouki, R. Legros, Investigation of the mean and turbulent particle velocity fields in a spouted bed using radioactive particle tracking, Can. J. Chem. Eng. 76 (1998) 190–195. doi:10.1002/cjce.5450760205.

[50] R. Zhu, S. Li, Q. Yao, Effect of cohesion on granular-fluid flows in spouted beds: PIV

measurement and DEM simulations, AIP Conf. Proc. 1542 (2013) 979–982. doi:10.1063/1.4812097.

[51] A. Benkrid, H.S. Caram, Solid flow in the annular region of a spouted bed, AIChE J. 35 (1989) 1328–1336. doi:10.1002/aic.690350811.

[52] D. Roy, F. Larachi, R. Legros, J. Chaouki, A study of solid behavior in spouted beds using 3-D particle tracking, Can. J. Chem. Eng. 72 (1994) 945–952. doi:10.1002/cjce.5450720602.

[53] Z. Wang, H.T. Bi, C.J. Lim, Measurements of local Flow Structures of conical spouted beds by optical fibre probes, Can. J. Chem. Eng. 87 (2009) 264–273. doi:10.1002/cjce.20157.

[54] H. Altzibar, G. Lopez, I. Estiati, J. Bilbao, M. Olazar, Particle cycle times and solid circulation rates in conical spouted beds with draft tubes of different configuration, Ind. Eng. Chem. Res. 52 (2013) 15959–15967. doi:10.1021/ie401412j.

CHAPTER 9

FINAL REMARKS AND MAIN CONCLUSIONS

This thesis advances the understanding of the intermittent drying and draft tube design for spouted beds in the processing of particulate solids, providing key contributions to the development of equipment with suitable and feasible features for industrial applications, mainly considering energy and scale up aspects. Despite the focus on spouted bed applications, the current study has also shed some light on the theoretical basis of intermittent drying for application in different moving beds (e.g., fluidized beds, vibrofluidized beds, rotary drum dryers, etc.). Therefore, the main findings obtained in this thesis are listed below, fulfilling the specific objectives described in Chapter 1:

- The application of intermittent drying significantly improved the energy performance of spouted beds. This methodology provided higher energy efficiency and better use of the energy supplied than the continuous process. Likewise, significant decreases in energy consumption were provided by the intermittency, as reductions in the range from 13.2% to 67.2% were obtained compared to the continuous process. The intermittent methodology also decreased the energy losses in the spouted bed. Such findings showed that intermittent drying is a promising alternative to optimize energy consumption in spouted beds.
- In the quality analysis, a distinct trend of intermittent drying was obtained in the spouted bed compared to other dryers. Surprisingly, the continuous process provided the lowest degree of seed deterioration, considering both physical and physiological

aspects, followed by the intermittent process with the shortest period of reduced air flow, both processes at 50 °C. Furthermore, mechanical damages of continuous drying in the spouted bed were not as harmful to physiological properties as heating damages, implying further studies under lower temperatures for good quality results. Nevertheless, the mechanical damages caused by intermittency with periodic interruption of the air flow were more harmful to physiological properties than damages caused by intermittency with periodic reductions. Such unexpected findings were attributed mainly to the gas-solid flow pattern of spouted beds.

- A fully predictive model for continuous and intermittent drying was proposed and good agreements between predicted and experimental results were obtained for continuous drying under moderate air temperature, as well as for intermittent drying with medium and long resting periods. However, the assumptions adopted are less accurate for the processes under high air temperatures and short resting periods, as the heat losses and particle-particle interactions were neglected. Therefore, different terms should be implemented in the model. Nevertheless, the model proposed provided predictions physically consistent of the internal gradients of moisture and temperature. Such findings are fundamental in the intermittent drying for energy optimization and product quality.
- In the hydrodynamic analysis, a methodology based on the analysis of pressure fluctuation signals and spectral analysis was proposed for estimating the minimum spouting velocity. Such methodology proved to be especially suitable for systems characterized by pulsating spouting. Thus, these systems were represented by configurations without and with draft tubes in the processing of fine and irregular

particles, as well as systems without tubes in the processing of large spherical particles (e.g., soybean particles). Regarding configurations with more stable regimes, pressure fluctuation signals analysis monitoring the qualitative behaviour at different air velocities was able to identify the different flow regimes. Therefore, the findings obtained in the hydrodynamic analysis are relevant for industrial processes, mainly when the aim is process control and scaling up, as spectral analysis is more feasible than visual methodologies.

- The analysis of the drying of particulate solids in draft tube spouted beds showed the influence of these devices in the processing of different particulate solids, i.e., alumina, soybean, and barley particles. As the removal of moisture from diffusive materials is less affected by the reduced air percolation and poorer gas-solid contact obtained with draft tubes, these internal devices tend to provide better energy performance in the processing of these materials. Besides the removal of moisture, the influence of draft tube in the hydrodynamic parameters also played an important role in energy performance. Thus, the open-sided draft tube provided the best energy utilization for alumina particles, whereas the nonporous draft tube provided the best energy performance for barley and soybean particles. Therefore, these findings contribute to support the draft tubes as promising devices for improving energy issues in spouted beds, mainly in the processing of low moisture materials.
- A new design criterion for the development of draft tubes to be used in spouted beds was proposed. Such a criterion was based on the average spout diameter measured by a borescopic technique in conical spouted beds without draft tubes. Thus, the new draft tubes designed provided a more efficient gas-solid contact than any

conventional one, mainly the new open-sided tube. The latter also presented an interesting hydrodynamic similarity with the configuration without tube, which was evidenced by both the spout geometry and hydrodynamic parameters (differences in the range from 2% to 6%). Furthermore, the new internal devices also presented the pertinent advantages of the conventional ones, such as high bed stability and better solid circulation control. Therefore, this study meant a step further to overcome the spouted bed limitations related to scale up and applications in large-scale industrial processes by using internal devices tailored to the actual spout geometry.

Therefore, the results of this thesis will push forward the knowledge frontier involving the use of intermittency and draft tubes in spouted beds. A natural progression of this research is to perform studies in the spouted bed with heat recovery system designed in this thesis, which was presented in Chapter 2 (Figure 2.1), coupling methodology of the intermittency and the use of the draft tube. Furthermore, this research has thrown up many questions in need of further investigation. Thus, the following suggestions for future research are described below:

- Analysis of drying and energy performance of the spouted bed with heat recovery system designed, evaluating different recycling ratios;
- Optimization of the intermittent drying, based on the model proposed in this thesis and a suitable objective function able to reflect the product quality;
- Analysis of the spout geometry for different particulate materials and configurations, mainly involving the spouted bed with heat recovery system;
- Development and design of draft tubes based on the new design criterion proposed in this research for the different configurations evaluated.
- Coupling the intermittent methodology with the new draft tubes developed.

APPENDIX

LIST OF PUBLICATIONS

JOURNAL PAPERS

---

1. **BRITO, R. C**.; TELLABIDE, M.; ATXUTEGI, A.; ESTIATI, I.; FREIRE, J. T.; OLAZAR, M. Draft tube design based on a borescopic technique in conical spouted beds. ADVANCED POWDER TECHNOLOGY, In Press, 2021.
2. **BRITO, R. C.**; TELLABIDE, M.; ESTIATI, I.; FREIRE, J. T.; OLAZAR, M. Drying of particulate materials in draft tube conical spouted beds: Energy analysis. POWDER TECHNOLOGY, v. 388, p. 110-121, 2021.
3. **BRITO, R. C.**; TELLABIDE, M.; ESTIATI, I.; FREIRE, J. T.; OLAZAR, M. Estimation of the minimum spouting velocity based on pressure fluctuation analysis. Journal of the Taiwan Institute of Chemical Engineers, p. 56-65, 2020.
4. BARROS, J. P. A. A.; **BRITO, R. C.**; FREIRE, F. B.; FREIRE, J. T. Fluid Dynamic Analysis of a Modified Mechanical Stirring Spouted Bed: Effect of Particle Properties and Stirring Rotation. Industrial & Engineering Chemistry Research, v. 59, p. 16396-16406, 2020.
5. BATISTA, J. N. M.; **BRITO, R. C.**; FREIRE, J. T.; BETTEGA, R. Experimental and CFD Study of Heat Transfer in Spouted Beds: Analysis of Nusselt Number Correlations. THEORETICAL FOUNDATIONS OF CHEMICAL ENGINEERING, v. 54, p. 1314-1326, 2020.
6. **BRITO, R. C.**; ZACHARIAS, M. B.; FORTI, V. A.; FREIRE, J. T. Physical and physiological quality of intermittent soybean seeds drying in the spouted bed. DRYING TECHNOLOGY (ONLINE), v. 39, p. 1-14, 2020.
7. PAULA, E. R.; **BRITO, R. C.**; FREIRE, J. T.; FREIRE, F. B. Soft sensor based on a lumped parameter model of solids drying in a spouted bed. DRYING TECHNOLOGY (ONLINE), v. 39, p. 1-14, 2020.

8. **BRITO, R. C.**; BÉTTEGA, R.; FREIRE, J. T. Energy analysis of intermittent drying in the spouted bed. DRYING TECHNOLOGY (ONLINE), v. 37, p. 1498-1510, 2019.
9. **BRITO, R. C.**; SOUSA, R. C.; BÉTTEGA, R.; FREIRE, F. B.; FREIRE, J. T. Analysis of the energy performance of a modified mechanically spouted bed applied in the drying of alumina and skimmed milk. CHEMICAL ENGINEERING AND PROCESSING, v. 130, p. 1-10, 2018.
10. BATISTA, J. N. M.; **BRITO, R. C.**; BÉTTEGA, R. Influence of inlet air distributor geometry on the fluid dynamics of conical spouted beds: A CFD study. Chemical Industry & Chemical Engineering Quarterly, v. 24, p. 369-378, 2018.
11. **BRITO, R. C.**; FREIRE, J. T.; PADUA, T. F.; BETTEGA, R. Effect of mechanical energy on the energy efficiency of spouted beds applied on drying of sorghum [Sorghum bicolor (L) moench]. CHEMICAL ENGINEERING AND PROCESSING, v. 117, p. 95-105, 2017.

BOOK CHAPTERS

1. **BRITO, R. C.**; BETTEGA, R.; FREIRE, J. T. Intermittent Drying: principles and fundamentals. In: José Teixeira Freire; Geisa Albini. (Org.). Special Topics in Particulate Systems. 1ed. São Carlos/SP: 2019, v. 5, p. 205-231 (in Portuguese).
2. **Brito, Ronaldo Correia de**; Bettega, Rodrigo; Freire, José Teixeira. Application of intermittence in the drying process of particulate material in spouted bed. In: Luís Fernando Paulista Cotian. (Org.). Engineering, science and technology. 1st edition: Antonella Carvalho de Oliveira, 2019, v. 1, p. 18-33 (in Portuguese).

CONFERENCE PAPERS

1. **BRITO, R. C.**; BÉTTEGA, R.; FREIRE, J. T. APLICAÇÃO DA INTERMITÊNCIA NA SECAGEM DE ALUMINA EM LEITO DE JORRO: ANÁLISE DA HOMOGENEIDADE DO MEIO. In: XXII Congresso Brasileiro de Engenharia Química,

2018, São Paulo. Blucher Chemical Engineering Proceedings. São Paulo: Editora Blucher, 2018. v. 1. p. 882.

2. PAULA, E. R.; **BRITO, R. C.**; FREIRE, J. T.; FREIRE, F. B. SENSOR VIRTUAL DE UMIDADE DO SÓLIDO PARA SECAGEM EM LEITO DE JORRO. In: XXII Congresso Brasileiro de Engenharia Química, 2018, São Paulo. Blucher Chemical Engineering Proceedings. São Paulo: Editora Blucher, 2018. v. 1. p. 3805.
3. BATISTA, J. N. M.; **BRITO, R. C.**; BÉTTEGA, R. TRANSFERÊNCIA DE CALOR EM LEITO DE JORRO UTILIZANDO CFD: ANÁLISE DA CONDIÇÃO DE CONTORNO TÉRMICA NA PAREDE. In: XXII Congresso Brasileiro de Engenharia Química, 2018, São Paulo. Blucher Chemical Engineering Proceedings. São Paulo: Editora Blucher, 2018. v. 1. p. 2969.
4. ESTECA, G. F.; **BRITO, R. C.**; BÉTTEGA, R. CARACTERIZAÇÃO FÍSICA E CINÉTICA DE SECAGEM DE SORGO (SORGHUM BICOLOR L. MOENCH). In: Congresso Brasileiro de Engenharia Química em Iniciação Científica, 2017, São Carlos. Blucher Chemical Engineering Proceedings, 2016. p. 2159.
5. SOUSA, R. C.; **BRITO, R. C.**; BÉTTEGA, R.; FREIRE, F. B.; FREIRE, J. T. ANÁLISE DO DESEMPENHO ENERGÉTICO DO LEITO DE JORRO MECÂNICO APLICADO NO PROCESSO DE SECAGEM DE ALUMINA. In: XXXVIII Congresso Brasileiro de Sistemas Particulados, 2017, Maringá-PR. XXXVIII Congresso Brasileiro de Sistemas Particulados, 2017.
6. **BRITO, R. C.**; BÉTTEGA, R.; FREIRE, J. T. ANÁLISE ENERGÉTICA DA APLICAÇÃO DA INTERMITÊNCIA SOBRE O PROCESSO DE SECAGEM DE ALUMINA EM LEITO DE JORRO. In: XXXVIII Congresso Brasileiro de Sistemas Particulados, 2017, Maringá-PR. XXXVIII Congresso Brasileiro de Sistemas Particulados, 2017.
7. **BRITO, R. C.**; PAULA, E. R.; FREIRE, J. T.; FREIRE, F. B. MODELO REALIMENTADO EM CASCATA PARA SECAGEM DE ALUMINA EM LEITO DE JORRO. In: XXXVIII Congresso Brasileiro de Sistemas Particulados, 2017, Maringá-PR. XXXVIII Congresso Brasileiro de Sistemas Particulados, 2017.